HYDRO-MECHANICAL BEHAVIOR OF UNSATURATED SPECIMENS ISOTROPICALLY RECONSTITUTED FROM SLURRY AND COMPACTED SPECIMENS

A THESIS SUBMITTED TO
THE GRADUATE SCHOOL OF NATURAL AND APPLIED SCIENCES
OF
MIDDLE EAST TECHNICAL UNIVERSITY

BY

REZA AHMADI NAGHADEH

IN PARTIAL FULFILLMENT OF THE REQUIREMENTS
FOR
THE DEGREE OF DOCTOR OF PHILOSOPHY
IN
CIVIL ENGINEERING

JANUARY 2016

Approval of the thesis:

**HYDRO-MECHANICAL BEHAVIOR OF UNSATURATED SPECIMENS
ISOTROPICALLY RECONSTITUTED FROM SLURRY AND
COMPACTED SPECIMENS**

submitted by **REZA AHMADI NAGHADEH** in partial fulfillment of the
requirements for the degree of **Doctor of Philosophy in Civil Engineering
Department, Middle East Technical University** by,

Prof. Dr. Gülbin Dural Ünver
Dean, Graduate School of **Natural and Applied Sciences** ———————————

Prof. Dr. İsmail Özgür Yaman
Head of Department, **Civil Engineering** ———————————

Assist. Prof. Dr. Nabi Kartal Toker
Supervisor, **Civil Engineering Dept., METU** ———————————

Examining Committee Members:

Prof. Dr. Kemal Önder Çetin
Civil Engineering Dept., METU ———————————

Assist. Prof. Dr. Nabi Kartal Toker
Civil Engineering Dept., METU ———————————

Prof. Dr. Erdal Çokça
Civil Engineering Dept., METU ———————————

Assoc. Prof. Dr. Mehmet Barış Can Ülker
Earthquake Engineering and Disaster Management
Institute., ITU ———————————

Assoc. Prof. Dr. Sami Oğuzhan Akbaş
Civil Engineering Dept., Gazi University ———————————

Date: 19 JANUARY 2016

I hereby declare that all information in this document has been obtained and presented in accordance with academic rules and ethical conduct. I also declare that, as required by these rules and conduct, I have fully cited and referenced all material and results that are not original to this work.

Name, Last name : Reza Ahmadi Naghadeh

Signature   :

ABSTRACT

HYDRO-MECHANICAL BEHAVIOR OF UNSATURATED SPECIMENS ISOTROPICALLY RECONSTITUTED FROM SLURRY AND COMPACTED SPECIMENS

Ahmadi Naghadeh, Reza

Ph.D., Department of Civil Engineering

Supervisor: Assist. Prof. Dr. Nabi Kartal Toker

January 2016, 328 pages

Response of unsaturated soils constitutes an important consideration for many problems in geotechnical engineering. The main objective of this study is to understand coupling hydro-mechanical behavior of the unsaturated reconstituted specimens from slurry and moist-tamped compacted specimen, and to develop practical and cost-effective testing equipment and procedure. The innovations that will be put forth by this study will make the unsaturated soil mechanics more accessible and appealing to those practical engineers working.

A prediction type exponential equation is introduced to predict the shear strength of the unsaturated soil. Equation involves three constant parameters. Two of which are effective shear strength parameters (i.e. ϕ' and c' can be determined through conventional saturated shear strength tests). The third parameter is ultimate shear strength, c''_{max}, introduced in this study, which can be determined through soil-water characteristic curve (SWCC). The proposed equation was validated through laboratory tests conducted. In addition, validity of the equation is investigated regarding test results of five types of soils published in the literature. Comparison on

prediction of shear strength was performed between proposed equation and six published shear strength equations.

Within the scope of experimental studies, the existing testing equipment (automated the triaxial setup) was modified to be able to perform the unsaturated soils tests (which require matric suction control, volume change measurements) and to measure the SWCC of the soil.

A novel procedure is developed to measure the total volume change of the saturated and unsaturated soils in triaxial testing. The principle of the proposed method is based on cell fluid volume measurements corrected by the assumption of viscoelastic behavior for the triaxial setup. Calibration and parameter determination procedures of the model are devised, and the presented model is implemented into a MATLAB code. The performance of the proposed method is validated through a series of consolidated drained (CD) triaxial tests on saturated specimens, by comparing the changes in volume measurement of proposed method and conventional measurement (pore fluid inflow/outflow). The accuracy in volume measurement during consolidation and shear stages of these tests was between 0.03 - 0.22 cm^3, which is on par with or better than more complex and expensive alternatives found in the literature. Repeatability of the proposed technique in measurement of the volume change was also investigated through a set of identical suction controlled unsaturated soil tests.

A new procedure for preparation of specimens isotropically reconstituted from slurry is developed for use in both saturated and unsaturated soil testing. The uniformity of the specimen (regarding void radio), segregation and repeatability was investigated to confirm the performance of the method. New preparation method results in a homogenous specimen, which has a simple structure and stress history. The strength and volumetric behavior of specimens prepared by the introduced method are compared with those of specimens that are moist-tamped compacted as well as one-dimensionally reconstituted from slurry, by performing consolidated drained (CD) triaxial tests.

A comprehensive laboratory-based study has been carried out, with the modified triaxial setup, to investigate the effects of matric suction and suction history (drying-wetting) as well as net mean stress on shear strength of moist-tamped compacted

specimens and specimens isotropically reconstituted from slurry. The results show that the shear strength of the studied soil increases nonlinearly at a decreasing rate toward an asymptotic value as suction increases. The response of the specimens change from strain-hardening in saturated condition to strain-softening as suction increases. For the same net confining stress, specimens with higher suction values reach a peak deviator stress at lower axial strain. In general, it is found that total volumetric deformation behavior became more dilative as the suction increases. Stiffness and maximum shear strength are found to depend on the direction of the suction path (wetting or drying), where specimens on the drying path exhibit higher shear strength and stiffness for a given suction than those on the wetting path. However, shear strength in the critical state is found to be independent of the direction of the suction path. For a given net confining stress and suction (through drying or wetting paths) specimen approaches a critical state.

For the entire testing range of suction (0 - 400 kPa), it was found that specimens on the wetting path reach a peak deviator stress at lower axial strain than those at the same suction and net confining stress on the drying path. During shearing, for a given net confining stress and suction, specimens on the wetting path exhibit more dilative behavior than those on the drying path. The laboratory test results were also interpreted under elasto-plastic framework. For MT compacted specimens, inclined semi-elliptical yield curves were fitted to each series of constant suction yield points. The inclination of the yield locus was attributed to inherent anisotropic nature of the one-dimensionally compacted specimens. For IRS specimens, an elliptical yield surface with the axis of net mean stress as the major axis were fitted successfully to yield points. For both MT and IRS, it was shown that, the size of the yield locus is suction dependent and expands as the suction increases. For IRS specimens with drying-wetting, the shape (elliptical) of the yield loci remain unchanged independent of suction history. However, specimens with a drying-wetting cycle have larger yield locus.

Keywords: unsaturated soil, shear strength, triaxial test, volume change measurement, viscoelasticity, slurry consolidation

ÖZ

NUMUNE ÇAMURUNA İZOTROPİK GERİLME UYGULAMA VE SIKIŞTIRMA YÖNTEMLERİ İLE OLUŞTURULAN SUYA DOYGUN OLMAYAN NUMUNELERİN HİDROMEKANİK DAVRANIŞI

Ahmadi Naghadeh, Reza

Doktora, İnşaat Mühendisliği Bölümü

Tez Yöneticisi: Yrd. Doç. Dr. Nabi Kartal Toker

Ocak 2016, 328 sayfa

Suya doygun olmayan zemin davranışı birçok geoteknik mühendisliği problemi için önem teşkil eder. Bu çalışmanın ana amacı, numune çamurundan konsolidasyon veya nemli numuneden sıkıştırma ile oluşturulan suya doygun olmayan numunelerin hidro-mekanik davranışını anlamaktır ve pratik, ekonomik test ekipmanları ve yöntemleri geliştirmektir. Bu çalışma ile ortaya koyulacak yenilikler suya doygun olmayan zemin mekaniği konseptini mühendisliğin pratik uıygulamaları için daha kullanılabilir ve cazip hale getirecektir.

Suya doygun olmayan zeminin kayma dayanımını tayin edebilmek için üssel türde bir denklem önerilmiştir. Denklem üç adet sabit parametre içermektedir. Bu üç parametreden ikisi standart suya doygun zemin mekaniği deneyleri ile belirlenen efektif kayma dayanımı parametreleridir ($\phi´$ ve $c´$). Üçüncü parametre ise bu çalışmada ortaya koyulan ve zemin-su karakteristik eğrisi kullanılarak elde edilen maksimum emme kohezyon ($c´´_{max}$) parametresidir. Önerilen denklemin geçerliliği yürütülen laboratuvar deneyleri ile teyit edilmiştir. Ayrıca, literatürde yayımlanmış beş farklı zeminden elde edilen deney sonuçları kullanılarak da denklemin geçerliliği

araştırılmıştır. Önerilen kayma dayanımı denklemi ile daha önce yayımlanmış diğer altı adet kayma dayanımı denkleminin tahminleri karşılaştırılmıştır.

Deneysel çalışmalar kapsamında, suya doygun olmayan zemin deneylerinin yapılabilmesi için gerekli matrik emme kontrolü, hacim değişimi ölçümü gibi işlevleri yerine getirebilecek ve zeminin zemin-su karakteristik eğrisinin ölçülmesini sağlayacak şekilde, mevcut üç eksenli deney ekipmanına eklemeler yapılmıştır. Üç eksenli kesme deneylerinde suya doygun ve suya doygun olmayan numunelerin toplam hacim değişiminin ölçülmesinde yeni bir yöntem geliştirilmiştir. Önerilen yöntem, üç eksenli deney aletinin viskoelastik davranış gösterdiği kabulü ile hücre suyu hacmi ölçümlerine düzeltme yapmak ilkesine dayanır. Kalibrasyon ve parametre belirleme yöntemleri tasarlanmış ve sunulan model için bir MATLAB kodu hazırlanmıştır. Önerilen yöntemin geçerliliği, suya doygun zeminler kullanılarak yapılan konsolidasyonlu drenajlı (CD) üç eksenli deneylerinde, önerilen yöntemle yapılan hacim değişimi ölçümleri standart ölçüm yönteminden (boşluk suyu giriş ve çıkışının ölçülmesi) elde edilen hacim değişimi ölçümleri ile karşılaştırılarak incelenmiştir. Konsolidasyon ve kesme aşamalarında hacim değişimi ölçümlerindeki hata payı, literatürde bulunan daha karmaşık ve daha pahalı alternatiflere eşit veya daha iyi şekilde 0.03 - 0.22 cm^3 arasındadır. Ayrıca, hacim değişimi ölçümü için önerilen tekniğin tekrarlanabilirliği özdeş emme kontrollü suya doygun olmayan zemin deneyleri ile incelenmiştir.

Hem suya doygun hem de suya doygun olmayan zemin deneylerinde kullanmak üzere numune çamuruna izotropik gerilme uygulamaya dayanan yeni bir numune hazırlama yöntemi geliştirilmiştir. Yöntemin gücünü teyit etmek için boşluk oranına bağlı olarak numune üniformluğu, segregasyon ve tekrarlanabilirlik konuları incelenmiştir. Yeni numune hazırlama yöntemi ile basit bir mikro-yapıya ve gerilme geçmişine sahip homojen numuneler elde edilebilmektedir. Önerilen yöntem ile hazırlanmış numunelerin dayanım ve hacimsel davranışları, konsolidasyonlu ve drenajlı (CD) üç eksenli deneyleri yapılarak tokmaklama ile sıkıştırarak veya numune çamurundan tek boyutlu konsolide edilerek oluşturulan numunelerin dayanım ve hacimsel davranışları ile karşılaştırılmıştır.

Modifiye üç eksenli deney düzeneği ile matrik emmenin, emme geçmişinin (kuruma-ıslanma) ve net ortalama gerilmenin, tokmaklama ile sıkıştırılarak veya numune

çamuruna izotropik gerilme uygulayarak oluşturulan numunelerin kayma dayanımına etkisinin incelendiği kapsamlı bir deneysel çalışma yürütülmüştür. Elde edilen sonuçlar, çalışmalarda kullanılan zeminin kayma dayanımının emme gerilmesi arttıkça doğrusal olmayan ve azalan bir şekilde asimtotik bir değere doğru arttığını göstermiştir. Numunelerin davranışı, suya doygun durumdaki pekleşme davranışından emme gerilmesi arttıkça yumuşama davranışına doğru değişmektedir. Aynı net gerilme değeri için, emme gerilmesi yüksek numuneler daha düşük eksenel birim şekil değiştirme değerlerinde nihai deviyatör gerilme değerine ulaşmıştır. Genel olarak toplam hacimsel deformasyon davranışı emme gerilmesi arttıkça daha fazla dilatasyon gerçekleştirmiştir. Sertliğin ve maksimum kayma dayanımının emme gerilmesi yönüne (ıslanma veya kuruma) bağlı olduğu bulunmuş ve aynı emme gerilmesi değerinde kuruma yönünde olan numunelerin ıslanma yönündekilerine kıyasla daha fazla sertlik ve kayma dayanımı gösterdiği ortaya çıkarılmıştır. Ancak, kritik durumdaki kayma dayanımı değerinin emme gerilmesi yönünden bağımsız olduğu gözlenmiştir. Numuneler, belirli bir net gerilme ve emme gerilmesi (ıslanma veya kuruma yönünde) değerinde kritik duruma yakınsamışlardır.

Testlerde uygulanmış tüm emme gerilmesi aralığı (0 - 400 kPa) için ıslanma yönündeki numuneler aynı emme gerilmesi ve net gerilme değerindeki kuruma yönünde olan numunelere göre daha düşük eksenel birim şekil değiştirme değerlerinde nihai deviyatör gerilme değerine ulaşmıştır. Belirli bir net gerilme ve emme gerilmesi değeri için ıslanma yönündeki numuneler kuruma yönündekilere göre kesme işlemi sırasında daha fazla dilatasyon göstermiştir. Deney sonuçları ayrıca bir elastoplastik model kapsamında değerlendirilmiştir. Tokmaklama ile sıkıştırılmış (TS) numuneler için eğimli, yarı eliptik akma eğrisi sabit emme gerilmesi akma noktalarına yerleştirilmiştir. Akma bölgesinin eğimli oluşu tek eksenli olarak hazırlanmış numunelerin anizotropik oluşu ile ilişkilendirilmiştir. İzotropik gerilme uygulama yöntemi (İGU) ile oluşturulmuş numuneler için net gerilme ekseni majör eksen olacak şekilde oluşturulmuş eliptik akma yüzeyi başarılı bir şekilde akma noktalarına yerleştirilmiştir. Hem TS hem de İGU numuneleri için akma bölgesi büyüklüğünün emme gerilmesine bağlı olduğu ve emme gerilmesi arttıkça akma bölgesinin de genişlediği gösterilmiştir. Islanma ve kuruma yönünde İGU numuneleri için emme gerilmesi tarihçesinden bağımsız olarak akma bölgesinin şekli (eliptik)

sabit kalmaktadır. Ancak ıslanma kuruma çevrimine tabi tutulmuş numuneler daha büyük akma bölgesine sahip olduğu ortaya çıkarılmıştır.

Anahtar Kelimeler: Suya doygun olmayan zemin, kayma dayanımı, üç eksenli deneyi, hacim değişimi ölçümü, viskoelastik, numune çamuru

To My Parents, Who Taught Me to Believe in Myself

To My Wife, Who Believed in Me More Than I Believed in Myself

ACKNOWLEDGMENTS

TABLE OF CONTENTS

LIST OF TABLES

LIST OF FIGURES

xxiv

xxv

xxxiii

CHAPTER 1

INTRODUCTION

Terzaghi's effective stress principle (1925), or in other words the classical soil mechanics is formulated based on the two-phase media assumption (either totally saturated or completely dry soil). In the light of the simplistic and conservative design, the assumption of total saturation is still being adopted by practicing engineers. However, in most of the geotechnical projects, engineers encounter soils in partially saturated condition. Soils in the field could be subjected to changes in degree of saturation (i.e. wetting-drying cycles) owing to climate and environmental variation or human activity. The bearing capacity (strength and deformability) could be considerably affected by these variations and cause significant problems especially in projects including expensive and collapsible soils, slope stability and landfills. All of these deviations from the conventional theory makes it necessary to understand the behavior of the unsaturated soils, to predict and prevent natural instabilities.

In the case of partially saturated soils, total volume of soil mass should be considered as a three-phase system (solids, water and gas). Therefore, the two-phase effective stress principle is not valid for partially saturated soil.

1.1   Problem Statement

- Complexity and cost of unsaturated soil testing equipment have made it difficult to enter among the common equipment of soil mechanics lab and geotechnical practice, limiting it just to research institutions. In conventional testing of saturated soils (assuming soil particles and pore fluid are incompressible) volume change can be measured by monitoring the inflow or outflow of pore water from the specimen. However, such techniques are not applicable to unsaturated soils, which have both air and water phases in their

pores, as a portion of the volume change happens due to the compressibility, dissolution, and inflow or outflow of the air phase. Even in a saturated triaxial test, during the backpressure saturation stage, the specimen is unsaturated and its volume may change significantly due to swelling or collapse. Measuring this volume change at this stage, for further calculation (such as area correction or void ratio during shear), is crucial. However, volume change in unsaturated specimens is not measurable except with research-grade modification setups.

- The stress-strain behavior of low-plastic silts has not been investigated as thoroughly as clays and sands. Generally, silty soils have been considered to behave either as sands or as clays. In addition, most of the constitutive models are developed based on the lab testing of clays and sands and with the assumption of isotropic behavior. This can be attributed somewhat to the difficulty such soils present in obtaining intact samples or reconstituting uniform specimens to simulate the field condition.

  As far as unsaturated soil mechanics is concerned, the past two decades have seen increasingly rapid advances in both constitutive modeling and laboratory study. However, most of these achievements are obtained in the light of compacted specimens. Sheng et al. (2008) have raised unanswered questions about behavior and modeling of specimens dried or consolidated from the initial state of slurry. In the literature on unsaturated soil testing, there are only a few studies that had been conducted on specimens reconstituted from the slurry (Jennings and Burland 1962, Cunningham et al. 2003). This is due to time requirement and difficulties in preparing and desaturating slurry specimens.

  Generally, reconstituted specimens are prepared one-dimensionally and then subject to isotropic pressure in the hope that it will erase the precedent loading history. However, this procedure can lead to a complex stress history in the specimen.

- Estimating shear strength of a soil element in most of the geotechnical projects is inevitable. The shear strength of saturated soils is well defined through the effective stress concept in classical soil mechanics. However,

2

despite impressive advances in unsaturated soil mechanics, unanswered questions still exist from both theoretical and experimental points of view. Presence of the air phase in unsaturated soil brings considerable difficulties to both lab measurements, and formulation of the shear strength. To predict the shear strength of unsaturated soils different methods have been developed and reported in literature. However, there is still room for further elaboration and model enhancements.

1.2   Objective and Scope of the Research

The main objective of this study is to understand and compare the coupled hydro-mechanical behavior of the unsaturated reconstituted specimens from slurry and moist-tamped compacted specimens, and also to develop practical and cost-effective testing equipment and procedures.

In line with the objective, the present study involves three main parts:

1. Developing and modifying testing setup and procedures to perform saturated and unsaturated soil tests:

   ▪ Developing novel method to measure the total volume change of the saturated and unsaturated soils in triaxial testing.

   ▪ Modifying the existing triaxial setup to be able to control and induce desired values of matric suction using axis translation technique.

   ▪ Developing a procedure to prepare isotropically reconstituted specimens from slurry for use in both saturated and unsaturated soil testing.

2. Theoretical approach:

   ▪ literature review on unsaturated soils shear strength equations, and evaluating their predictions by comparisons between predicted and measured values,

   ▪ Developing an equation to predict shear strength of the unsaturated soils,

   ▪ Validate the proposed equation through laboratory tests performed in this study,

3

- Validate the proposed equation through the results of the laboratory tests on other soils, published in the literature.

3. Performing laboratory tests on both reconstituted specimens from slurry and moist-tamped compacted specimens:

  - A series of constant-suction CD triaxial tests on reconstituted specimens from slurry to investigate the effects of matric suction and net confining stress on shear strength, and volumetric behavior of unsaturated soils,

  - A series of constant-suction CD triaxial tests on reconstituted specimens from slurry with drying-wetting to investigate the effect of hydraulic hysteresis,

  - A series of constant-suction CD triaxial tests on moist-tamped compacted specimens to investigate the effects of specimen preparation on shear strength, and volumetric behavior of unsaturated soils,

  - Obtaining SWCC of the soil (both reconstituted specimens from slurry and moist-tamped compacted specimens) with hysteresis (drying and wetting paths).

1.3 Outline of the Thesis

The overall structure of the study takes the form of ten chapters, including this introductory chapter. Each chapter involves a separate section which provides a pertinent literature review. Therefore, a separate chapter that contains the entire "Literature Review" is not presented. However, **chapter two** provides a detailed background and reviews the fundamental concepts of unsaturated soils and viscoelasticity. In addition, a background review of constitutive models of unsaturated soils is also provided.

The **third chapter** is concerned with the Theoretical approach of the study. A literature review on unsaturated soils shear strength equations is presented. The development of the proposed shear strength equations for unsaturated soils is presented and parameter determination procedures of the model are devised.

Chapter four describes the modification of triaxial setup for testing unsaturated soils, presents the employed laboratory equipment and their calibration and testing procedures.

A comprehensive literature review on existing "volume change measurement" methods in triaxial testing of unsaturated soils is presented in **Chapter five**. The chapter continues with the development of the proposed novel method for the measurement of volume change of saturated and unsaturated soils in triaxial testing. Calibration and parameter determination procedures of the model are devised. The performance verification through consolidated drained triaxial tests on saturated specimens concludes this chapter.

Chapter six begins with a comprehensive literature review on existing specimen preparation methods. Then, presents the development of a new procedure for preparation of specimens isotropically reconstituted from slurry for use in both saturated and unsaturated soil testing. Examines the uniformity and segregation in the specimens and investigate repeatability of the method in preparing identical specimens.

Chapter seven describes the testing material and testing program and procedures.

Chapter eight presents and interprets experimental test results corresponding to the testing programs presented in Chapter seven.

Chapter nine compares and discusses saturated and unsaturated triaxial tests result (presented in chapter 8) performed on specimens with different preparation and suction history. The proposed strength equation is validated through the laboratory test results presented in chapter eight and also using the results of the laboratory tests published in the literature by comparing predicted and measured values.

Chapter 10 summarizes the main conclusions of this study and presents recommendations for future research.

CHAPTER 2

REVIEW OF FUNDAMENTAL CONCEPTS OF UNSATURATED SOIL

The theoretical and experimental investigations of unsaturated soils date back to 1960's (Bishop, 1959; Bishop et al, 1960). Despite this, the development of experimental and constitutive models for the behavior of unsaturated soils has lagged significantly behind that of saturated soils.

2.1 Soil Suction

Soil suction is one of the most important factors that influences the behavior of unsaturated soils. Water in unsaturated soils is absorbed and stored (retained) by the soil, and the energy required to remove the water from the soil, per unit volume of water is called total suction (Lee and Wray, 1995).

Total suction (negative pressure) is the sum of two components: the matric suction that is directly related to the capillary phenomenon and the osmotic suction which is due to the presence of dissolved ions in the pore water. Ground surface (fill materials, retaining walls, slopes, etc.) above the water table may subject to different suction values. It is one of the most important parameters and is of interest in analyzing geotechnical engineering problems. Although thermodynamical aspects of the problem of soil suction (water tension, water potential, or capillarity) have been addressed in a theoretical manner by several scientists over the centuries (van der Waals 1879; Einstein, 1901; Fisher, 1923; Aitchison, 1965; Coussy and Fleureau, 2002), its mechanical aspects have mostly been studied from a practical point of view.

2.1.1 Osmotic Suction

The presence of dissolved ions in water decreases the soil vapor pressure, increasing the relative humidity, which then increases the total soil suction. It can be observed in soils with soluble materials. Osmotic suction (h_s) can be expressed as:

$$h_s = \frac{n}{V} . R . T \qquad (2.1)$$

where n/V is the total ion concentration (molar), R is the universal gas constant, T is the absolute temperature in Kelvins. In most practical problems encountered in geotechnical engineering, significant changes in osmotic suction do not occur (Nelson & Miller, 1992).

2.1.2 Matric Suction

Matric suction comes from the capillary phenomenon as a result of surface tension of the air-water interface. The matric suction (u_a-u_w) can be defined as "*the equivalent suction derived from the measurement of the partial pressure of the water vapor in equilibrium with the soil water, relative to the partial pressure of the water vapor in equilibrium with a solution identical in composition with the soil water*" (Aitchinson, 1965).

Matric suction ($u_a - u_w$) is the pressure difference across the curved air-water interface, as given by the Young-Laplace Equation (Laplace, 1806):

$$u_a - u_w = 2\kappa . \sigma_{ST} \qquad (2.2)$$

Where κ is the mean curvature, and σ_{ST} is the air-water interfacial tension. Under equilibrium conditions, potential differences are constant, therefore soil suction, and hence the mean curvature of the interface, is constant.

Soil suction variation will affect the strength, deformation and hydraulic conductivity. Therefore, it has a great role in unsaturated soil mechanics. According to Rumpf (1962), suction and interfacial tension combined are among the mechanisms that keep particle agglomerations together.

2.1.3 Inducing and Measuring Soil Suction

A comprehensive description of the commonly used methods for inducing or measuring soil suction can be found in previous studies (Fredlund and Rahardjo 1993; Lee and Wray 1995; Toker 2007).

The techniques that are used for inducing a desired value of suction in the soil specimen are commonly equilibrium techniques that either reduce water tension to conventionally measureable magnitudes by applying air pressure, or manipulate the relative humidity of the environment. Both methods have been known to be used in unsaturated triaxial tests.

Methods of suction measurement can be grouped into three categories according to their working principles:

1. Relative Humidity Techniques: Psychrometers and the Filter Paper technique (ASTM D5298-94) measure the relative humidity in the pore air, and calculate the suction through thermodynamics.

2. Indirect Measurement Techniques: Filter Paper in contact with the soil (ASTM D5298-94), Time Domain Reflectometry (Conciani, Herrmann, & Soares, 1996), heat dissipation sensors and gypsum porous blocks in contact with the soil are all indirect methods used to measure the matric suction.

3. Direct Measurement Techniques: Tensiometer provide the only means of direct matric suction measurement. The basic principle is that the pressure of water contained in a high air entry material will come to equilibrium with the soil water pressure making it possible to measure negative soil water pressures. There have been several examples of incorporating tensiometers into static (Wong et al. 2001; Jotisankasa et al. 2007; Toker 2007) and cyclic (Becker & Meißner, 2002) triaxial setups.

2.2   Soil-Water Characteristic Curve (SWCC)

The soil-water characteristic curve (SWCC) plays a key role in applying unsaturated soil mechanics in engineering practice. Soil-water characteristic curves are widely used in geotechnical engineering for predicting various aspects of mechanical behavior (Fredlund 2006). Results of previous studies demonstrate a consistent relationship of the soil-water characteristic curve (SWCC) with unsaturated shear strength properties (discussed in chapter 3). Most of the equation reviewed in chapter 3 use SWCC to predict the shear strength of the unsaturated soils. The soil-water characteristic curve explains the relationship between the soil suction and the amount of water in the soil. The amount of water could be express as gravimetric water

content, degree of saturation or volumetric water content. White et al. (1970) were the first to define the different saturation stages of a soil. Vanapalli et al. (1996) modified their idea and defined three stages of desaturation: the boundary stage, the transition stage (primary and secondary transition zone) and residual stage. Air entry value and the onset of residual stage, which are the limits between the stages, are key components of SWCC, and can be determined graphically (Figure 2.1).
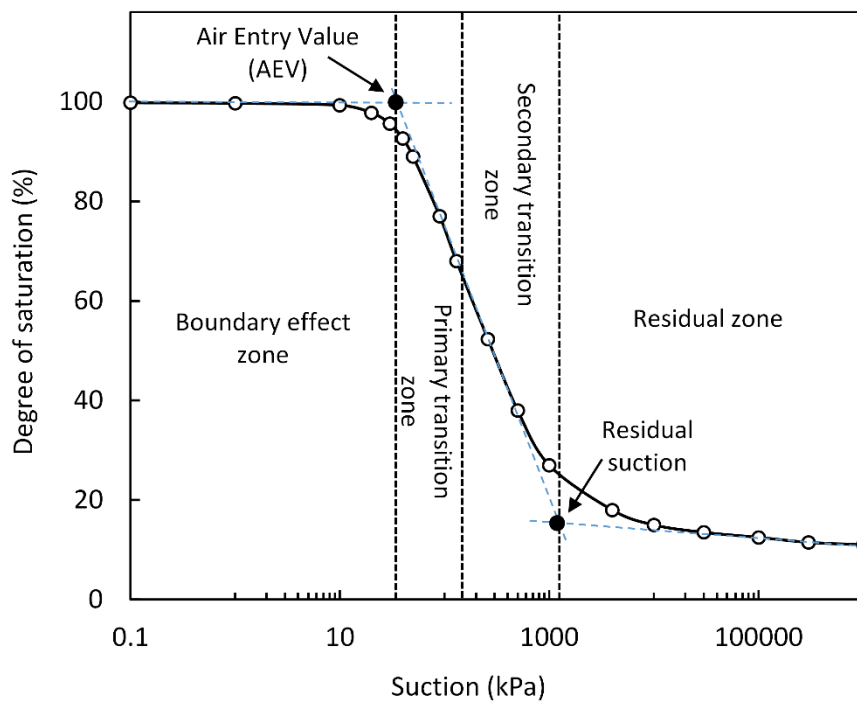
Figure 2.1 Typical soil-water characteristic curve showing different stages (modified from: Vanapalli et al., 1999).

Various methods (pressure plate, Tensiometer, filter paper) have been developed to obtain the SWCC experimentally. However, these methods have their own limitations and weaknesses. Most of these methods are incapable, or have some difficulties, in measuring or inducing high suction values. Therefore, to obtain the entire SWCC, the need for a fitting equation, especially when working with fine-grained soils with high residual suction, is inevitable. For this purpose, different empirical fitting equations have developed (Gardner 1958, Brooks and Corey 1964, Brutsaert 1967, Van Genuchten 1980, and Fredlund and Xing 1994) (Table 2.1). Among them, the Fredlund and Xing's expression is one of the more

acceptable approaches in the literature. In this study, this equation is used to obtain SWCC for the entire range of the suctions.

Table 2.1 Fitting equations for Soil Water Characteristic Curve.

References	Expressions	Fitting parameters	Eq
Gardner (1958)	$\theta(\psi) = \dfrac{\theta_s}{1 + a\psi^n}$	a, n	(2.3)
Brooks and Corey (1964)	$\begin{cases} \theta(\psi) = \theta_s & for\ \psi \leq \psi_{ae} \\ \theta(\psi) = \theta_s(\psi/a)^{-n} & for\ \psi \geq \psi_{ae} \end{cases}$	a, n	(2.4)
Brutsaert (1967)	$\theta(\psi) = \dfrac{\theta_s}{1 + (\psi/a)^n}$	a, n	(2.5)
Van Genuchten (1980)	$\theta(\psi) = \dfrac{\theta_s}{[1 + (a\psi)^n]^m}$	a, m, n	(2.6)
Fredlund and Xing (1994)	$\theta(\psi) = \dfrac{\theta_s}{\{ln[1 + (a\psi)^n]^m\}}$	a, m, n	(2.7)

where:

θ = volumetric water content

θ_s = residual volumetric water content

ψ = matric suction of soil

ψ_{ae} = air entry value

2.2.1 Hydraulic Hysteresis

The soil-water characteristic curve can be obtained in two ways: 1) drying an initially saturated specimen by increasing suction, 2) gradually wetting an initially dry specimen by reducing suction. Previous studies (Haines 1930; Croney 1952; Miller and Miller 1956; Mualem 1984; Fredlund et al. 2012) have demonstrated that the SWCC obtained with drying and wetting path are not identical and for a given suction, and soil has a higher water content in drying path than those in wetting path. This directional dependency of the SWCC is called hysteresis. Figure 2.2 shows hysteresis in a soil-water characteristic curve. To complicate things further, drying or wetting from intermediate suction values results in "scanning curves" that lie in between the virgin drying and virgin wetting curves (see Figure 2.2).
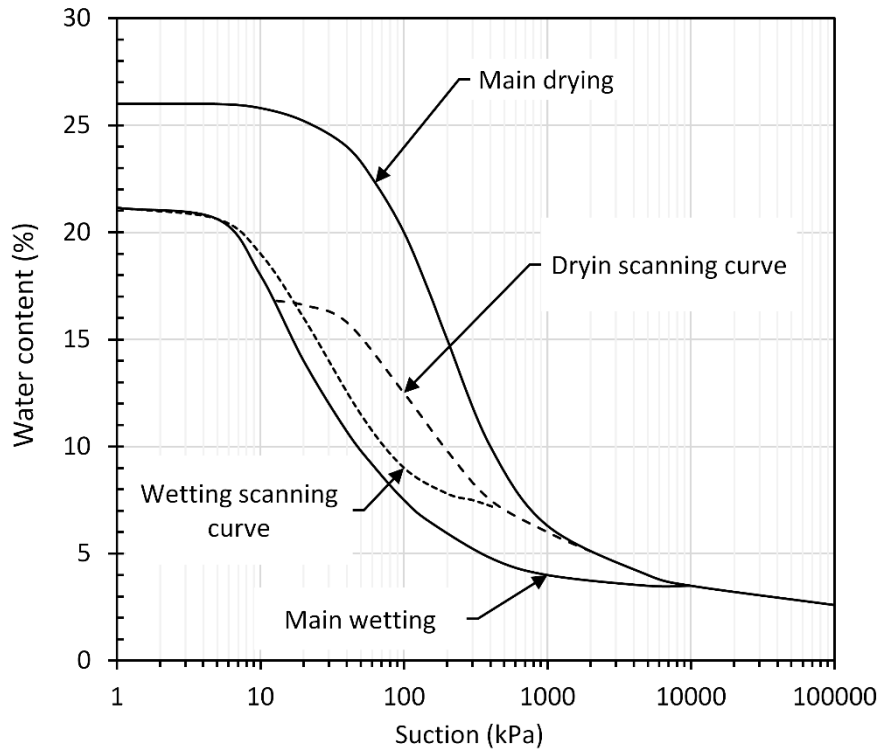
Figure 2.2 Illustration of hydraulic hysteresis in soil-water characteristic curve.

2.3 Stress State Variables

Selection of appropriate stress variables is the first step to describe the mechanical behavior of the soil. There are two common approaches to describe the mechanical behavior (i.e. volume change and the shear strength behaviors) of unsaturated soils: the effective stress and the two independent state variables.

2.3.1.1 Effective Stress Approach

Terzaghi's effective stress principle ($\sigma = \sigma' + u_w$) is formulated based on the two-phase media assumption (either totally saturated or completely dry soil). In the case of the partially saturated soils, total volume of soil mass should be considered as a three-phase system (solids, water and gas). Therefore, the two-phase effective stress principle is not valid for partially saturated soils. Bishop (1959) expanded the effective stress principle to unsaturated soils as below:

$$\sigma' = (\sigma - u_a) - \chi(u_w - u_a) \qquad (2.8)$$

12

Where u_a is the pressure in gas phase (air and vapor), u_w is the pressure in liquid phase (water), and χ is Bishop's effective stress parameter (for saturated condition it is one, and it decreases with the degree of saturation, to zero).

In recent decades, determining Bishop's effective stress parameter, χ, has given rise to a new challenge. To date, most of the modification regarding the effective stress has been related to developing an appropriate procedure to determine the effective stress parameter. Bishop and Donald (1961) and Jennings and Burland (1962) studies, indicated an inconsistent relationship between χ and degree of saturation for different soil types (Figure 2.3).


```
1   COMPACTED BOULDER  CLAY (-2μ·4%)  ] BISHOP
2   COMPACTED SHALE (-2μ·22%)         ] ET AL (1960)
3   BREAHEAD SILT.  BISHOP AND DONALD (1961)
4   SILT (-2μ·3%)
5   SILTY CLAY (-2μ·23%)
6   THEORETICAL   DONALD (1960)
```
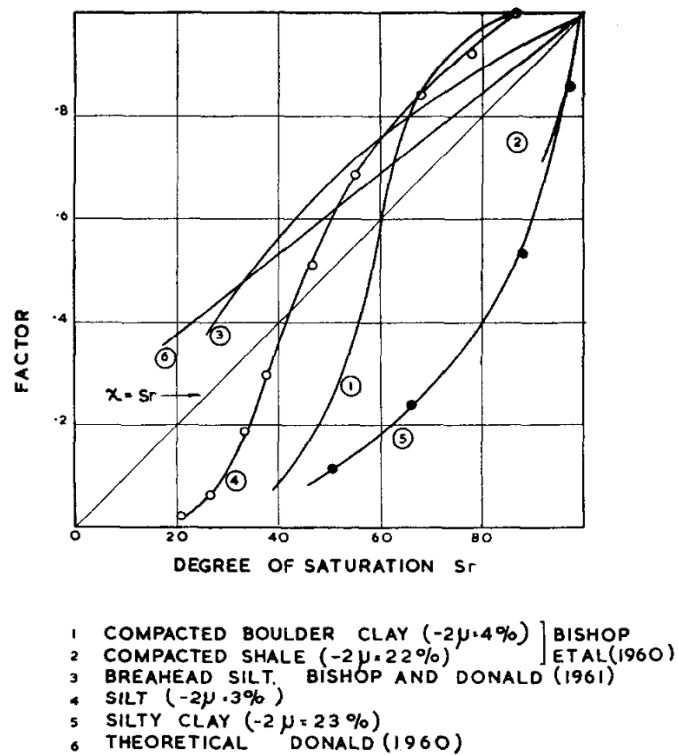
Figure 2.3 Variation of the effective stress parameter (χ), with degree of saturation (Sr) (Jennings and Burland 1962).

2.3.2   Two Independent Stress Variables Approach

The difficulties in using effective stress equation (as mentioned in section 2.3.1.1) to describe the mechanical behavior of unsaturated soil gradually led to adopting the

13

two independent stress state variables. (Bishop and Blight 1963; Matyas and Radhakrishna 1968; Fredlund and Morgenstern 1976)

Fredlund and Morgenstern (1977) proposed two independent stress variables: namely the net normal stress, $(\sigma_n - u_a)$, and matric suction, $(u_a - u_w)$ to describe the state of stress in unsaturated soils.

Formulation of the first elasto-plastic constitutive model for unsaturated soils was due to Josa (1988), Josa et al. (1987), Alonso et al. (1987), Alonso et al. (1990) which is extension of the Modified Cam-Clay (MCC) model to involve matric suction as a separate stress variable to model unsaturated soil behavior. This model, also known as the "Barcelona Basic Model" (BBM), is developed based on the two independent sets of stress state variables. BBM includes three stress parameters (mean net stress P, deviator stress q, and suction s) and two strain parameters (volumetric strain $d\varepsilon_v$ and deviatoric strain $d\varepsilon_d$) to define the critical state framework. The volumetric strain is related to specific volume (v). These parameters in triaxial space can be defined as:

Mean net stress	$p = \dfrac{\sigma_1 + 2\sigma_3}{3} - u_a$	(2.9)
Deviator stress	$q = \sigma_1 - \sigma_3$	(2.10)
Matric suction	$s = u_a - u_w$	(2.11)
Specific volume	$v = 1 + e$	(2.12)

2.4   Constitutive Modelling for Unsaturated Soils

This section explains basis of constitutive modeling, with every explained component exemplified by how it is in the BBM.

In order to model the elasto-plastic response of the soil three essential ingredient need to be defined (Shen & Kushwaha, 1998):

1. Yield surface
2. Strain hardening law
3. Flow rule

In an elasto-plastic material, the total deformation can be decomposed additively into elastic component and plastic component.

$$\varepsilon = \varepsilon^e + \varepsilon^p \tag{2.13}$$

A yield surface in stress-strain space defines a boundary between the elastic and plastic locus. For any stress state within the yield surface the deformation is purely elastic or recoverable.

2.4.1 Yield Surface

2.4.1.1 Elastic Deformation

As long as stress state remains inside the yield surface, variation in net stress and suction results in elastic deformations. In the BBM the elastic variation in specific volume due to net stress (dp) and suction (ds) increment is formulated as below:

$$dv^e = -\kappa \frac{dp}{p} - \kappa_s \frac{ds}{s + p_{atm}} \tag{2.14}$$

where κ elastic constant due to net stress and κ_s elastic constant due to suction. The atmospheric pressure p_{atm} was incorporated to avoid infinite dv^e when suction is zero.

The elastic shear strain due to deviator stress q is given by:

$$d\varepsilon_s^e = \frac{dq}{3G} \tag{2.15}$$

where G is the elastic shear modulus which is assumed to be independent of the suction.

2.4.1.2 Yielding and Plastic Deformation

In BBM, Similar to Cam-Clay model for saturated soil, the virgin compression line for a given constant-suction is assumed to be straight line on a v-lnp plot:

$$v = N(s) - \lambda(s) \ln \frac{p}{p^c} \tag{2.16}$$

where p^c is a reference pressure, N (s) is the specific volume at the reference pressure, and $\lambda(s)$ is the gradient of the compression line. The $\lambda(s)$ and N (s) are both assumed to depend on suction.

The variation of N(s) with suction in BBM is assumed as:

$$N(s) = N(0) - \kappa_s \ln\left(\frac{s + p_{atm}}{p_{atm}}\right) \qquad (2.17)$$

As shown in Figure 2.4, BBM assumes that the $\lambda(s)$ decreases monotonically with increasing suction through the following equation:

$$\lambda(s) = \lambda(0)[(1 - r)\exp(-\beta s) + r] \qquad (2.18)$$

where $\lambda(0)$ is the gradient of the NCL in saturated conditions ($\lambda(s)$ at zero suction), r $= \lambda(s \to \infty) / \lambda(0)$ and β is a soil constant which controls the rate of increase of soil stiffness with matric suction.

The BBM defines these sets of yield loci that bound the elastic behavior.

The BBM involves a Loading–Collapse (LC) yield locus (in the s-p plane), which defines the increases in yield stress due to increasing suction (see Figure 2.4). The combination of Eqs. (2.14), (2.16) and (2.18), allows to define the shape of the Loading-Collapse (LC) yield locus:

$$\left(\frac{p_{0(s)}}{p^c}\right) = \left(\frac{p_0^*}{p^c}\right)^{\frac{\lambda(0)-\kappa}{\lambda(s)-\kappa}} \qquad (2.19)$$

where $p_{0(s)}$ is the yield stress at a given suction and p_0^* is the yield stress for those in saturated condition.

During drying path (increasing suction), additional plastic volumetric strains could be occurred for suction values beyond the previously applied maximum suction. To incorporate this effect, BBM includes a second yield surface, known as the Suction-Increase (SI) yield locus. The BBM assumes that SI has a straight line parallel to the p axis (see Figure 2.4) given by:

$$s = s_0 \qquad (2.20)$$

where s_0 is the current location of the yield surface (i.e. maximum suction experienced by the soil).

The BBM, in parallel with modified Cam-Clay model, assumes an elliptical shape for yield surface in q-p plane (at a constant suction). The yield surface intercepts the p axis in $p_{0(s)}$ and $-\kappa s$. The slope of the critical stress (M) is assumed as a constant (same as the saturated value) and the intercept with q axis is assumed to increase linearly with suction (see Figure 2.4). The critical state lines at given values of suction in q-p plane is given by:

$$q = Mp + M\kappa s \tag{2.21}$$

The elliptical yield surface on a constant-suction cross-section given by:

$$q^2 - M^2(p + \kappa s)\big(p_{0(s)} - p\big) = 0 \tag{2.22}$$

Wheeler and Sivarkumar (1995) found that the model can not predict well the relationship of the critical state value v to p and s. Hence a refinement of the model was suggested to include a non-linear increase of strength with suction and to allow the aspect ratio of the elliptical yield curve to vary with suction so as to capture the critical state values of v at various suctions. On the basis of the data for compacted kaolin, Wheeler and Sivarkumar (1995) defined the CSL for unsaturated soils as follows:

$$q = M(s)p + \mu(s) \tag{2.23}$$

$$v = \Gamma(s) - \phi(s)\ln(\frac{p}{p_{atm}}) \tag{2.24}$$

The parameters M(s), μ(s), Γ(s) and ϕ(s) all varied with suction.

For both the models of Alonso et al. (1990) and Wheeler and Sivarkumar (1995), it was assumed that one axis of the elliptical yield curve is coincident with the p axis.
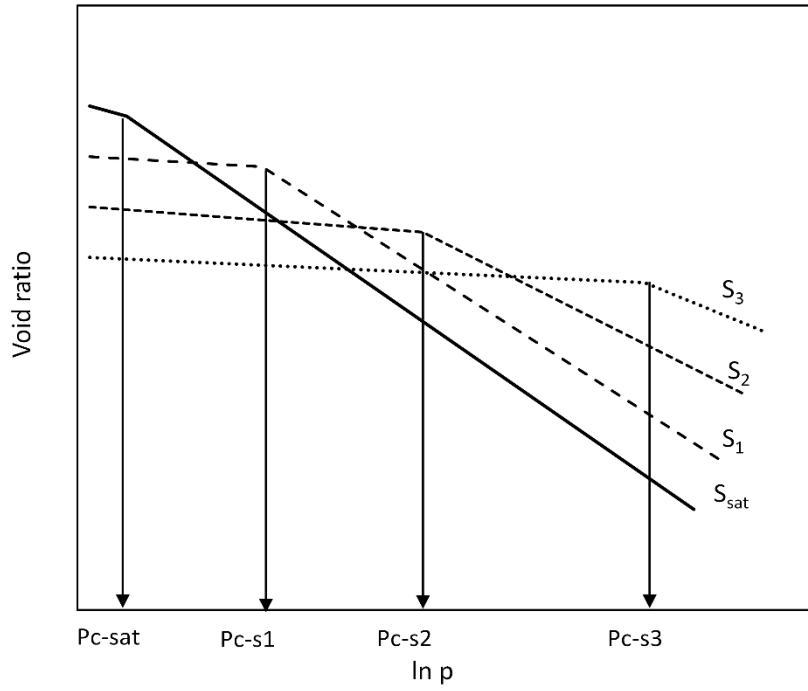
(a)
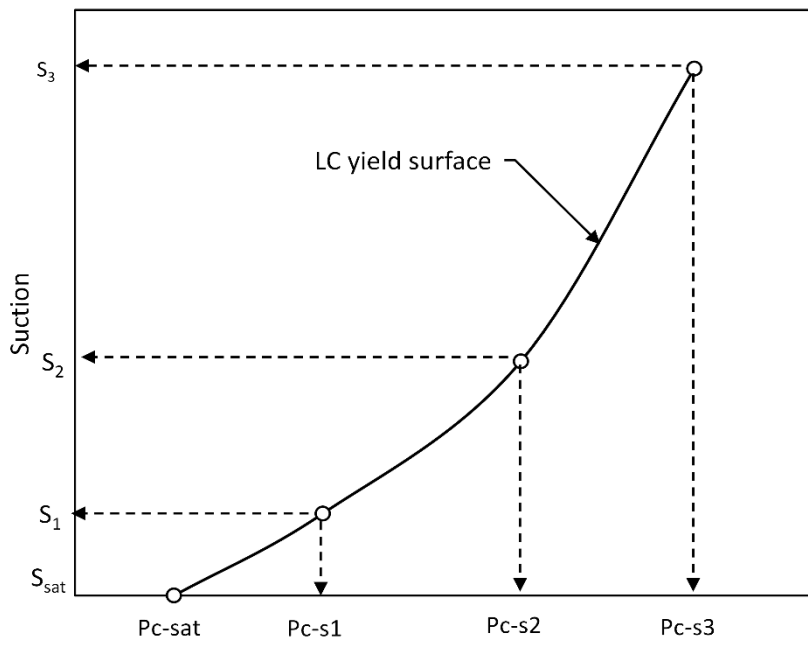
(b)

Figure 2.4 Schematic of Barcelona model formulation in (p: q: s) space
(Alonso et al. 1990).

18
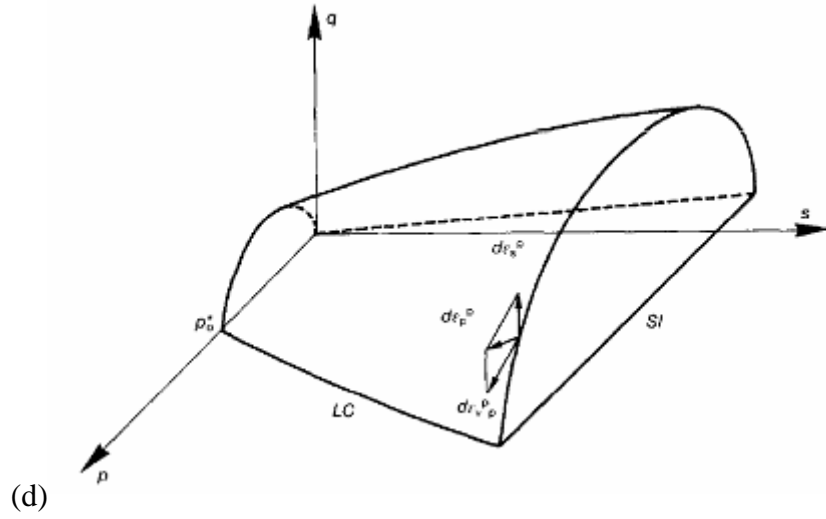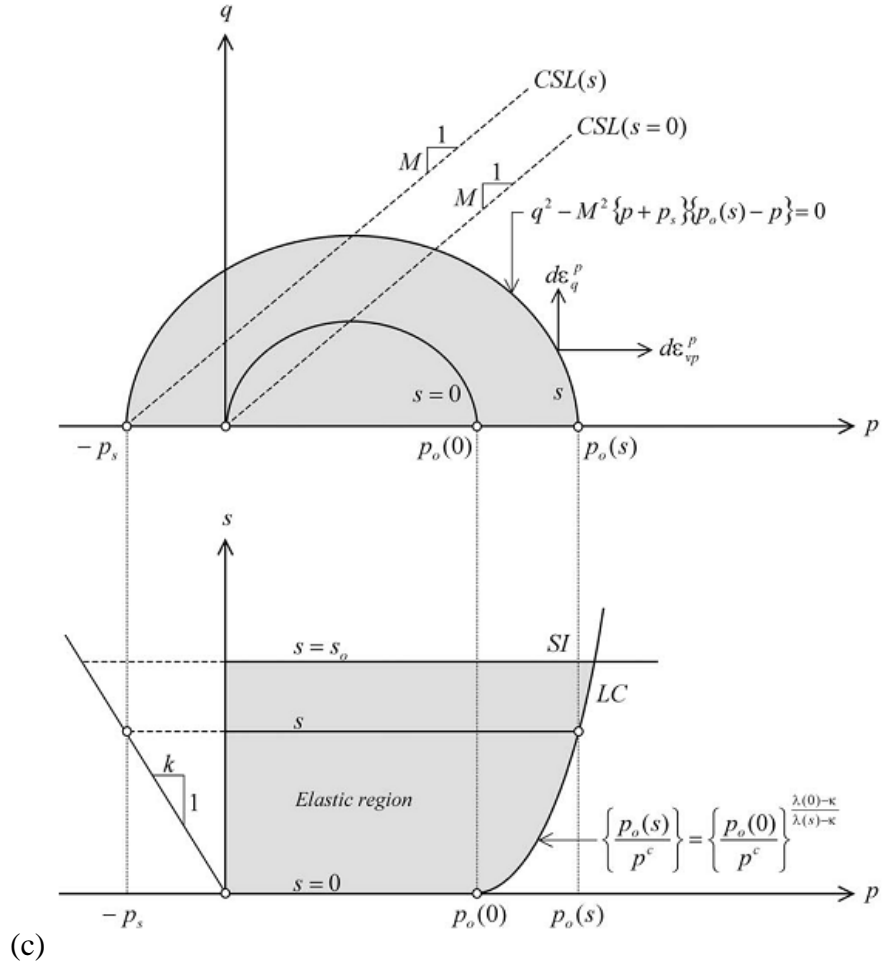
Figure 2.4 continued.

2.5   Viscoelasticity

Behavior of perfectly elastic (Hookean) material with mechanical analogue could simply be modeled as a spring (Figure 2.5) in which the applied stress, σ, (in compression or extension) is proportional to the strain, ε. The constitutive equation may be written as Eq. 2.25. Applying and maintaining a constant stress, σ_0, cause an instantaneous response of spring and unloading cause immediate and completely recovery.

$$\sigma^e = E\varepsilon^e \qquad\qquad (2.25)$$
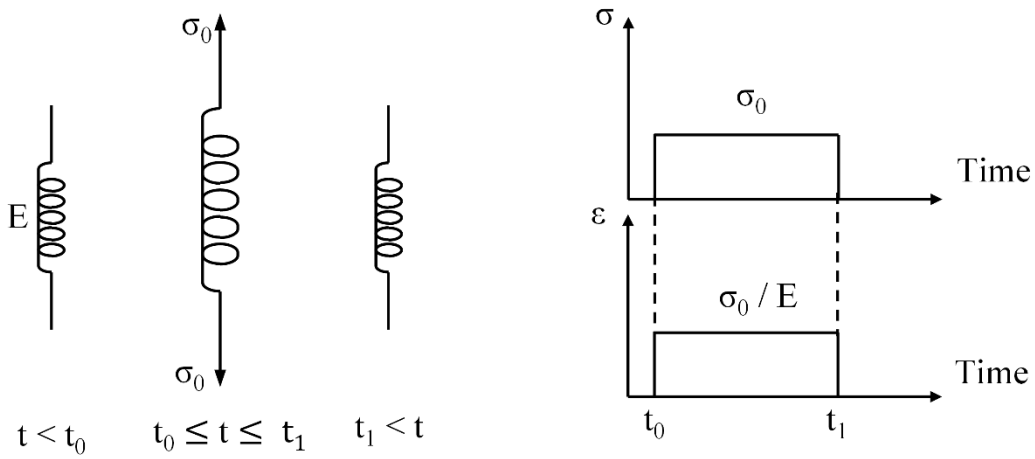
Figure 2.5 Hookean model, linear response of spring to constant stress.

Where E is referred to as the elasticity modulus of the material, and the superscripts e refers to elastic behavior.

For an incompressible and isotropic Newtonian fluid the applied shear stress, is proportional to the rate of deformation (dy/dt) and the relationship may be written as eq. 2,

$$\sigma^v = \eta \frac{d\varepsilon}{dt} = \eta \dot{\varepsilon}^v \qquad\qquad (2.26)$$

Where η is referred to as the viscosity [Pa.s], superscript v stands for viscous behavior and dot denotes the time derivative (i.e. = de/dt).

In literature, viscous behavior is adopted to model with a dashpot. Dashpots (viscous material), as shown in Figure 2.6, behave as a rigid member under immediate loading, and then deform gradually (flows like a liquid). During unloading, recovery does not occur and dashpot remains open or close (depends on loading direction, i.e. compression or extension).
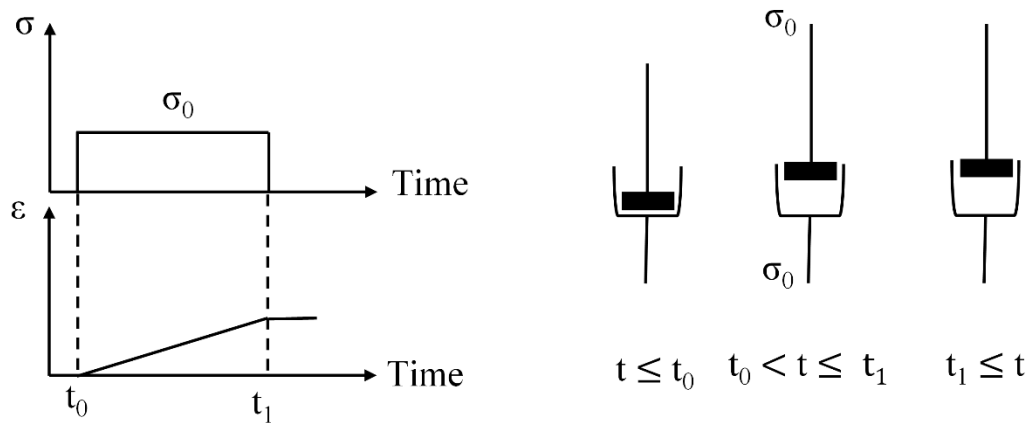
Figure 2.6 Newtonian model, response of linear viscous dashpot to constant stress.

However, to describe the mechanical behavior of most of the materials under different loading condition merely utilizing the spring or dashpots is not sufficient and a specific combination of both spring and dashpots, which gives alternative rheological structures, is required. The materials, which exhibit both elastic and viscous action, are known as viscoelastic material. Time dependent response is a special feature of viscoelastic materials. The time dependency of stress under constant strain is known as relaxation and time dependency of strain to applied constant stress is known as creep. In this material stress is a function of both strain and time.

Maxwell model, a series combination of an elastic spring and dashpot depicted in Figure 2.7, is one of the simplest mechanical models to predict the behavior of viscoelastic materials.

21
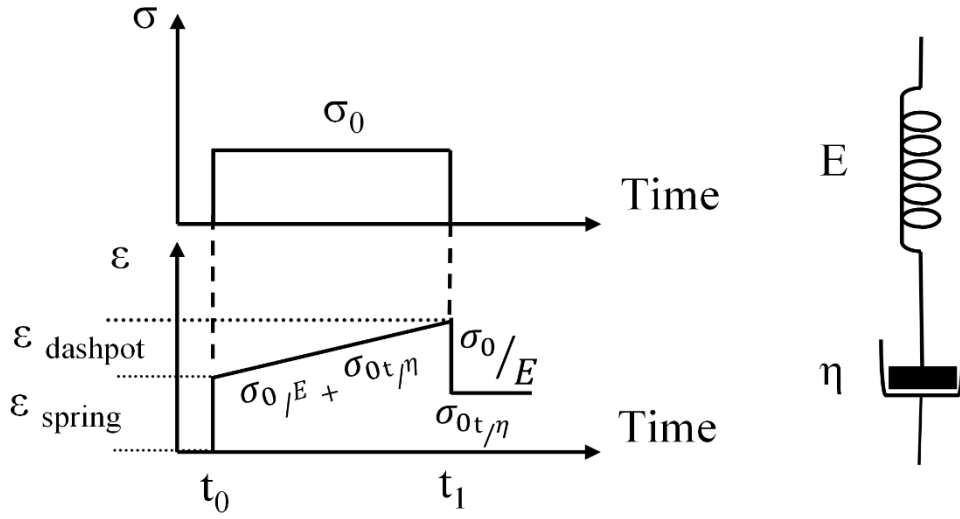
Figure 2.7 The Rheological diagram of the Maxwell model and its stress-strain-time response.

In this model since both elements are arranged in series connection, stress is identical in both elements but strain decomposes additively into instantaneous elastic strain in spring, and creep strain in dashpot. Under a constant stress, the total strain at any time, employing the constitutive relations for both spring and dashpot, calculated from the following equation:

$$\varepsilon(t) = \frac{\sigma}{E} + \frac{\sigma t}{\eta} \quad \forall\, t_0 \leq t \leq t_1 \tag{2.27}$$

Where, t is the elapsed time.

Once the system is unloaded, an instantaneous elastic recovery due to Hookean elastic element is occurs, however, as mentioned, dashpot behave as a rigid member so that there is no recovery of viscous strain. This can be mathematically formulated as following equation:

$$\varepsilon(t) = \frac{\sigma t}{\eta} \quad \forall\, t > t_1 \tag{2.28}$$

22

Despite acceptable behavior of Maxwell model in the case of relaxation, it fails to predict the creep and recovery.

The Kelvin model, shown in Figure 2.8, is another alternative viscoelastic model which is parallel combination of a spring and a dashpot. In this model, strain is identical in both elements, as they are connected in parallel, however, stress decomposes additively to both elements.
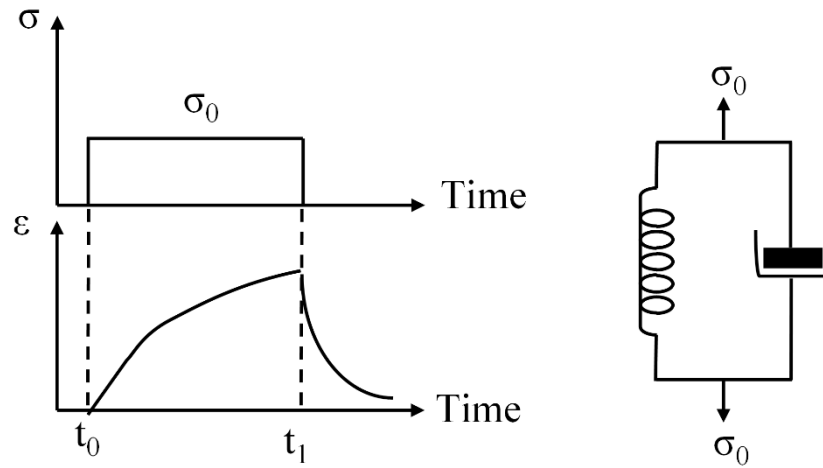
Figure 2.8 The Rheological diagram of the Kelvin model and its stress-strain-time response.

Under constant stress, σ, employing constitutive relation of spring (Eq. 2.25) and dashpot (Eq. 2.26) the total strain calculated by the below expression:

$$\varepsilon(t) = \frac{\sigma}{E}\left(1 - e^{-\frac{Et}{\eta}}\right) \tag{2.29}$$

In contrast to Maxwell model, this model is not suitable to describe the relaxation behavior of the materials.

Despite mathematical simplicity of Kelvin and Maxwell models, these models are inadequate to describe the behavior of most of the real materials. The Maxwell model is adequate to describe stress relaxation however, incapable of describing time-dependent recovery and creep, on the other hand the kelvin model can account for

23

creep and recovery, however, it cannot consider for stress relaxation. Combination of these two simple models in mechanical series, as shown in Figure 2.9, gives an alternative comprehensive viscoelastic model known as Burgers (or four parameter viscoelastic) model introduced by Burgers (1935).

Since Maxwell and Kelvin elements are connected in series, the strain response of this model under constant stress are given by

$$\varepsilon = \varepsilon_{Maxwell} + \varepsilon_{Kelvin} \tag{2.30}$$

Where $\varepsilon_{Maxwell}$ is the strain of the Maxwell element and ε_{Kelvin} is the strain in the kelvin element therefore, the total strain calculated with following equation:

$$\varepsilon_{Burger} = \frac{\sigma}{E_1} + \frac{\sigma t}{\eta_1} + \frac{\sigma}{E_2}\left(1 - e^{-\frac{E_2 t}{\eta_2}}\right) \tag{2.31}$$

Where E_1, E_2 are the elastic moduli and η_1, η_2 are the viscous coefficient of the Maxwell and Kelvin section respectively. The problem is the estimating these unknown parameters based on the experimental data.
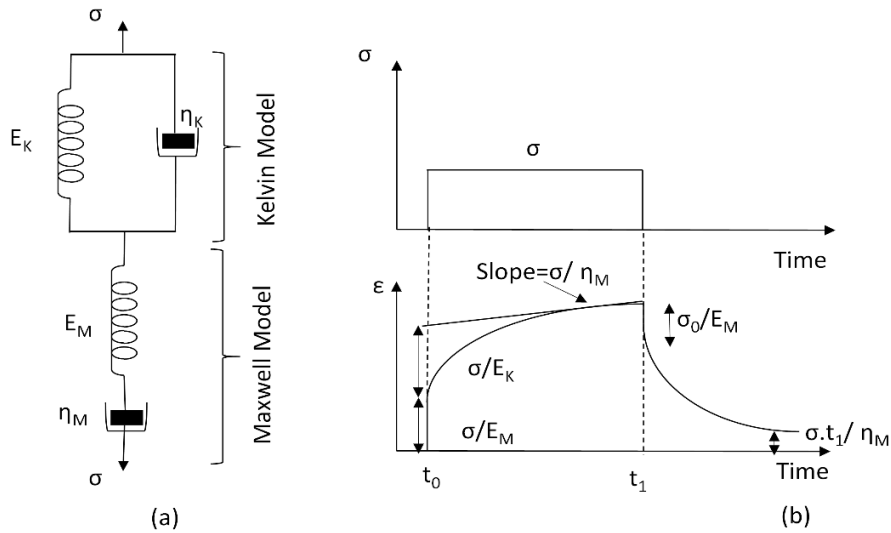
Figure 2.9 The Rheological diagram of the Burger model and its stress-strain-time response.

CHAPTER 3

THEORETICAL APPROACH

In this chapter a comprehensive literature review on shear strength equations for unsaturated soil is presented. An exponential relation is introduced to predict the shear strength of the unsaturated soils. The procedure for the parameter determination of the model is devised. Equation involves three parameters; two of which are effective shear strength parameters (i.e. $\phi´$ and $c´$ can be determined through conventional saturated shear strength tests). The third parameter is ultimate shear strength, c_{max}, introduced in this study, which can be determined through the SWCC.

3.1 Literature Review

Estimating shear strength of a soil element in most of the geotechnical projects is inevitable, no need to emphasize its importance. The shear strength of saturated soils is well defined through the effective stress concept in classical soil mechanics. Coulomb's linear shear-strength equation along with Terzaghi's effective stress principle have been widely used in estimating the shear strength of saturated soils,

$$\tau = c' + \sigma'.tan\phi' \tag{3.1}$$

where τ is the shear strength, c' is a cohesion, and ϕ' is the internal friction angle of the soil sample.

To predict the shear strength of unsaturated soils, different methods have been developed and reported in literature. In general, most of the methods are developed based on Coulomb's shear-strength equation (Eq. 3.1) following the two fundamental approaches of effective stress: the effective stress (Bishop, 1959) and independent stress state variables (Fredlund and Morgenstern, 1977). These methods can be divided into two categories of the prediction and fitting type equations. Prediction

type equations have been developed to predict the shear strength of a soil through easy obtainable parameters (like saturated shear strength parameters) while exempt from performing complex and expensive unsaturated laboratory tests. The fitting type equations are developed to best fit to unsaturated test data. The fitting type equations are not the subject of discussion in this study.

Rewriting the Eq. (3.1) for the Bishop effective stress (Eq. 2.8), the shear strength equation takes the following form:

$$\tau = c' + (\sigma - u_a).tan\phi' - \chi(u_w - u_a).tan\phi' \tag{3.2}$$

In recent decades, determining Bishop's effective stress parameter, χ, has given rise to a new challenge. To date, most of the modification regarding the effective stress is related to developing an appropriate procedure to determine the effective stress parameter. Bishop and Donald (1961) and Jennings and Burland (1962) studies, indicated an inconsistent relationship between χ and degree of saturation for different soil type.

Öberg and Sällfors (1997) used the degree of saturation for χ, and proposed the following equations:

$$\tau = c' + (\sigma - Su_w - (1 - S)u_a)tan\phi' \tag{3.3}$$

or rewriting as:

$$\tau = c' + (\sigma - u_a)tan\varphi' + (u_a - u_w)[S]tan\phi' \tag{3.4}$$

Vanapalli et al. (1996) and Karube et al., (1996) employed the soil-water characteristic curve to define the effective stress parameter, χ. They introduced a linear relationship of degree of saturation (or volumetric water content) as below:

$$\chi = \frac{S - S_r}{100 - S_r} \tag{3.5}$$

or

$$\chi = \frac{\theta - \theta_r}{\theta_s - \theta_r} \tag{3.6}$$

where S and θ are current degree of saturation and the current volumetric water content, S_r and θ_r are the residual degree of saturation and residual volumetric water content and θ_s is the volumetric water content at saturated condition. Inspection of these equations indicate that χ is 1.0 at full saturation and zero at the residual state. For these parameters, the shear strength equation takes the following form:

$$\tau = c' + (\sigma - u_a)tan\varphi' + (u_a - u_w)\left(\frac{S - S_r}{100 - S_r}\right)tan\phi' \tag{3.8}$$

$$\tau = c' + (\sigma - u_a)tan\varphi' + (u_a - u_w)\left(\frac{\theta - \theta_r}{\theta_s - \theta_r}\right)tan\phi' \tag{3.9}$$

Brooks and Corey (1964), proposed the Eq (3.10) to describe the SWCC.

$$\Theta = \left[\frac{(u_a - u_w)_{AE}}{(u_a - u_w)}\right]^f \tag{3.10}$$

Where $(u_a - u_w)_{AE}$ is the air entry value and "f" is the fitting parameter. Fredlund et al. (1995) employed this equation as a shear strength fitting type equation. Therefore, the shear strength equation takes the following form:

$$\tau = c' + (\sigma - u_a)tan\varphi' + (u_a - u_w)\left[\frac{(u_a - u_w)_{AE}}{(u_a - u_w)}\right]^f tan\phi' \tag{3.11}$$

Khalili and Khabbaz (1998) analyzed the shear strength data published in the literature and introduced an empirical relation between the effective stress parameter χ and soil suction. They employed the SWCC to define the air-entry value suction. They assumed the effective stress parameter χ is 1.0 for the suctions less than air entry value. There are similarities between this expression and the equation proposed

by Brooks and Corey (1964), and just the fitting parameter of the *f* is replaced with -0.55. Therefore, the shear strength equation takes the following form,

$$\chi = \left[\frac{(u_a - u_w)}{(u_a - u_w)_{AE}}\right]^{-0.55} \tag{3.12}$$

$$\tau = c' + (\sigma - u_a)tan\phi' + (u_a - u_w)\left[\frac{(u_a - u_w)}{(u_a - u_w)_{AE}}\right]^{-0.55}.tan\phi' \tag{3.13}$$

Bao et al. (1998) proposed a relation (Eq. 3.14) for the effective stress parameter that involves the air entry value and residual suction value, in log-scale.

$$\zeta = \chi = \frac{log(u_a - u_w)_r - log(u_a - u_w)}{log(u_a - u_w)_r - log(u_a - u_w)_{AE}} \tag{3.14}$$

Therefore, the shear strength equation takes the following form:

$$\tau = c' + (\sigma - u_a)tan\phi' + (u_a - u_w)\frac{log(u_a - u_w)_r - log(u_a - u_w)}{log(u_a - u_w)_r - log(u_a - u_w)_{AE}}.tan\phi' \tag{3.15}$$

where $(u_a - u_w)_r$ is the residual suction.

Vanapalli et al. (1996) proposed a fitting type equation involving normalized water content (Θ) with a fitting parameter κ:

$$\Theta = \frac{\theta_w}{\theta_s} \tag{3.16}$$

where θ_w is the volumetric water content at given matric suction, and θ_s is the volumetric water content in saturated condition.

$$\tau = c' + (\sigma - u_a)tan\phi' + (u_a - u_w)(\Theta)^\kappa tan\phi' \tag{3.17}$$

Vanapalli and Fredlund (2000) and Garven and Vanapalli (2006) proposed correlation between fitting parameter κ, and the plasticity index given in Eq 3.18 and 3.19, respectively:

$$\kappa = -0.008.\, I_p{}^2 + 0.0801.\, I_p + 1 \qquad (3.18)$$

$$\kappa = -0.0016.\, I_p{}^2 + 0.0975.\, I_p + 1 \qquad (3.19)$$

The alternative for effective stress approach (Eq 3.2) is using the independent stress variable concept which was introduced by Fredlund and Morgenstern (1977):

$$\tau = c' + (\sigma - u_a).\tan\phi' - (u_w - u_a).\tan\phi^b \qquad (3.20)$$

where ϕ^b is the shear strength contribution due to suction. The general shape of the equation is similar to Eq (3.2) where the effective stress parameter could be explained as below:

$$\tan\phi^b = \chi \tan \phi$$

or $\qquad\qquad\qquad\qquad\qquad\qquad\qquad\qquad\qquad\qquad (3.21)$

$$\chi = \tan\phi^b / \tan \phi$$

Therefore, a non-constant value could be expected for the ϕ^b, which has been confirmed experimentally (Gan et al. 1988; Escario and Juca 1989; Oloo and Fredlund 1996; Vanapalli et al. 1996).

Tekinsoy et al. (2004) introduced an empirical relation relating the shear strength equation to SWCC through air entry value.

$$\tau = c' + (\sigma - u_a).\tan\phi' + ((u_a - u_w)_{AE} + P_{atm})ln\left[\frac{(u_a - u_w) + P_{atm}}{P_{atm}}\right]\tan\phi' \quad (3.22)$$

where P_{atm} is the atmospheric pressure.

Not that all of these equations suggest that suction has no influence over the ϕ', and the contribution of suction is an increase in cohesion (Figure 3.1), generally called apparent cohesion ca (or capillary cohesion c˝ (Lu and Likos 2004)).

$$\tau_{ff} = c + (\sigma_f - u_a)_f \tan \phi'$$

or

$$\tau_{ff} = c' + (u_a - u_w)_f \tan \phi^b + (\sigma_f - u_a)_f \tan \phi'$$
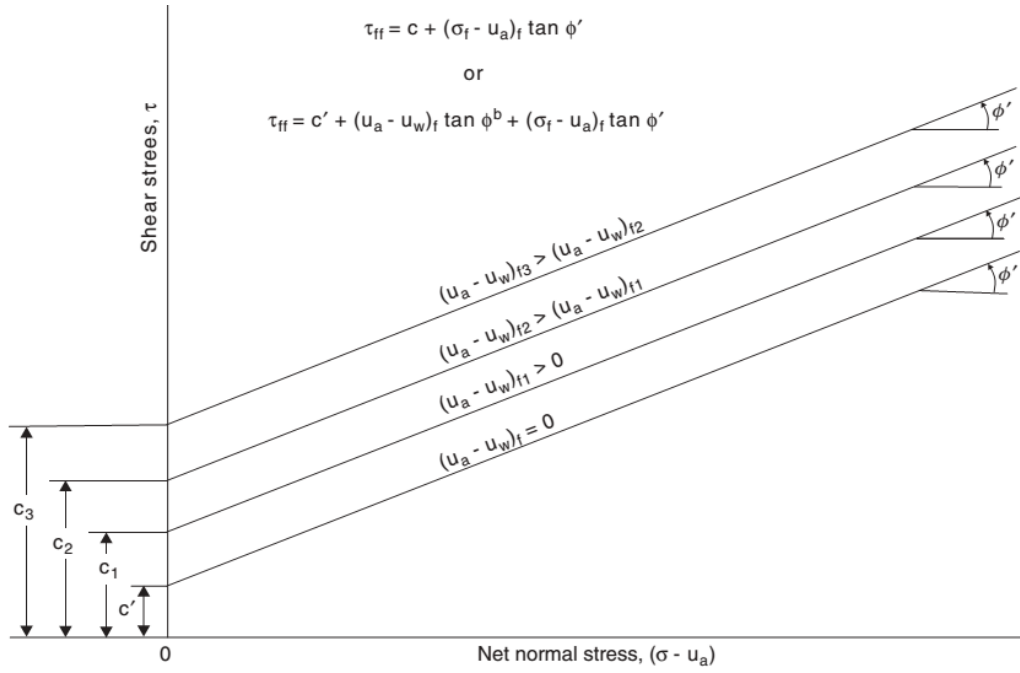
Figure 3.1 Projections of failure envelopes for different values of matric suctions (adopted from Fredlund et al. 2012).

Table 3.1 summarizes the shear strength equations that were reviewed.

In this study an exponential equation is introduced to predict the shear strength of the unsaturated soil. Equation involves three constant parameters. Two of which are effective shear strength parameters (i.e. ϕ' and c´ can be determined through conventional saturated shear strength tests). The third parameter is ultimate shear strength, c''_{max}, introduced in this study, which can be determined through SWCC. A series of suction-controlled triaxial tests performed to verify the proposed equation. In addition, validity of the equation is investigated (see chapter 9) regarding shear strength test results of five soil published in the literature and compared with predicted values of equations summarized in Table 3.1.

Table 3.1 Summary of the equations for shear strength of unsaturated soil.

Reference	Shear strength equations
Oberg and Sallfors (1995 and 1997)	$c'' = (u_a - u_w)[S]\tan\varphi'$
Vanapalli et al., (1996) and Karube et al., 1996	$c'' = (u_a - u_w)\left(\dfrac{S - S_r}{100 - S_r}\right)\tan\varphi'$ or $c'' = (u_a - u_w)\left(\dfrac{\theta - \theta_r}{\theta_s - \theta_r}\right)\tan\varphi'$
Khalili and Khabbaz (1998)	$c'' = (u_a - u_w)\left[\dfrac{(u_a - u_w)}{(u_a - u_w)_{AE}}\right]^{-0.55}.\tan\varphi'$
Bao et al. (1998)	$c'' = (u_a - u_w).\left(\dfrac{log(u_a - u_w)_r - log(u_a - u_w)}{log(u_a - u_w)_r - log(u_a - u_w)_b}\right).\tan\varphi'$
Garven and Vanapalli (2006)	$c'' = (u_a - u_w)(\varTheta)^{\kappa}\tan\varphi'$ $\kappa = -0.0016.I_p{}^2 + 0.0975.I_p + 1$
Tekinsoy et al. (2004)	$c'' = ((u_a - u_w)_{AE} + P_{atm})\, ln\left[\dfrac{(u_a - u_w) + P_{atm}}{P_{atm}}\right]\tan\phi'$

3.2 Introduced Equation

As shown in Figure 3.2 (a) and (b), the shear strength of a soil increases at a decreasing rate toward an asymptotic value, c''_{max}, as suction tends to residual value. The c''_{max} is the maximum apparent cohesion that could be achieved due to suction. In this study, the non-linear variation of the shear strength (i.e. apparent cohesion) with suction is formulated with an exponential equation. The general form of the introduced equation is as below:

$$\tau = c' + (\sigma - u_a).\tan\phi' + c''_{max} \times (1 - exp^{(-\psi\times\,\tan\phi')/(c''_{max})}) \qquad (3.23)$$

where

$$c'' = c''_{max} \times (1 - exp^{(-\psi\times\,\tan\phi')/(c''_{max})}) \qquad (3.24)$$

where c´´ is the apparent cohesion, ϕ' is the effective internal friction angle, c´ is the effective cohesion, and ψ is the current matric suction (u_a-u_w). This equation involves

three constant parameters to be evaluated. The first two parameters (i.e. ϕ' and c´) can be determined through conventional saturated shear strength tests (like direct shear and triaxial tests). The maximum apparent cohesion, c''_{max} , could be obtained by performing suction-controlled shear strength tests on specimens at high suction values. However, the long duration and complexity of the unsaturated soil testing prods towards using indirect estimation procedures. Additionally, when axis translation technique is applied, the maximum suction is limited to the AEV of the ceramic. Low hydraulic conductivity in ceramics with high AEV (1500 kPa), and the issue of air-diffusion at high values of air pressure make ceramics with low AEV (i.e. $\leq$ 500-kPa) preferable in unsaturated soil testing. Therefore, measuring the ultimate shear strength of the specimen at high suction (residual values), which matters most in fine soils, will be problematic. A graphical procedure is introduced to estimate the maximum apparent cohesion, c''_{max} , through soil water characteristic curve (SWCC). As shown in Figure 3.2, if shear strength were to be increased with suction at its initial rate (i.e. $\psi \times tan\phi'$), it would intersect the asymptotic value, i.e. c''_{max} , at suction ψ_t , called with the transition value in this study. Therefore, if the transition value was known, the c''_{max} , could be estimated as follow:

$$c''_{max} = (tan\phi' \times \psi_t) \tag{3.24}$$

Therefore, the object is determining the transition value, ψ_t, from the SWCC. The transition value is defined as the onset of the secondary transition zone of the SWCC beyond the air entry value. A graphical procedure were adopted to estimate ψ_t. First, for SWCC, a point, similar to yield point in consolidation tests, was identified using Casagrande's graphical construction procedure (this is demonstrated in Figure 3.3 for SWCC related to Madrid clay sand (Escario and Juca 1989). First, as shown in Figure 3.4 (a) and (b) (SWCC related to Madrid clay sand, Escario and Juca, 1989), for suctions beyond the air entry value, the SWCC is plotted in arithmetic scale (instead of semi-logarithmic scale). By visual observation, the initial linear portion of the curve is identified and extended. The transition value, ψ_t , is a point where the SWCC deviates from the straight-line. In the example, the transition value, ψ_t , of the related soil is determined to be 150 kPa.

By determining the transition value in this way, ψ_t, the c''_{max} can be determined through Eq (3.24), and finally the shear strength can be estimated with Eq (3.23).

(a)

(b)
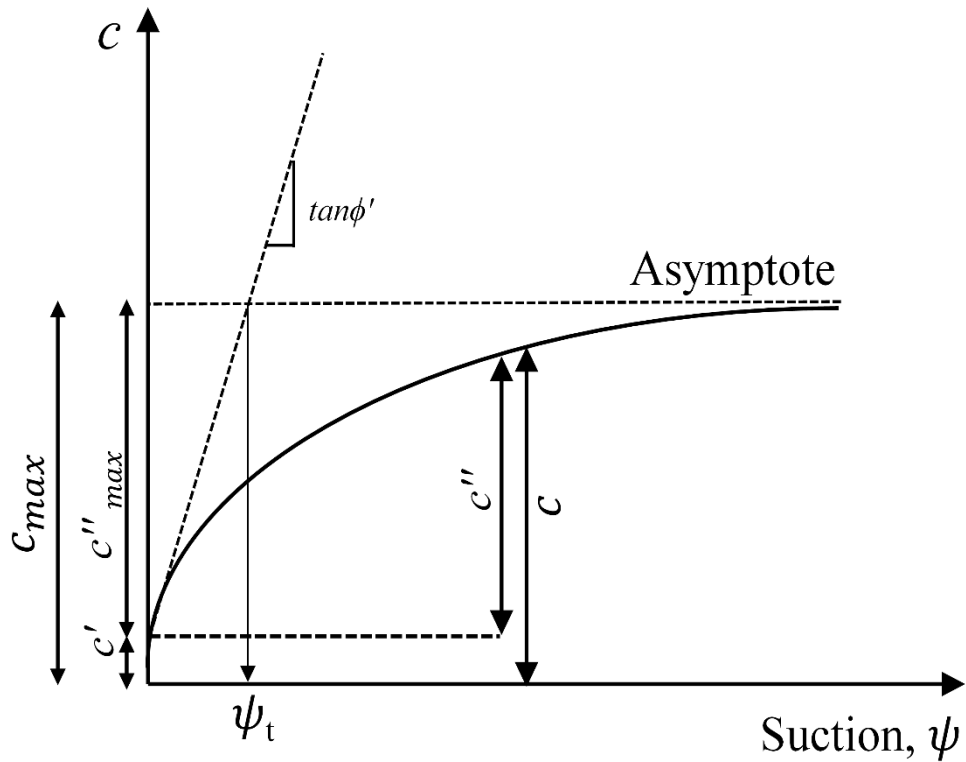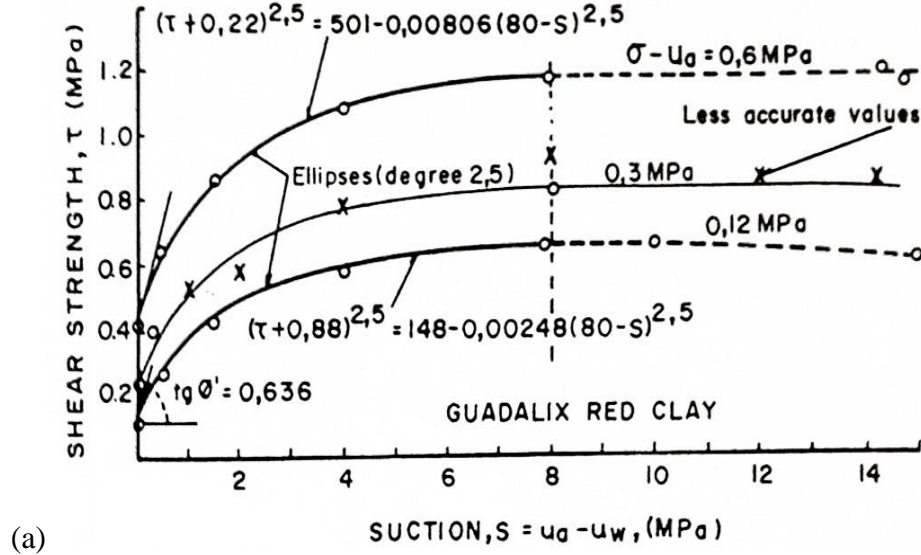
Figure 3.2 (a) Non-liner variation of the shear strength with suction (Escario and Juca 1989) (b) position of the transition value and c_{max}.
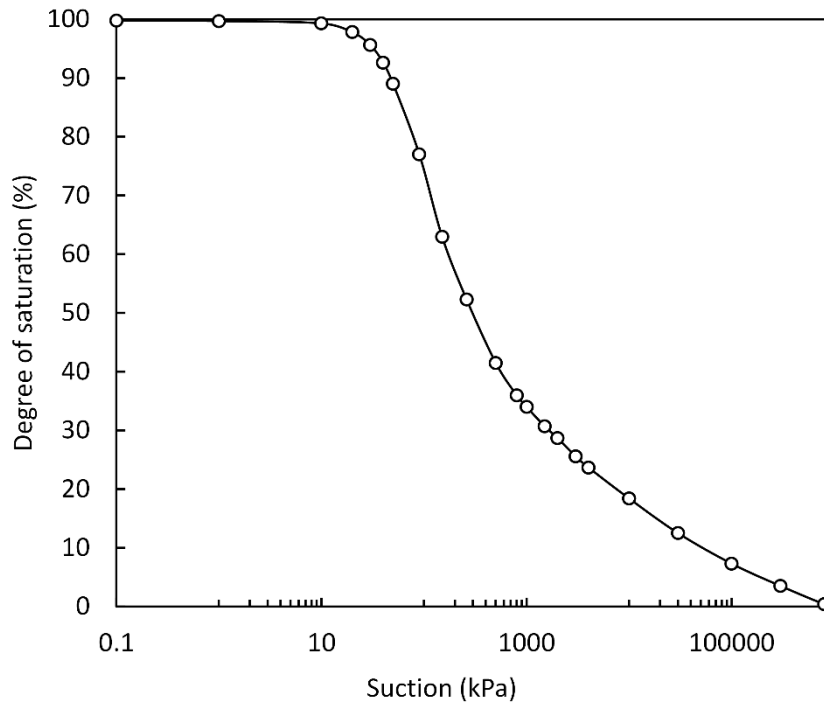
Figure 3.3 Determination of the yield suction in SWCC (Madrid clay sand adopted from Escario and Juca (1989).
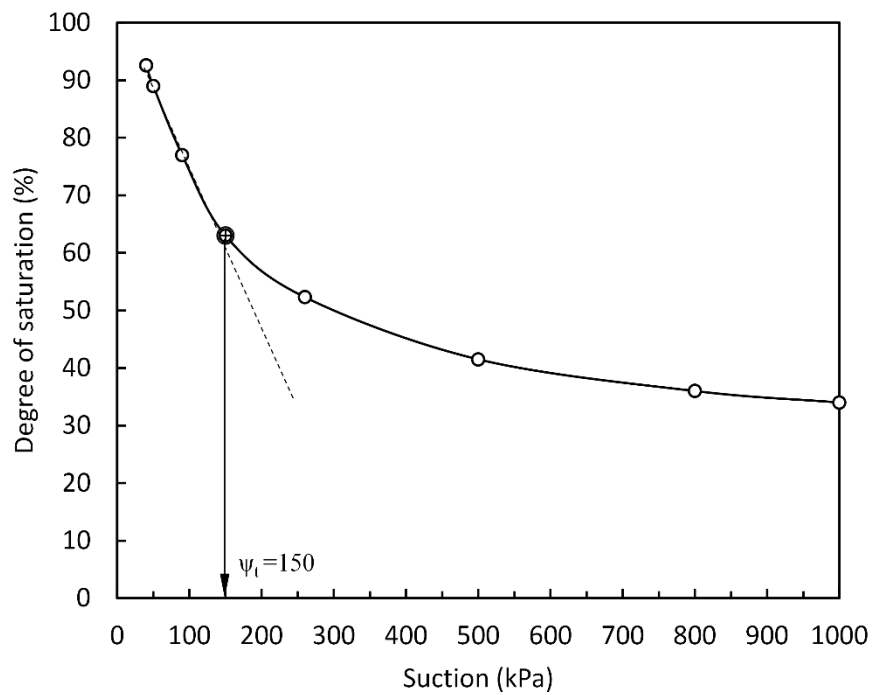
Figure 3.4 SWCC in arithmetic scale and graphical representation of transition value, ψ_t.

CHAPTER 4

EQUIPMENT DEVELOPMENT AND TECHNIQUES

4.1 Introduction

Testing unsaturated soils is much more sophisticated than at of saturated soils. Non-standard equipment and procedures are required for testing unsaturated specimens. Therefore, the conventional techniques used for saturated soils are not directly applicable to unsaturated soil testing, and require some modification of the apparatus.

Within this project, specialized components for these purposes were developed onto the triaxial test setup, and test procedures are modified accordingly. Soil suction is controlled and measured by axis translation. With these modifications the test setup is able to measure the soil behavior in both saturated and unsaturated condition under monotonic loading.

In this study, a conventional triaxial setup is modified to perform unsaturated soil tests. For this purpose, a new triaxial base with new features was designed and built. The entire testing setup employed to perform unsaturated soil shear strength testing and to obtain the SWCC is shown in Figure 4.1. The testing setup involves: a load frame, triaxial cell, cell and sample pressure volume actuators (PVA), air pressure control system, diffused air volume indicator (DAVI) and data logging system.

Axis translation technique is employed to control and induce the desired values of suction. The double drainage (top and bottom) is used for reducing the test duration.

Image processing, independent measurement of air and water volume change, inner cell and single cell fluid measurement methods were examined to measure the volume change of the unsaturated soil specimens. Each method has own advantages and

limitations in measuring the volume change of the unsaturated soils. Ultimately, measuring the variation of single cell fluid volume method was adopted to measure the total volume change of the unsaturated soil specimen. Each of these methods is discussed in detail in the chapter 5.

To correct the amount of the water volume change due to air diffusion, a diffused air volume indicator (DAVI) system was developed according to (Fredlund 1975). In this way flushing of the diffused air in regular intervals, become possible.
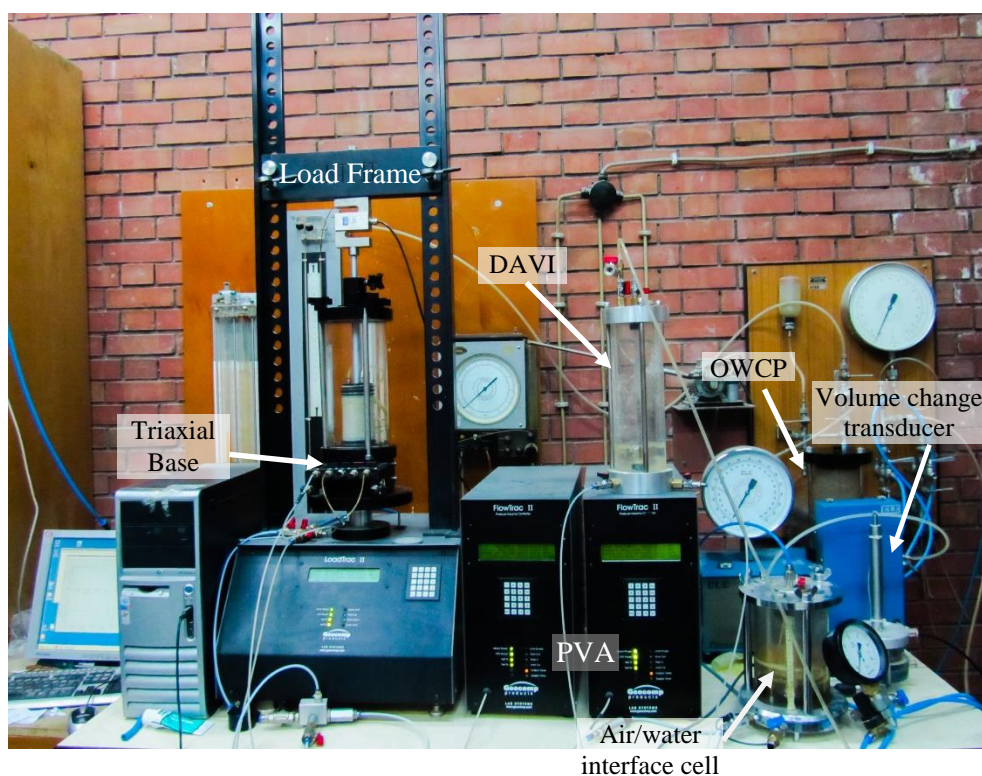
Figure 4.1 General layout of modified triaxial setup for unsaturated soil testing.

4.2   Triaxial Testing Systems

4.2.1   Cell and Sample Pressure-Volume Actuator (PVA)

Two FlowTrac-II units, manufactured by Geocomp, are employed to control and measure the cell pressure, pore water pressure and the volume change measurement.

FlowTrac-II unit includes a flow pump, a pressure sensor and a control board. The flow pump involves a high speed, micro stepper motor to regulate the pressure and volume. FlowTrac-II is capable of maintaining either a constant pressure or volume, ramping up the pressure with a constant rate to a desired value. As shown in Figure 4.2 the volume change is related to stepper motor movement multiplied by area of the piston. Capability of the FlowTrac-II in maintaining a given pressure is within 0.35 kPa and monitoring volume changes within 0.001 cc (Geocomp 2010).
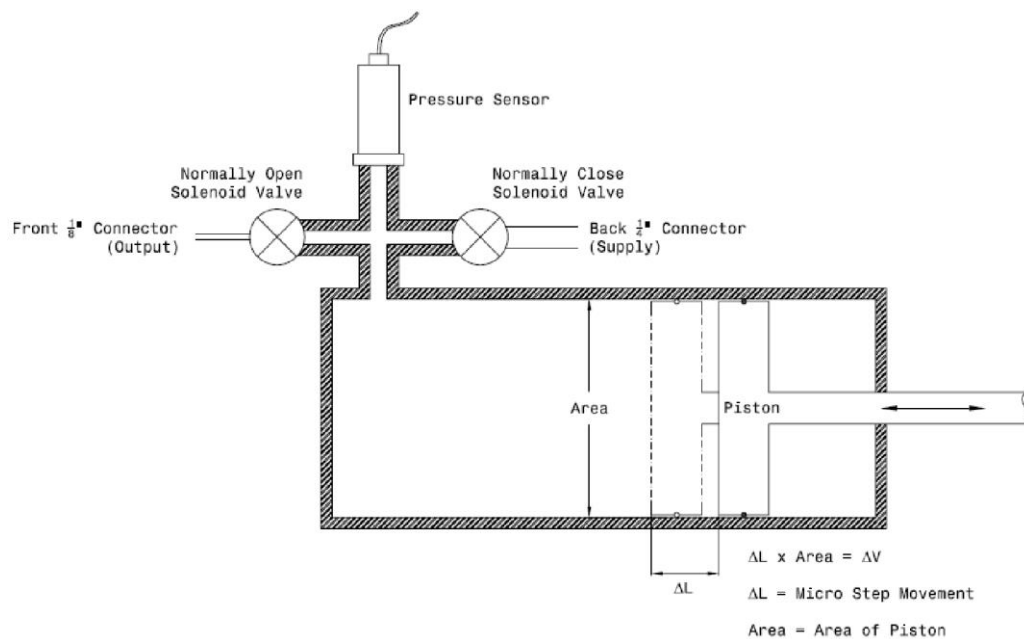
Figure 4.2 Schematic layout of a FlowTrac-II Unit (Geocomp 2010).

4.2.2 Load Frame

The unit is capable of performing both stress and strain controlled tests. The load frame includes a LVDT and load cell to measure the displacement and the applied force.

4.3 Modifications of Triaxial System for Suction Control

One of the main challenges when testing unsaturated soils is applying soil suction, which can cause cavitation in the measurement system. This can be prevented by axis translation technique (Hilf 1956). This represents replacing conventional porous

stone with a high air entry (HAE) ceramic disk at the bottom pedestal. In this way, independent control of pore-water (with HAE ceramic disk at the bottom pedestal) and pore-air pressures (with coarse porous stone at the top cap) is applicable (Bishop and Donald 1961; Ho and Fredlund 1982; Rampino et al. 1999).

In this configuration the drainage length is equal to the length of the specimen.

In recent years, double-drainage systems have been used for triaxial testing of unsaturated soils (Romero et al. 1997; Sharma 1998).

In this study, axis translation technique with double drainage (to reduce the length of the drainage to half and therefore to reduce the testing time) is employed to control and induce soil suction in triaxial testing of unsaturated soils.

For this purpose, a triaxial base, top cap and pedestal with new features were developed (see Figure 4.3 and Figure 4.4).

The pedestal and top cap include a peripheral annular coarse porous metal alloy (for pore air pressure) and HAE ceramic at center (for pore water pressure). The details of new pedestal and top cap is shown in Figure 4.5.

To flush diffused air bubbles and allow for an adequate amount of water in contact with the ceramic, two drainage holes (water inlet and outlet) are connected by a groove that meanders under the ceramic seat in both pedestal and top cap.

Ceramics with HAE value of 5-bar is used in this study. Epoxy-based adhesive is utilized to seal the HAE ceramic into a recess of the top cap and pedestal. In this way, the pore-air cannot find any way to the cavities the system.

Therefore, the new modified triaxial system is capable of obtaining SWCC and running isotropic compression tests under different suction and net confining stress. In addition, by using the new modified triaxial setup, performing consolidated drained (constant suction, CD) and constant water content (CW) tests are possible. All the procedure in this setup is automated except applying and controlling the air pressure.
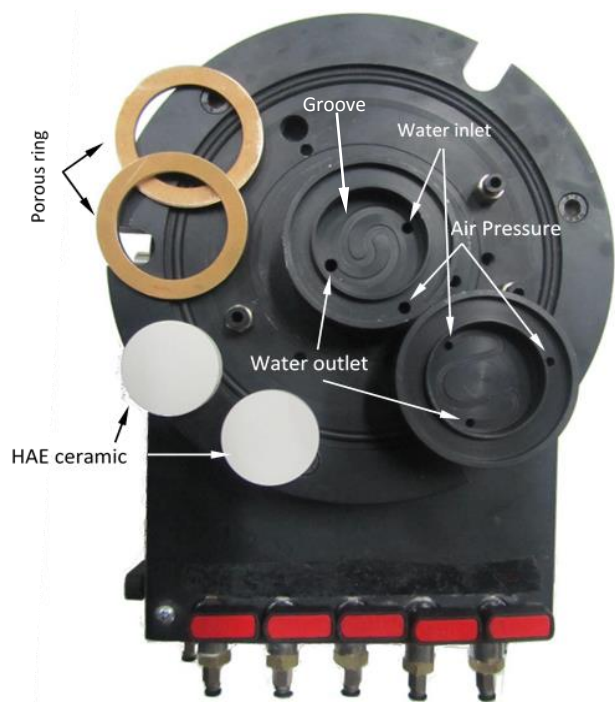
Figure 4.3 New triaxial base with top-cap and pedestal.
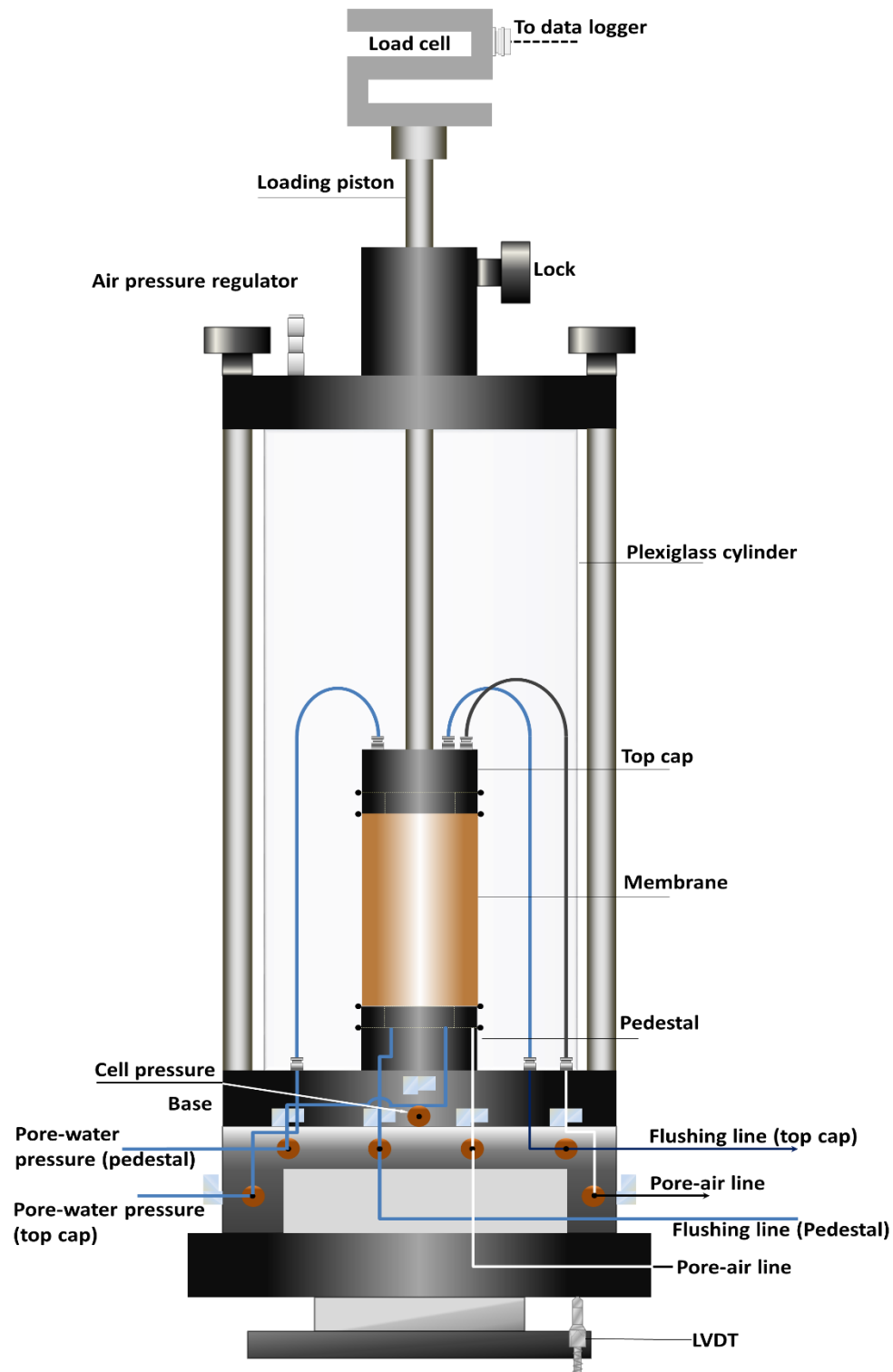
Figure 4.4 Schematic of triaxial cell.
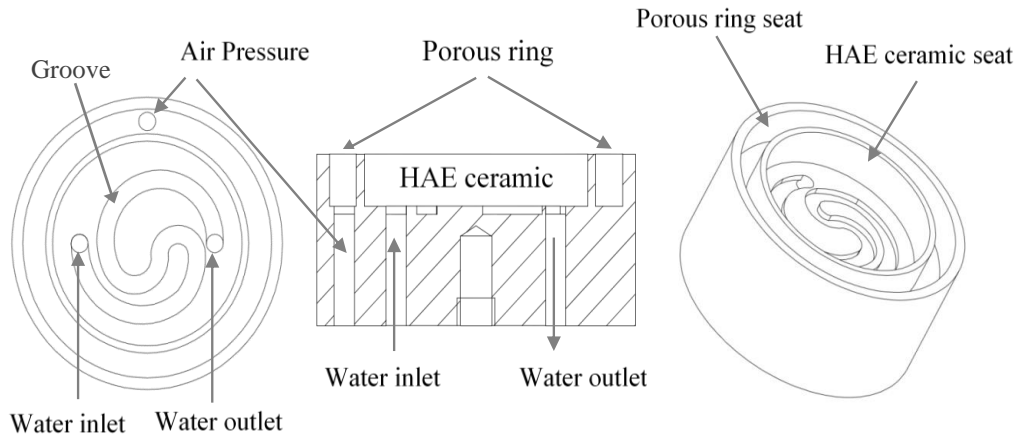
Figure 4.5 Schematic design of top-cap and pedestal.

4.3.1   Pore-Air Pressure Control and Measurement

Pore-air pressure was initially controlled by a pressure regulator supplied by a compressor. However, air pressure fluctuation was observed during preliminary tests. Different regulators were tried, but none had the sufficient precision. To solve this problem, a new pore-air pressure control system was designed.

A schematic layout of the pore-air pressure control system is shown in Figure 4.6. This arrangement includes an oil-water constant pressure system (OWCP) connected to an air/water interface cell. The desired values of air pressure is achieved by a pressure regulator supplied by a compressor. Then, the OWCP is used to maintain the air-pressure constant. A pressure transducer is placed between the triaxial base and air/water interface cell and connected to the data logger system (see section 4.3.4), to monitor the applied pressure.
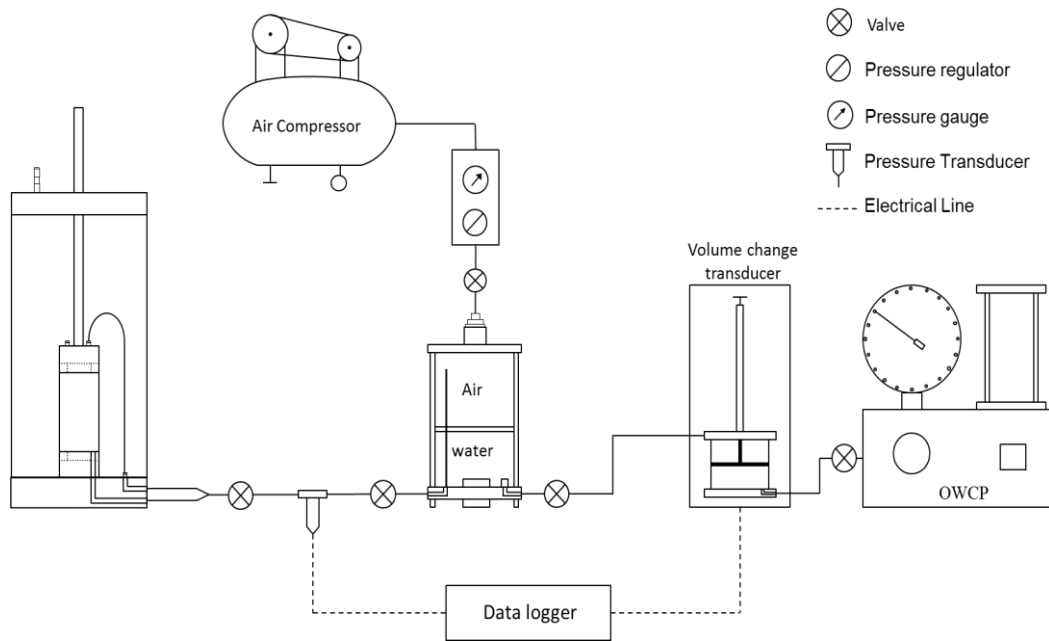
Figure 4.6 schematic layout of the pore-air control system.

4.3.2 Pore-water Pressure and Volume Control and Measurement

As mentioned in section 4.2, a FlowTrac-II unit is employed to monitor pore-water pressure and volume changes. Figure 4.7 shows schematic layout of the pore-water pressure-volume control system. To flush the diffused air, a diffused air volume indicator is developed and added to the system. The detail procedure of the DAVI and flushing system is explained in section 4.3.3.
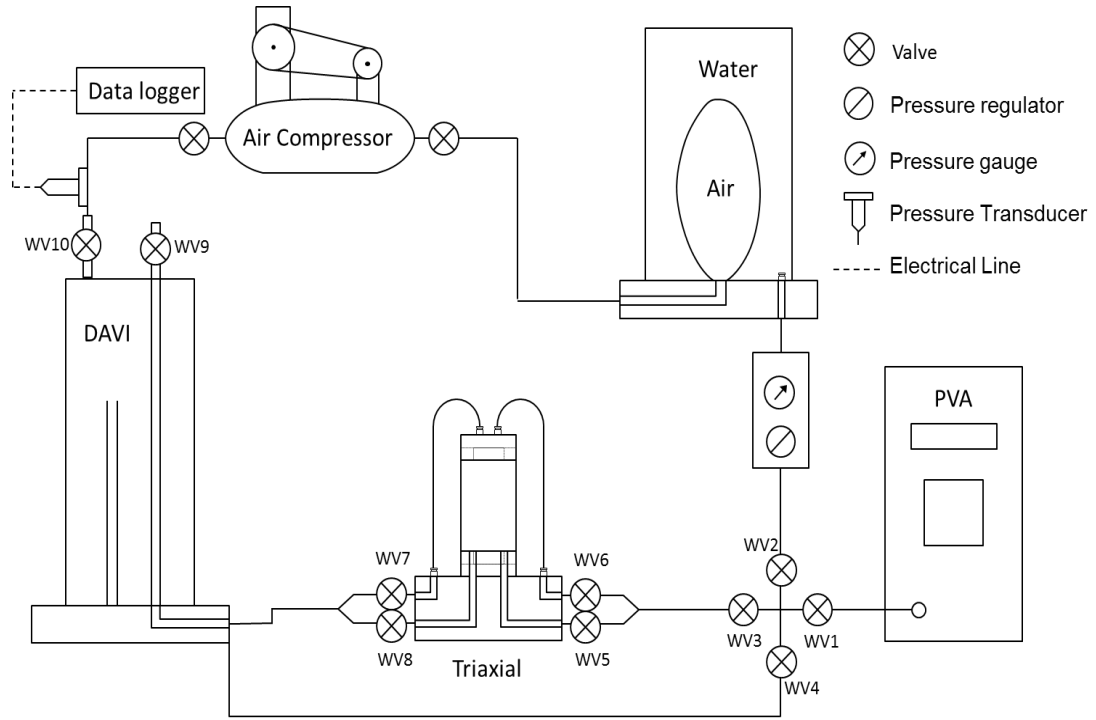
Figure 4.7 Schematic layout of the pore-water control system.

4.3.3 Flushing system

Theoretically, as long as HAE ceramic is in saturated condition and the applied suction is less than the AEV, air cannot pass through the pores of the ceramic. However, dissolved air in water can diffuse through the ceramic and accumulate beneath the ceramic. Diffused air bubbles cause misinterpretation of the applied pressure, and water volume change measurements. Therefore, the air bubbles should be flushed out, and its volume should be measured regularly to correct the water volume change measurements.

Fredlund (1975) developed diffused air volume indicator (DAVI) to measure the volume of diffused air through the HAE ceramic independently.

In this study, a diffused air volume indicator (DAVI) was developed, following Fredlund (1975), to flush and measure the volume of the diffused air. Figure 4.8 shows the schematic layout of the developed DAVI.

43

DAVI includes a graded burette (filled with water) and an exit tube (see Figure 4.8). The exit tube provides a constant head in the burette. There are two vent on top of the DAVI. The first one connected to the burette and opens only when filling the burette. The pressure inside the DAVI (burette and exit tube) can be controlled through air compressor connected to second vent on top of the DAVI.

Two vents are also located in the bottom of the DAVI. As shown in the Figure 4.8, one is used for daring the water inside the DAVI. Another vent is connected to the triaxial base (beneath the ceramic in the top cap and pedestal) to flush the accumulated diffuse air into the burette (by creating a desired pressure gradient across the ceramic). Water level inside the burette falls as the air bubbles go inside the DAVI. The volume of diffused air is related to the changes in the water elevation inside the burette.
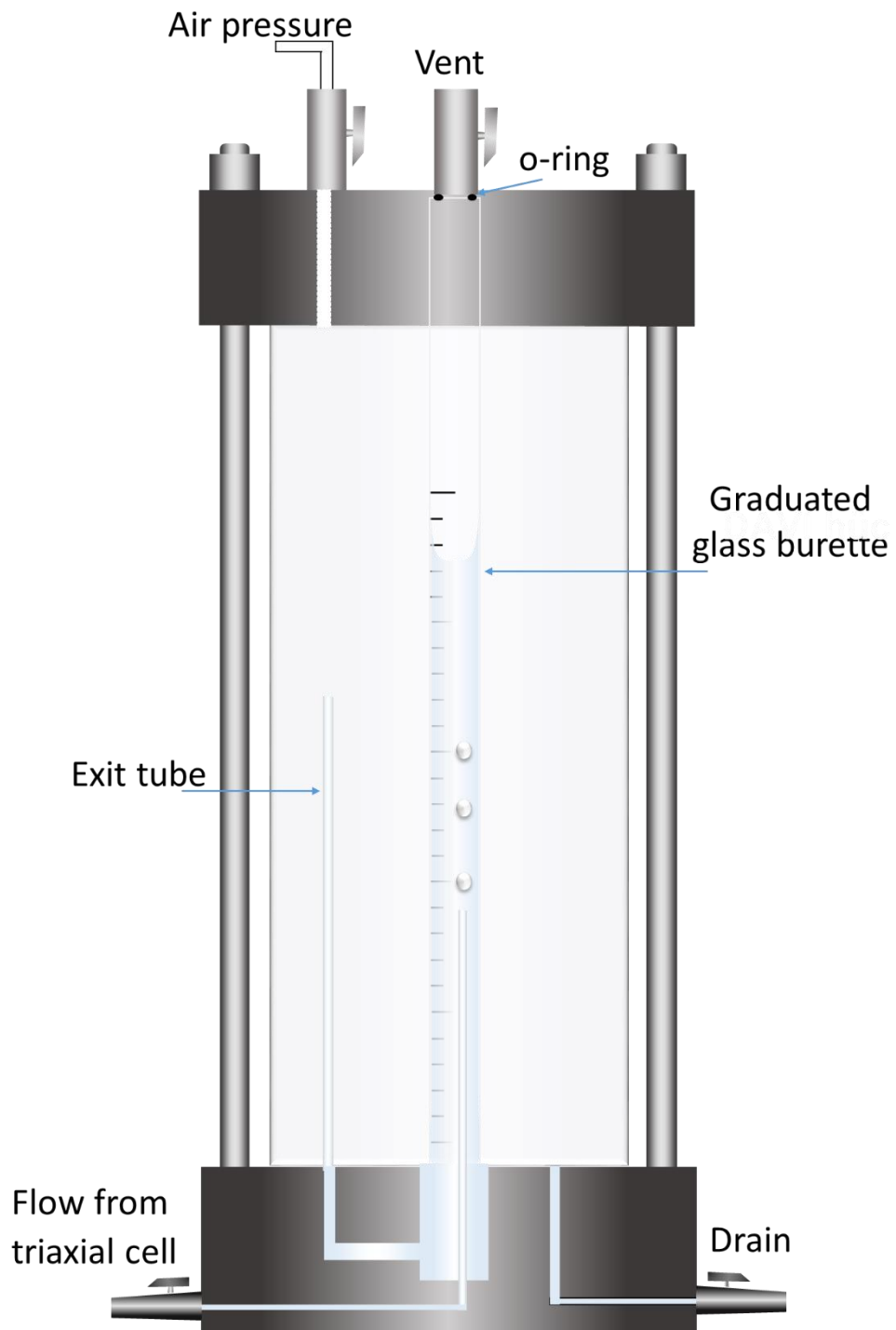
Figure 4.8 Schematic of diffused air volume indicator (DAVI).

4.3.4 *Data Acquisition System (data logger)*

All the data from PVAs, LVDT and load cell were collected via the data acquisition system embedded in triaxial setup and controlled through the commercially provided software. All of these transducers are calibrated by the manufacturer. However, additionally, a volume change transducer, and two air pressure transducers (see sections 4.3.1 and 4.3.2) are used in this study. A Testbox1001(TDG) data-acquisition system and a process interface were used to collect and record the additional data channels. These additional transducers were calibrated using PVAs, and their calibration graphs are in appendix A.

4.4 Testing Equipment Maintenance and Preparation

4.4.1 *Saturation of High Air Entry (HAE) Ceramics*

Saturation of the HAE ceramic is one of the most important steps when using axis translation technique. A saturated ceramic provides continuity between the pore-water in specimen and the water beneath the ceramics, while preventing air passage through the ceramic. Both top cap and pedestal were saturated inside the triaxial cell. The following procedures were adopted for saturation of the ceramic:

- Distilled de-aired water is prepared to saturate the ceramics.

- The pressure volume actuators (PVA) (both sample and cell) and the drainage lines were saturated with de-aired water to ensure removing any air bubbles.

- Then the triaxial cell (including pedestal and top cap) was filled with de-aired water.

- A perforated cylinder is used to carry the top cap.

- The back pressure line connected to the pedestal and top cap and cell pressure line to triaxial cell.

- Both back pressure and cell pressure valves are opened.

- First, a cell pressure and back-pressure of 100 kPa gradually was applied and maintained for about an hour. Then the backpressure line valve (valve 5 and 6) are closed. After about two hours, the backpressure line is opened for at least 15 min to flush the dissolved air.

- Then the cell pressure was increased with 100-kPa intervals to 600 kPa following the same procedure as mentioned in the previous step.

- Coefficient of permeability of the ceramics was calculated regularly to control saturation. This is a suitable way to control the saturation and the undesirable presence of a crack in the ceramic.

- After ensuring saturation, the cell pressure and backpressure are decreased gradually and triaxial cell is disassembled to proceed to the test.

- After each test, ceramics were re-saturated following the above procedures.

Inappropriate sealing of ceramic also provides air breach into the water system. Therefore, a sealing examination is performed after the first time the ceramics are saturated. For this purpose, the water drainage line was placed inside a water container. The triaxial cell with pedestal and top cap are subjected to air pressure. The air pressure gradually is increased to 450 kPa (slightly less than the air entry vale) and maintained for a while. At this time, the output line was monitored. If no bubbles come out, the seal works properly.

4.4.2   Flushing Procedure of the Diffused Air

In this study, the diffused air was flushed from the system almost every 12 hours. The following steps were followed to flush out the diffused air (the first two steps were performed before the test):

1) First, the graduated glass burette (inside the DAVI) is filled with water. For this, the valves 1, 3, 7, 8 and 10 were closed, and the valves 2, 4, and 9 are

opened. After filling the burette, valves 2, 4, and 9 are closed. The arrangement of the valves is shown Figure 4.7.

2) Then pressure inside the DAVI is adjusted (using the air compressor) to a value less than pore water pressure (below the ceramic). In this study, a difference of 20-kPa was adopted to flush out the air bubbles.

3) To flush out the air bubbles during the test, first, the burette reading is taken. Pressure behind the valve 2 is adjusted to the same value as the PVA. Then the valve 1 is closed and valves 2, 7 and 8 is opened.

4) Due to pressure gradient between the water pressure beneath the ceramic and pressure inside the DAVI, water and air bubbles flow to the DAVI.

5) Then, valves 2, 7 and 8 are closed and the valve one is opened to the system.

6) Then, the final burette reading is taken.

7) The quantity of the diffused air is estimated based on the ideal gas law as described by Fredlund (1975).

4.5   Pressure Plate Extractor (PPE)

In this study, the modified triaxial system (for testing unsaturated soils) and a pressure plate were independently used to obtain the SWCC of the testing soil. The pressure plate was employed to select the proper soil sample. After identifying soil sample the triaxial system was used to obtain the SWCC. The PPE was custom-built by FOREA (Ahmadiadli 2014).

The working principle of the pressure-plate is based on the axis translation technique. The schematic of the pressure plate (with 15 bar high air entry ceramic) is shown in Figure 4.9. A water compartment below the ceramic disk is connected to a burette. The burette is opened to the atmospheric pressure.
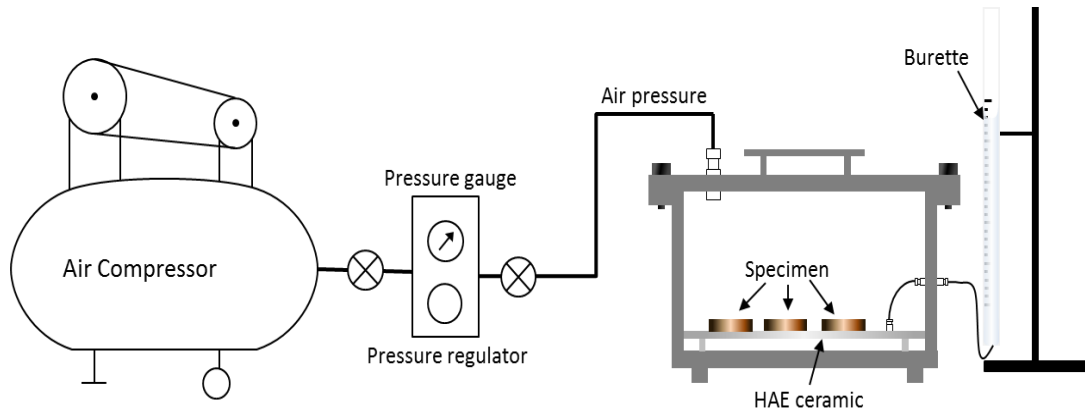
Figure 4.9 Schematic of pressure plate.

Before the test, the HAE ceramic should be saturated. For this purpose, up to half of the pressure plate chamber is filled with distilled de-aired water. An air pressure of 100 kPa is applied and maintained for one day to force air bubbles in the ceramic to go into solution. Then the drainage line of the water compartment is opened to burette, for at least 15 min, to flush the dissolved air. The opening and closing of the drainage valve are performed at regular intervals. The next day, the air-pressure is increased to 250 kPa. Similarly, the dissolved air was flushed out regularly. After two days, the air pressure was gradually decreased and the water is drained.

CHAPTER 5

VOLUME CHANGE MEASUREMENT IN TRIAXIAL TESTS

A novel procedure is developed to measure the total volume change of the saturated and unsaturated soils in triaxial testing. The principle of the proposed method is based on cell fluid volume measurements corrected by the assumption of viscoelastic behavior for the triaxial setup. Calibration and parameter determination procedures of the model are devised, and the presented model is implemented into a MATLAB code. The performance of the proposed method is validated through a series of consolidated drained triaxial tests on saturated specimens, by comparing the changes in volume measurement of proposed method and conventional measurement (pore fluid). The accuracy in volume measurement during consolidation and shear stages of these tests was between 0.09 - 0.32 cm^3, which is on par with or better than more complex and expensive alternatives found in the literature. Repeatability of the proposed technique in measurement of the volume change was also investigated through a series of suction controlled unsaturated soil tests.

5.1 Literature Review

Complexity and cost of unsaturated soil testing equipment have made it difficult to enter among the common equipment of soil mechanics laboratory and geotechnical practice, limiting it just to research institutions. In conventional testing of saturated soils (assuming soil particles and pore fluid are incompressible) volume change can be measured by monitoring the inflow or outflow of pore water from the specimen. However, such techniques are not applicable to unsaturated soils, which have both air and water phases in their pores, as a portion of the volume change happens due to the compressibility, dissolution, and inflow or outflow of the air phase. Even in a saturated triaxial test, during back pressure saturation stage, the specimen is unsaturated and its volume may change significantly due to swelling or collapse.

51

Measuring this volume change at this stage, for further calculation (such as area correction), is crucial. However, volume change in unsaturated specimens is not measurable with conventional methods at present.

Even though measurement of volume changes in the air phase have been reported (Laudahn, Sosna, & Boháč, 2005), majority of unsaturated triaxial test setups rely on external measurement of specimen volume. This is due to the high compressibility of air phase and as the membranes are not completely impermeable with respect to air, diffusion could happen into the cell fluid over time.

Practical methods, which have been suggested in the literature to measure the volume changes of unsaturated soils externally in triaxial test setups, may be classified into three categories as direct measurement on the specimen, optical measurement techniques, and cell liquid variation measurement.

In direct measurement techniques, the volume measurement in a triaxial test can be performed by locally monitoring the axial and radial strains of the samples. As shown in Figure 5.1, axial and radial strains can be measured directly by using various local displacement measurement devices(Clayton, Khatrush, Bica, & Siddique, 1989; Costa-Filho, 1985; Klotz & Coop, 2002). However, the utility of these techniques are limited to small strains (when shear plane is not expected) and relatively dense specimens.

Figure 5.1 Local transducers for measuring volume change in a triaxial apparatus
a) LVDT local strain transducers, b) hall effect local strain transducers (GDS,
2014).

Optical measurement techniques include laser mapping and image-processing. Romero et al. (1997) suggested mapping the specimen with lasers mounted outside the triaxial cell (Figure 5.2). Despite high precision of this technique, it is expensive, sophisticated and requires long calibration and installation procedures (Hoyos et al. 2008). Macari et al. (1997) proposed the use of digital photography during the test at regular intervals, then analyzing pictures through image-processing software (Figure 5.3). This method can be employed in a conventional triaxial setup to measure volume change without any modification to the setup. Note that multiple cameras are necessary unless the specimen deforms symmetrically (i.e. without strain localization). In this method, the real time observation of volume change is not possible and a time-consuming operation is required for processing each picture. Another problem is distinguishing the edge of the specimen from the shadow of the top drainage tube for which professional lighting is required to take good-quality pictures.
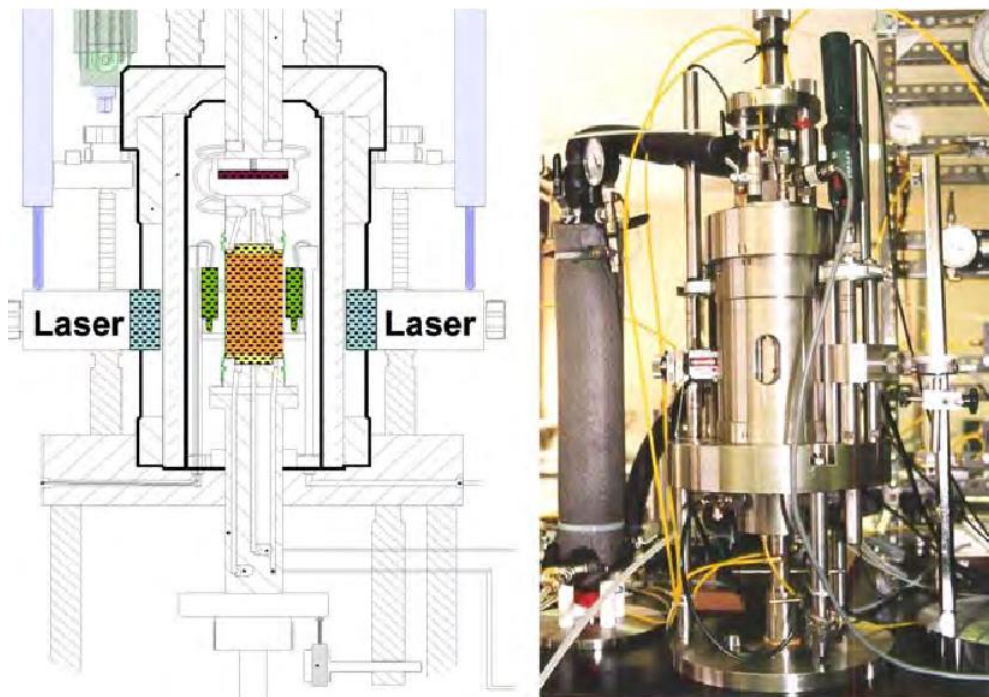
Figure 5.2 Measuring of volume change in triaxial apparatus by electro optical lasers (Romero et al. 1997, adopted from Hoyos et al. 2008)
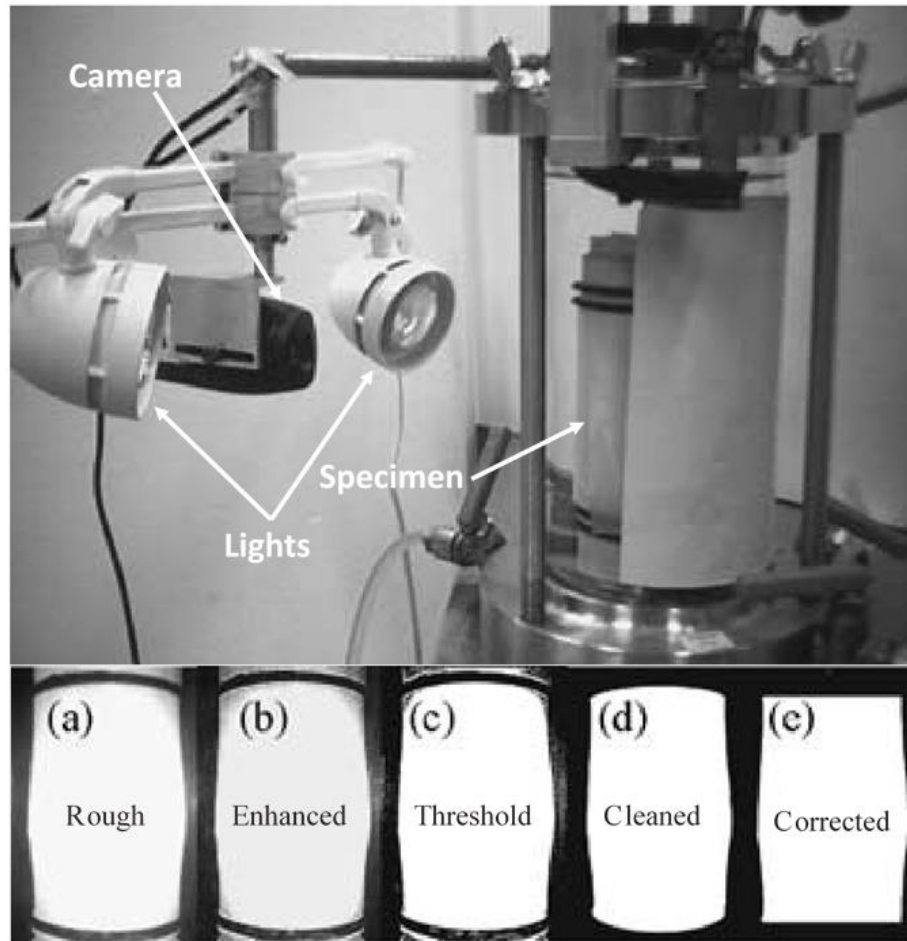
Figure 5.3 Measuring of volume change in triaxial apparatus by image processing (Rifaı et al. 2002).

The last category is the cell liquid measurement, where volume change of the specimen is related to measurement of changes in the volume of the liquid in the triaxial cell. This can be done by monitoring the inflow and outflow of fluid surrounding the specimen.

Monitoring the cell fluid volume change in a conventional triaxial setup is a simple to use, and inexpensive method of volume change measurement. However, immediate expansion and time dependent changes in volume of the triaxial system occur in addition to specimen volume change, and calibration is necessary to take these effects into account.

To eliminate the errors related to the expansion and creep of the triaxial cell, Bishop and Donald (1961) proposed inclusion of an additional inner cell, which is an open-

ended Perspex cylinder sealed from the outer cell at the base (Figure 5.4). The inner cell is filled with mercury, and outer cell is filled with water, both up to level of the top cap. As the pressures inside and outside the inner cell are equal, the inner cell does not expand due to variations in cell pressure. Then, soil volume change can be related to variation of fluid level in the inner cell. This level change was monitored by tracking the movement of a steel ball floating over the mercury surface, using a cathetometer. For safety reasons Cui and Delage (1996) replaced the mercury with colored water and a layer of silicone oil is placed on top of water surface to decrease evaporation.
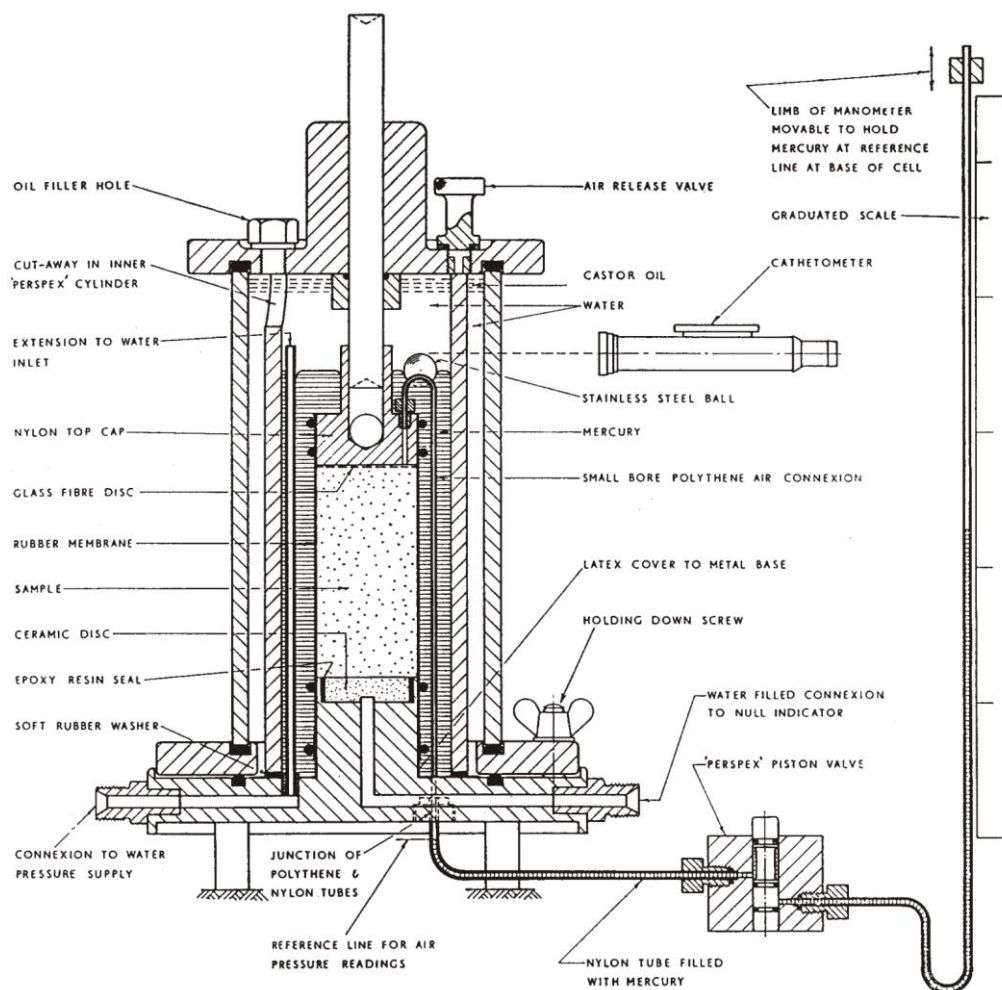
Figure 5.4 Modified double wall volume measuring triaxial setup (Bishop and Donald, 1961).

Ng et al. (2002) introduced a new setup in which, the volume change of the specimen is deduced by recording the differential pressure between water inside a bottle-shaped open-ended inner cell and water inside a reference tube using the differential pressure transducer (Figure 5.5). However, in this way the total volume change that could be measured is limited to the volume of the neck section of the open-ended inner cell. To eliminate the problem related to creep and hysteresis of the system the aluminum inner cell and bronze tubes are employed. A thin layer of paraffin is placed on top of the water surface, inside both inner cell and reference tube, to reduce the water evaporation and air diffusion into the water. This setup has a few problems. If a non-transparent inner cell is required to increase the accuracy of measurement, it offers no advantage over a conventional triaxial setup with (rigid, non-transparent) steel cell. Using paraffin may lead to some measurement errors and pressurization of Plexiglas cell with compressed air is somewhat unsafe (Sivakumar et al., 2006). Despite using an aluminum inner cell and bronze tubes, the system could register apparent changes in volume in addition to actual changes (Ng et al. 2002) (both immediate and time dependent). Therefore, a calibration procedure has to be performed.
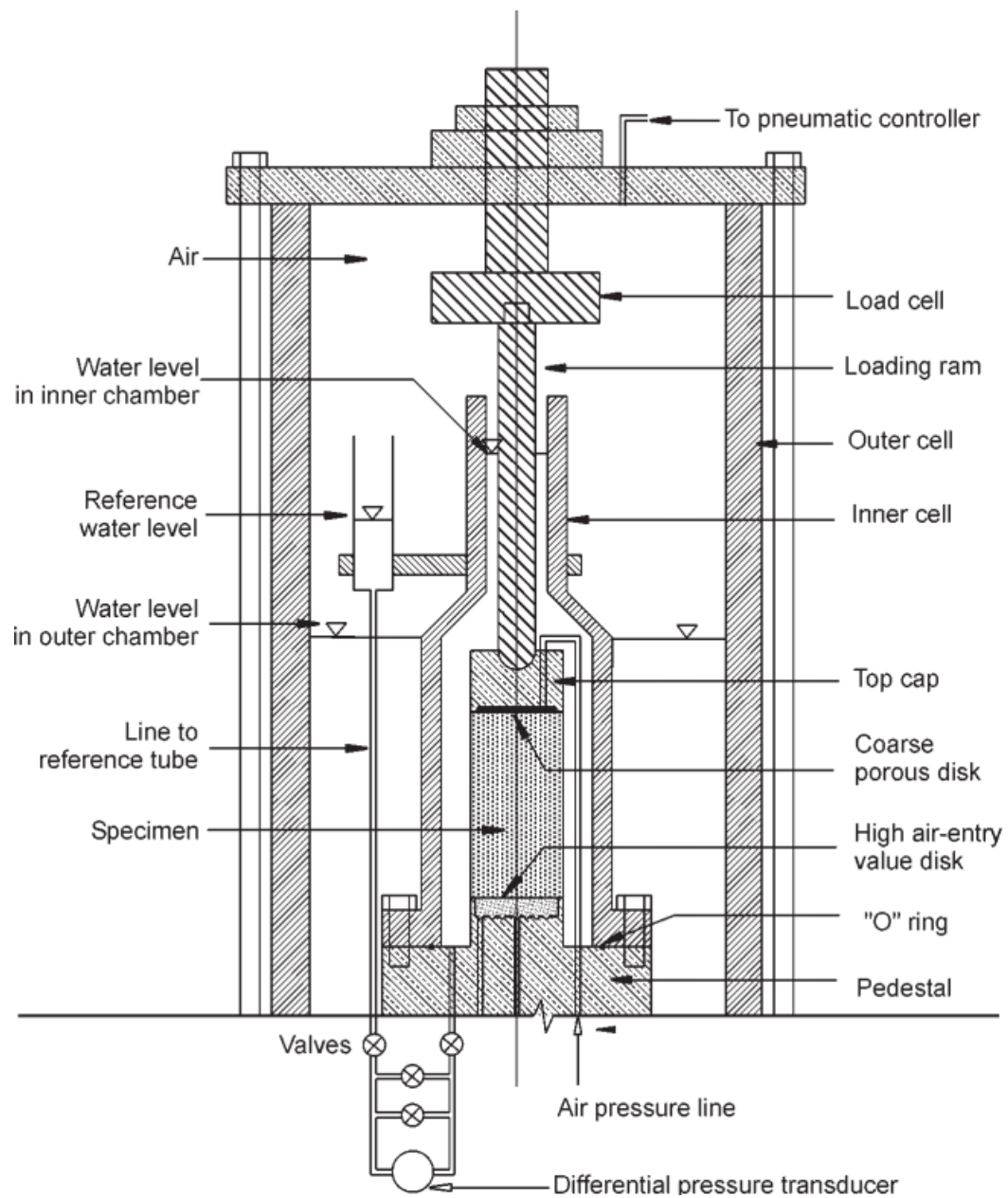
Figure 5.5 Modified inner cell volume measuring triaxial setup (Ng et al. 2002).

Wheeler (1988) developed a double-walled triaxial apparatus in which, the inner chamber is sealed at both ends (Figure 5.6). The volume change of the specimen is deduced from the inner chamber's fluid exchange. Theoretically as the pressures inside and outside of the inner chamber is the same, the change in volume of the inner chamber due to variations in pressure must be zero. However, due to various effects, such as temperature fluctuation, difficulties in setting up of the specimen in the triaxial cell and water absorption of the acrylic cell, volume of the inner chamber can change with pressure and time (Sivakumar et al. 2006). In this case, calibration procedure similar to that of the single-cell method is inevitable. The other problem is related to the air bubbles that could be trapped in the inner cell. Moreover, when the vertical load is measured externally as in Wheeler (1988)'s setup, the effect of piston friction is greater, as it goes through two seals or one long shaft seal, unless the inner and outer chambers share a single top plate.
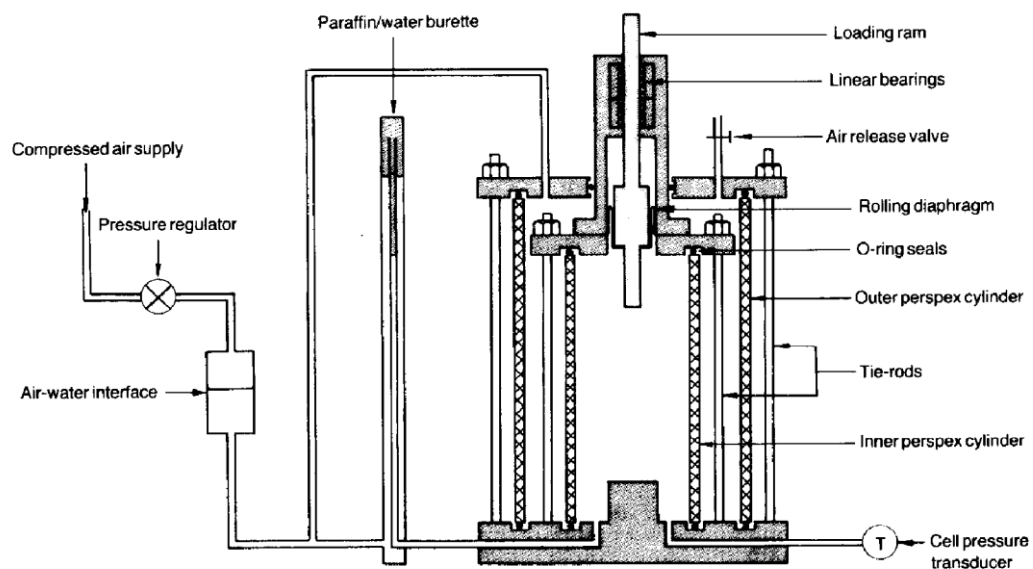
Figure 5.6 Modified double wall volume measuring triaxial setup (Wheeler 1988).

Table 5.1 provides a summary of the advantages and disadvantages of volume-change measurement methods found in the literature.

All of these methods require expensive and complex modifications to the conventional triaxial setup or involve additional pieces of equipment. The double-wall and inner cell methods have been widely employed for testing unsaturated soils and in both method calibration for immediate and creep behavior of the system is required (like using the single-cell technique). However, employing these setups with this level of complexity (added to that of suction control) is not commercially practical and therefore, unsaturated soil tests do not see widespread use in soil mechanics laboratories.

Table 5.1 Advantages and disadvantages of volume change measurement methods.

Method	Disadvantage	Advantage	Accuracy
Local displacement transducers	▪ Limited to small strains and relatively dense specimens. ▪ Requires modification to setup and preparation procedure	▪ Real time monitoring	▪ -
Laser mapping	▪ Expensive, sophisticated and long calibration and installation procedures	▪ High precision ▪ Non-contact ▪ Real time monitoring	▪ 0.6 to 1.02cm^3
Image processing	▪ Suitable for specimen with symmetric deformation, ▪ Real time observation of volume change is not possible, ▪ A time consuming processing operation is required for each picture.	▪ Do not need modification* to conventional triaxial setup ▪ Can be inexpensive (depends on camera type)	▪ 0.25 cm^3
Double wall	▪ Requires modification* of conventional triaxial setup (expensive and complex).	▪ Real time monitoring	▪ 0.6 to 1.02cm^3
Inner cell	▪ Requires modification* of conventional triaxial setup (expensive and complex), ▪ Problem relating to using air pressure to control cell pressure (discussed in the text)	▪ Real time monitoring	▪ 0.1 cm^3
Single cell	▪ Difficult calibration is required	▪ Simplicity, employing conventional setup without modification*. ▪ Inexpensive ▪ Real time monitoring if calibration is incorporated into control software	▪ 0.45 cm^3

5.2 Volume Change Measurement

In this study, image processing, independent measurement of the air and water volume change, inner cell and single cell methods were examined to measure the volume change of the unsaturated soils. Advantages and disadvantages of each of the 4 methods were investigated to select the suitable measurement method.

5.2.1 Image Processing Technique

Macari et al. (1997) proposed the use of digital photography to measure the volume change of the unsaturated soils. This method can be employed in a conventional triaxial setup to measure volume change without modification to the setup.

In this study, a Canon Powershot SX210, digital camera was used for this application. The camera was fixed at a constant distance from the triaxial cell using a tripod. The images were processed using the procedure suggested by Macari et al. (1997). An image-processing code was developed in MATLAB following Uchaipichat et al. (2011). Different colors for background were tested to reduce the noise during edge detection. The black and green background seems to be suitable to take acceptable pictures. Lighting is an important factor to take pictures with clear and detectable boundaries. Lighting of the specimen in saturated soil testing was performed with fewer difficulties. In unsaturated soil testing, the problem is distinguishing the edge of the specimen from the shadows of the top drainage tubes (two water and one air drainage lines) for which professional lighting is required to take good-quality pictures. Different arrangements of lightning were examined, however, none of them were successful. Therefore, a manual edge tracing becomes inevitable, which makes this method tedious and time consuming. The real time observation of volume change is not possible and a time-consuming operation is required for processing each picture. Another problem was encountered at-large displacements, where the deformation is not symmetric, therefore, multiple cameras were necessary. All of these difficulties made this method inappropriate for this study, therefore, this method was abandoned.

5.2.2 Independent Measurement of Air and Water Volume Change

In this method the volume change due to air phase and water phase is monitored separately. The overall volume change of the specimen is equal to the sum of the changes in volume of the air and water components. The change in volume of the water phase simply is measured through pore-water drainage line as it is done in saturated tests. In order to measure the changes in volume of the air phase, a volume change transducer (VCT) is added to the system (see sections 4.3.1 and Figure 4.6). The VCT is placed between the air-water interface cell and OWCP. The change in volume of the air phase can be deduced from the volume of the water inflow and outflow to the OWCP. However, during the preliminary tests, the inadequacy of the system recognized. This is due to the sensitivity of air volume to temperature fluctuations, which considerably affect the volume of the air phase. In addition sealing the entire system to air leakage is difficult, and also diffusion of the air through the tubs and membrane is inevitable. Therefore, considering all of these issues, this method was also abandoned.

5.2.3 The Inner Cell Method

Inner cell method is an alternative to measure the volume change in unsaturated soil testing. A new triaxial cell was developed to measure the volume change according to inner cell technique following Ng et al. (2002). The Schematic layout of the modified triaxial cell is shown in Figure 5.7. The triaxial cell includes an additional open-ended bottle-shaped inner cell and a reference tube. The overall volume change in an unsaturated–saturated specimen is related to pressure difference between the water inside the open-ended, bottle-shaped inner cell and the water inside a reference tube (Ng et al. 2002). A high-accuracy differential pressure transducer (DPT) is required to measure this pressure difference. Unfortunately due to high cost of the DPT (was not possible to buy within the budget of this study) and its limitation this method was not used in this study.
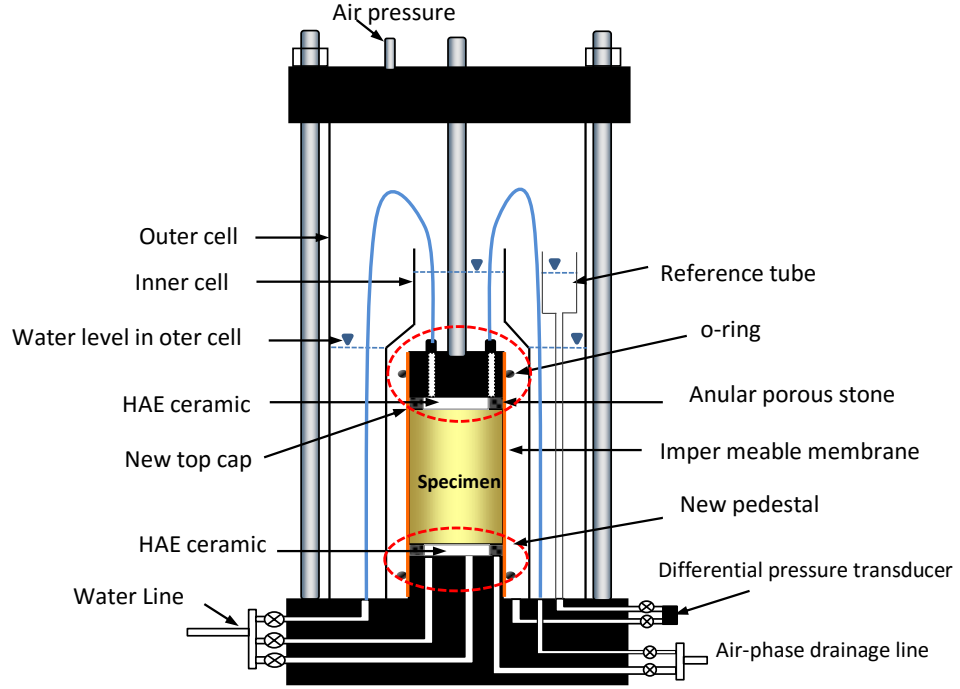
Figure 5.7 Schematic layout of the modified triaxial cell with inner cell.

This complexity can be abated by employing conventional triaxial cell and monitoring the cell fluid exchange. However, the accuracy of single cell method relies heavily on calibration accuracy (Ahmadi-Naghadeh & Toker, 2012). Despite its simplicity, this method was gradually abandoned due to severe calibration requirement.

In this study, a novel and simple calibration procedure that assumes viscoelastic constitutive model for triaxial cell is developed to take the immediate and time dependent volume changes of the triaxial setup into consideration. Volume change of the triaxial cell fluid is related to the soil specimen volume change, immediate and time dependent volume changes of the cell and tubing (expansion of the system) and piston intrusion into the cell, as follows:

$$\Delta V_{\text{Cell Fluid}} = \Delta V_{\text{specimen}} + \Delta V_{\text{expansion of the system}} + \Delta V_{\text{piston intrusion}} \qquad (5.1)$$

The volume change related to movement of the piston (i.e. loading ram) simply could be corrected by the product of axial displacement and cross section area of the piston. However, a calibration process requires to account for not only the immediate expansion of the cell caused by pressure increase, but also time dependent volume changes of the triaxial setup under constant stress. Immediate and time dependent deformation are typical characteristics of viscoelastic materials. Therefore, the behavior of the triaxial setup could be simulated using viscoelastic constitutive models.

The following section of this paper explains the theoretical aspects of the viscoelastic constitutive model. Then the procedure and required tests for calibrating the viscoelastic model for the given triaxial cell is explained. Finally, the accuracy of proposed method is investigated using a series of validation tests on saturated specimen with conventional volume change measurement of the pore fluid.

5.3   Theoretical Background on Viscoelasticity

To describe the mechanical behavior of most of the materials under different loading conditions, combinations of springs and dashpots, are employed to the stress (σ) and strain (ε). A perfectly elastic "spring" ($\sigma = E\varepsilon$, where E is the modulus of the elasticity) has no time-dependent deformation. A "dashpot" is a viscous element ($\sigma = \eta \cdot \dot{\varepsilon}$, where η is viscosity coefficient) that deforms infinitely under sustained stress. Materials that exhibit both elastic and viscous action, are known as viscoelastic materials. In such materials, time dependency of stress under constant strain is known as relaxation and time dependency of strain to applied constant stress is known as creep. This is formulated by expressing, stress as a function of both strain and time.

Maxwell (1868) combined an elastic spring and dashpot in series, to create one of the simplest mechanical models to predict the behavior of viscoelastic materials. In this model since both elements are arranged in series connection, stress is identical in both elements but strain decomposes additively into instantaneous elastic strain in spring, and creep strain in dashpot. Under a constant stress, the total strain at any time, employing the constitutive relations for both spring and dashpot, is calculated from the following equation:

$$\varepsilon_{Maxwell} = \frac{\sigma}{E_M} + \frac{\sigma \times t}{\eta_M} \qquad \forall \ t_0 \leq t \leq t_1 \tag{5.2}$$

where, t is the elapsed time, E_M, is the elastic moduli and η_M is the viscous coefficient of the Maxwell model.

Once the system is unloaded, an instantaneous elastic recovery due to Hookean elastic element occurs, however, there is no recovery of viscous strain. This can be mathematically formulated as following equation:

$$\varepsilon(t) = \frac{\sigma \times \ t_1}{\eta_M} \qquad \forall \ t > t_1 \tag{5.3}$$

Despite acceptable behavior of the Maxwell's model in the case of relaxation, it fails to predict the creep and recovery after unloading.

The Kelvin model (also called Kelvin-Voight model), is another alternative viscoelastic model, which is parallel combination of a spring and a dashpot (Kelvin 1875; Voigt 1892). In this model, strain is identical in both elements, as they are connected in parallel. However, stress decomposes additively to both elements.

Under constant stress, σ, employing constitutive relation of spring and dashpot the total strain calculated by the expression:

$$\varepsilon_{Kelvin} = \frac{\sigma}{E_K}\left(1 - exp^{-\frac{E_K \times t}{\eta_K}}\right) \tag{5.4}$$

where, t is the elapsed time, E_K, η_K are the elastic moduli and the viscous coefficient of the Kelvin model respectively.

In contrast to the Maxwell model, this model is improper to describe the relaxation behavior of the materials, as the entire strain is recovered after unloading.

5.3.1 Burgers Model

Kelvin and Maxwell models, are inadequate to describe the behavior of most of the real materials. The Maxwell model is adequate to describe stress relaxation, however it is incapable of describing time-dependent recovery and creep, on the other hand,

the Kelvin model can account for creep and recovery, however, it cannot consider for stress relaxation. Combination of these two simple models in mechanical series, as shown in Figure 5.8(a), gives an alternative comprehensive viscoelastic model known as the Burgers (or four parameter viscoelastic) model (Burgers, 1935).
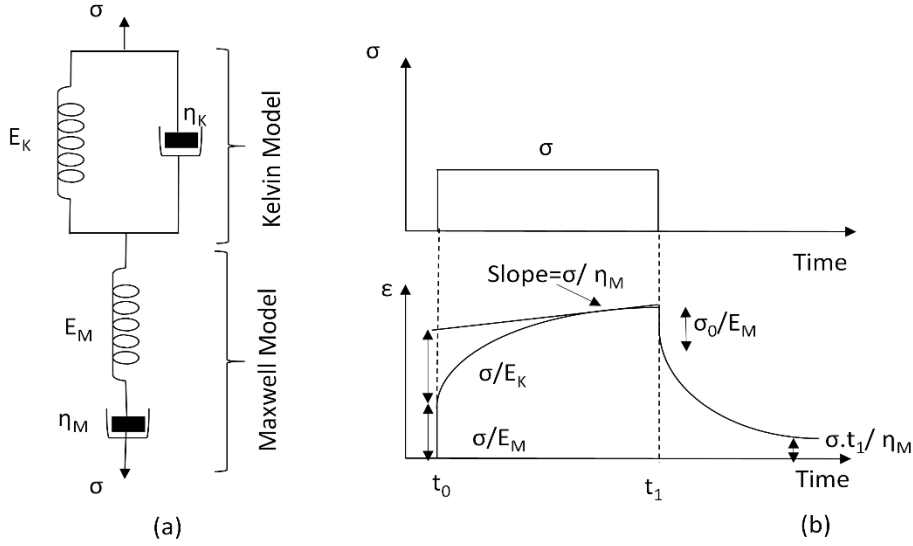
Figure 5.8 (a) Burgers spring-dashpot model, and (b) typical creep and recovery response of Burgers model.

Since Maxwell and Kelvin's elements are connected in series, the strain response of this model under constant stress is given by:

$$\varepsilon_{Burgers} = \varepsilon_{Maxwell} + \varepsilon_{Kelvin} \tag{5.5}$$

where $\varepsilon_{Maxwell}$ is the strain in the Maxwell element and ε_{Kelvin} is the strain in the Kelvin element. Therefore, the total strain calculated by the following equation:

$$\varepsilon_{Burgers} = \frac{\sigma}{E_M} + \frac{\sigma \times t}{\eta_M} + \frac{\sigma}{E_K}\left(1 - exp^{-\frac{E_K \times t}{\eta_K}}\right) \tag{5.6}$$

A typical creep and recovery response of the Burgers model for a constant stress is shown in Figure 5.8(b). At t = 0, the spring in the Maxwell portion instantaneously deforms to its ultimate capacity and can be estimated by the first term of the Eq (5.6). Then the Kelvin element starts to deform. Within the Kelvin portion, first, all the

66

stress is sustained by the dashpot and then it is gradually transferred to spring element of the Kelvin model. This portion of deformation is known as delayed elasticity (Findley, Lai, & Onaran, 1976) and formulated by the last term of the Eq (5.6). Eventually, the only remaining deformation is Maxwell dashpot's flow at a rate of σ/η_M.

The observed behavior of a sealed triaxial system (triaxial cell, tubing, valves, etc.) at different pressures is similar to what we see in the Burgers model. The instantaneous deformation of the triaxial system, due to cell pressure, can be attributed to elastic and delayed elasticity of the Burgers model. The creep behavior of the triaxial system can be modeled with Maxwell dashpot portion.

5.4   Determination of Burgers Model Parameters for Triaxial System

In this study, the behavior of the pressurization system (cell, tubing, PVA, etc.) is assumed to obey the linear viscoelastic principles of the Burgers model. Therefore, calculation of changes in cell fluid volume in response to stress and stress history requires, firstly, estimating unknown parameters of the Eq (5.6) based the experimental data.

The input parameters of the Eq (5.6) are not fit in the same concept of the system properties. For instance, here instead of strain, the volume change of the system is considered and the instantaneous strain (related to Young's modulus) of the model is not equal to modulus of elasticity of the cell and is related to instantaneous volume change of the system. Therefore, the Eq (5.6) is rewritten for volume change as:

$$\Delta V = \Delta V_i + \frac{\sigma \times t}{\eta_M} + \frac{\sigma}{E_K}\left(1 - exp^{-\frac{E_K \times t}{\eta_K}}\right) \tag{5.7}$$

where ΔV is the volume change of the triaxial pressurization system and ΔV_i is its instantaneous component. Here the first term (linearly elastic component of the Maxwell model) is replaced by the more general ΔV_i term because of the slight nonlinearity of the system response observed in the preliminary tests.

5.4.1 *Instantaneous Component of ΔV*

To estimate the instantaneous volume change of the triaxial pressurization system, ΔV_i, rapid loading tests are performed. For this purpose, the triaxial cell is filled with distilled de-aired water. Then the cell is pressurized by controlled increase of the cell pressure as fast as possible (depends on system capability of applying pressure and measurement intervals) to a target value. To assess the repeatability of the observed behavior, this test is conducted several times. Figure 5.9 compares the results of the rapid loading tests for three different target pressures (800, 1000 and 1200 kPa). As shown in Figure 5.9, all target pressures result in coinciding curves. A nonlinear response between cell pressure and volume change is observed in the range of zero to 100 kPa whereas for cell pressures beyond 100 kPa the behavior is linear. Given that the nonlinear portion does not have a large curvature a separate linear function is fitted onto it, resulting in a simplified approach to estimate the first term, ΔV_i, of the Eq (5.8). In this way, this curve could be divided into two linear sections and formulated as a partial function as below:

$$\Delta V_i = \begin{cases} a_i \times \sigma_{cell}, & \sigma < 100 \\ b_i \times \sigma_{cell} + c_i, & \sigma \geq 100 \end{cases} \tag{5.8}$$

where $a_i = 0.0183$ (cc/ kPa), $b_i = 0.0158$ (cc/ kPa), $c_i = 0.384$ (cc), for the setup used in this study.
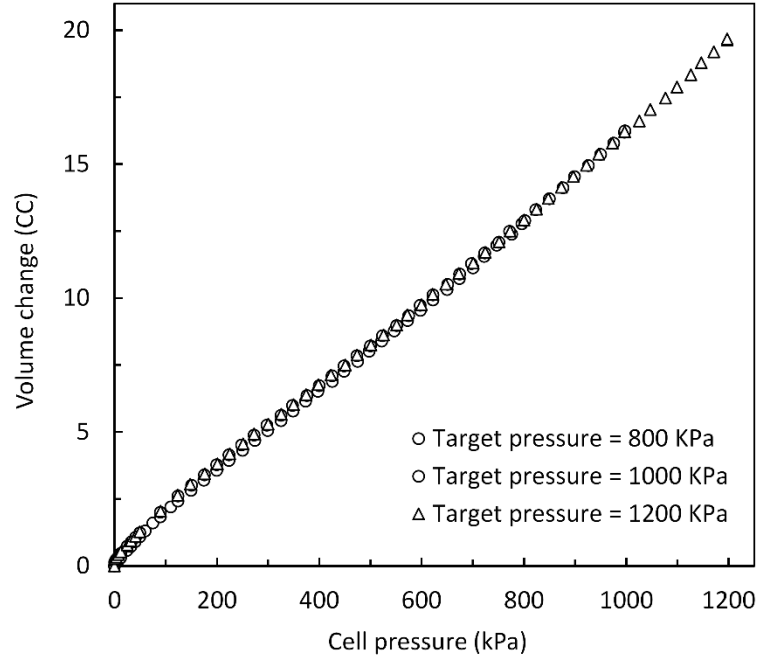
Figure 5.9 Relationship between instantaneous volume change and cell pressure for different target pressure.

5.4.2 Maxwell Viscous Coefficient (η_M) Determination

Creep-recovery tests were carried out in order to estimate the remaining unknown parameters of the Burgers model. These tests include continuous volume change measurement over 600-minute creep (maintaining constant stress) followed by 600-minute recovery (zero stress) periods for each loading step. Sequential creep-recovery loading history and its response is shown in Figure 5.10. Creep-recovery tests were performed in eight loading-unloading steps (i.e., 50, 100, 200, 400, 600, 800, 1000 and 1200-kPa cell pressure).

The Maxwell viscous coefficient, η_M, is related to slope of the creep section, shown in Figure 5.8 (b), in the steady state region of the creep-recovery test results. The steady-state region can be recognized by drawing the slope of the creep test versus the elapsed time, which is shown in Figure 5.11 for 100-kpa constant cell pressure. Figure 5.11 shows that the steady state of the loading step reach around 200 min after loading. As shown in Figure 5.12, therefore, the η_M could be estimated by relating

69

the slope of the creep section of each step, after steady state region, to related cell pressure and estimating the slope of this line.

$$\eta_M = \frac{\sigma}{dV/dt}$$ (5.9)

For the setup used in this study the amount of η_M is estimated to be 1.4×10^7 kPa.min/cm^3.
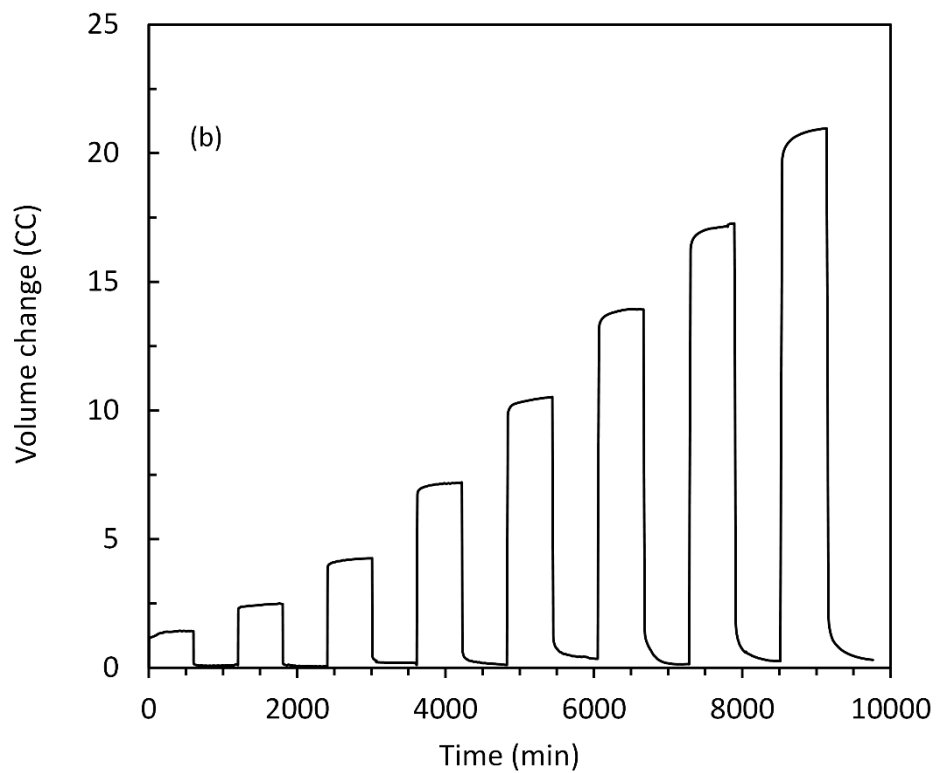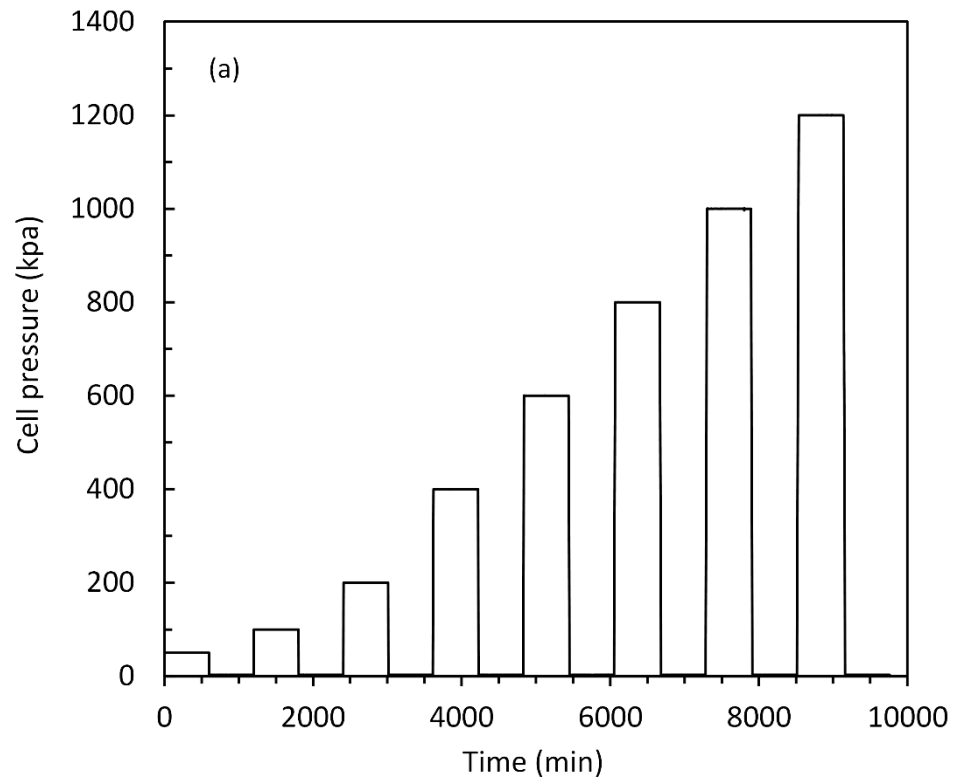
Figure 5.10 (a) Loading history and (b) volume change versus time for creep-recovery test.
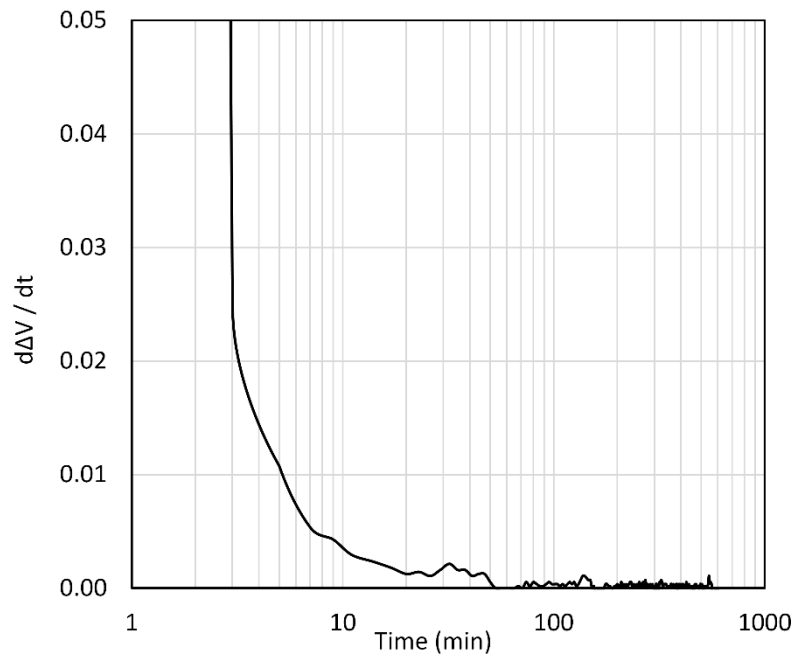
Figure 5.11 Variation of the slope of the creep-recovery test with time for
100-kPa cell pressure to determine the steady state region.

$y = 14054288x$
$R^2 = 0.985$
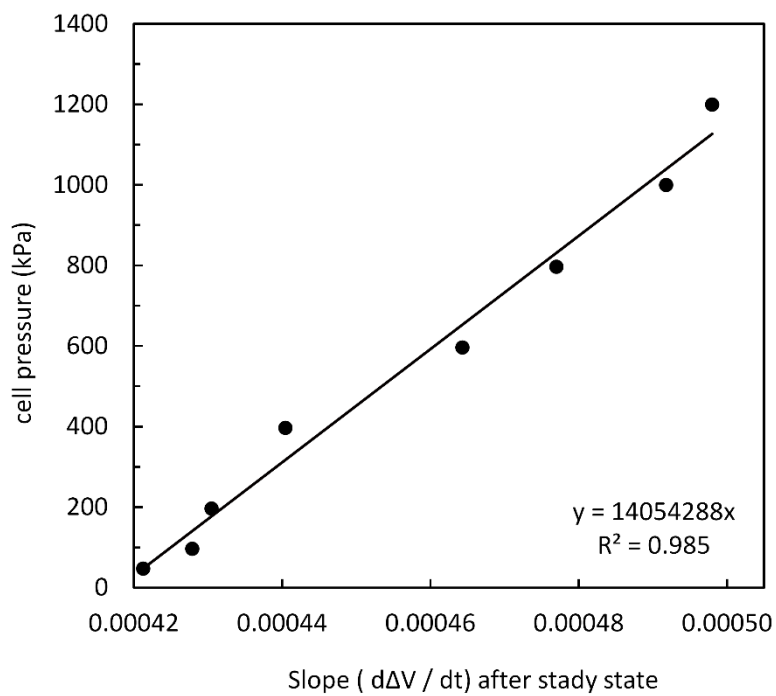
Figure 5.12 Maxwell viscous coefficient, (ηM), estimation.

5.4.3   Kelvin-Voigt Modulus (EK) Determination

In order to estimate the spring constant for the Kelvin element, E_K, (which is related to maximum delayed volume change, ΔV_d, expressed as σ/E_K in Eq (5.7)), a geometrical approach is utilized. As illustrated in Figure 5.13, ΔV_d is the subtraction of the tangential line of creep strain and ΔV_i (which is calculated in previous sections using bilinear formula). The value of ΔV_d can be calculated from the following procedure:

$$\Delta V_d = X - \frac{\sigma}{\eta_M} t - \Delta V_i \tag{5.10}$$

where, X is the volume change (any point after steady state) selected from the steady-state region, t is the time from the stress application to the selected data point and σ/η_M is the slope of the tangential line.
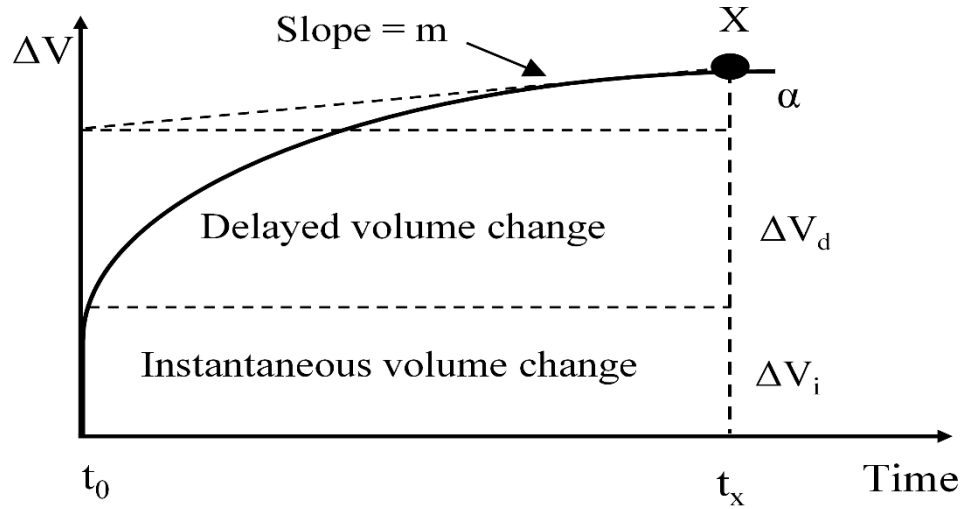
Figure 5.13 Geometrical approach to determine the delayed volume change ΔV_d.

E_K is the ratio of the applied constant stress to delayed volume change (i.e. $E_K = \sigma / \Delta V_d$), and can be estimated through the slope of the linear fit to the calculated ΔV_d, of each creep recovery test, versus corresponding cell pressures. For our setup, E_K is estimated to be 716 kPa/cm3, as shown in Figure 5.14.
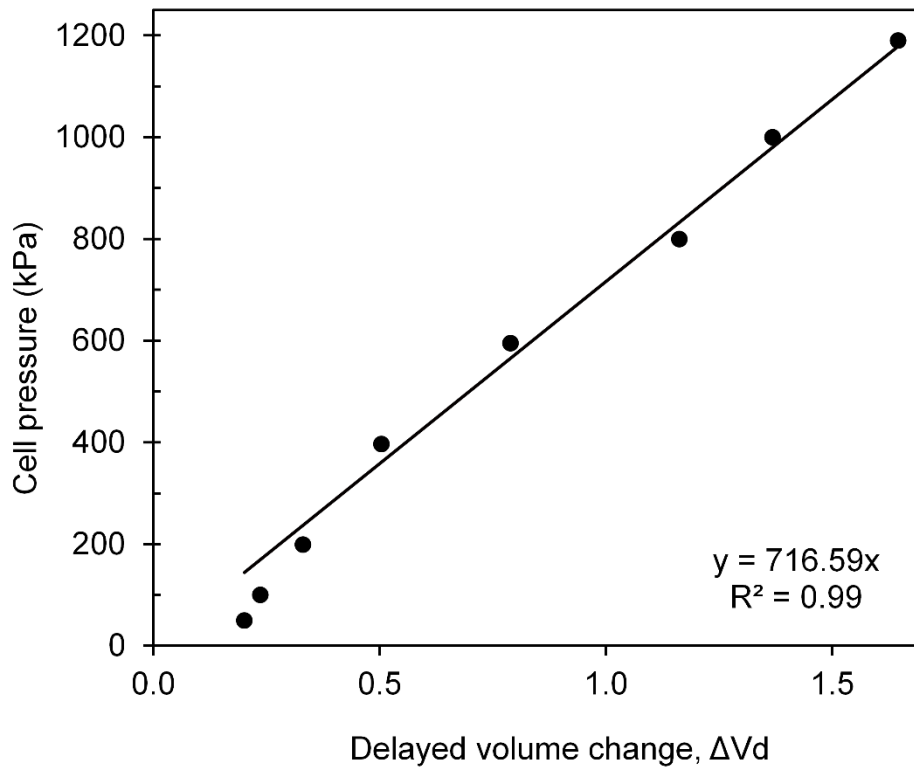
Figure 5.14 Cell pressure versus delayed volume change used to determine the
Kelvin Modulus, EK.

5.4.4 Kelvin-Voigt Viscous Coefficient (ηK) Determination

The dashpot constant, η_K, of the Kelvin-Voigt element can be determined by
resolving the Eq (5.7) for η_K at any selected time and substituting corresponding ΔV
between elastic and steady state from the creep curves into equation. For the
equipment used in this study, $\eta_K = 4\times10^8$ kPa.min/cm^3 is estimated.

5.5   Implementation of the Burgers Model into MATLAB and Its Validation

As the Burgers model constants are determined, the volume change of the triaxial
system could be predicted for any given loading-time history. Employing the
Boltzmann superposition (Irgens 2008), the Burgers model was implemented into
MATLAB. The Boltzmann superposition principle implies that, for a linear
viscoelastic material, the final deformation in response to a combined loading is
simply the sum of the deformation from each component of the loading. Figure 5.15
presents the flowchart for implementation of the Burgers equation. Figure 5.16

compares the results of the experimental data from the creep-recovery cycles and model fit using the estimated four parameters. A good agreement is obtained between model calculations and the experimental data. The observed maximum cumulative absolute error is 0.45 cm^3.
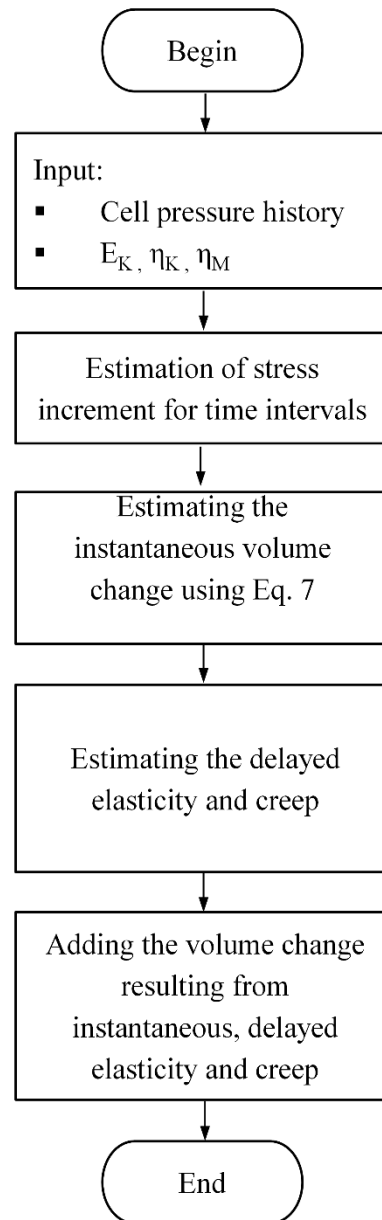
Figure 5.15 Flowchart for implementation of the Burgers equation.
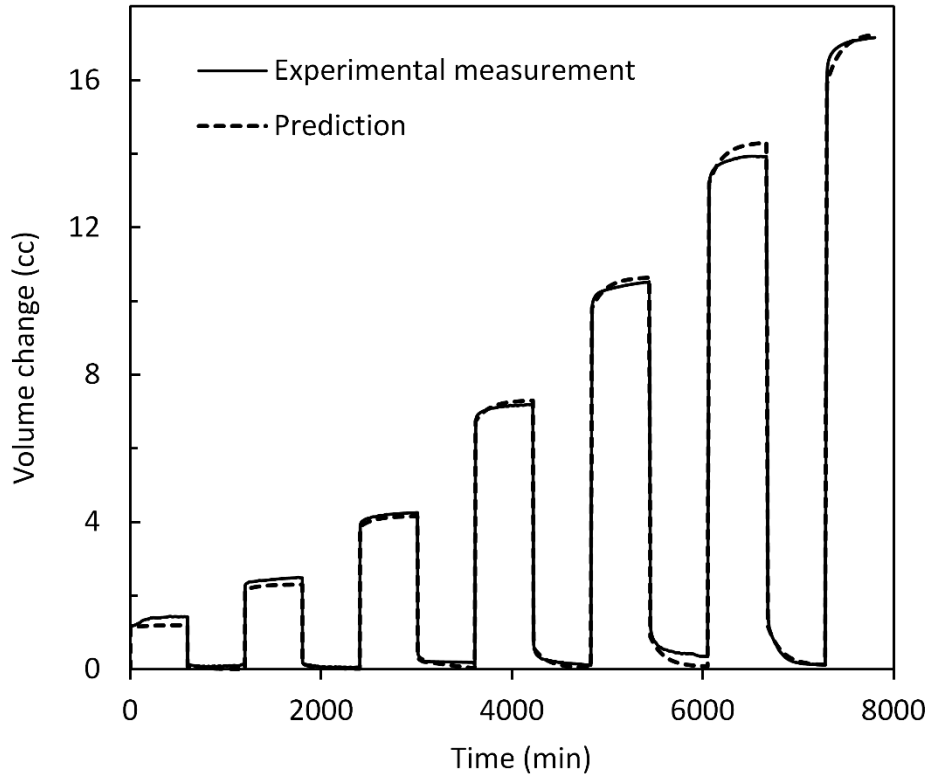
Figure 5.16 Comparison of predicted volume change of the triaxial system under loading and unloading cycles.

5.6 Verification of the Model and Estimated Parameters

5.6.1 Volume Change Measurement in Saturated Specimen

In order to evaluate and validate the performance of the proposed method, a series of isotopically consolidated drained compression tests were done on saturated soil specimens. Volume change of the specimen was measured by both conventional method (measuring inflow and outflow of water from the specimen through the pore PVA) and proposed method (monitoring the variation of cell liquid volume through the cell PVA) simultaneously.

A silty soil from Mersin, Turkey, was used as the testing material. The properties of the soil sample is presented in Chapter 6. The soil sample is classified as low plasticity silt ML according to the Unified Soil Classification System (ASTM D2487-11).

Two sets of triaxial tests were accomplished on saturated specimen prepared by two distinctive preparation methods: set 1) compacted specimen and set 2) isotopically consolidated specimen from the slurry.

Specimen is 5-cm in diameter and 10-cm in height. After the specimen is prepared on the triaxial pedestal, the cell is filled with distilled de-aired water. The triaxial test is controlled by the computer from start to finish. In all tests, first the specimen is back-pressure saturated until B value reaches 0.96. To speed up the saturation of the compacted specimens, their pores were vacuumed, followed by circulation of carbon dioxide followed by another application of vacuum before back pressure saturation. Then, for each set, the specimen is consolidated at all-round stresses of 25, 100, 200 and 400 kPa.

The consolidation of the specimen could be accomplished in two different manner: Ramped (gradual) loading and step-loading consolidation. The step-loading consolidation is the conventional method of consolidation in saturated soils testing and the ramped loading compression method mostly adopted in unsaturated soil testing. Finally, the specimen is sheared in compression.

In step-loading consolidation, it is common to increase the cell pressure up to desired effective pressure, in undrained condition. Then consolidation is initiated by opening the pore-water drainage valves. However, this is not a suitable method when the objective is the evaluation of the measurements of the volume change using cell fluid method. This is because when the cell pressure is increased in undrained condition, changes in volume of the saturated specimen would be zero while the triaxial cell expands. Time scales for expansion of the system and specimen would have different starting points. Therefore, in this study ramped loading method employed in consolidation step of all triaxial tests (since this is the conventional method of compression in unsaturated soil testing and also to have the system respond to pressure changes instantaneously).

During consolidation and shearing stages, changes in volume of the specimen is measured by monitoring both specimen pore water exchange and variation in cell fluid independently. Movement of the loading ram into or out of the cell need to be taken into consideration in addition to system volume change. For this purpose, the

volume change could be corrected by the product of axial displacement, during the test, and cross section area of loading ram (i.e. $\Delta L \times S$).

The cell fluid volume change data is corrected by loading ram intrusion, as well as time and stress dependent expansion of the triaxial cell and piping (which is calculated through Boltzmann superposition of Eq (5.7)). Figure 5.17 (a) and Figure 5.18 (a) compare measurements of proposed and conventional volume change measurement for the test set prepared from slurry. Same comparison is done for the test set on compacted specimen in Figure 5.19 (a) and Figure 5.20 (a).

Difference between the volume change measurement of the conventional method and proposed method is calculated as the absolute error and depicted in Figure 5.17(b)-13b. The maximum error for each test, in both consolidation and shear stage and their sum, and the average value of the maximum error for all tests presented in Table 5.2. In these tests, maximum absolute error in volume measurement during consolidation and shear stages was between 0.03 - 0.22 cm^3. Considering specimen of 5-cm diameter and 10-cm height, the values corresponded to volumetric strain values of about 10^{-3} on average.

Table 5.2 Absolute errors in volume change measurement using proposed method.

Tests series	Max errors in specimen from slurry (cm^3)		Max errors in compacted specimens (cm^3)	
	consolidation	shear	consolidation	shear
25 kPa	0.03	0.06	0.17	0.07
100 kPa	0.07	0.03	0.11	0.03
200 kPa	0.09	0.11	0.12	0.18
400 kPa	0.15	0.14	0.22	0.10
Average maximum error	0.09	0.09	0.16	0.10
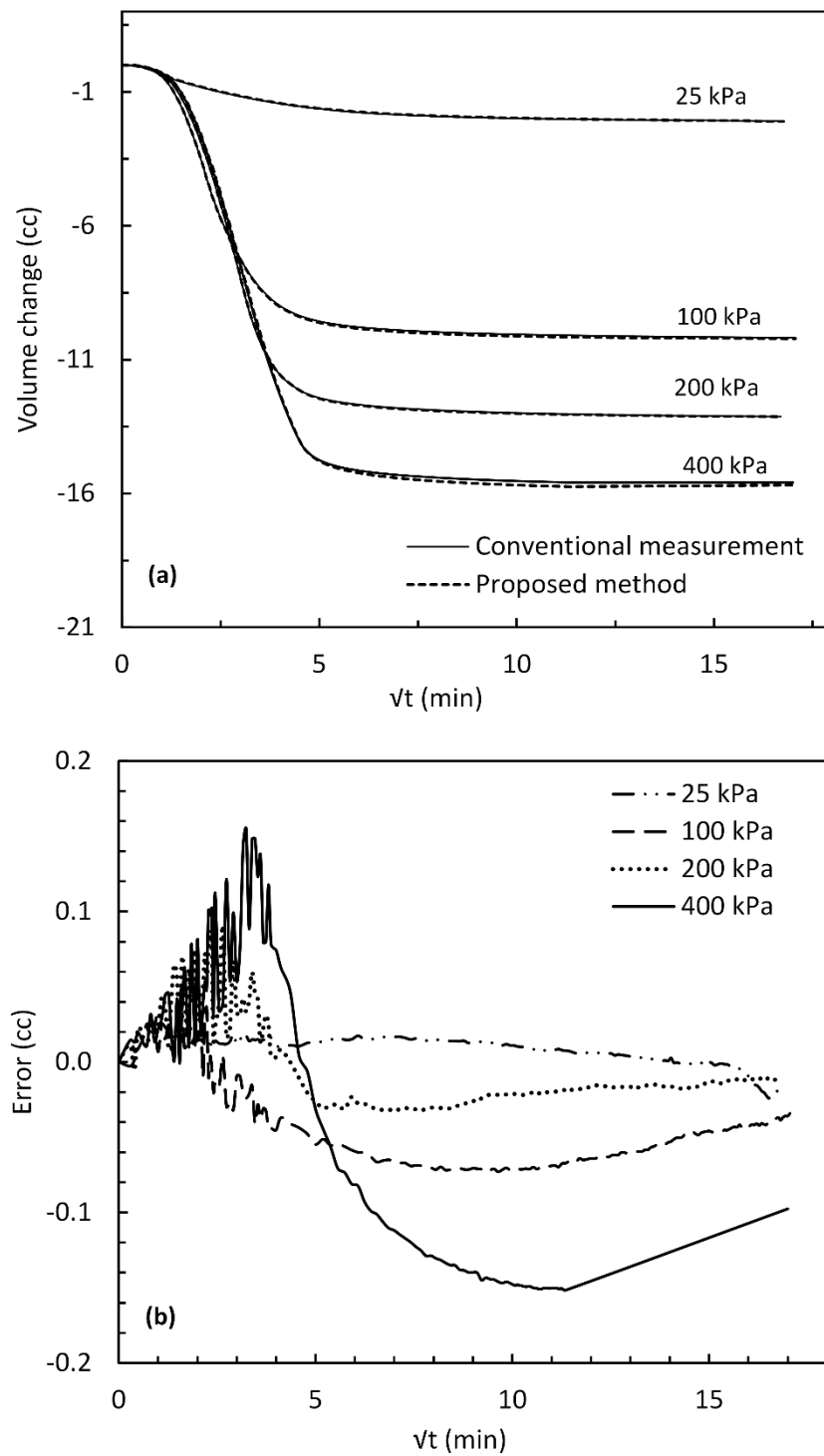
Figure 5.17 (a) Comparison of measured volume change during isotropic consolidation for specimen prepared from slurry, (b) amount of accumulated error versus squared time.
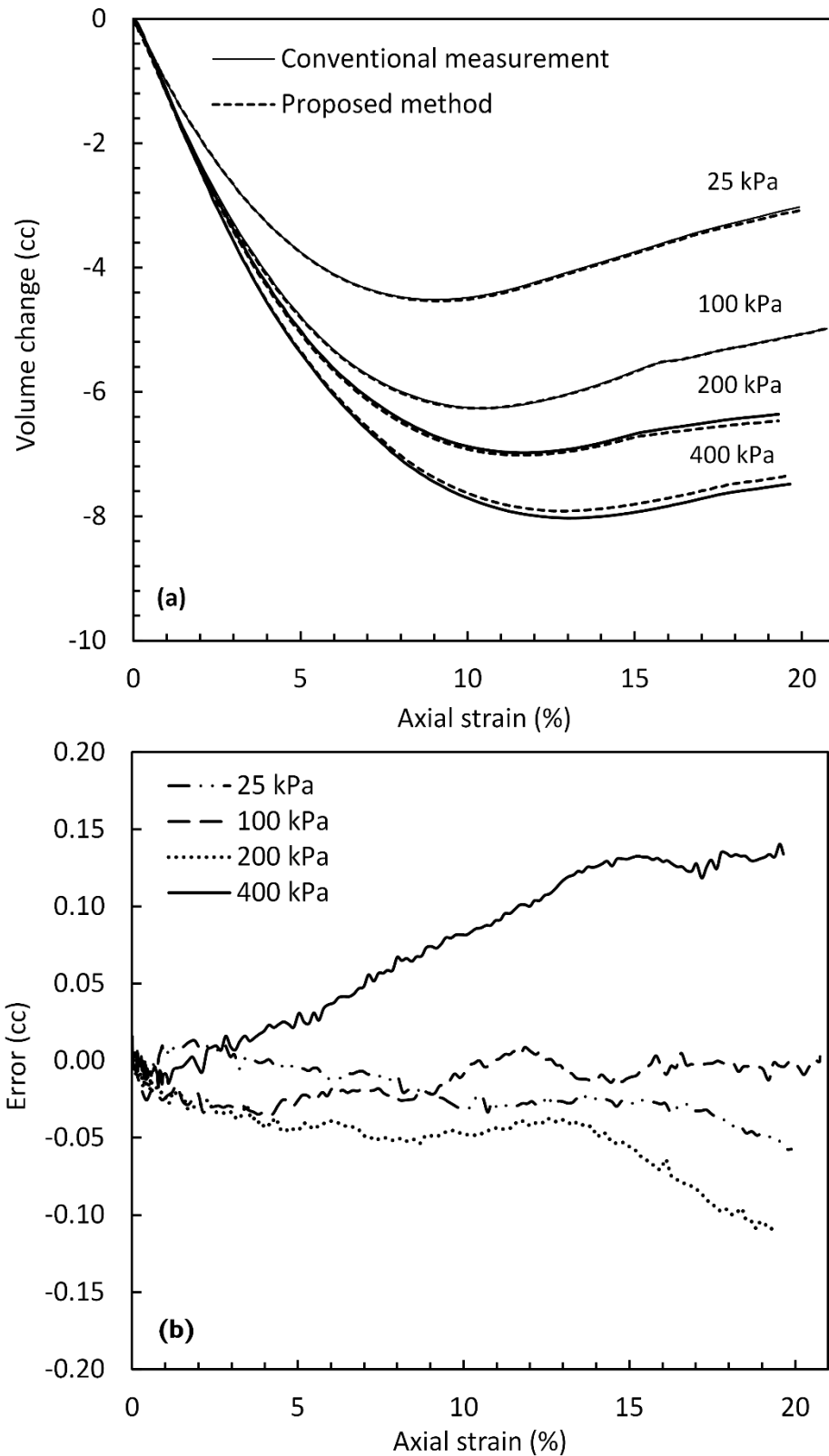
Figure 5.18 (a) Comparison of measured volume change during triaxial shearing for specimen prepared from slurry, (b) amount of error versus squared time.
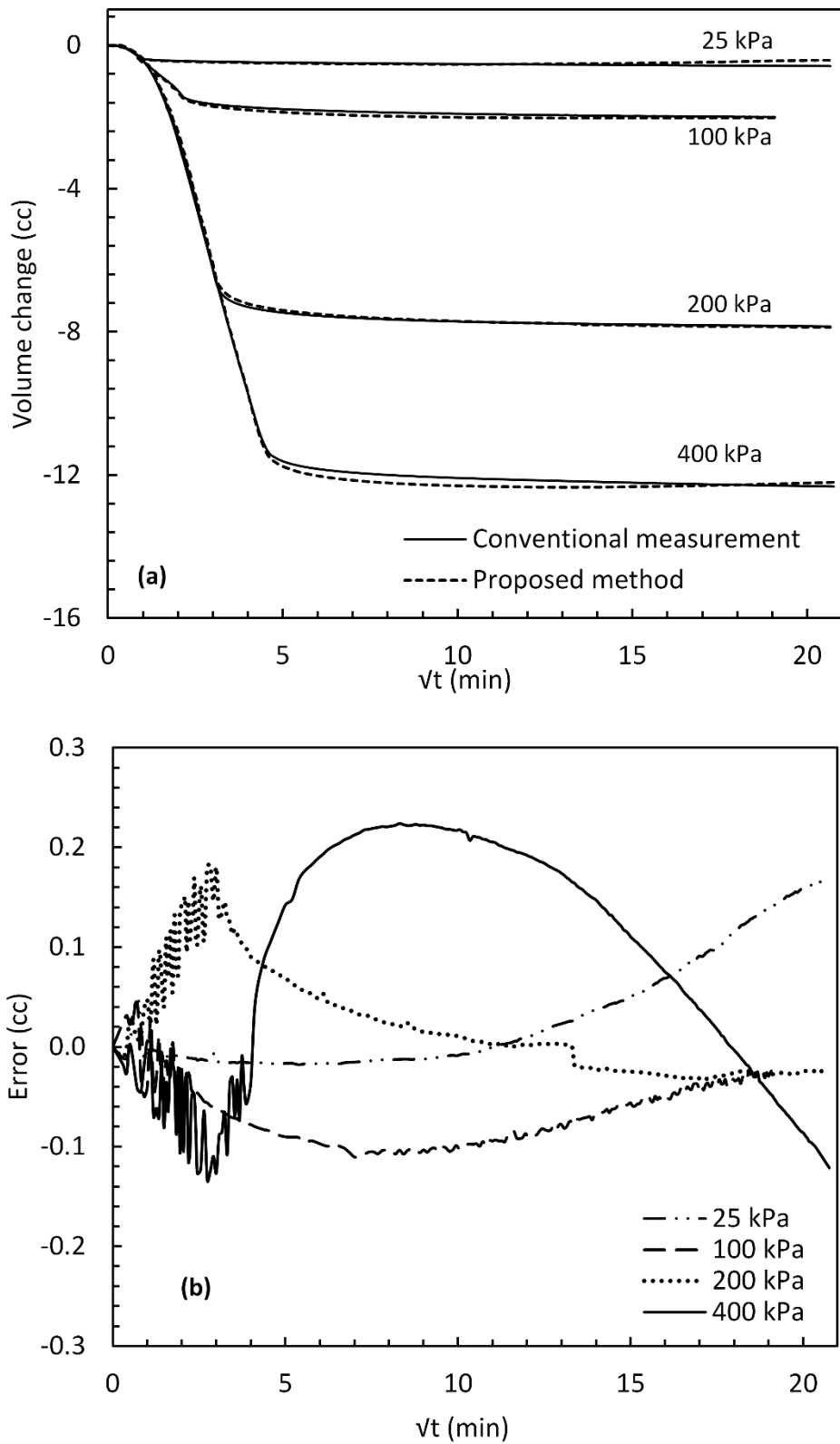
Figure 5.19 (a) Comparison of measured volume change during isotropic consolidation of compacted specimen, (b) amount of error versus squared time.
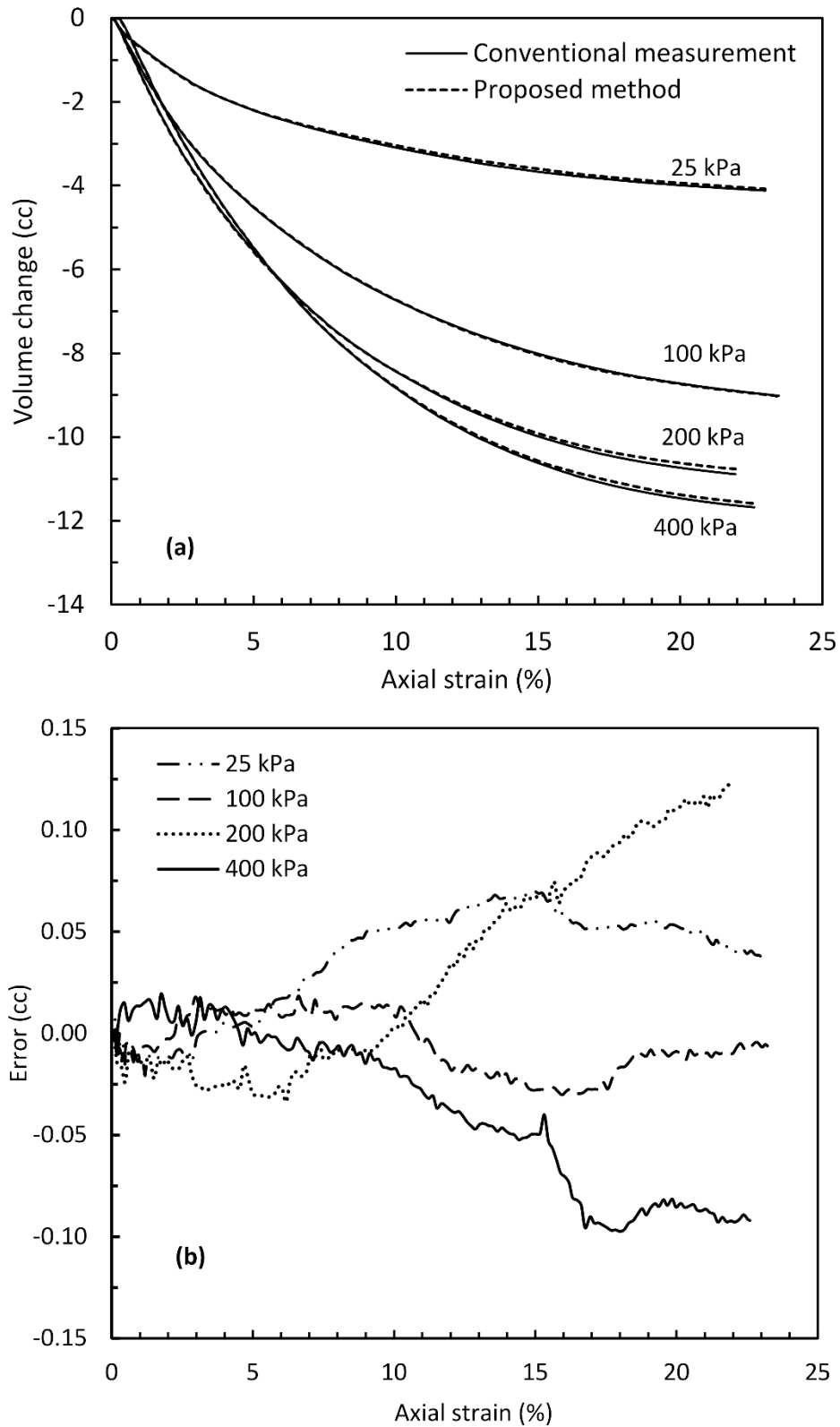
Figure 5.20 (a) Comparison of measured volume change during triaxial shearing of compacted specimen, (b) amount of error versus squared time.

To illustrate the capability of the technique in more complex stress history conditions, (i.e. loading and unloading cycles), a test of isotropic consolidation under five loading increments (25, 50, 100, 200 and 400 kPa) followed by five unloading steps were performed (the loading increment is kept for almost 10 hours). As shown in Figure 5.21, there is an almost perfect agreement between measurements of pore fluid flow and results of proposed method during loading.
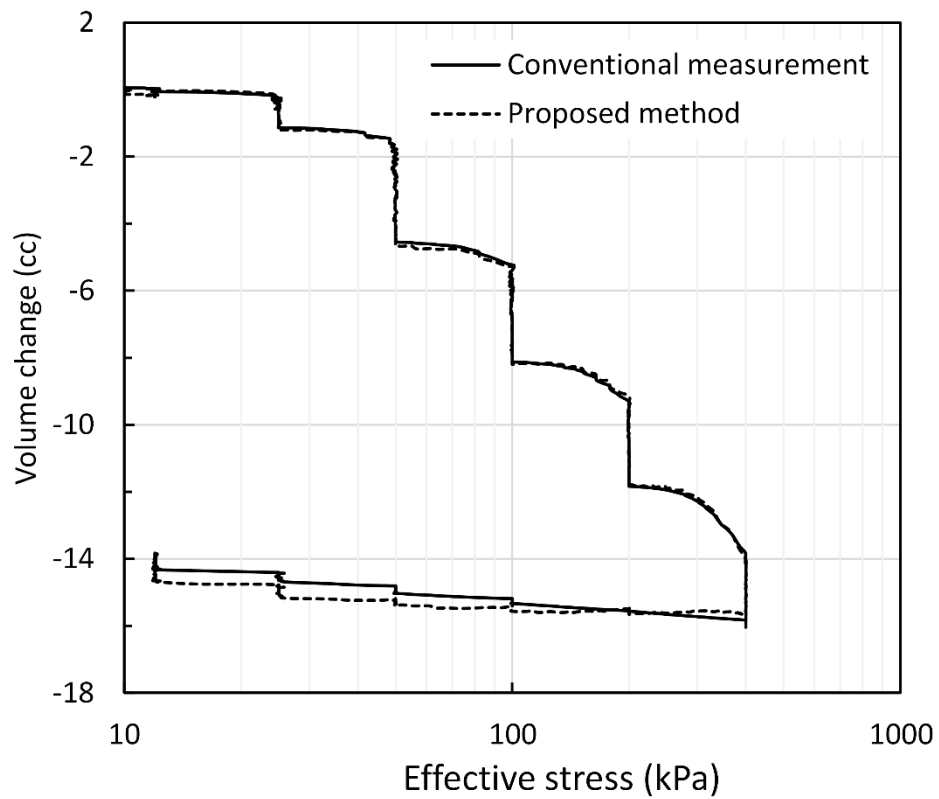
Figure 5.21 Comparison of measured volume change during isotropic consolidation.

83

5.6.2   Volume Change Measurement for Unsaturated Soil Testing

A series of suction controlled tests are performed to assess the repeatability of the proposed technique in unsaturated soil testing. Same tests were repeated thrice at each of 100 and 400 kPa suction on identically prepared specimens that are isotopically consolidated from slurry. Suction was controlled by axis translation technique (Hilf, 1956). The volume change of each specimen under given suction is measured with the proposed methods. Figure 5.22 compares these measurements, which appear consistent with each other at both suction values.
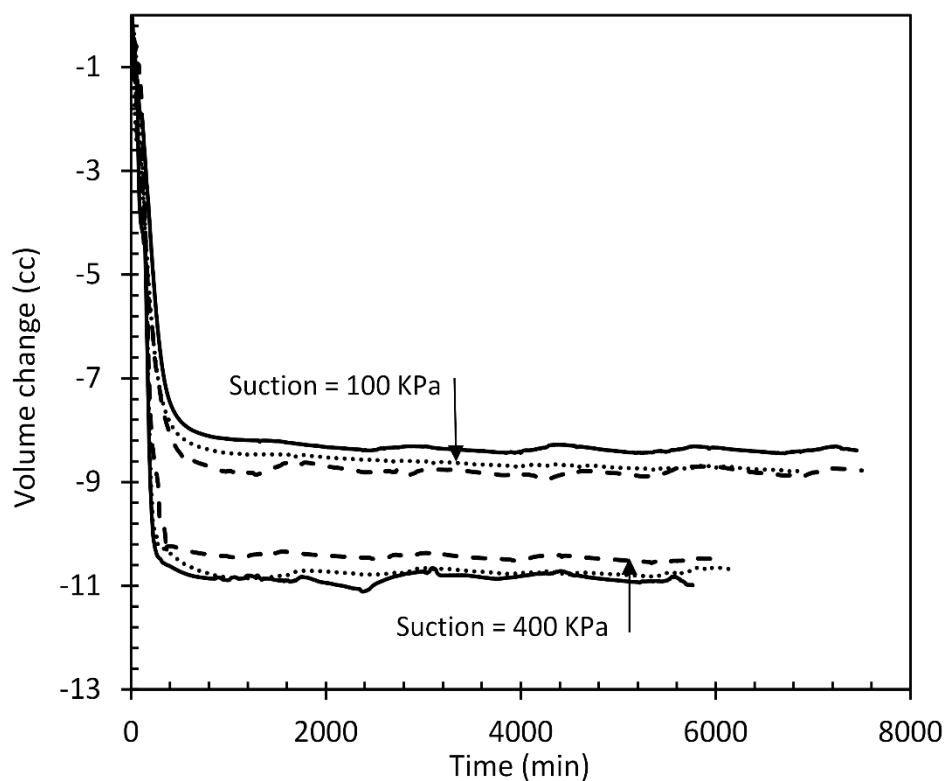
Figure 5.22 Comparison of measured and predicted volume change during suction equalization for 100 and 400-kPa suction.

CHAPTER 6

SPECIMEN PREPARATION PROCEDURE

A new procedure for preparation of low-Plasticity silt specimens isotropically reconstituted from slurry is developed for use in both saturated and unsaturated soil testing. The uniformity of the specimen (regarding void radio and segregation) and repeatability was investigated to confirm the performance of the method. The strength and volume change behavior of specimens prepared by the introduced method are compared with those of compacted specimens as well as and one-dimensionally reconstituted slurry specimens, by performing consolidated drained (CD) triaxial tests. New preparation method results a homogenous specimen, which have a simple structure and stress history.

The stress-strain behavior of low-Plasticity silts has not been investigated as thoroughly as clays and sands. Generally, silty soils have been considered to behave either as sands or as clays. In addition, most of the constitutive models are developed based on the laboratory testing of clays and sands and assuming isotropy. To some extent, this can be attributed to difficulty of obtaining intact samples or reconstituting uniform laboratory specimen to simulate the field condition.

As far as unsaturated soil mechanics is concerned, past two decades have seen rapid advances in both constitutive modeling and laboratory study. However, most of these achievements are obtained in the light of testing programs on compacted specimens. Sheng et al. (2008) have raised some unanswered questions about behavior and modelling of specimens dried and loaded from slurry. A search of the literature on unsaturated soil testing revealed only few studies had been conducted on reconstituted specimens from the slurry (Jennings and Burland 1962, Cunningham et

al. 2003). This is due to long duration and practical difficulties, in preparing and desaturating slurry specimens.

Generally, specimens are prepared one-dimensionally and then subject to isotropic pressure in the hope that it will erase the precedent loading history. However, this procedure can lead to a complex stress history in the specimen.

In this study, a new slurry preparation procedure for testing both saturated and unsaturated soils is developed. The shear strength and volume change behavior of specimens prepared with the new procedure are compared with those of specimens prepared by moist tamping and one-dimensionally reconstitution from slurry.

6.1 Review on Specimen Preparation Techniques

It is difficult to ignore the effect of specimen preparation method (which translates into soil fabric) on the engineering behavior of the soil elements in laboratory tests. Preparing reconstituted specimens is inevitable especially when assessing the impact of changing certain parameters of the sample (i.e. parametric study). Key parameters to be controlled during reconstitution are water content and density (or void ratio).

Depending on initial and desired soil properties, various specimen preparation techniques have been developed. According to the literature, the most preferred specimen preparation techniques for triaxial testing are as follows:

1. Moist tamping, and moist tamping with under-compaction,
2. Funnel deposition
3. Air pluviation (or dry pluviation)
4. Water pluviation (or water sedimentation)
5. Reconstitution from slurry.

Preparing reconstituted specimens by employing moist tamping technique dates back to 1951 by Lambe. This technique is applicable for most soils and is capable to control both density and water content at small degrees of saturation such that the air phase is continuous (Germaine and Germaine 2009). The specimen is prepared by mixing the dry soil sample with water to achieve desired water content. Then the given

amount of soil sample is poured into preparation mold and compacted with a tamping rod to a height, which corresponds to the volume that achieves the desired density. The specimen is prepared in several layers to increase the homogeneity of the final product. Nevertheless, compacting consecutive layers can transfer extra energy to and cause undesired densification of the lower layers. The non-uniformity of specimens prepared with moist tamping is a well-known issue, and confirmed by several researchers (Castro et al. 1982; Gilbert and Marcuson 1988; Vaid and Negussey 1988; Vaid and Sivathayalan 2000; Frost and Park 2003).

To overcome this issue and produce more uniform specimens, Ladd (1978) proposed moist tamping with under-compaction technique. In this technique, the lower layers are under compacted (to a density lower than the target density) with a predetermined percentage of density reduction. The percent of under-compaction through the layers changes linearly from the maximum value at bottom to zero for the upper layers. Sample mixing and molding procedure in this technique is same as the moist tamping technique.

An issue, which we encountered in the preliminary tests of this study, is the deviations in the cross sectional area of the top and bottom of each layer that appeared after the consolidation, making the boundaries of each layer easily recognizable (see Figure 6.1). This is because of the non-uniform distribution of compaction energy within the layer (i.e. the surface of each layer receives more energy compared to its bottom and densifies to a higher density). This phenomenon is especially most common in the case of fine-grained soils and can be reduced, but not eliminated, by compacting in thinner layers. Even employing the under-compaction technique, the variations in density within each layer remain a problematic issue.

Air and water pluviation techniques have been developed and extensively employed to reconstitute sandy specimen (Emery et al. 1973; Rad and Tumay 1987; Vaid and Negussey 1988). In air pluviation, specimens are created by raining the dry sand through a small container with holes at the bottom (similar to a saltshaker). Density of the specimen could be controlled by adjusting the falling height of the particles. Water pluviation is done in a same procedure except that the pluviation medium is

water. The main disadvantage of these methods is the segregation of particles, which limit the applicability just to poorly-graded sands.

Figure 6.1 Deviations in the cross sectional area after consolidation stage.

To produce uniform, non-segregated and initially saturated specimens of cohesive soils, the material is consolidated from slurry. This method can be performed in three different procedures: 1) slurry sedimentation, 2) one-dimensionally consolidating and preparing a block specimen, and 3) preparing in place specimens.

Emery et al. (1973), Ishihara et al. (1978) and Kuerbis and Vaid (1988) employed a slurry deposition method for silty sand and sandy silt soils. This method includes mixing and shaking soil samples inside a capped ended cylindrical tube filled with

de-aired water to get a homogeneous slurry. The slurry could be subjected to vacuum for a while to eliminate entrapped air bubbles. After ensuring the uniformity of the sample by shaking the cylinder, the top cap of the cylinder is replaced with a porous stone and filter paper. The tube is transferred and inverted inside the triaxial split mold and membrane that are already filled with de-aired water. The slurry is deposited in the mold by raising the tube. The main objective of this method was reproducing specimen with soil fabric similar to natural sedimentation soils and overcome to the segregation of particles, which is the disadvantage of water pluviation method. Later, this method was employed by other researchers (Salgado et al. 2000; Carraro and Prezzi 2008) successfully. Tastan and Carraro (2013) modified the method adopted by Carraro and Prezzi (2008) to reconstitute hollow cylinder specimens of clean or silty sands, deposited under water. Ishihara et al. (1978) demonstrated that when the amount of fine content ranges between 30 to 80 percent, this method fails to produce a uniform specimen. In most of the cases in the literature the maximum amount of fine content of the sample is less than 20 percent.

The other procedure of the preparing specimen from slurry was introduced by Sheeran and Krizek (1971). This technique includes one dimensionally consolidating a slurry, prepared with initial water content of 2 to 2.5 times the liquid limit, in a large consolidometer to a desired pressure to create a block sample. The test specimen needs to be trimmed to the dimensions to perform the laboratory tests. Trimming is this technique's disadvantage, being a sophisticated and time-consuming procedure. During trimming, specimen may be damaged and disturbed. Therefore, it is required to prepare specimens under high consolidation pressure. In this case, at low confining pressures, which is the case in most of the engineering problems, specimen behaves like an overconsolidated specimen. This technique is more suitable for highly plastic fine-grained soils, preparing low plastic silts without some amount of disturbance is difficult.

There are several issues that may be disadvantageous when using this method. In this technique, a sample with large dimensions is created, therefore a long time is required to complete the consolidation. Secondly, from each block sample, several specimens are obtained and each specimen has to wait for its turn in the testing program. This

requires the development of additional procedures for sealing, handling and storing the specimens. Another issue is wasting large amount of possibly scarce material during the trimming process, as the re-drying and re-powdering is not desirable. Finally, due to sidewall friction in the consolidation tank, a non-uniform sample with noticeable water content gradient, which means variation of density, may be obtained. Mandeville and Penumadu (2004) reported a 15% variation of water content from top to bottom of their sample. To overcome this shortage and to minimize the frictional effects, they lined the consolidation tank with Teflon and sprayed the inner walls with silicon to minimize the frictional effects between the walls and the slurry. In this way, the water content was varied only by 2.85% from top to bottom.

To overcome some of the deficiencies of the one dimensionally consolidated specimen as a block, Donahue (2007), and Wang et al. (2011) prepared the specimen inside the triaxial mold. This technique includes pouring the slurry inside the mold and one dimensionally consolidating the specimen from top, to achieve the desired height. Like the previous method, the friction between the slurry and the membrane results a non-uniform density distribution along the specimen height. In order to reduce this effect the specimen is subjected to a vacuum equal to the vertical pressure from the bottom. Hyde et al. (2006) prepared the specimen from the slurry in the same procedure, however, instead of vertical loading, they applied 10 and 40-kPa negative pore water pressure through base of the sample to bring out the excess water.

6.2 Preparing Isotropically Reconstituted Specimens from the Slurry

In this study, a new slurry preparation procedure for testing both saturated and unsaturated low plastic silts is developed. The purpose is producing loose and homogenous specimens, starting the entire application of confining pressure from the normally

6.2.1 Materials

The soil used in this study (from Mersin, Turkey) is classified as low plasticity silt, ML, according to the Unified Soil Classification System (USCS). The index properties of the soil are presented in Table 6.1. The results of the modified Proctor

compaction test of the sample indicated a maximum dry density, 1.86 g/cm3 at an optimum water content of 14.2%.

Table 6.1 Summary of index properties of soil used in this study.

Soil properties	Description/value
Specific Gravity Gs	2.72
Liquid Limit (%)	25
Plastic Limit (%)	20
Plasticity Index, IP (%)	5
USCS classification	ML
Maximum dry density g/cm3	1.86

6.2.2 Preparation Procedures for saturated Soil Testing

The slurry was initially prepared by thoroughly mixing a given mass of air-dried soil with distilled de-aired water, at a water content of about 1.5 times the liquid limit. The preparation water content plays a key role in uniformity of the sample. Air bubbles could be occluded at lower water content and high-water content may cause stratification (Kuerbis and Vaid 1988).

The slurry is sealed and tempered in the humid room for at least 24 hours to achieve uniform water content. Then, the slurry is subjected to vacuum to eliminate the entrapped air pockets. Following vacuum, the sample is mixed thoroughly with a pestle to get a homogeneous slurry. It is noticed that about 0.2% of water content decreases during these procedures. Therefore, to compensate to this, the preparation water content should start at 0.2 % greater than the desired value. A saturated porous stone and a filter paper are placed on the triaxial pedestal. Then, a membrane is positioned around the pedestal. To prevent leaks, high-vacuum grease is applied around the pedestal before placing the membrane. Using a pair of O-rings, the membrane tightly is sealed to the pedestal.

The split mold is mounted on the triaxial base, around the membrane. In order to apply vacuum, and later, confining pressure, to between the membrane and the split mold, a filter paper covers the inner surface of the mold. Then the upper part of the membrane is folded around the mold. Vacuum is applied, between split mold and membrane, to stretch and hold the membrane tight to the mold. Then the entire triaxial base with the mold on it is placed on a digital balance to control the deposited mass of the slurry. The slurry is poured into the mold and gently mixed with a spoon to prevent entrapment of the air bubbles. After filling the split mold with the desired mass, the specimen is left for two hours to consolidate under its own weight, to lose some of its liquid consistency. To limit the evaporation, the split mold is covered with a wet towel. The change in volume of the water is monitored using the pressure volume actuator of the triaxial setup, which is set to keep the pore pressure at zero (i.e. atmospheric pressure). For all tests on this material, less than 1-cm^3 water outflow is measured at this step. Next, a filter paper and a saturated porous stone along with the triaxial top cap are placed on top of the specimen. Then the membrane is unfolded over the top cap, sealed with two O-rings and the vacuum line is removed. The specimen in this condition is in the loose state and prone to damage. Therefore, the split mold is kept in place to support the specimen. Then the triaxial cell is assembled, filled with water and pressurized. The objective is preparing normally consolidated specimens, thereby specimens are consolidated to 10-kPa effective confining pressure. The loading rate should be slow enough to avoid any excess pore pressure generation in the specimen. This is accomplished by ramping the cell pressure at a rate of 0.1 kPa/min. The filter paper between the split mold and membrane provides an equal distribution of stress throughout the specimen. This step takes almost eight hours to expel about 23-cm^3 of pore water for this sample material.

Once the consolidation is completed, the drainage valve is closed. The vacuum pump regulator is adjusted to 10 kPa, and connected to drainage line. Then the cell pressure is released, and simultaneously the drainage line is opened to the mild vacuum. As a result, an identical effective stress as consolidation pressure is applied to the specimen. In light of the applied vacuum, the risk of the specimen disturbance decreases to the minimum.

Following draining the cell fluid, the split mold is dismantled. The specimen is ready for testing, and its initial dimensions are measured. The triaxial cell is reassembled and filled with distilled de-aired water to perform the desired test.

6.2.3 Preparation Procedures for Unsaturated Soil Testing

The axis translation technique (Hilf, 1956) has been widely adopted to control and induce matric suction in unsaturated soil testing. In this technique, it is common to use high-air entry value (HAE) ceramic at the bottom (to control pore-water pressure) and a coarse porous stone (to control pore-air pressures) on the top of the specimen (Bishop and Donald 1961; Josa et al. 1987; Sivakumar 1993; Rampino et al. 1999). In the case of preparing the specimen on the triaxial pedestal for testing unsaturated soils, the low permeability (i.e. the impedance) of the ceramic considerably prolongs the time of preparation.

To overcome the mentioned shortcoming, a triaxial base (pedestal and top cap) with a new arrangement is developed. The details of new pedestal and top cap is shown in Figure 4.5. The pedestal and top cap both have HAE ceramic at center and a peripheral annular porous metal. Consequently, the pore-water can be expelled much faster from the peripheral coarse porous metal from top and bottom during specimen preparation. Preparation procedure is identical with that for saturated soils.

6.2.4 Evaluation of Specimen Homogeneity

Void ratio and segregation are two key parameters that should be evaluated to verify the uniformity of the specimen. For this purpose, a triaxial specimen was prepared following the introduced procedure. After consolidating the specimen at 10-kPa effective stress, the drainage valve is closed, and the specimen is retrieved. The specimen is divided to five horizontal slices for void ratio and grain size analysis. Assuming full saturation and using Eq (6.1), the void ratio is proportional to the water content.

$$S_r.e = G_s.w \tag{6.1}$$

Therefore, the water content of each slice was determined. Figure 6.2 shows the spatial variation of water content throughout the specimen height. A maximum absolute difference of 0.75% in water content was observed between the topmost and bottommost slices. This difference could be considered acceptable, as the absolute error margin for water content measurements is 0.5% (ASTM D2216). The results of tests indicate an average void ratio of 0.72.

The effect of further consolidation on spatial variation of the void ratio is also investigated. For this, first a specimen was isotropically consolidated at 400-kPa effective stress, then unloaded to 10 kPa. Similarly, the specimen is sliced and the water content of each slice is measured. As shown in Figure 6.2, the water content is almost constant throughout the specimen height. It may therefore be assumed that a little variation in water content (and void ratio) during preparation could be compensated during consolidation.
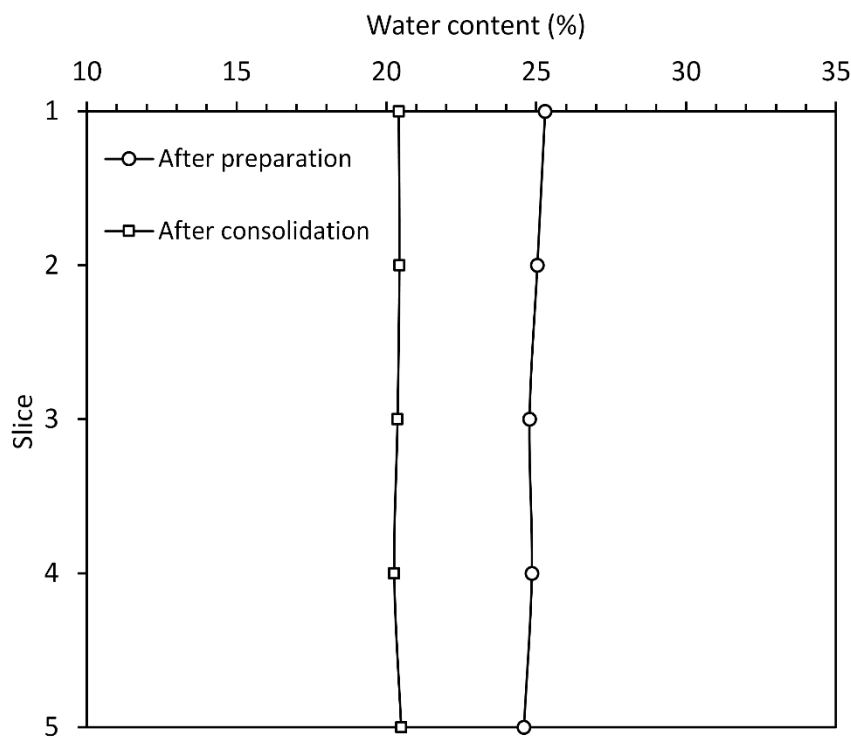
Figure 6.2 Spatial variation of water content after preparation (includes 10-kPa consolidation) and after consolidation under 400 kPa.

To examine particle segregation, grain-size analysis (ASTM D422) is performed on each slice (Figure 6.3). Figure 6.4 compares the grain-size distribution of the slices. The considerable agreement between layers confirms the success of the proposed method in preparing uniform specimens regarding grain-size distribution.

Figure 6.3 Hydrometer test on five divided horizontal slices.
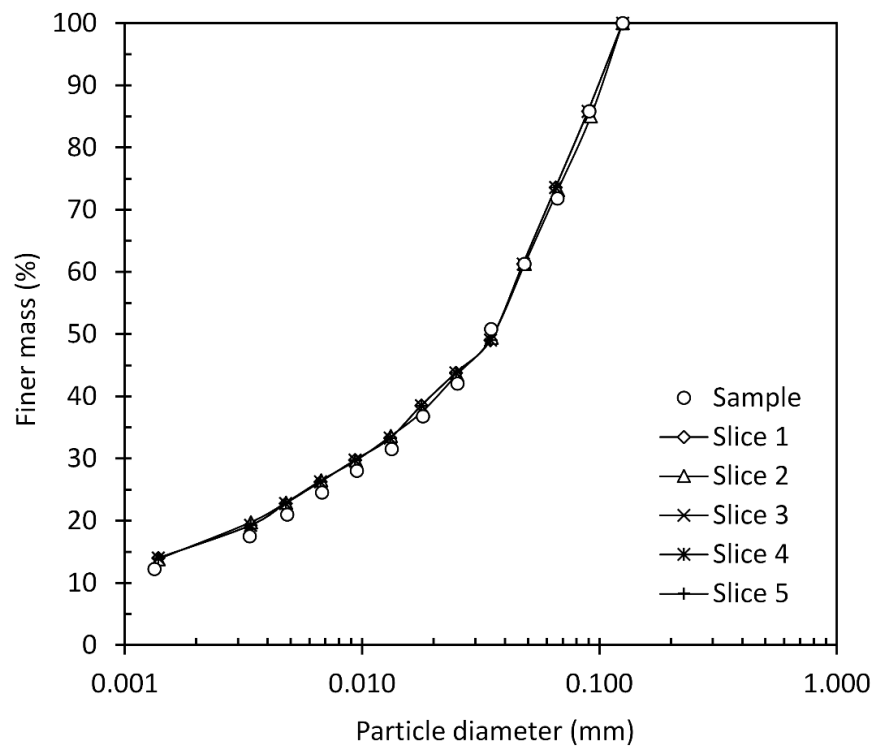
Figure 6.4 Comparison between the of grain size distribution of slices.

6.2.5   Evaluation of Repeatability

The repeatability of the proposed method in preparing identical specimens was investigated for both saturated and unsaturated soil testing. For saturated soil testing, a consolidated drained triaxial test was repeated twice at 100-kPa confining pressure on identically prepared specimens. Figure 6.5 (a) and (b) compare the stress-strain and volumetric response of the specimens. An excellent agreement between the results of two tests is evident, confirming the repeatability. Once tests are finished, the specimens are divided to five slices to measure the water content. Figure 6.6 illustrates the spatial variation in water content of the specimens. The results are very close, and the difference is within the acceptable error margin of the water content measurement (i.e. less than 0.5%)
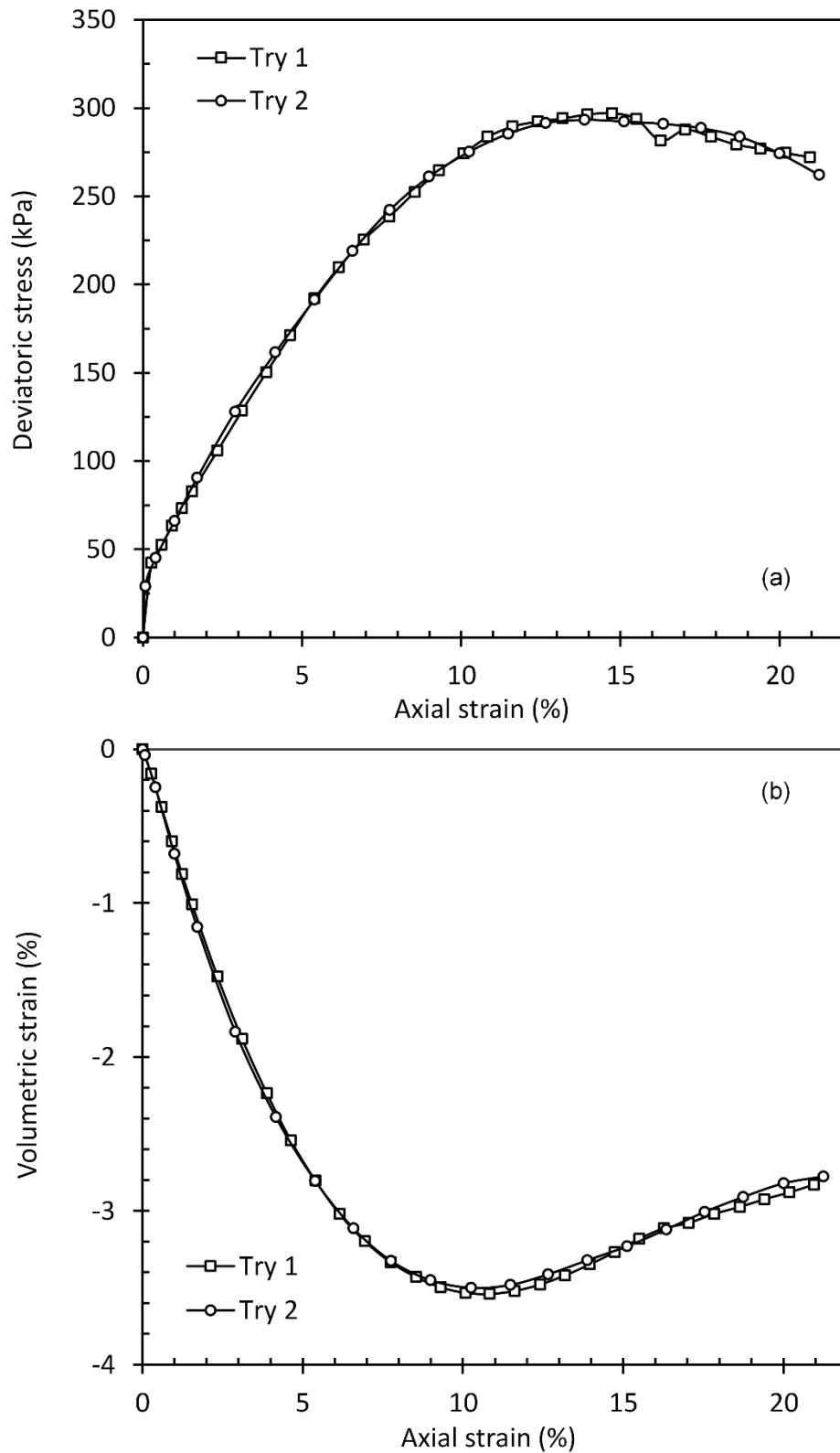
Figure 6.5 Repeatability of the proposed method for saturated soil testing (a) deviatoric stress-axial strain (b) volumetric strain-axial strain.
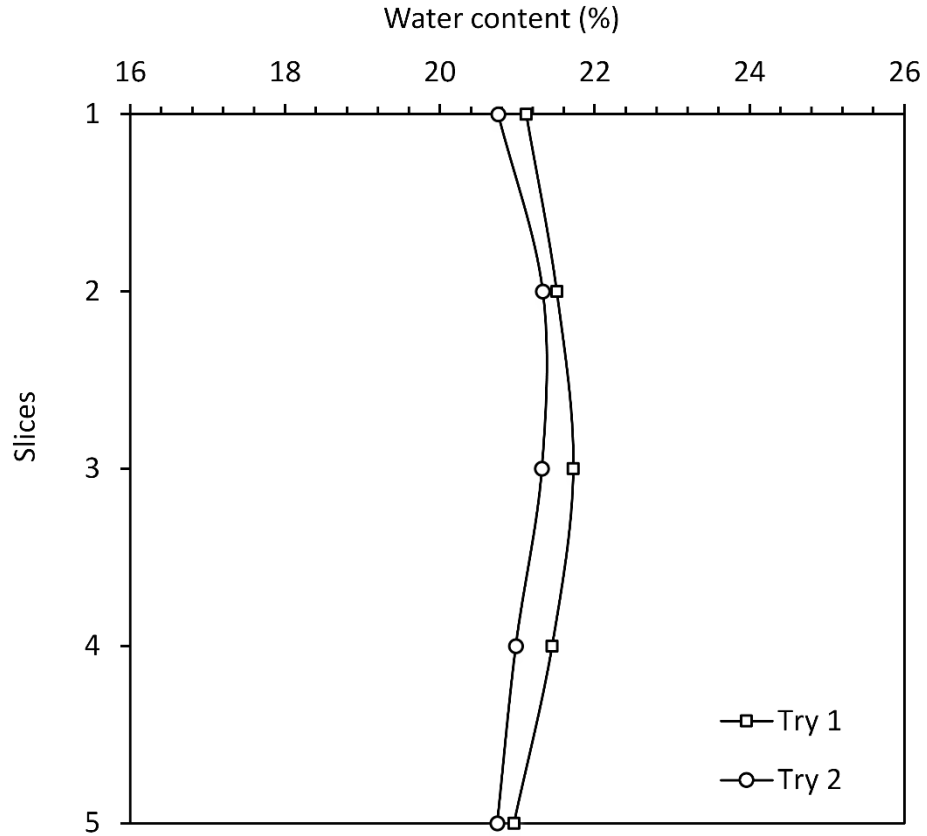
Figure 6.6 Spatial variation of water content.

For unsaturated soil testing, series of suction controlled tests were performed to evaluate the repeatability. For this, same tests were repeated thrice at each of 100 and 400-kPa suction on identically prepared specimens. Suction is controlled by axis translation technique. Figure 6.7 compares the pore-water volume change with time during suction equalization. Comparison of the results reveals agreement between the results, which confirm the repeatability of the proposed method for testing unsaturated soils.
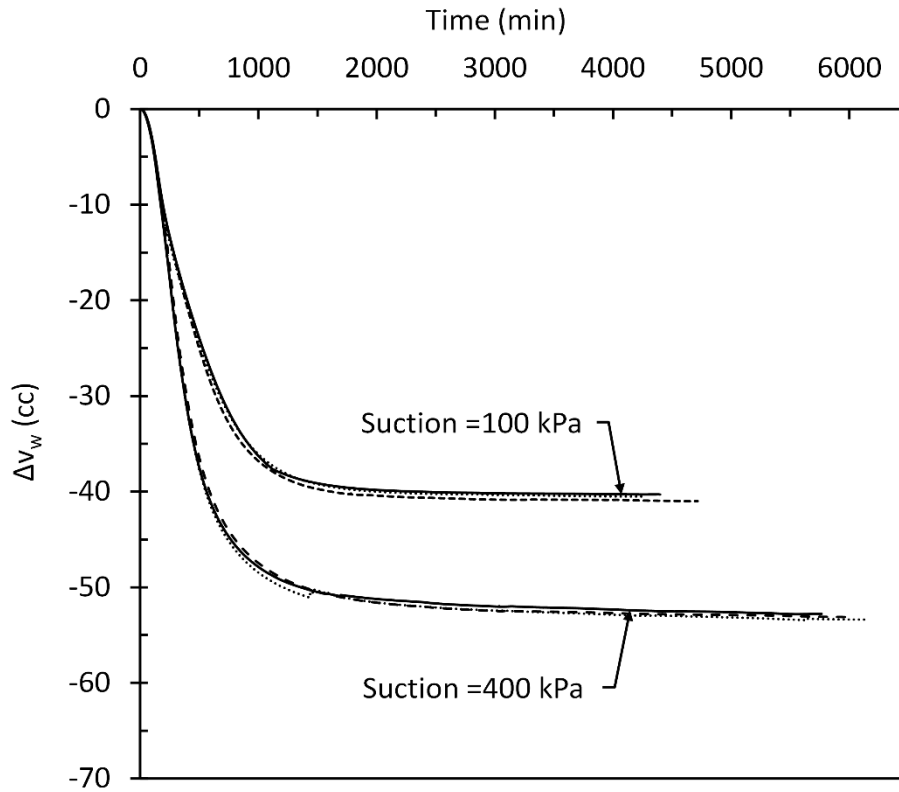
Figure 6.7 Repeatability of the proposed method for unsaturated soil testing.

6.3 Experiments Comparing Behavior of Specimens by Different Preparation Methods

The effects of preparation methods on strength and volumetric behavior of specimens are investigated (see chapter 9). For this, three sets of consolidated drained (CD) triaxial tests were performed on the saturated specimens prepared by three distinct preparation methods: a) isotropically reconstituted from slurry (IRS), b) one-dimensionally reconstituted from slurry (ORS) and c) moist tamping with under-compaction (MT) specimens (see chapter 7 for testing program).

6.3.1 Preparation Procedure of One-Dimensionally Reconstituted Specimens from Slurry (ORS)

The preparation procedure up to pouring slurry inside the membrane is identical to IRS. After that, the top cap and loading piston are placed on slurry and the specimen is left to consolidate in the split mold. The slurry was one-dimensionally consolidated by ramping the vertical loading at a rate of 1 kPa per hour. This rate was concluded

to be sufficient to complete the consolidation under each increment. The loading continues until the desired height is achieved. Following consolidation, the split mold is disassembled and the dimension of the specimen is measured. The results of tests indicate an average void ratio of 0.72.

6.3.2 Preparation Procedure of Moist Tamping Specimens with Under Compaction

To speed up the saturation, carbon dioxide is circulated along with vacuum before back pressure saturation.

Triaxial specimens with 5-cm diameter and 10-cm height and initial void ratio of 0.72 are prepared by the under-compaction method (Ladd, 1978) on the triaxial pedestal, in 10 layers.

The following expression (Germaine and Germaine 2009) is used to calculate the percentage of undercompaction for each layer:

$$U_n = U_1 \left(\frac{m - n}{m - 1}\right) \tag{6.2}$$

The height at the top of each layer was calculated using the following expression:

$$h_n = \frac{h}{m}[(n - 1) + (1 + u_n)] \tag{6.3}$$

where,

h_n = height to top of layer n (mm),

m = total number of layers

h = total height of specimen (mm)

n = layer number

U_n = undercompaction for layer n (decimal)

U_1 = undercompaction of the first layer, which is the bottom layer
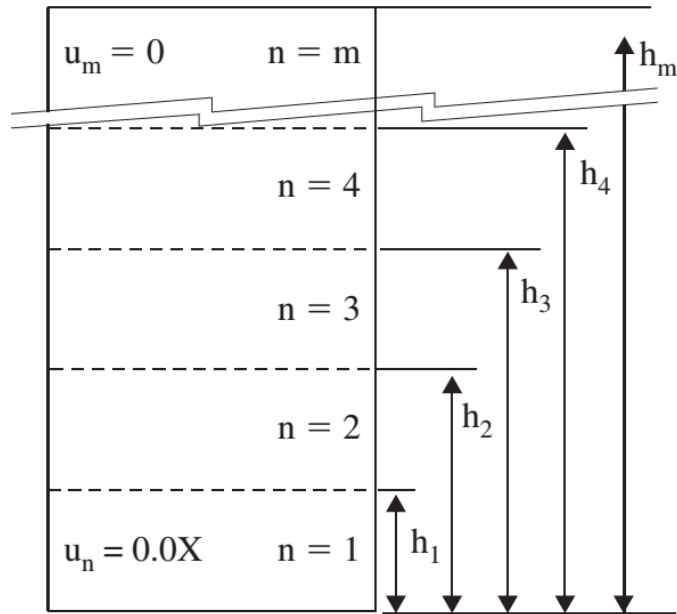
Figure 6.8 Schematic diagram of determining percentage of undercompaction and height of layers (Germaine and Germaine 2009).

The preparation equipment consists of a conventional split mold and custom made hammer (see Figure 6.9). This hammer includes a steel rod for tamping and an adjustable collar for precise control of layer height.
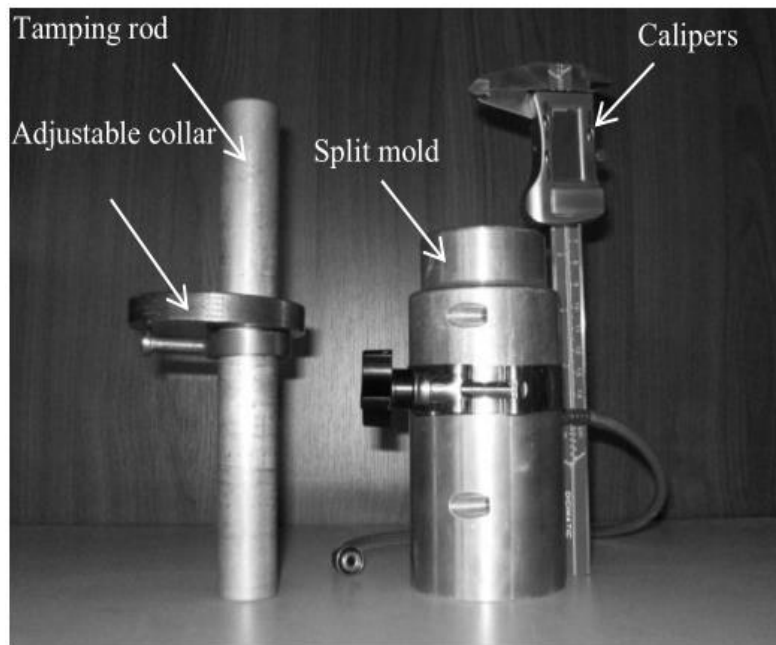
Figure 6.9 Equipment used for compaction.

Initially, the entire sample was mixed as a single batch, from which the soil was taken as small portions for each layer. However, this meant the lowermost layer, as it is placed first, had the highest water content, and as the soil of the following layers had waited longer, evaporating, they had gradually decreasing preparation water contents. To eliminate this error and to prepare uniform specimens, material is mixed in 10 different dishes, each with the desired water content. A syringe is used for precise control of the amount of water added to the soil. Before placing the material of each layer into the mold, its water content is measured prior to placement.

The membrane is placed around the triaxial pedestal and sealed with two O-rings at bottom. Then split mold is placed around the membrane. The membrane is then folded around the mold and vacuum is applied to hold the stretched membrane tight to the mold. Then each layer is placed and compacted to the desired density by controlling the height of the layer for a given mass of soil (see Figure 6.10). After preparing the specimen the top cap is placed on top of the specimen and the membrane is rolled around the top cap and sealed with two O-ring. A porous stone and a filter paper are placed on the triaxial pedestal. Then the membrane is unfolded over the top cap, sealed with two O-rings and finally split mold is dismantled. The specimen is ready for testing, and its initial dimension are measured. Then the triaxial cell is filled with distilled de-aired water. Next, the test conditions are specified and triaxial test is controlled by the computer from start to finish.
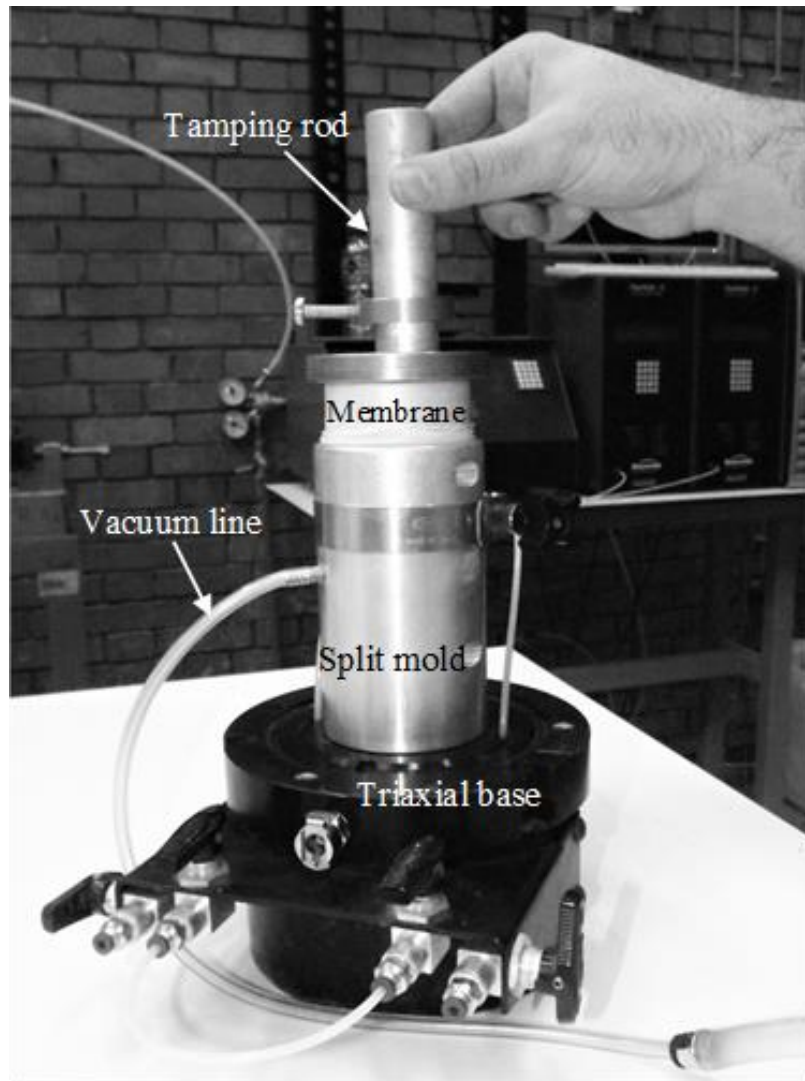
Figure 6.10 General arrangement for moist tamped compaction.

CHAPTER 7

TESTING PROGRAM AND PROCEDURE

This chapter first presents the properties and criteria used for selecting the testing soil. It is followed by presenting the testing program and related stress paths. Then, the procedures and methods to obtain SWCC and to perform suction controlled triaxial tests on both IRS and MT specimens are presented.

7.1 Testing Material

The main objective of this study is investigating the coupling of hydro-mechanical behavior of unsaturated reconstituted specimen. An appropriate soil had to be selected in order to achieve the objectives of this study. The following criteria were considered in selecting the sample:

- The grain size is the first important criterion when selecting the proper soil sample. The soil had to be fine enough to see the influence of the matric suction on the shear strength and volumetric behavior of the unsaturated soil specimens clearly. On the other hand, soil had to be coarse enough to exhibit significant changes in degree of saturation within the suction range of the testing apparatus (i.e. low residual matric suction)

- The soil sample had to be none or low-plastic to avoid difficulties associated with plasticity (such as possible effects of particle surface charges).

- The selected soil could not be potentially problematic soils (expansive or collapsible soils).

- The soil could exhibit solidification behavior with time due to its mineralogy. Therefore, this effect had to be investigated when selecting the soil sample.

Considering these criteria, low or non-plastic silty soils were deemed appropriate for this study. For this purpose, three different soil samples were examined; namely, M100, quartz, and Mersin silt.

M100 and quartz are artificial (and commercially available) soils. The grain size analysis were performed where all the particles were finer than 0.075 mm (No. 200 sieve). The hydrometer test, according to ASTM D 422, were performed and their grain size distributions are shown in Appendix A.

The Atterberg limits and specific gravity tests were performed to determine the index properties of the soil samples. The SWCC of the soil samples for compacted specimens with dry density of $\rho_d=1.3$ g/cm^3 were obtained from pressure plate test. The testing results are presented in appendix A. According to the Unified Soil Classification System, soils were classified as low-plastic silt, ML. In view of the testing results, quartz and M100 were felt to be the appropriate for testing program. Therefore, additional triaxial tests and consolidation tests were performed on saturated compacted specimens. However, it was recognized, that both soils are unsuitable for this study due to following reasons:

- For M100, during saturation phase in triaxial tests, collapsible behavior was observed. The procedure suggested by ASTM D5333 was followed to measure the collapse potential of the soil sample (at given density and water content). The Collapse Index (I_e) (for the applied vertical stress of 200 kPa) is determined to be 8.9 percent. According to ASTM, this "collapse potential" is classified as Moderately Severe.
- For quartz, the CD triaxial tests were performed on compacted specimens with no problem. However, for specimens prepared from slurry, solidification behavior was observed.

The same tests and procedure were repeated for silty soil from Mersin. The index properties of the sample are determined through laboratory tests as summarized in Table 7.1. The soil is ML according to the Unified Soil Classification System (ASTM D2487-11). The grain-size distribution is shown in Figure 7.1. The SWCC of the soil

samples for compacted specimens were obtained from pressure plate test (Figure 7.2). In view of the aforementioned criteria and testing results, the Mersin silt was chosen.

Table 7.1 Summary of index properties of Mersin silt used in this study.

Soil properties	Description/value
Specific Gravity Gs	2.72
Liquid Limit (%)	25
Plastic Limit (%)	20
Plasticity Index, IP (%)	5
USCS classification	ML
Maximum dry density g/cm3	1.86
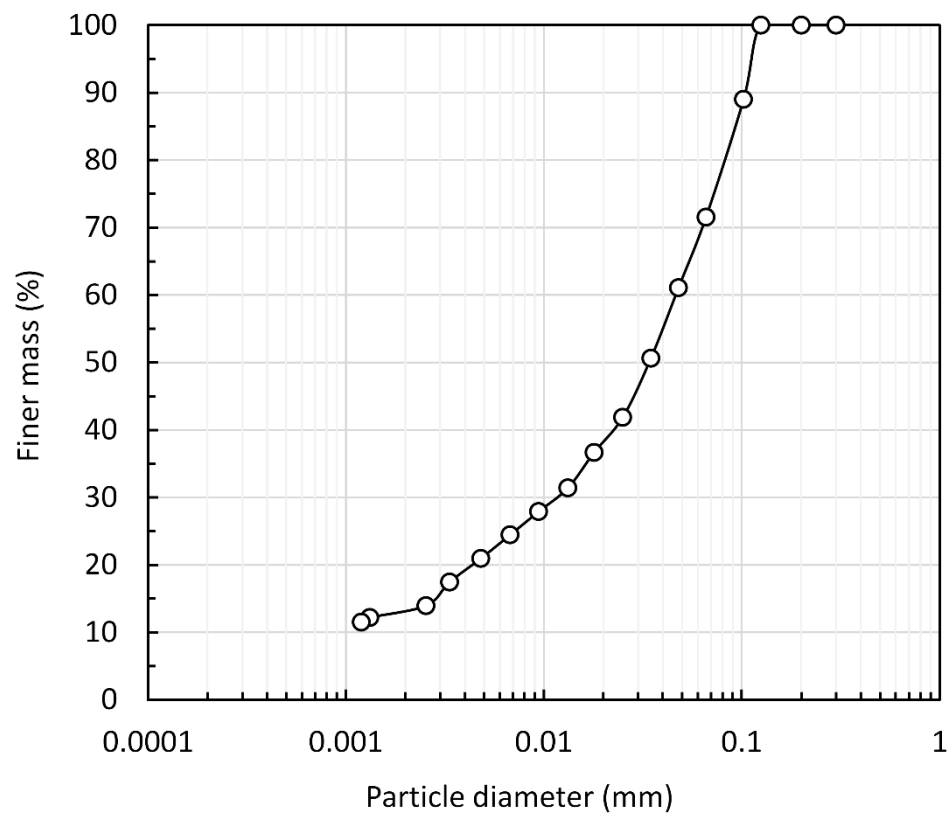
Figure 7.1 Grain size distribution of Mersin silt.
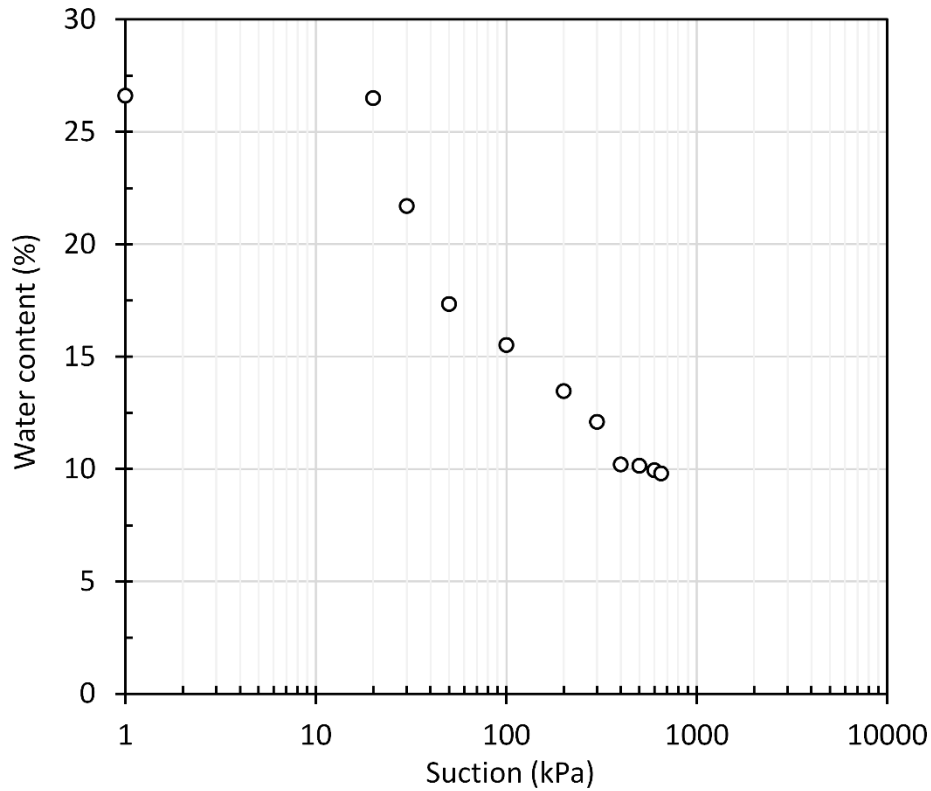
Figure 7.2 Soil water characteristic curve of Mersin silt from pressure plate test.

7.2 Testing Procedure for the Suction Controlled Triaxial Tests

7.2.1 Equalization Stage

The initial step in triaxial testing of unsaturated soils (after preparing and setting up the specimen), is to apply the desired suction. In this study, axis translation technique is employed to control and induce matric suction. Different values of suction (defined as the difference between pore air pressure, u_a, and pore water pressure, u_w) can be applied by regulating the air and water pressure. To prevent inflation of the membrane inside the triaxial cell, the air pressure should always be lower than the confining cell pressure (i.e. net confining stress must be positive). Water will flow into the specimen (wetting) if the applied suction is less than the initial value, and water will drain out (drying) if the applied suction is greater than the initial suction of the specimen. After reaching a desired suction, specimen is left to equalization under applied suction. The equalization implies full dissipation of the excess pore-water pressure under applied suction. The equalization stage can be terminated when the rate of water flow

decreases to less than 0.1 cm^3/day (Sivakumar 1993) for specimen with 5-cm in diameter and 10-cm in height.

The schematic layouts of the pore air pressure system and the pore water pressure system of the unsaturated soil testing setup are shown in Figure 4.6 and Figure 4.7. The following steps were followed during suction equalization stage:

- As a first step the cell pressure, air pressure, and water pressure are increased at a rate of 2 kPa/min to 75, 50 and 50 kPa respectively.
- The desired value of the suction, (at net confining stress of 25 kPa) is applied by gradually increasing (i.e. ramping) the cell pressure and air pressure a rate of 1.5 kPa/min. The cell pressure is controlled automatically through the TRIAXIAL software, but the air pressure is controlled manually through the air pressure regulator (see section 04.3.1 and Figure 4.6).
- The changes in volume of the pore water and the total volume of the specimen are monitored regularly. The equalization under the applied suction is completed when the rate of water flow decreased to less than 0.1 cc per day.

7.2.1.1 *Tests with Drying-Wetting*

Tests with drying-wetting include an equalization stage for the wetting path (at constant net stress) in addition to drying path. Once equalization for drying path was achieved, wetting path is initiated by reducing suction. This can be performed in two ways: (a) hold water pressure unchanged while reducing the air and cell pressure together (at the same rate, keeping a constant net confining stress) or (b) hold the air and cell pressure constant while increasing the water pressure.

Preliminary tests were performed to investigate the performance of each procedure. Problems were encountered when using the first procedure. During the long-term tests, the diffusion of air through the membrane could occur (despite all the measures). The dissolved air come out of solution in the form of the air bubbles with decreasing cell pressure (see Figure 7.3). In addition, it seems that the equalization time is shorter with the second procedure (i.e. when water pressure is increased). Beside these, in our setup the air pressure system is controlled manually, therefore,

holding air pressure constant and increasing the water pressure automatically through PVA is more convenient. Therefore, in this study the second procedure was adopted during wetting stage.

The suction was decreased at the same rate (1.5 kPa/min) during drying path i.e.. The same criterion as drying is adopted to end the equalization stage.

Figure 7.3 Photograph of air bubbles accumulated in triaxial cell after decreasing cell pressure.

7.2.2 Isotropic Compression

Following equalization stage specimens were isotropically compressed at constant suction. This can be achieved in two different manners: Ramped (gradual) loading and step-loading consolidation. The step-loading consolidation is the conventional method of consolidation in saturated soils testing and the ramped loading compression method mostly adopted in unsaturated soil testing.

Excess pore-water pressure can be generated with the step-loading compression that violate the assumption of constant suction.

In ramped compression method, it is possible to produce a continuous plot of the specific volume versus net mean stress to identify yield stress. The loading rate is selected slow enough to prevent generation of the excess pore-water pressure or maintain it within an acceptable margin.

Eq (7.1) proposed by Thomas (1987) to estimate the excess pore-water pressure, at the undrained face of the saturated specimens consolidated by ramped loading:

$$u_{ex} = \frac{Rh^2}{2c_v} \tag{7.1}$$

where R is the loading rate, h is the drainage path length and c_v is the coefficient of consolidation.

By selecting an acceptable value for excess pore water pressure, Eq (7.1) can be rearranged for R, as below:

$$R = \frac{2c_v\,u_{ex}}{h^2} \tag{7.2}$$

As mentioned this equation was initially suggested for saturated soils; however Sivakumar (1993) and Chiu (2001) commented that the generated excess pore-water pressure for unsaturated soil specimens is less than that for saturated specimen due to lower degree of saturation.

The loading rate of the ramped compression is estimated from Eq (7.2). For the range of confining effective stress, the coefficient of consolidation c_v, for saturated specimens prepared from the slurry is determined to be $c_v = 1.6 \times 10^{-6}$ m^2 /s. The value of maximum excess permissible pore water pressure is, selected to be 2.5 kPa. As mentioned in section 4.3, in this study, specimens were drained from both ends (double drainage) therefore, h is half the specimen height (i.e. h = 5 cm). Therefore, using Eq (7.2), the loading rate was determined to be 11 kPa per hour. To be conservative, the loading rate was selected to be 4 kPa/h for both specimen prepared from slurry and compacted specimens is:

The procedure followed during compression:

- A desired value of the net confining stress (σ_3 - u_a) is applied by keeping the air pressure and water pressure constant (i.e. constant suction) and increasing the cell pressure. The target cell pressure value and the corresponding rate is entered and controlled through the TRIAXIAL software.
- Once the desired value of the net confining stress is achieved, the specimen is left (under constant net stress and constant suction) for 24 hours, to ensure complete dissipation of the excess pore-water pressure.
- The changes in total and water volume and changes in height of the specimen are monitored throughout the test.
- The diffused air is flushed once a day following the procedure described in section 4.4.2.

7.2.3   Shearing at Constant Suction

Following consolidation, specimens is sheared at constant suction (i.e. drained condition for both air and water phase). The shearing is accomplished under strain-controlled (constant-rate) condition. The strain rate should be slow enough to ensure full dissipation of excess pore-water pressure during shearing. The strain rate can be represented as:

$$\dot{\varepsilon} = \frac{\varepsilon_f}{t_f} \qquad (7.3)$$

where ε_f is the strain at failure and the t_f is the corresponding time at failure. In order to determine the failure time Bishop and Henkel (1962) proposed the following equation for saturated soils:

$$t_f = \frac{H^2}{(\eta c_v (1 - U_f))} \qquad (7.4)$$

Where U_f is the average degree of consolidation at failure, H is the half the specimen height, and η is a parameter depending on drainage condition. η is equal to 0.75 for drainage from one end only and η is equal to 3 for drainage from both ends.

In unsaturated soil testing, the effect of the impeded flow through the high AEV ceramic should be considered as well. Bishop and Gibson, (1963) and Ho and Fredlund (1982) introduced the impedance factor λ that is defined within η and the Eq (7.4) take the following form:

$$t_f = \frac{L^2}{(\eta c_v (1 - U_f))} \qquad (7.5)$$

Where, $\eta = 0.75 / (1 + 3 /\lambda)$ for single drainage and $\eta = 3/ (1 + 3 /\lambda)$ for double drainage. Impedance factor λ formulated as follows:

$$\lambda = \frac{k_d d}{k_w L_d} \qquad (7.6)$$

where, k_d is the water coefficient of permeability of the high AEV ceramic, k_w is the coefficient of permeability of the unsaturated soil with respect to the water phase, d is the length of drainage path, and L_d is thickness of the high AEV ceramic.
As shown in Figure 7.4, Ho and Fredlund (1982) demonstrated that for the impedance factor greater than 10 (specimen with 140 mm height and single drainage) the time to failure, t_f, is almost constant for a given coefficient of consolidation.
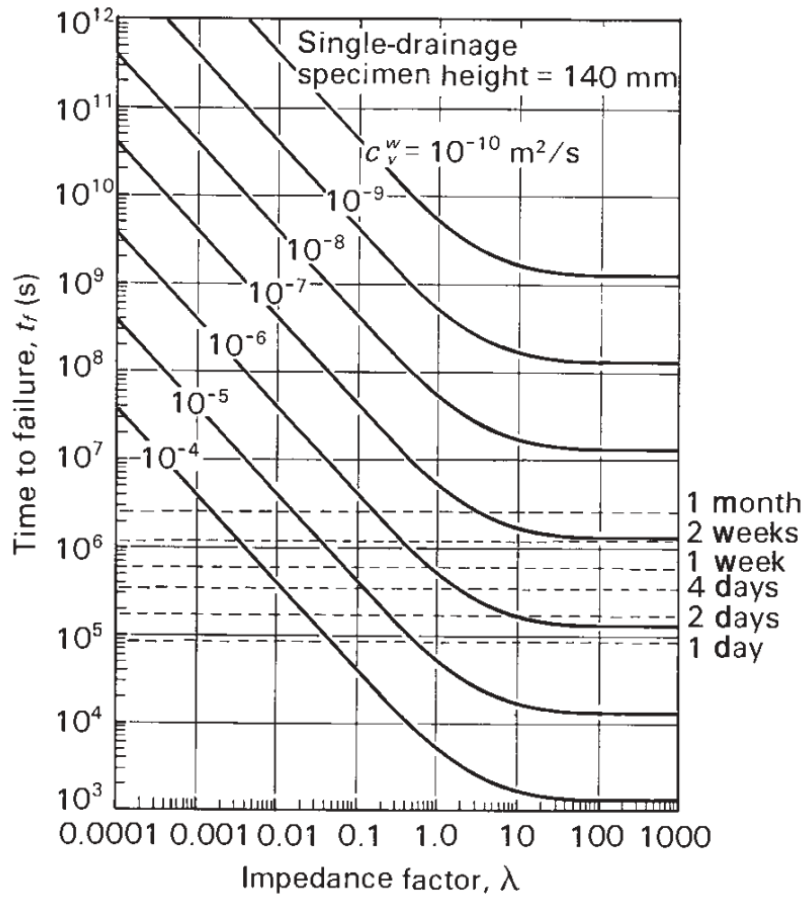
Figure 7.4 Time to failure t_f for drained triaxial test specimen
(adopted from Fredlund et al. (2012).

In this study the impedance factor, λ, of the 10 adopted in estimating the time required to fail the specimen. As mentioned in section 4.3, the drainage is provided from both sides therefore the drainage factor, η estimated as 2.3 using $\eta = 3/(1 + 3/\lambda)$.

By substituting, η=2.3 and $c_v = 1.6 \times 10^{-6}$ m^2 /s, the required time to failure was determined to be 4 hours.

Assuming failure will occur after 2 % axial strain (the tests results revealed that failure occurs after 8 % axial strain) the rate of the strain is determined to be 0.0088 %/min using Eq (7.3). To be conservative, the loading rate is selected to be 0.004 %/min for both specimen prepared from slurry and compacted specimens.

114

The changes in total and water volume and changes in height of the specimen are monitored throughout the test. The diffused air is flushed once a day following the procedure described in section 4.4.2.

7.2.4 Dismantling the Triaxial Cell and Specimen

Once the test was finished, pressures (the cell pressure, air pressure and water pressure) were all gradually decreased to zero while keeping positive net stress. All the valves were closed and the triaxial cell fluid is drained. All the pipes (i.e. cell, water and air pressure lines) were disconnected from the triaxial base and then the triaxial cell was taken off the loading frame.

The excess water from triaxial base, membrane and top was dried using toilet paper. The O-rings on top cap were removed and the membrane was stripped. The height and diameter of the specimen were carefully measured on top, middle and bottom of the specimen from two opposite directions. The diameter measurement at the middle of the specimen were used to control the estimation of the area correction.

It is common to measure the entire weight of the specimen to determine the overall water content of the specimen. In this study, water content of the specimen was taken from five levels along the height to investigate the spatial distribution of the water content. In addition, the spatial variation of the void ratio was examined by estimating void ratio at each level by wax-coated submersion. The following procedure was adopted to measure the water content and void ratio:

▪ Specimen was divided into five slices. Half of the slice was taken for water content determination, and the other half were taken for void ratio determination.

The following steps were followed to measure the void ratio of each slice, based on Archimedes' principle:

▪ Each slice is trimmed to get a regular shape. It is avoided to get angular and re-entrant angle specimens.
▪ Weigh the trimmed slice (M_1).

- Slice is coated by dipping in molten wax and removing it quickly. This step is repeated for several times to completely coat the specimen. A thermostatically controlled bath is employed for melting the wax. It should be noted that the overheated wax can cause cracks in the specimen. The wax should be heated to 60-70°c temperature.
- Weigh the waxed specimen after cooling, (M_2).
- A setup, as shown in Figure 7.5, is arranged to determine the apparent mass of the waxed specimen in water. A beaker is filled with distilled water and positioned on the digital balance. A tray, shown in Figure 7.5, is suspended from the supporting frame and completely immersed in water. The balance is zeroed.
- The waxed specimen is placed on the tray so that it is completely immersed in water.
- The mass of the immersed waxed specimen in water is measured (M_3). This is the difference between the specimen weight in air and under water.

The mass of wax is (M_w) given by:

$$M_w = M_2 - M_1 \tag{7.5}$$

The volume of the wax (V_{wax}) is given by

$$V_{wax} = \frac{M_{wax}}{\rho_{wax}} \tag{7.6}$$

where ρ_w is the density of the wax, which is determined to be 0.88 g/cm³.

Therefore, the volume of the specimen is given by:

$$V_s = \frac{M_3}{\rho_w} - V_{wax} \tag{7.7}$$

From this and water content of each slice, the bulk density, dry density and void ratios are determined.
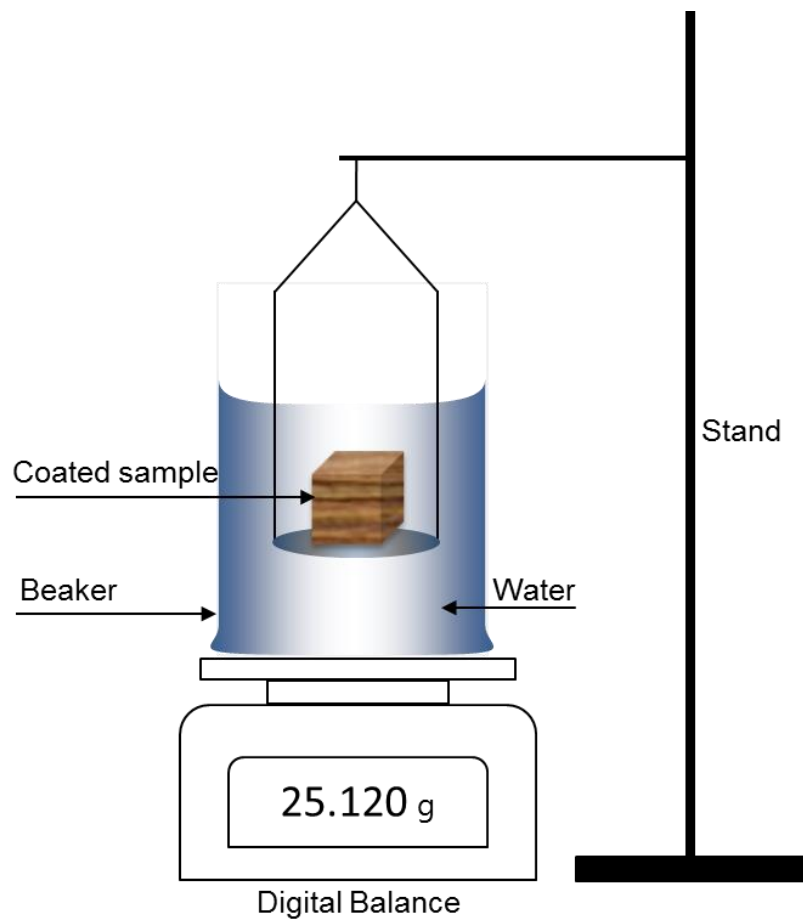
Figure 7.5 Setup for determining volume of the specimen.

7.3 Testing Program

Effect of matric suction and suction history (wetting-drying) as well as effect of net mean stress (p) on shear strength and volumetric behavior of specimens that are either isotropically reconstituted from the slurry (IRS) or moist-tamped compacted (MT) was examined. For this purpose, mainly two series of suction controlled CD triaxial tests were carried out.

To investigate the effect of suction magnitude and net mean stress, suction controlled CD triaxial tests were performed at each test point, as shown in Figure 7.6, on both IRS and MT specimens.

To investigate the effect of suction history, suction controlled CD triaxial tests involving drying and wetting were performed on IRS specimens.

Note that each saturated CD test took about 5 days and each unsaturated CD test took 20 days on average. Table 7.2 and Table 7.3 summarize the testing program for MT and IRS specimen respectively.
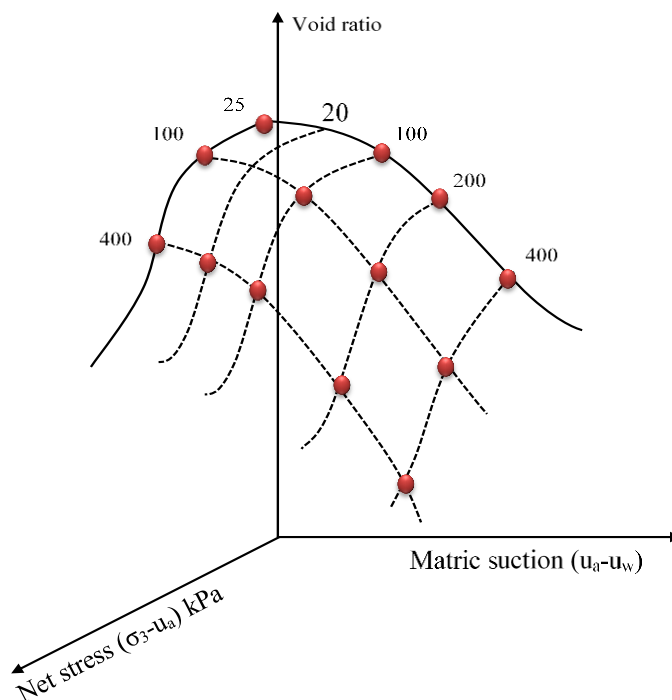
Figure 7.6 Summary of test points in unsaturated testing (series 1 for both MT and IRS), with conditions at the start of shearing.

Table 7.2 Summary of testing program for isotropically reconstituted specimen from slurry (IRS).

NO	Test ID	Prep. method	Prep. void ratio	Prep. water content (%)	Suction condition (kPa)			Net confining stress (kPa)		Sheared
					Initial	Drying to	Wetting to	Loading	Unloading	
1	Series1, 25	IRS	0.72	slurry	Zero	-	saturated	25	-	✓
2	Series1, 100					-		100	-	✓
3	Series1, 100					-		100	-	✓
4	Series1, 200									
5	Series1, 400					-		400	-	✓
6	Series1, step loading					-		400	12	✓
7	Series1, 25	IRS	0.72	slurry	Zero	-	saturated	400	25	✓
8	Series1, 100					-		400	100	✓
9	Series1, 100					-		400	200	✓
10	S 100 25	IRS	0.72	slurry	Zero	100	-	25	-	✓
11	S 100 100						-	100	-	✓
12	S 100 400						-	400	-	✓
13	S 200 25					200	-	25	-	✓
14	S 200 100						-	100	-	✓
15	S 200 400						-	400	-	✓
16	S 400 25					400	-	25	-	✓
17	S 400 100						-	100	-	✓
18	S 400 400						-	400	-	✓
19	S 20 400	IRS	0.72	slurry	Zero	20	-	400	-	✓
20	S 400-0, 25	IRS	0.72	slurry	Zero	400	0	25	-	✓
21	S 400-0, 100						0	100	-	✓
22	S 400-0, 400						0	400	-	✓
23	S 400-100, 25	IRS	0.72	slurry	Zero	400	100	25	-	✓
24	S 400-100, 100						100	100	-	✓
25	S 400-100, 400						100	400	-	✓
26	S 400-200, 25						200	25	-	✓
27	S 400-200, 100						200	100	-	✓
28	S 400-200, 400						200	400	-	✓
29	Series3, 400-25	ORS	0.72	slurry	Zero	-	saturated	25	-	✓
30	Series3, 400-100					-		100	-	✓
31	Series3, 400-200					-		100	-	✓

Table 7.3 Summary of testing program for MT compacted specimens.

NO	Test ID	Prep. method	Prep. void ratio	Prep. Water content (%)	Suction condition (kPa)			Net confining stress (kPa)		Sheared
					Initial	Drying to	Wetting to	Loading	Unloading	
1	Series1, 25	MT	0.72	10.2	400	-	saturated	25	-	✓
2	Series1, 100					-		100	-	✓
3	Series1, 400					-		400	-	✓
4	Series1, step loading					-		400	12	
4	Series2, 25	MT	0.72	17	50 to 100	-	saturated	25	-	✓
5	Series2, 100					-		100	-	✓
6	Series2, 200					-		200	-	✓
7	Series2, 400					-		400	-	✓
8	Series3, 25	MT	0.82	17	-	-		25	-	✓
9	Series3, 100					-		100	-	✓
10	Series3, 200					-		200	-	✓
11	Series3, 400					-		400	-	✓
12	MT 100 25	MT	0.72	10.2	400	-	100	25	-	✓
13	MT 100 100					-		100	-	✓
14	MT 100 400					-		400	-	✓
15	MT 200 25					-	200	25	-	✓
16	MT 200 100					-		100	-	✓
17	MT 200 400					-		400	-	✓
18	MT 400 25					-	400	25	-	✓
19	MT 400 100					-		100	-	✓
20	MT 400 400					-		400	-	✓

7.3.1 Test Program for Suction Controlled CD Triaxial Tests on Reconstituted Specimens

A total of 31 consolidated drained tests were performed on isotropically reconstituted specimens from the slurry (IRS). This involves 11 conventional consolidated-drained tests on saturated specimens and 20 unsaturated suction-controlled CD triaxial tests.

7.3.1.1 Saturated Soil Tests

Three series of conventional consolidated drained triaxial tests were performed on isotropically reconstituted specimens from the slurry (IRS), and one-dimensionally reconstituted from the slurry (ORS).

- Series 1 involves CD tests on IRS specimens at 4 effective confining stress of 25, 100, 200, and 400 kPa.

  The saturated shear strength parameters of the IRS were determined through the test results of series 1. In addition, these tests were used as a reference state to interpret the results of unsaturated soil tests. Four tests were performed at 25, 100, 200, and 400-kPa effective stress. A consolidated drained triaxial test was repeated twice at 100-kPa effective stress on identically prepared specimens to verify the repeatability of the specimen preparation method (see section 0).

- Series 2 involves CD tests on IRS specimens with loading and unloading in consolidation stage.

  In series 2, specimens were first consolidated to effective stress of 400 kPa, then unloaded to 200, 100 and 25 kPa to yield an OCR = 2, 4 and 16, respectively. Finally, specimens were sheared at constant effective stress. Yield points (that were used to generate yield surface) in saturated condition were determined through the results of test with loading and unloading (i.e. series 2).

- Series 3 involves CD tests on ORS specimens at three effective confining stress of 100, 200, and 400 kPa.

The results of series are compared to results of series 1, to investigate the effect of the preparation method (see chapter 6).

7.3.1.2 Unsaturated Soil Tests

Two series of suction-controlled consolidated drained triaxial tests were performed to investigate the effect of suction magnitude, suction history (drying-wetting) and net mean stress on shear strength and volume change characteristics of IRS specimens. In series 1, the effect of the suction magnitude was investigated and in series 2 that involves drying-wetting, the effect of hydraulic hysteresis was investigated.

- Series 1 involves suction controlled CD tests on IRS specimens at constant matric suctions of 100, 200 and 400 kPa and mean net stress of the 25, 100 and 400 kPa. An additional test was also performed at suction of 20 kPa and net stress of 400 kPa.
- Series 2 involves suction controlled CD test on IRS specimens with drying-wetting.

Initial states of the test of specimens of the series 1 are shown in Figure 7.6, and the corresponding stress paths in mean net stress-deviator stress-suction (p: q: s) space are shown in Figure 7.7 to Figure 7.15.

After setting up the specimen, a 25-kPa net confining stress was applied to each specimen (A→B). Then, specimens were subjected to a given value of the suction (i.e. 100, 200 and 400 kPa). The IRS specimens are initially in saturated condition (suction is zero). Therefore, under net mean stress of 25 kPa, specimens were brought to a given suction following drying path of B→C.

Following equalization, specimens were isotropically compressed (C→D) (at a constant suction) by ramping the cell pressure a mean net stress of 100, or 400 kPa. Since the suction equalization was carried out at 25-kPa net confining stress, therefore, additional step was not followed during compression stage for tests at 25 kPa net confining stress.

Finally specimens were sheared (D→E) at constant suction and constant cell pressure (i.e. $\Delta q/\Delta p = 3$).

Figure 7.7 Stress paths for Series 1 of IRS specimens, s = 100 kPa, p = 25 kPa.

Figure 7.8 Stress paths for Series 1 of IRS specimens, s = 100 kPa, p = 100 kPa.

Figure 7.9 Stress paths for Series 1 of IRS specimens, s = 100 kPa, p = 400 kPa.

Figure 7.10 Stress paths for Series 1 of IRS specimens, s =200 kPa, p = 25 kPa.

Figure 7.11 Stress paths for Series 1 of IRS specimens, s = 200 kPa, p = 100 kPa.

Figure 7.12 Stress paths for Series 1 of IRS specimens, s = 200 kPa, p = 400 kPa.

Figure 7.13 Stress paths for Series 1 of IRS specimens, s = 400 kPa, p = 25 kPa.

Figure 7.14 Stress paths for Series 1 of IRS specimens, s = 400 kPa, p = 100 kPa.

Figure 7.15 Stress paths for Series 1 of IRS specimens, s = 400 kPa, p = 400 kPa.

The stress paths in (p: q: s) space followed in series 2 are shown in Figure 7.16 to Figure 7.24. At net mean stress of 25 kPa, specimens were brought to a suction of 400 kPa for equalization following drying path of B→C.

Once the equalization is achieved, following wetting path of C→D, suction is reduced to 0, 100, and 200 kPa for equalization. Then, specimens were isotropically compressed (D→E) at (a constant suction) by ramping the cell pressure (to a mean net stress of 100, and 400 kPa). Finally specimens were sheared (E→F) at constant suction and constant cell pressure (i.e. $\Delta q/\Delta p = 3$).

Figure 7.16 Stress paths for Series 2 of IRS specimens, s = 400-0 kPa, p = 25 kPa.

Figure 7.17 Stress paths for Series 2 of IRS specimens, s = 400-0 kPa, p =100 kPa.

128
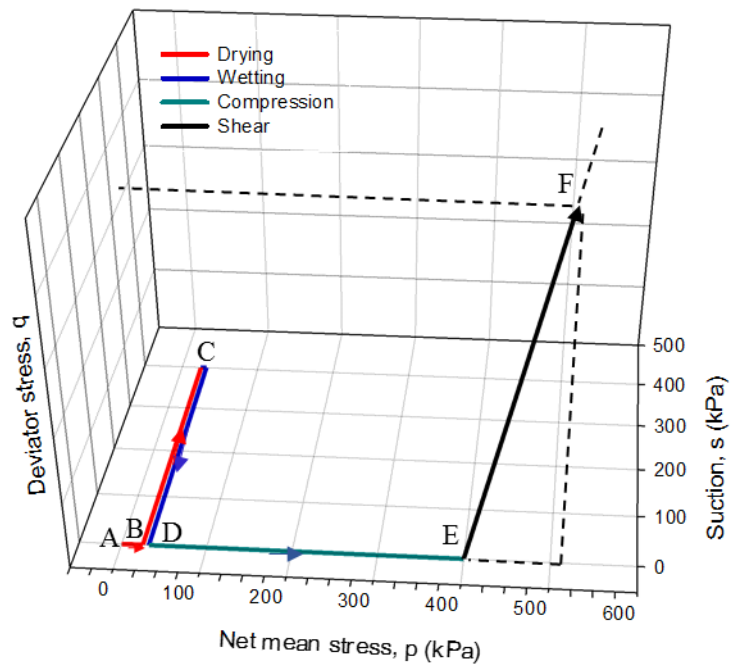
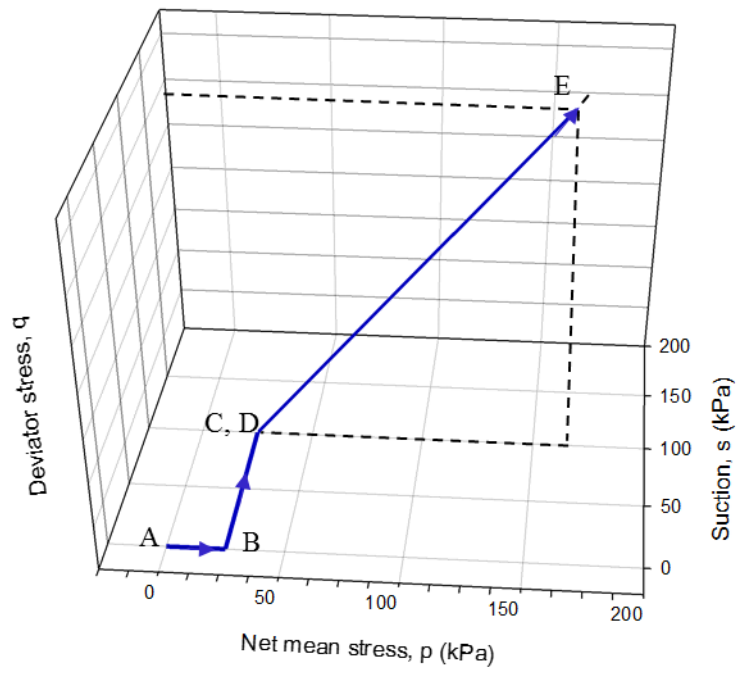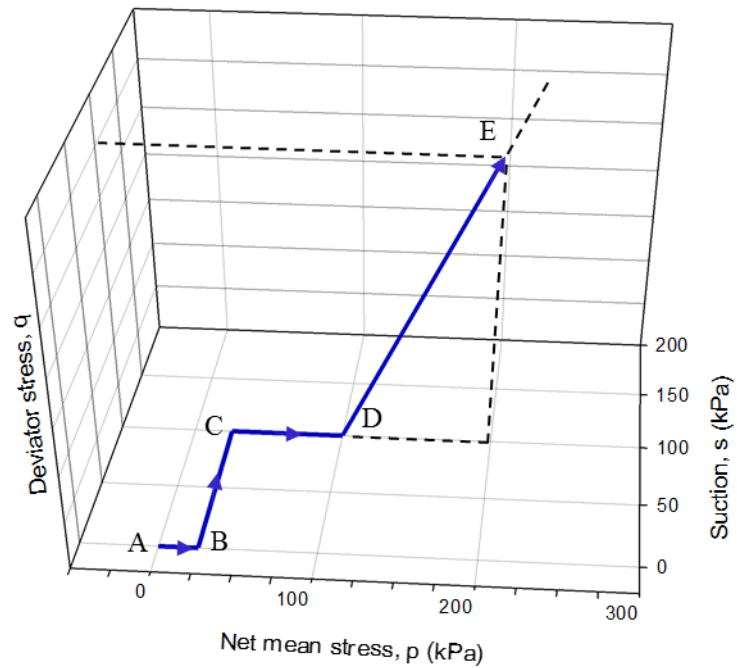Figure 7.18 Stress paths for Series 2 of IRS specimens, s = 400-0 kPa, p =400 kPa.
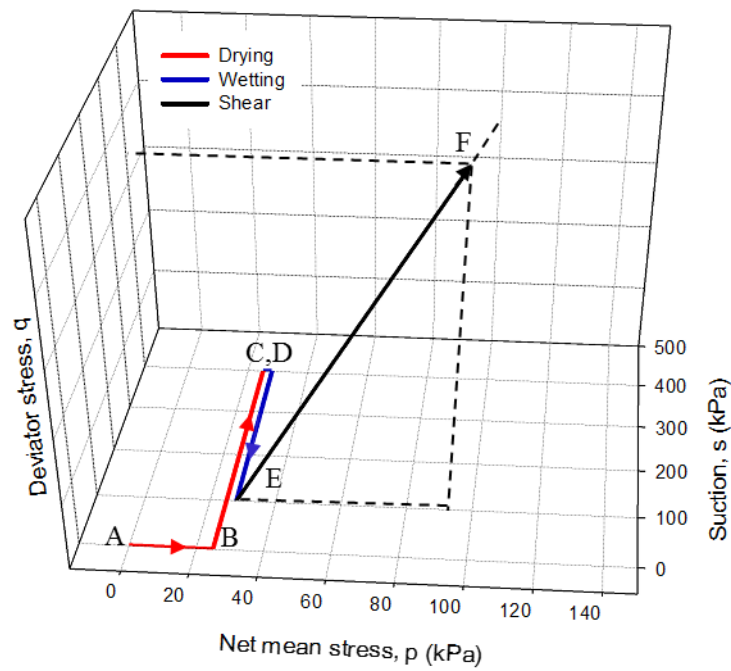
Figure 7.19 Stress paths for Series 2 of IRS specimens, s = 400-100 kPa,
p =2 5 kPa.
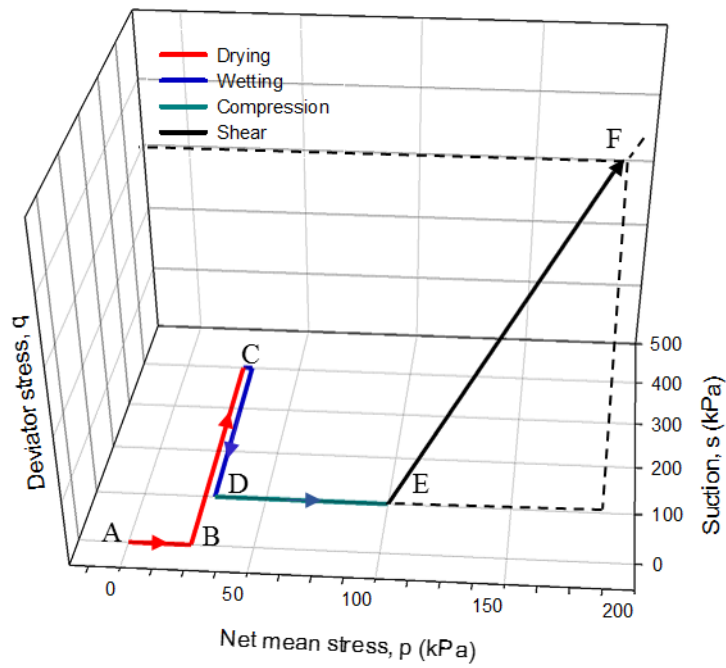
Figure 7.20 Stress paths for Series 2 of IRS specimens, s = 400-100 kPa,
p = 100 kPa.
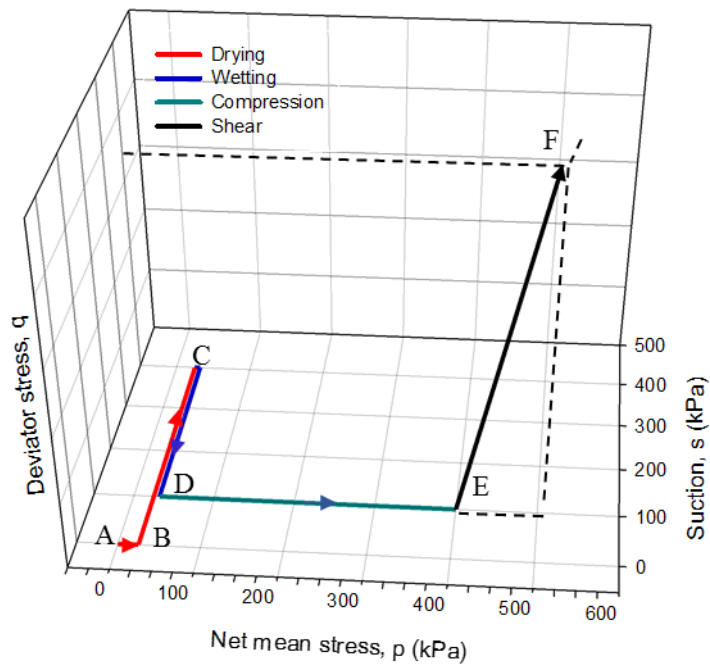
Figure 7.21 Stress paths for Series 2 of IRS specimens, s = 400-100 kPa,
p = 400 kPa.
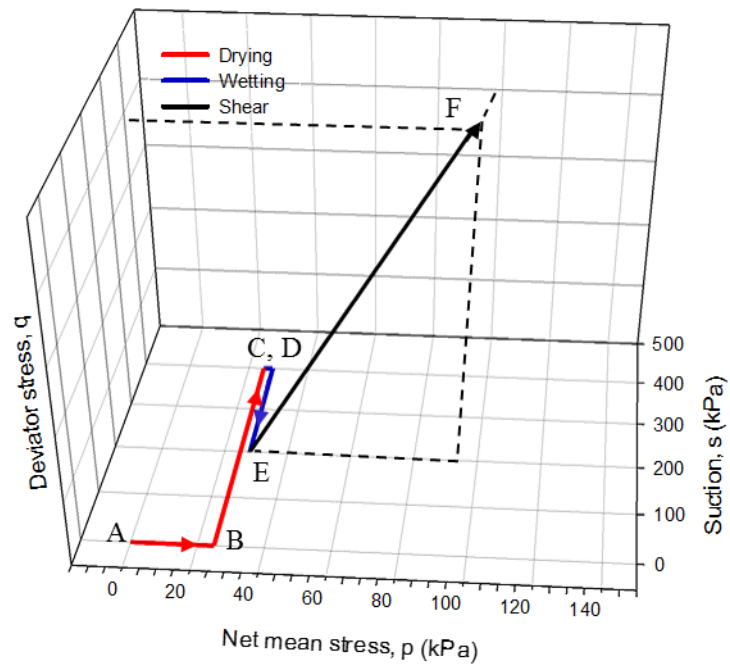
Figure 7.22 Stress paths for Series 2 of IRS specimens, s = 400-200 kPa, p = 25 kPa.
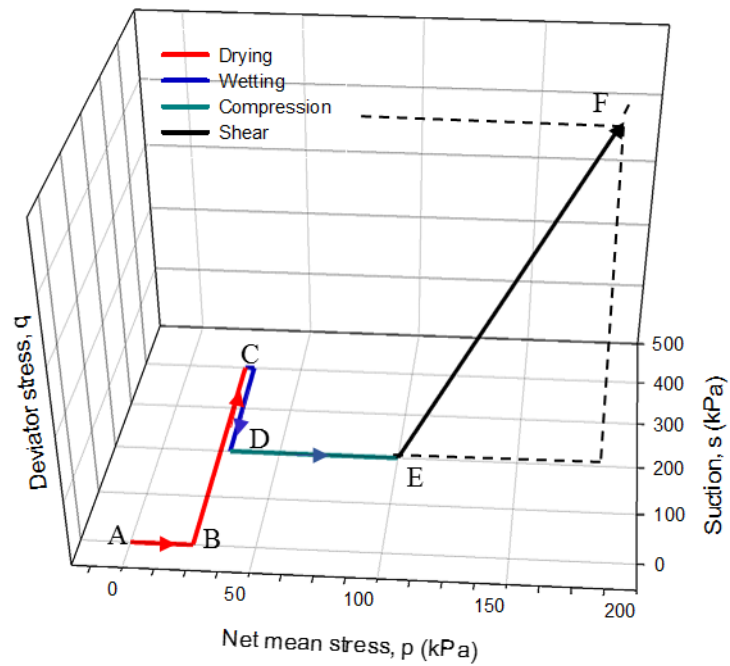
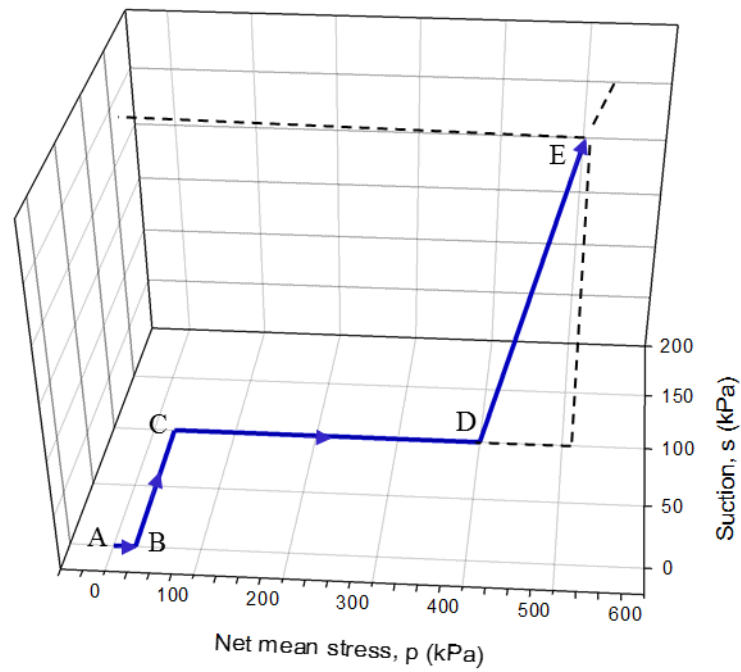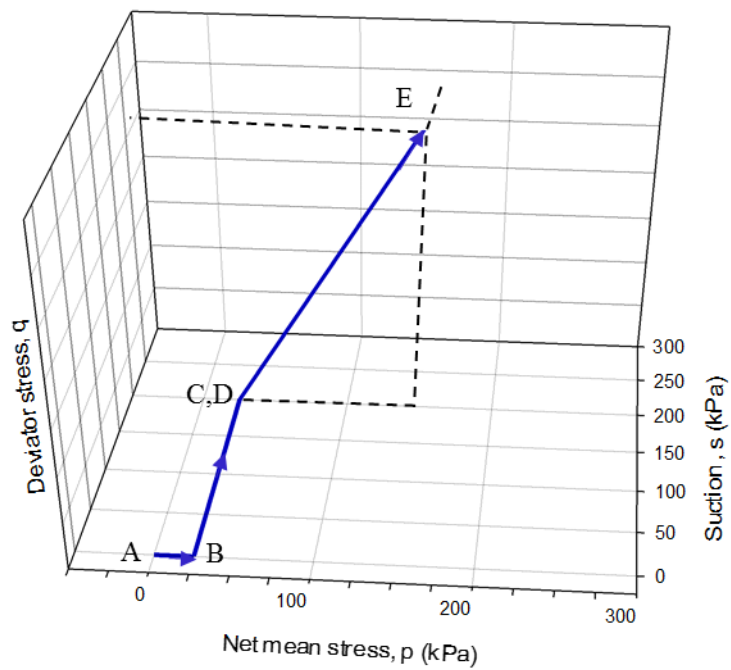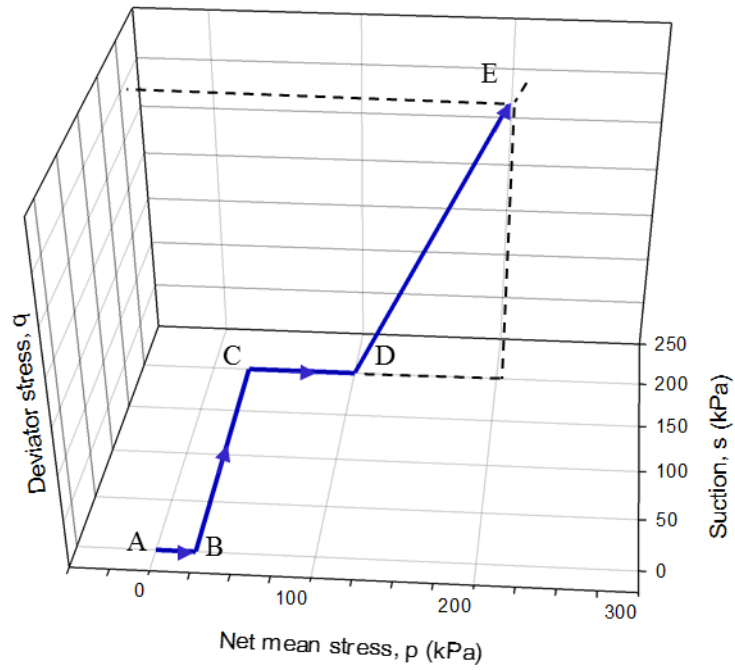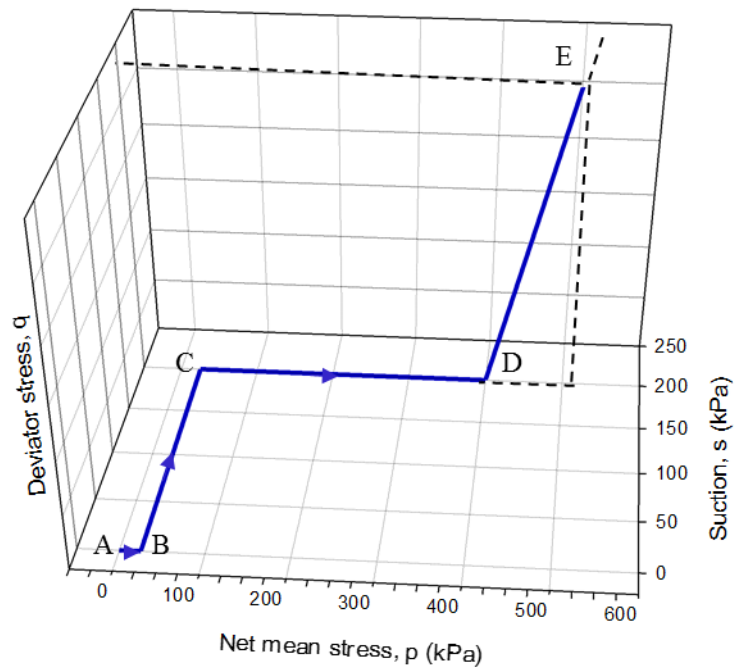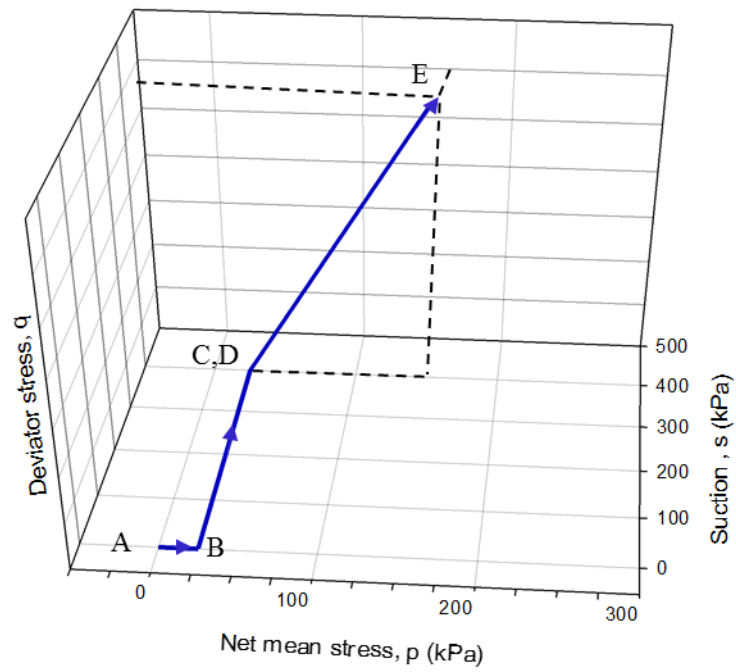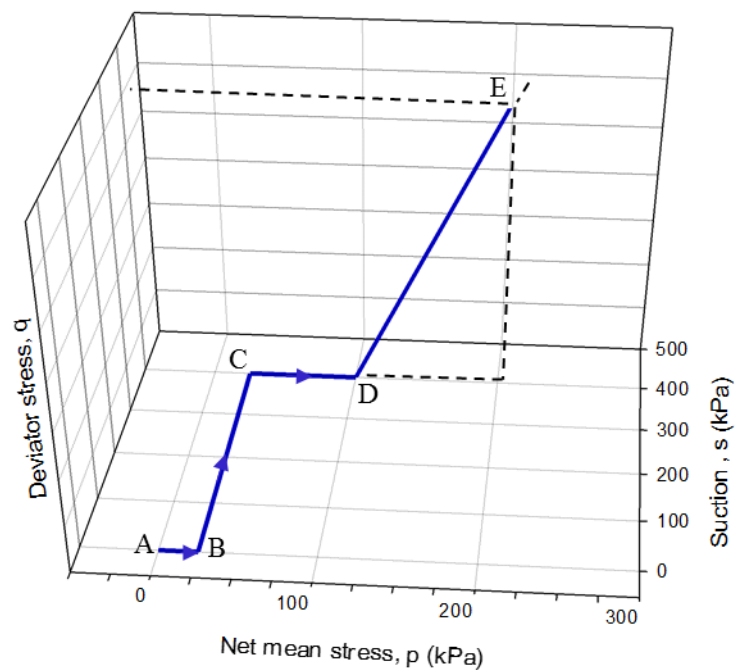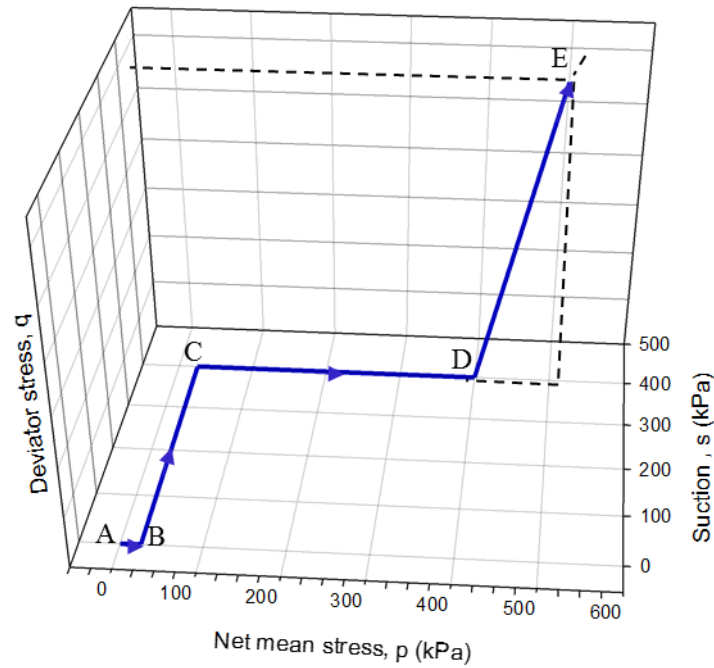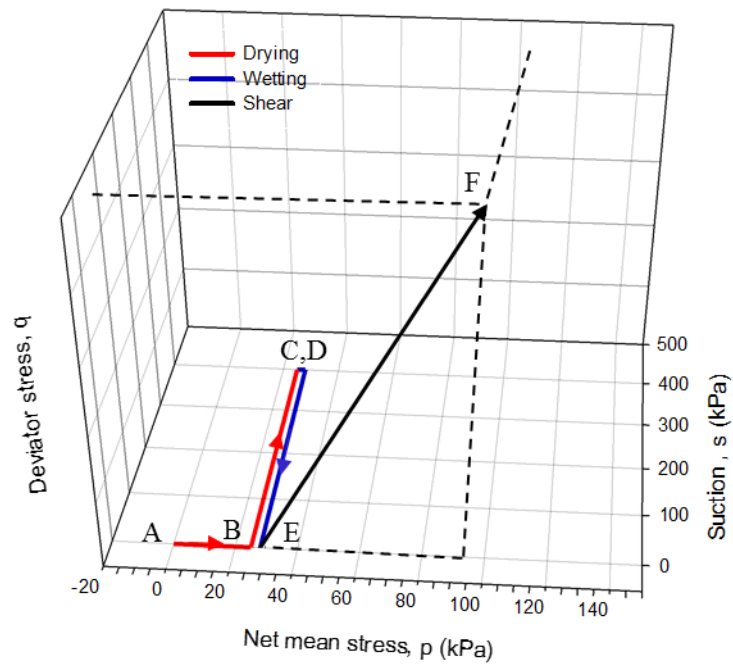Figure 7.23 Stress paths for Series 2 of IRS specimens, s = 400-200 kPa, p = 100kPa
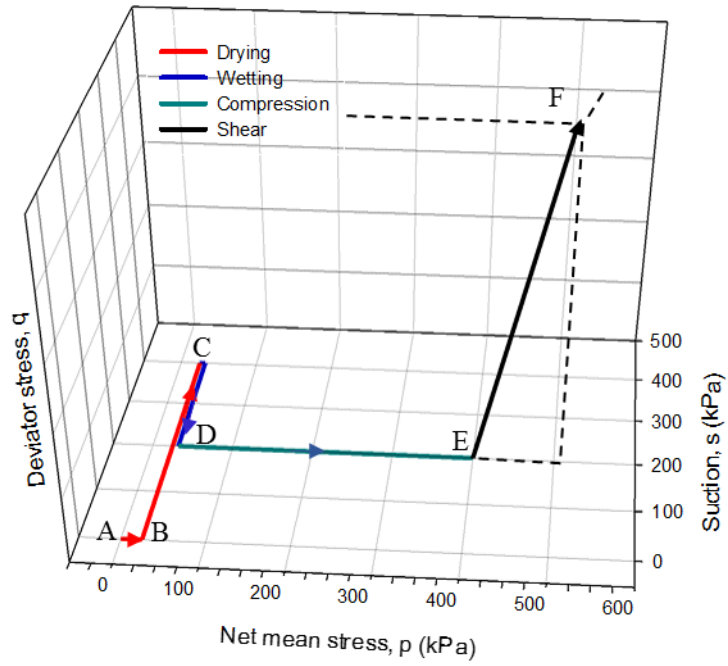
Figure 7.24Stress paths for Series 2 of IRS specimens, s=400-200 kPa, p=400kPa

7.3.2 Test Program for Suction Controlled CD Triaxial Tests on MT Specimens

A total of 20 consolidated drained tests were performed on compacted specimens, which involves 11 tests on saturated specimens and nine unsaturated soil testing.

7.3.2.1 Saturated Soil Tests

Three series of consolidated drained triaxial tests, including different void ratio and preparation water content, were performed on compacted specimens. Series 1 involves three tests on specimen with initial void ratio of $e_0 = 0.72$ and preparation water content of 10.2%. Series 2, involves four tests, the void ratio is unchanged but preparation water content increased to w=17%. Series 3 includes three tests on specimen with initial void ratio of $e_0 = 0.82$ and preparation water content of 17%. These tests could be summarized as below:

- Series 1: Three tests on specimen with initial void ratio of $e_0 = 0.72$ and preparation water content of 10.2%.
- Series 2: Four tests on specimen with initial void ratio of $e_0 = 0.72$ and preparation water content of 17%.
- Series 3: Four tests on specimen with initial void ratio of $e_0 = 0.82$ and preparation water content of 17%.

The saturated shear strength parameter of the MT specimens were determined through the test results of series 1. In addition these tests were used as a reference state to interpret the results of unsaturated soils.

7.3.2.2 Unsaturated Soil Tests

A series of suction controlled consolidated-drained tests were performed on compacted specimens, with 10.2% preparation water content and with initial void ratio of $e_0 = 0.72$. The testing program is the same as that for series 1 tests on IRS specimen (see Figure 7.6). The stress paths in (p: q: s) space is shown in Figure 7.25 to Figure 7.33.

Therefore, under net mean stress of 25 kPa, specimens were brought to a given suction following drying path of B→C.

The initial suction in MT specimens (after compaction) was found to be 400 kPa from the SWCC (for 10.2% preparation water content) which is indicated by point A. After setting up, a 25-kPa net stress was applied to each specimen (A→B). Specimens were brought to a given suction (400, 200, and 100 kPa) for equalization following drying path of B→C.

Then, specimens were isotropically compressed (C→D) (at a constant suction) by ramping the cell pressure (to a mean net stress of 100, and 400 kPa). Finally specimens were sheared (D→E) at constant suction and constant cell pressure (i.e. $\Delta q/\Delta p = 3$).

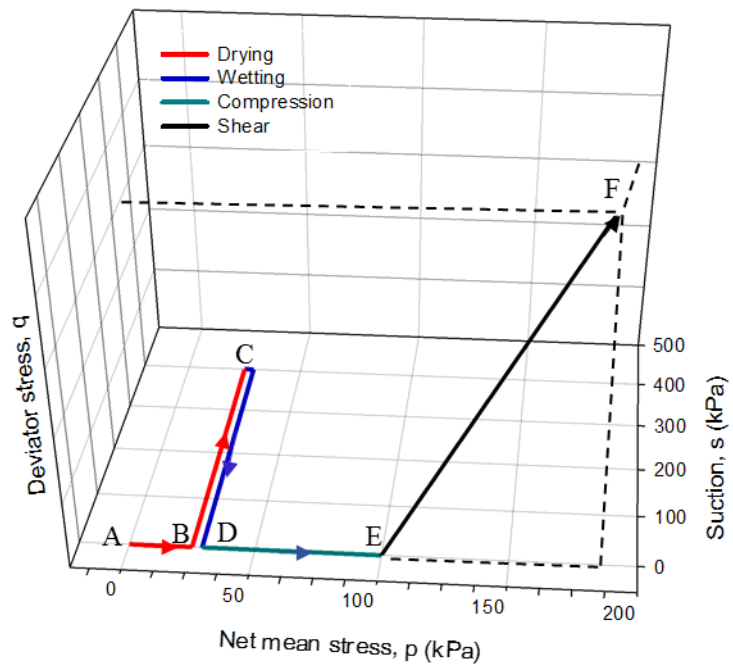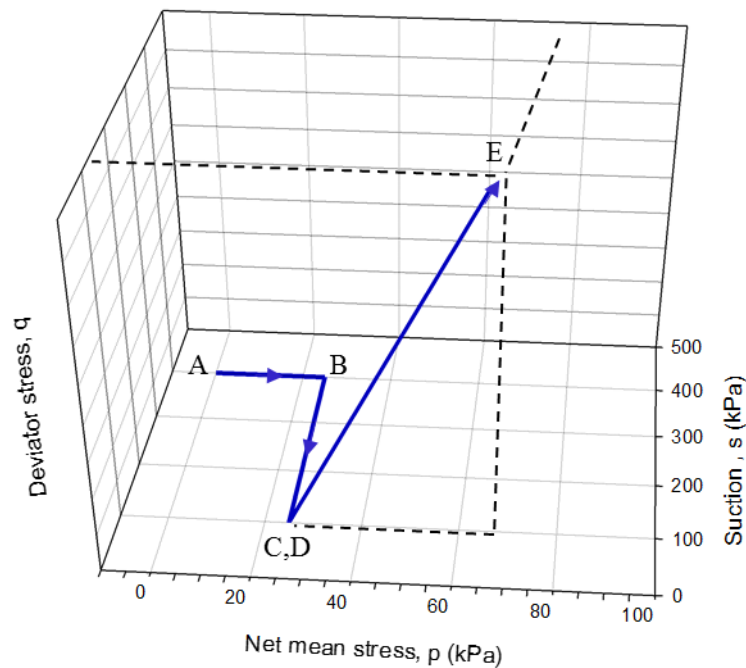Figure 7.25 Stress paths for MT specimens, s = 100 kPa, p = 25 kPa.
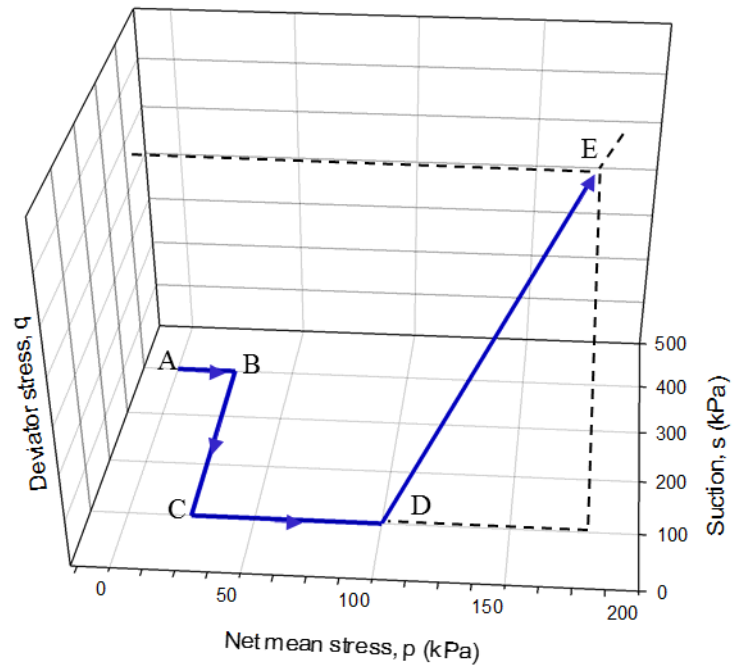
Figure 7.26 Stress paths for MT specimens, S = 100 kPa, P = 100 kPa.
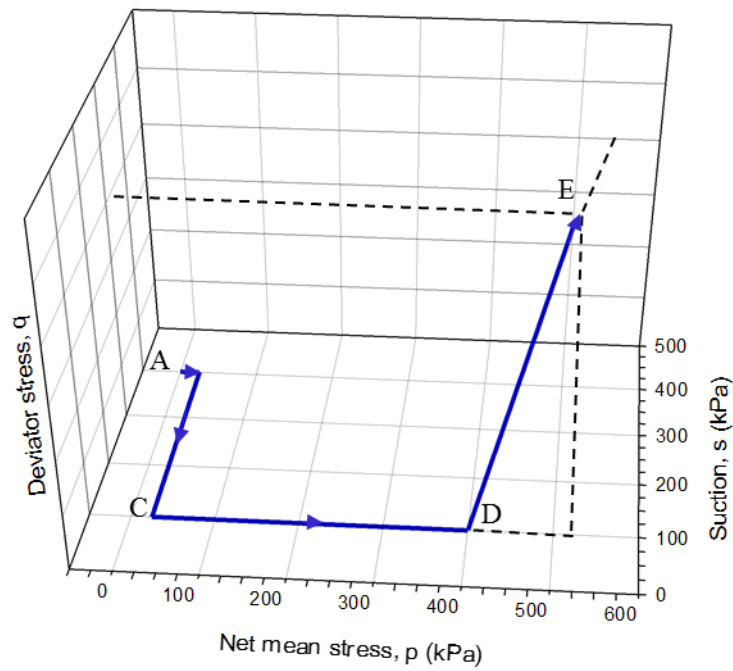
Figure 7.27 Stress paths for MT specimens, s = 100 kPa, p = 400 kPa.
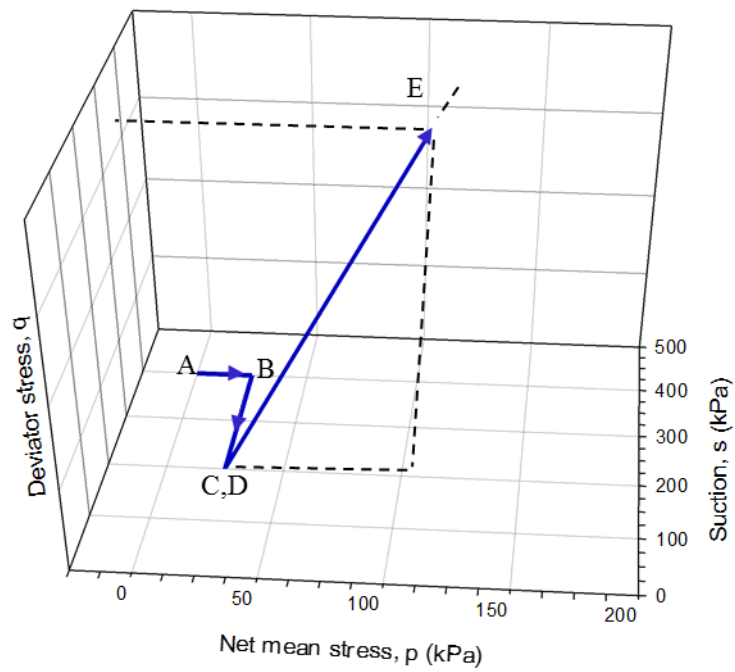
Figure 7.28 Stress paths for MT specimens, s = 100 kPa, p = 25 kPa.
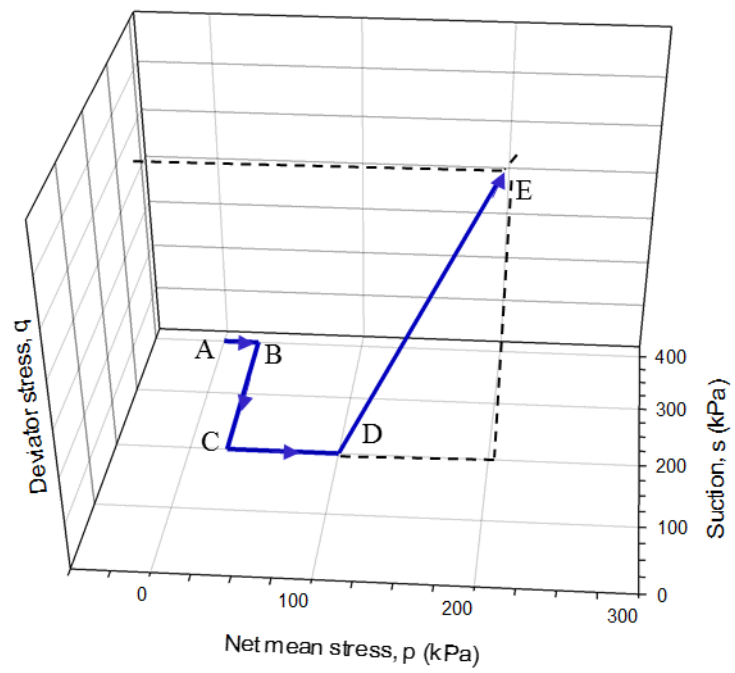
Figure 7.29 Stress paths for MT specimens, s = 200 kPa, p = 100 kPa.
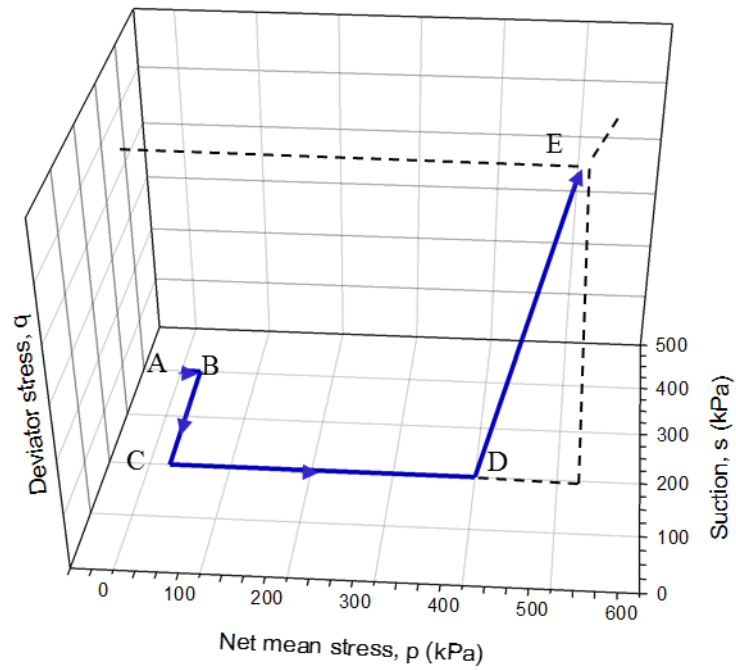
Figure 7.30 Stress paths for MT specimens, s = 200 kPa, p = 400 kPa.
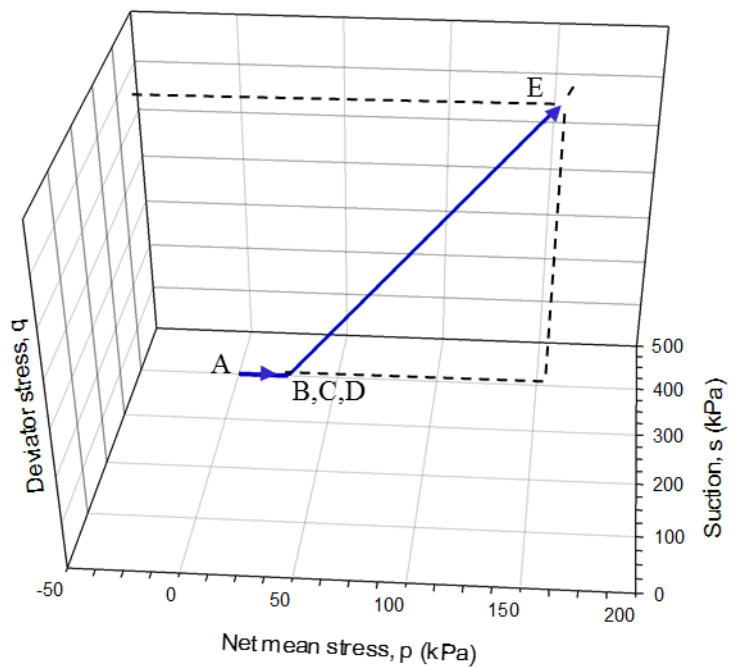
Figure 7.31 Stress paths for MT specimens, s = 400 kPa, p = 25 kPa.
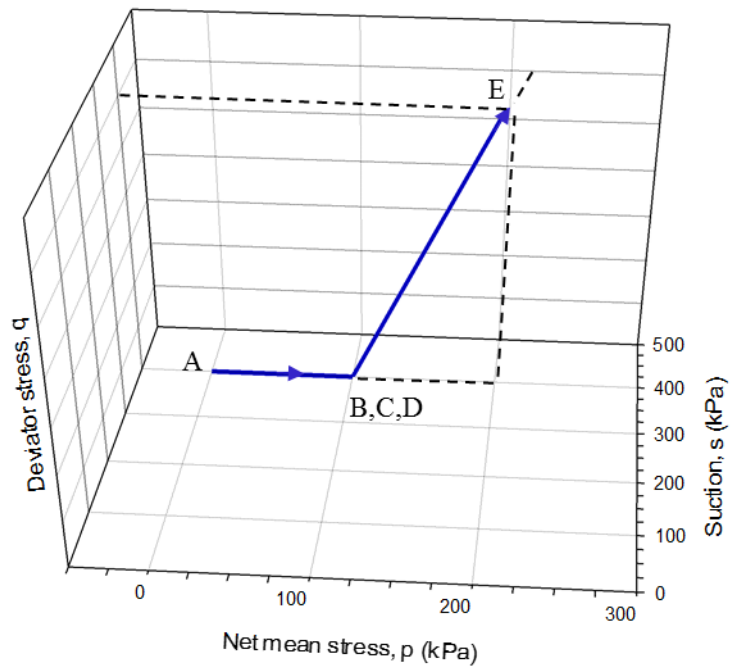
Figure 7.32 Stress paths for MT specimens, s = 400 kPa, p = 100 kPa.
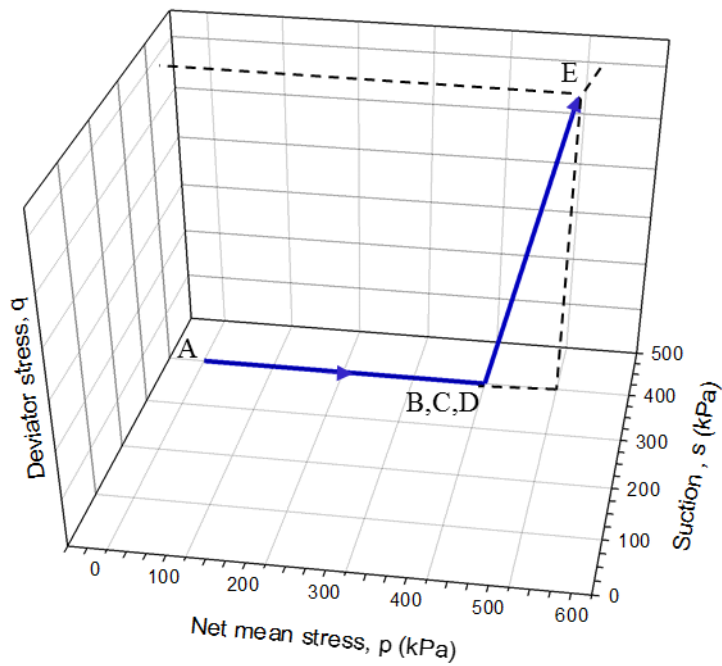
Figure 7.33 Stress paths for MT specimens, s = 400 kPa, p = 400 kPa.

CHAPTER 8

PRESENTATION AND INTERPRETATION OF RESULTS

This chapter presents the experimental results that are obtained from the testing program that was explained in chapter 7. The results of the saturated consolidated drained triaxial tests and the unsaturated suction controlled triaxial tests, under different values of matric suctions and net confining stress, for both isotropically reconstituted specimens from the slurry (IRS) and moist tamp compacted (MT) specimens are presented.

8.1   Experimental Results of the Moist Tamped Compacted Specimens

A total of 20 consolidated drained tests were performed on compacted specimens, which involve 11 tests on saturated specimens and nine on unsaturated soil.

8.1.1   Behavior of Saturated Specimens during Triaxial Tests

Three series of consolidated drained triaxial tests were performed on compacted specimens (see section 7.3.2.1 for detail).

Each test includes three distinguished stages: saturation, consolidation and shearing stage. The results corresponding to each stage are discussed as separate subsections.

8.1.1.1   Saturation

During the saturation process, depending on the state of the specimen and soil type, volume of the specimen may increase (swelling), or decrease (collapse) or remain unchanged. The states of the specimens before and after the saturation are presented in Table 8.1. It can be seen from the data in Table 8.1 the void ratio of the specimens in tests series 1 are increased from the initial value of the 0.72 to 0.75. However, in tests series 2 and 3, the void ratio is remained almost unchanged. This can be

attributed to the preparation water content, in which for series 1 that is lower than those in series 2 and 3 (even lower than the optimum water content).

Table 8.1 State of the specimen at each stage of the triaxial tests of the compacted specimens.

Tests series	Test Name	Initial condition			Void ratio after saturation	Void ratio after consolidation	Void ratio end of the test
		Water content %	Degree of saturation	Void ratio before test			
Series 1	MT 25 e=72, wc=10.2%	10.2	38.5	0.72	0.75	0.74	0.69
	MT 100 e=72, wc=10.2%	10.2	38.5	0.72	0.74	0.72	0.6
	MT 200 e=72, wc=10.2%	10.2	38.5	0.72	0.75	0.64	0.5
Series 2	MT 25 e=72, wc=17%	17	64	0.72	0.71	0.71	0.67
	MT 100 e=72, wc=17%	17	64	0.72	0.72	0.69	0.61
	MT 200 e=72, wc=17%	17	64	0.72	0.72	0.65	0.56
	MT 400 e=72, wc=17%	17	64	0.72	0.72	0.62	0.52
Series 3	MT 25 e=82, wc=17%	17	56	0.83	0.83	0.82	0.71
	MT 100 e=82, wc=17%	17	56	0.83	0.8	0.73	0.61
	MT 200 e=82, wc=17%	17	56	0.83	0.82	0.69	0.57
	MT 400 e=82, wc=17%	17	56	0.83	0.82	0.62	0.5

8.1.1.2 Isotropic Consolidation

Following saturation, the consolidation stage was initiated by elevating cell pressure at a rate of 20 kPa/min. The state of the specimen after consolidation are presented in

Table 8.1Table 8.1. Figure 8.1 to Figure 8.4 compare the volumetric changes and void ratio during the isotropic consolidation for all series at different consolidation pressures. A clear yield point (pre-consolidation pressure) could be identified from consolidation curves in tests with 400-kPa effective consolidation pressure. As expected, the yield point in specimen with high initial void ratio (i.e. e = 0.82) is smaller than those in series 1 and 2. In tests at 25-kPa consolidation pressure, (which is less than yield point), minor change in the void ratio occurred and the difference in the void ratio is obvious at the end of the consolidation. For higher consolidation pressures (especially for those greater than the yield point), the differences in void ratio decrease, and finally converge at 400-kPa consolidation pressure. In other words, despite initial condition, the post-yield compression lines tend to converge to a unique virgin compression line as the effective stress increases beyond the preconsolidation pressure that was applied during tamping.

An isotropic step-loading consolidation test was also carried out on a MT compacted specimen (with an initial void ratio of $e_0 = 0.72$ and preparation water content of 17%). Isotropic compression curve is shown in Figure 8.4. It can be seen that isotropic consolidation curve represent a clear yield point as well. The isotropic consolidation curve from step loading test coincides with compression curve of an identical specimen that is isotropically consolidated by ramped loading.
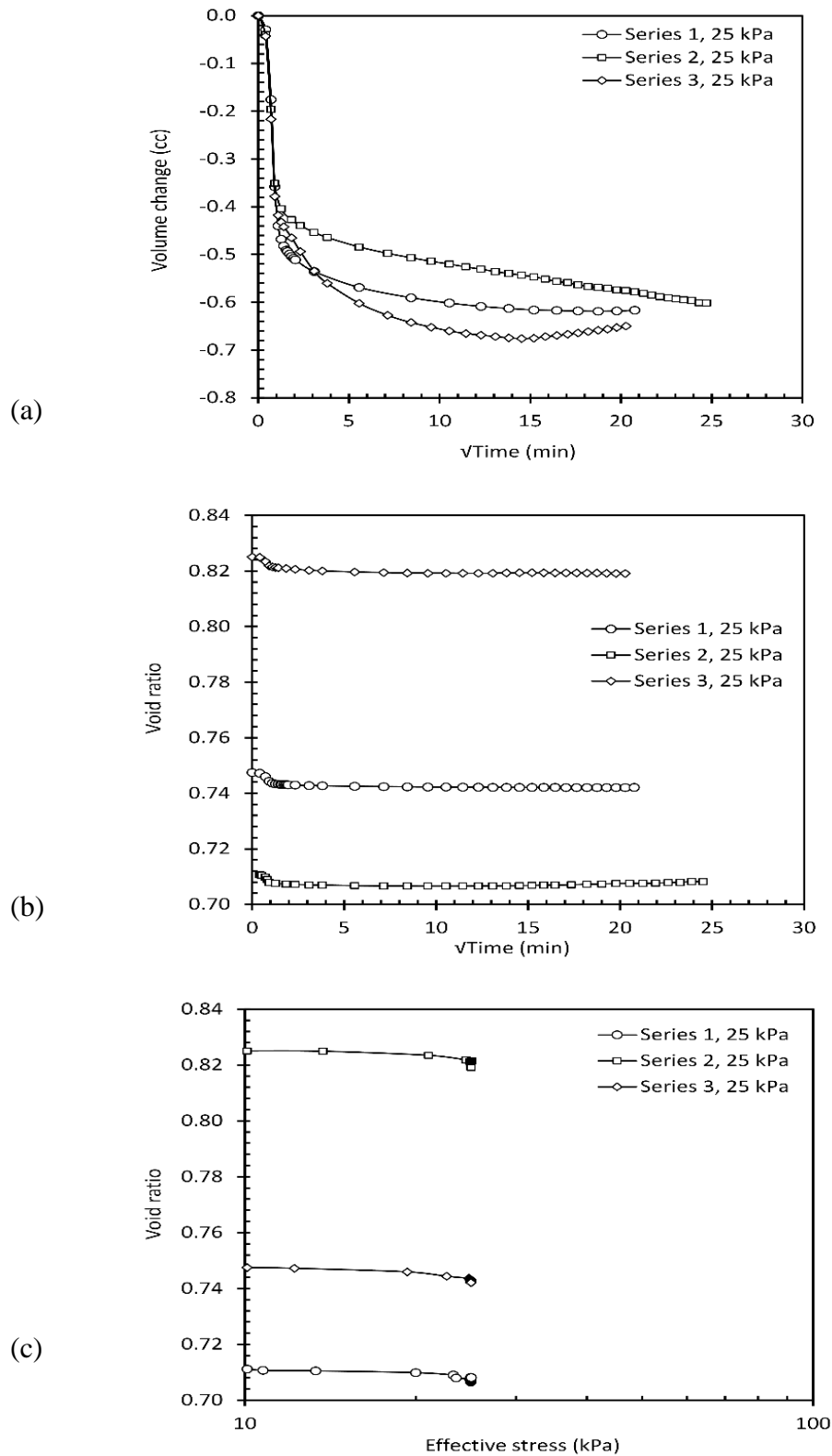
Figure 8.1 Comparison of the volumetric behavior during isotropic consolidation at 25 kPa effective stress: (a) volumetric changes versus time, (b) void ratio versus time, (c) Isotropic consolidation curves.

142

(a)

(b)

(c)
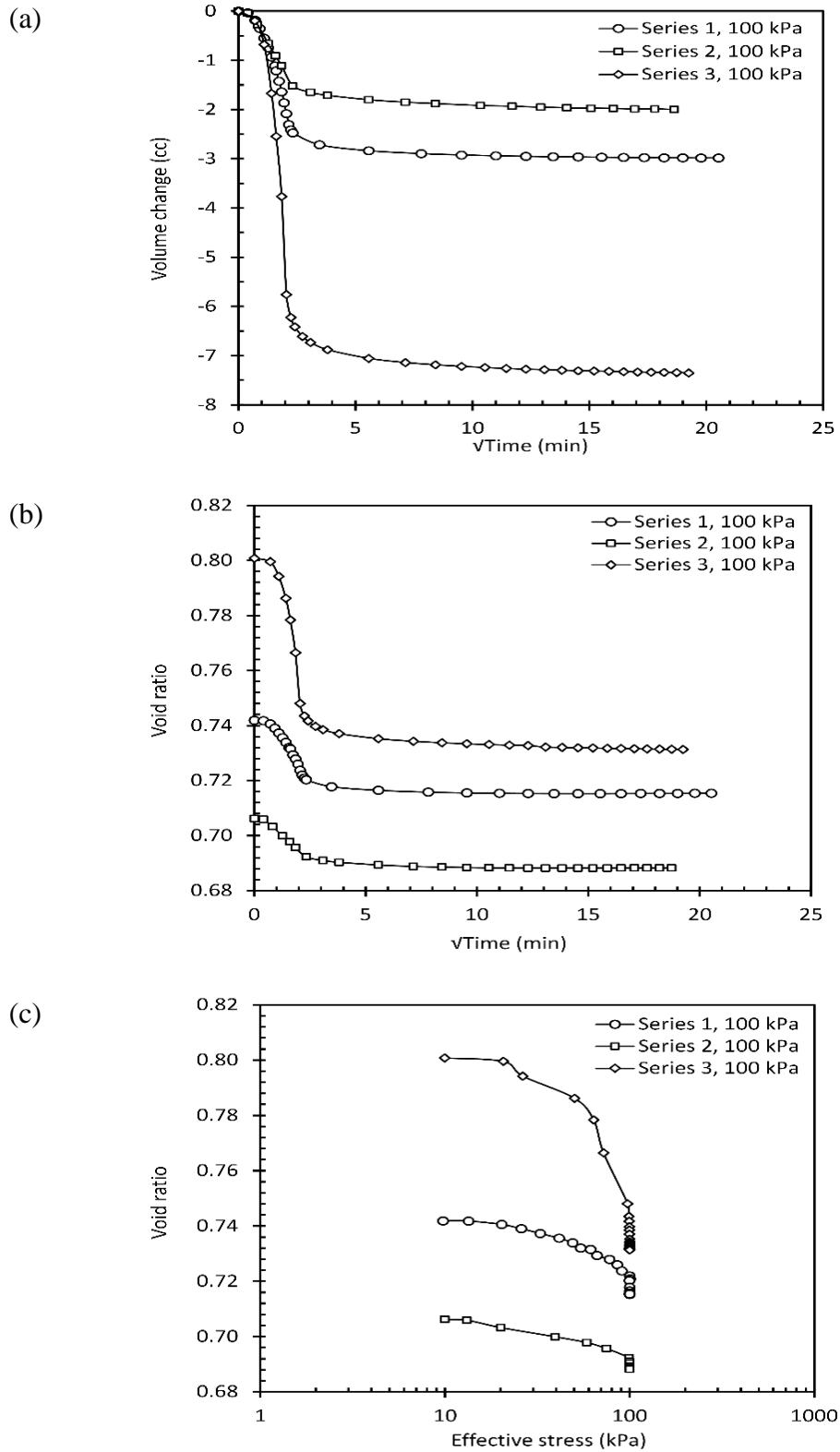
Figure 8.2 Comparison of the volumetric behavior during isotropic consolidation at 100 kPa effective stress: (a) volumetric changes versus time, (b) void ratio versus time, (c) Isotropic consolidation curves.

143
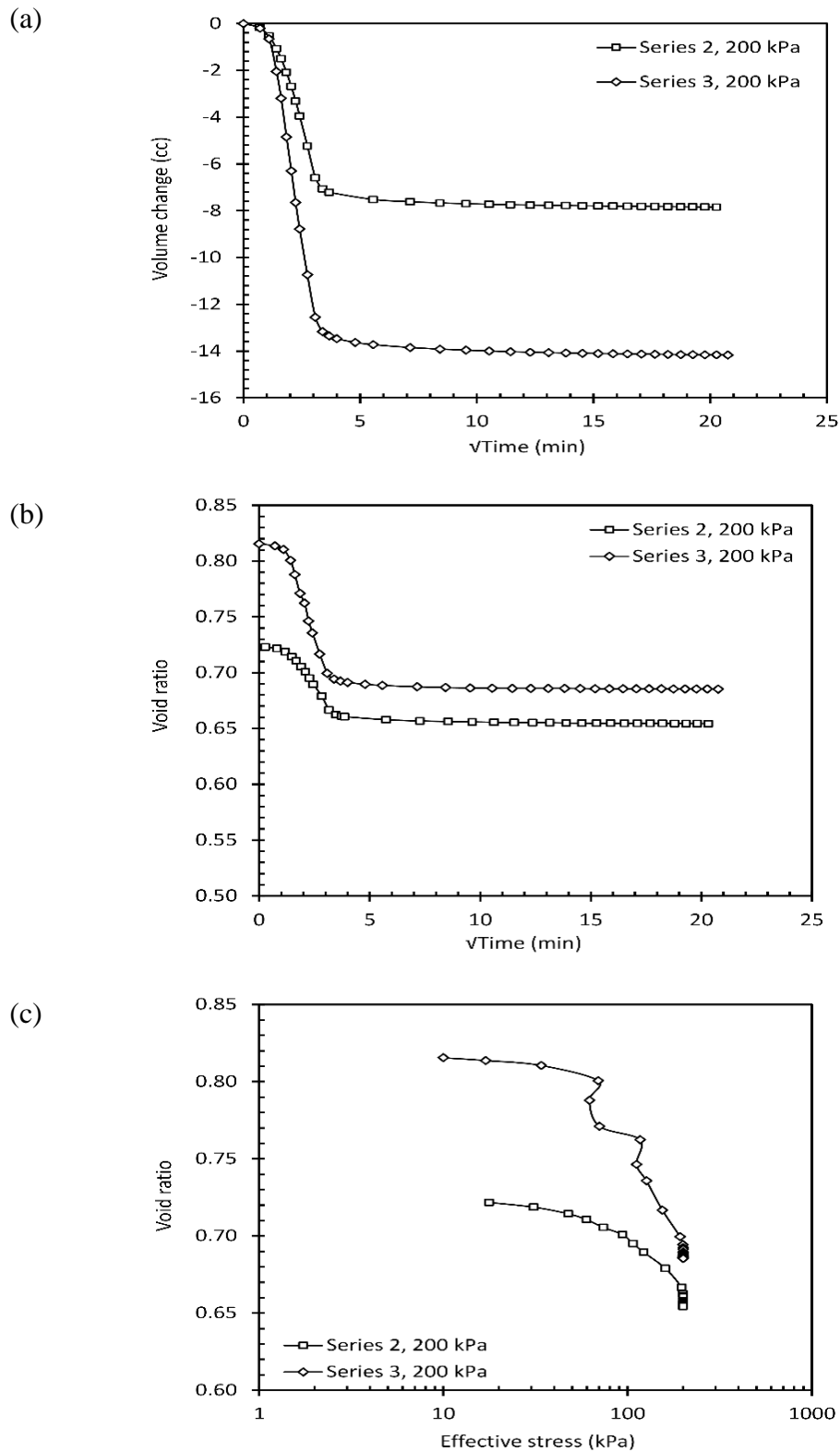
Figure 8.3 Comparison of the volumetric behavior during isotropic consolidation at 200 kPa effective stress: (a) volumetric changes versus time, (b) void ratio versus time, (c) Isotropic consolidation curves.

144

(a)

(b)

(c)
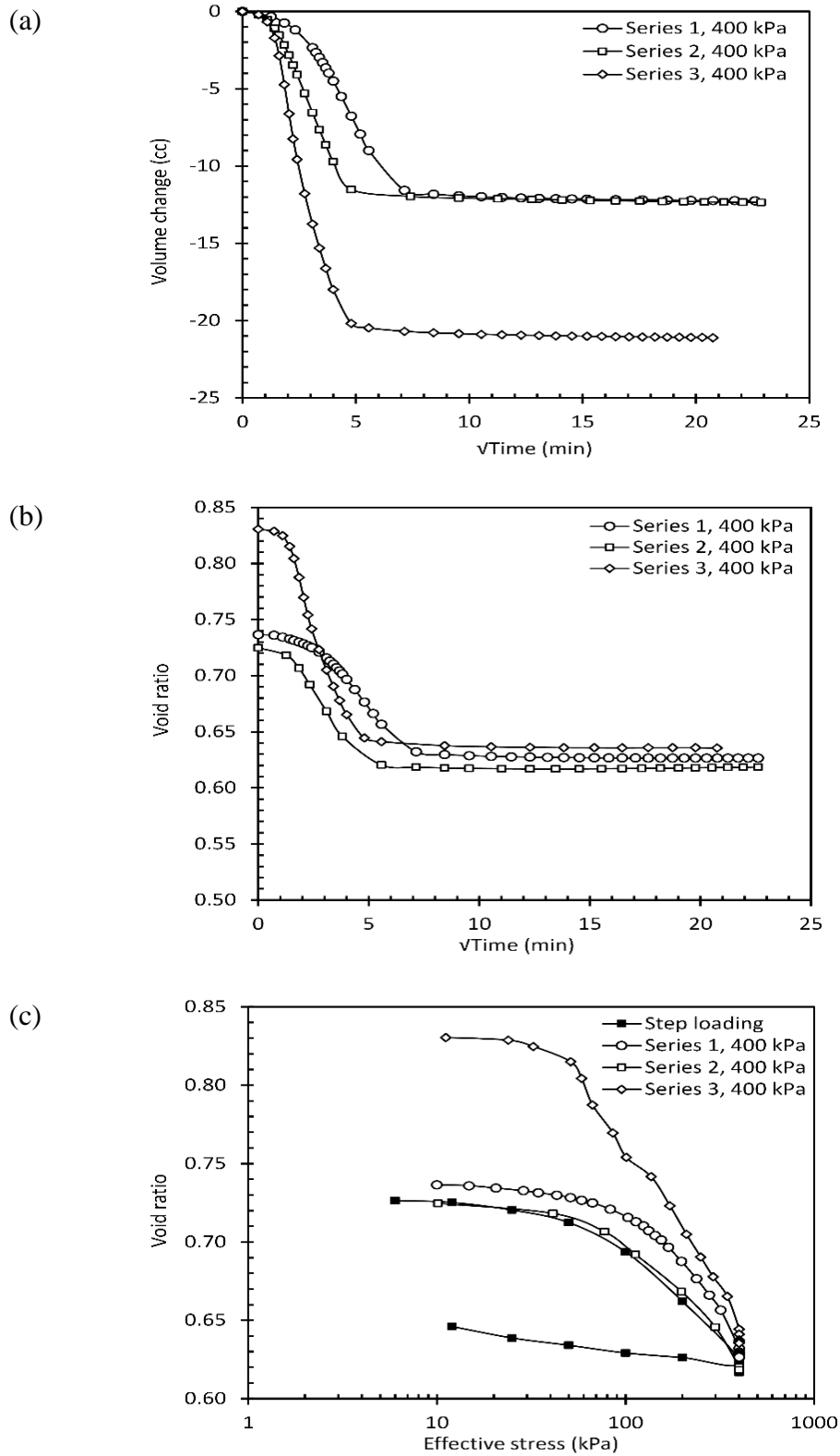
Figure 8.4 Comparison of the volumetric behavior during isotropic consolidation at 200 kPa effective stress: (a) volumetric changes versus time (b) void ratio versus time, (c) Isotropic consolidation curves.

145

8.1.1.3 Shearing Stage

Following consolidation, specimens were sheared at constant confining pressure. The state of the specimens after triaxial shearing tests are presented Table 8.1. Typical results of triaxial tests (variation of the deviatoric stress q, and volumetric strain versus axial strain) for each series (i.e. 1, 2 and 3) are presented in Figure 8.5-Figure 8.7. It can be seen from stress-strain curves that all the specimens exhibit strain-hardening behavior up to axial strain around 15% and eventually reach the critical state condition. Inspection of the figures related to volume change reveal a contractive behavior of the specimens in all the tests. All the specimens demonstrated a bulging failure without any distinct failure plane at the end of the tests. All these observation implies a normally consolidated behavior of the specimens.

Figure 8.8 to Figure 8.11 compare the stress-strain and volumetric response of all series at the same effective confining stress. Inspection of these figures reveal that, despite different preparation water content and void ratio, specimens reach the critical state condition. As expected, specimens with a higher initial void ratio exhibit more contractive behavior than those with a low void ratio. Finally, all specimens converge to a unique value of the void ratio (regardless of the initial void ratio and preparation water content). Therefore, it can be concluded that regardless of the initial condition (void ratio and preparation water content) all specimens approach to an ultimate value of the shear strength and void ratio. All of these observations are in agreement with critical state concept.

 Figure 8.12 Figure 8.14 show the critical state line in q-p´ and v-log p´ plane. The gradient of the critical state line q-p´ is determined to be M = 1.44, 1.39 and 1.42 for series 1, 2 and 3 respectively.

146
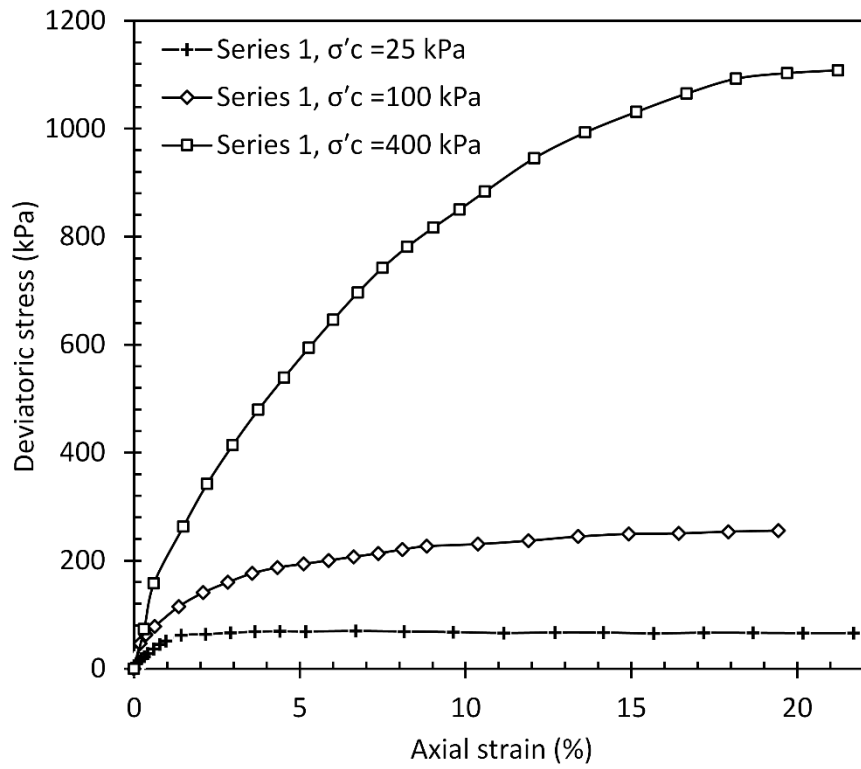
(a)
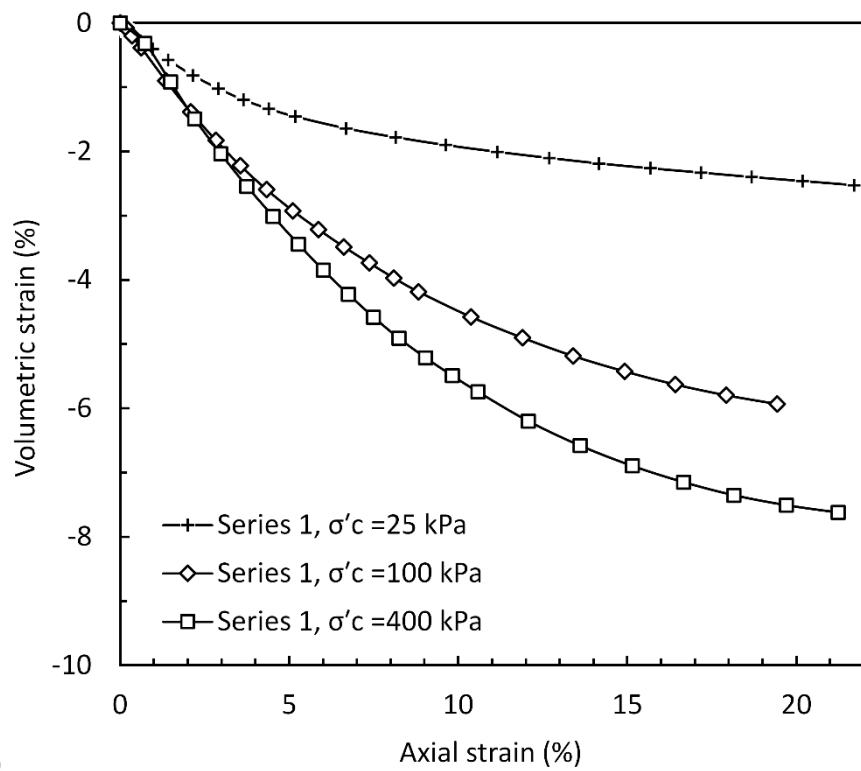
(b)

Figure 8.5 Triaxial tests results on series 1, (a) stress-strain (b) volumetric strain-axial strain.
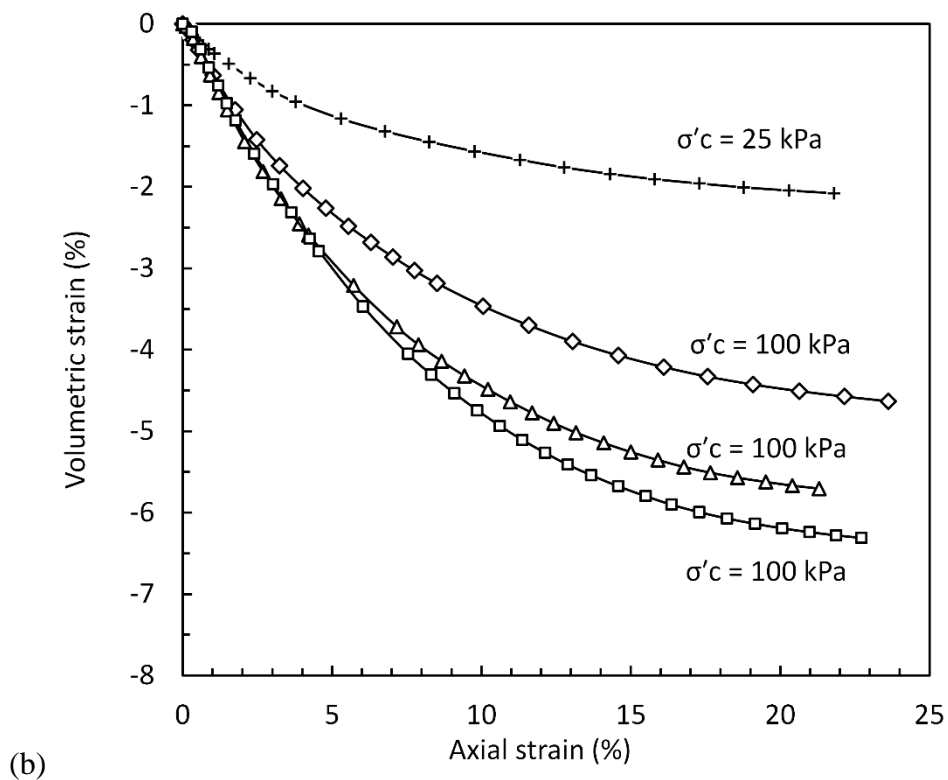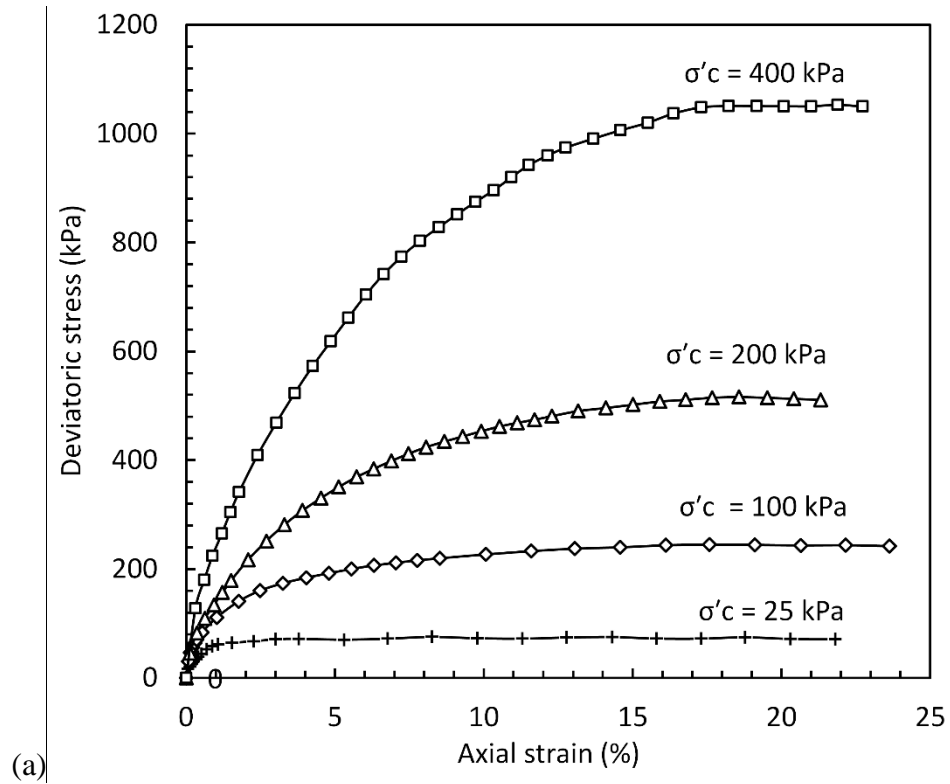
Figure 8.6 Triaxial tests results on series 2, (a) stress-strain (b) volumetric strain-axial strain.

148
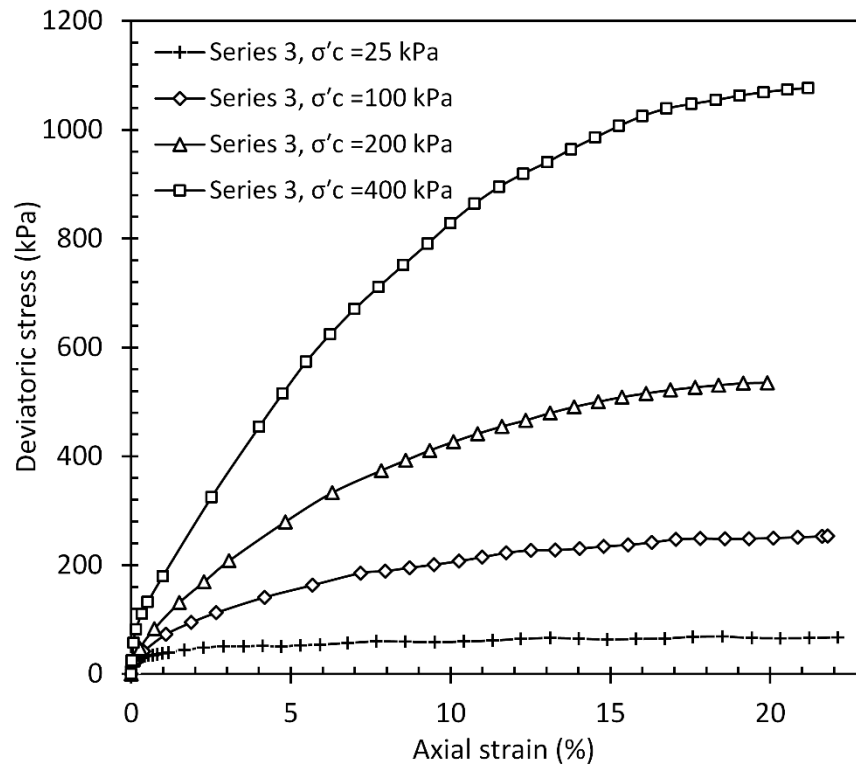
(a)
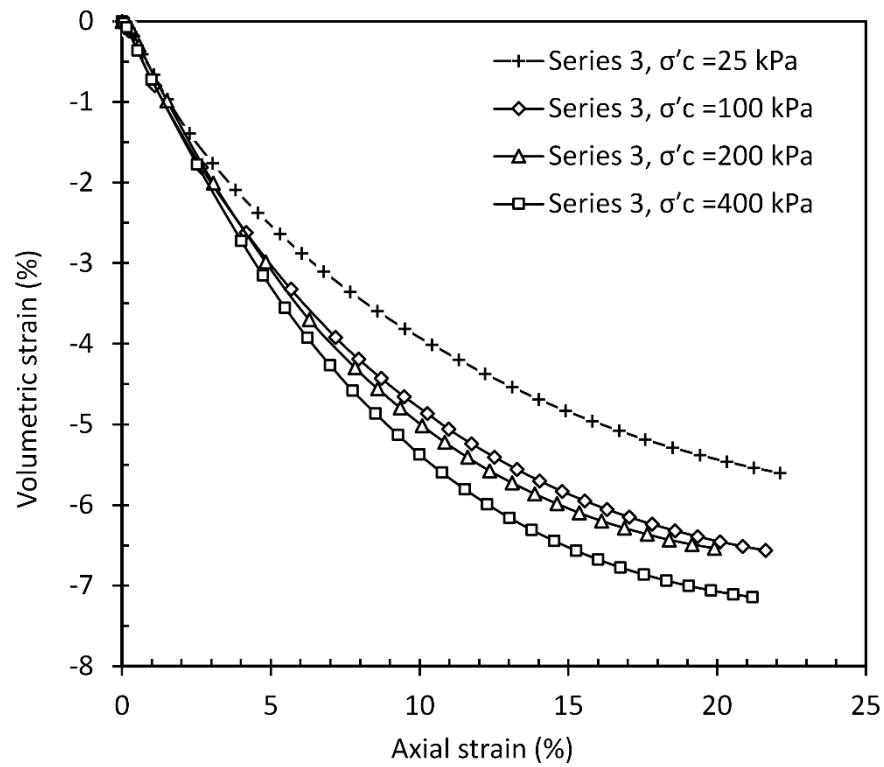
(b)

Figure 8.7 Triaxial tests results on series 3, (a) stress-strain (b) volumetric strain-axial strain.
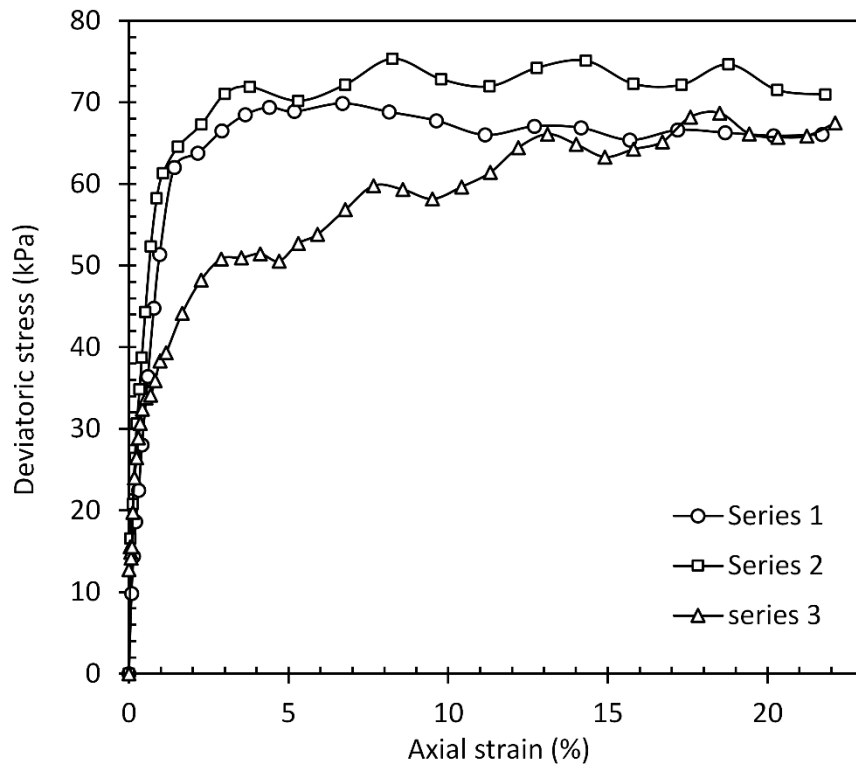
(a)
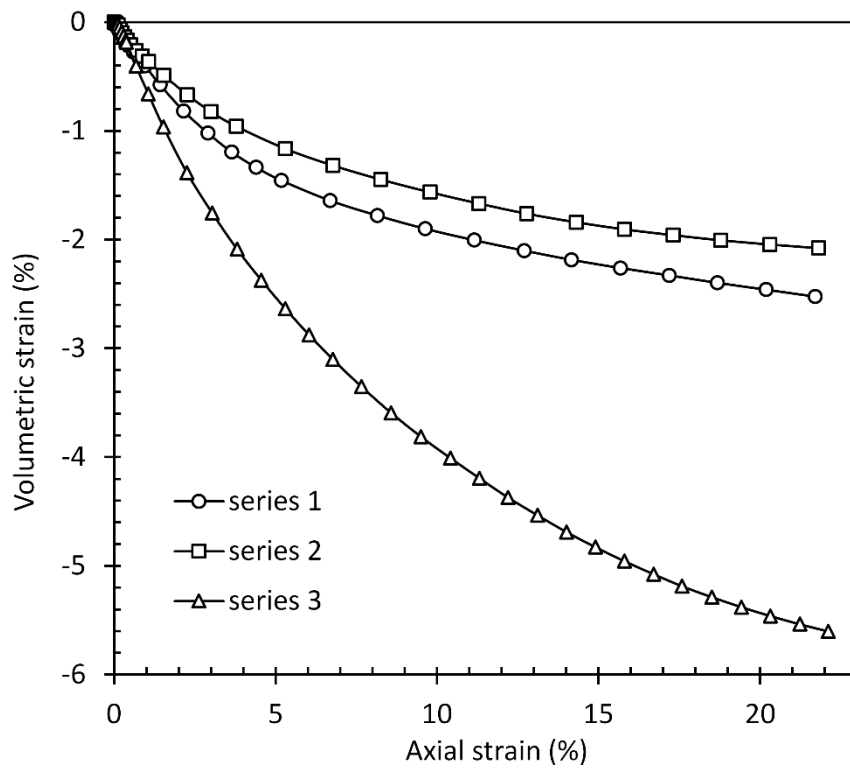
(b)

Figure 8.8 Comparison of triaxial tests results in series 1, 2 and 3 for
σ'_c=25 kPa, (a) stress-strain (b) volumetric strain-axial strain.

150
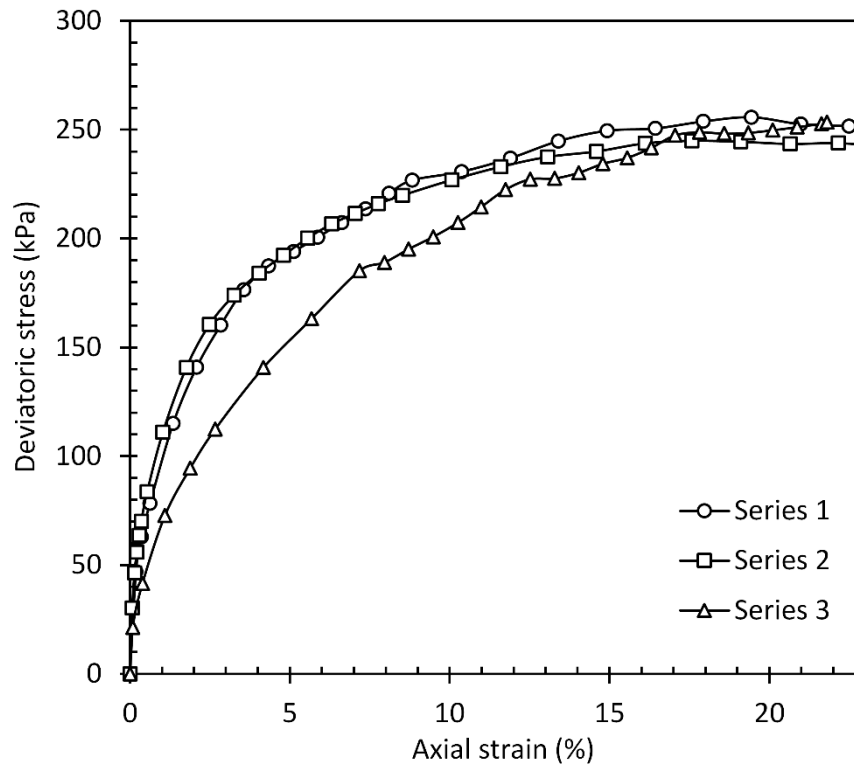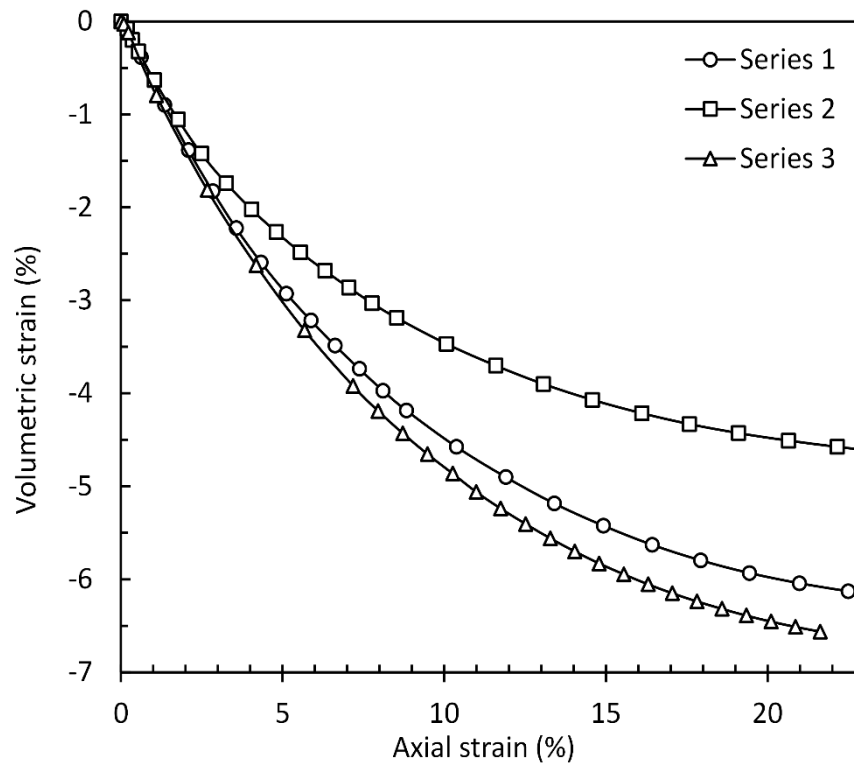
Figure 8.9 Comparison of triaxial tests results in series 1, 2 and 3 for
$\sigma'_c = 100$ kPa, (a) stress-strain (b) volumetric strain-axial strain.
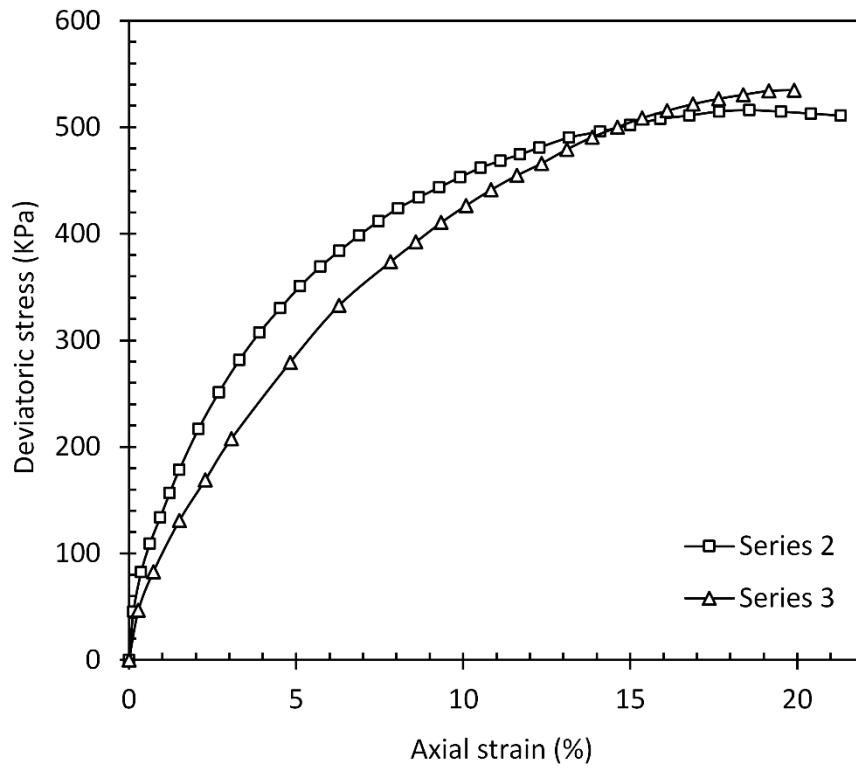
(a)
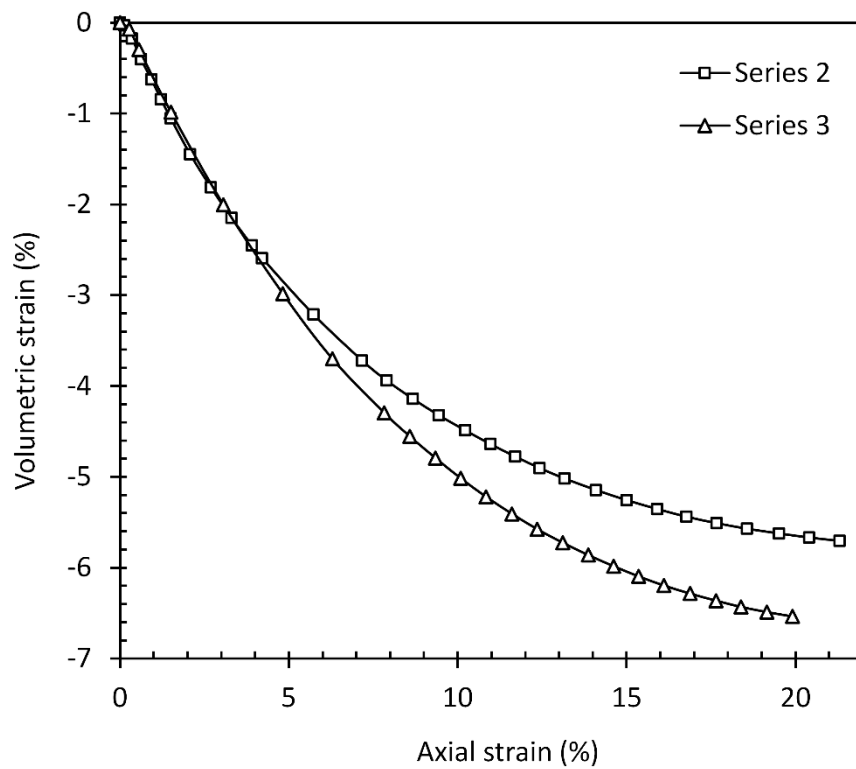
(b)

Figure 8.10 Comparison of triaxial tests results in series 2 and 3 for $\sigma'_c = 200$ kPa, (a) stress-strain (b) volumetric strain-axial strain.
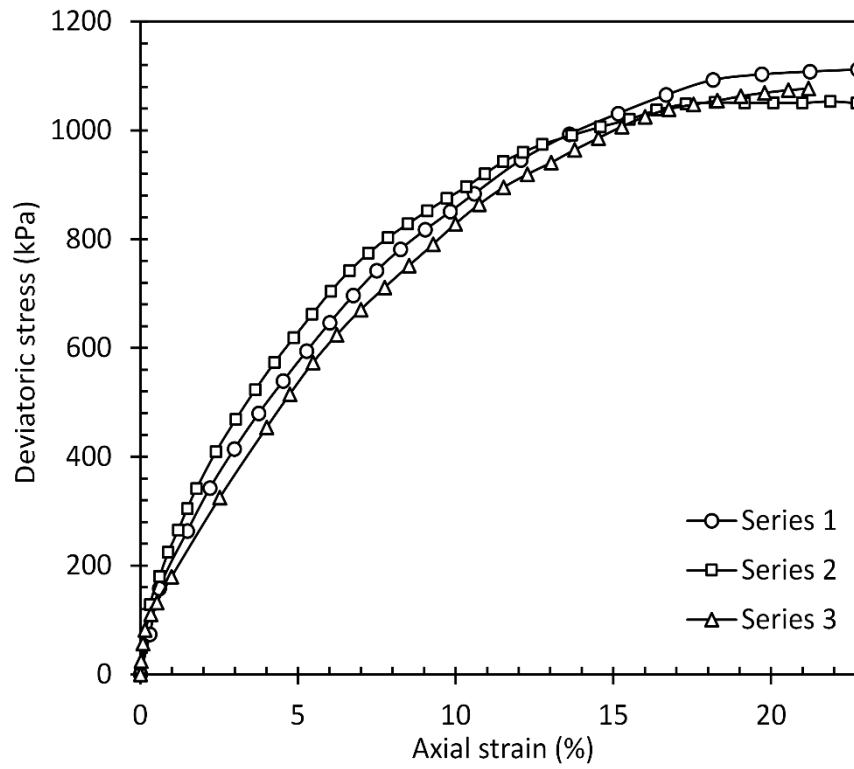
(a)
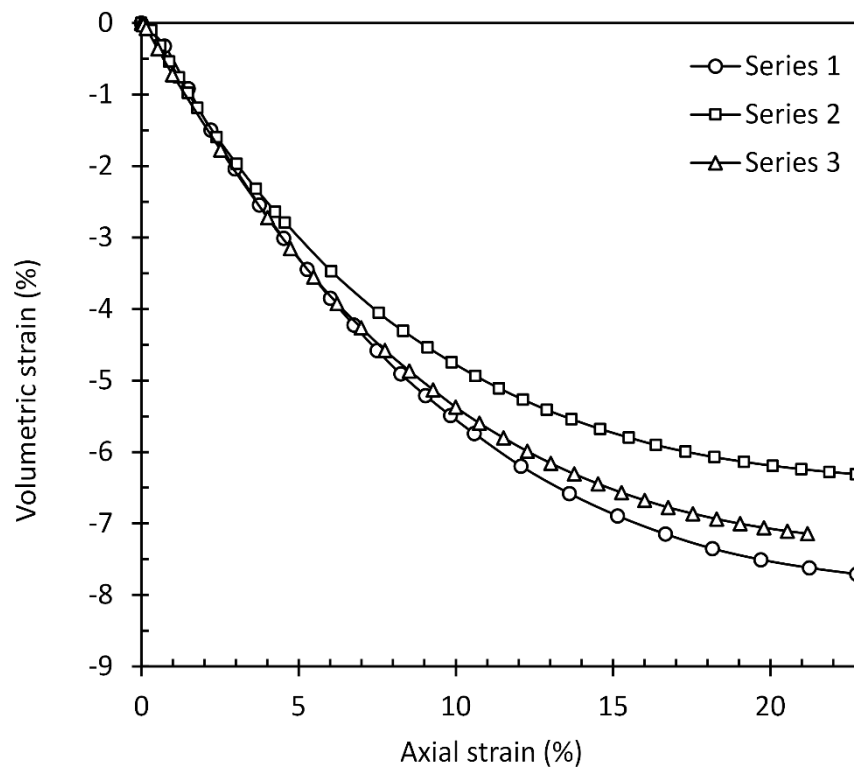
(b)

Figure 8.11 Comparison of triaxial tests results in series 2 and 3 for
$\sigma'_c = 400$ kPa, (a) stress-strain (b) volumetric strain-axial strain.
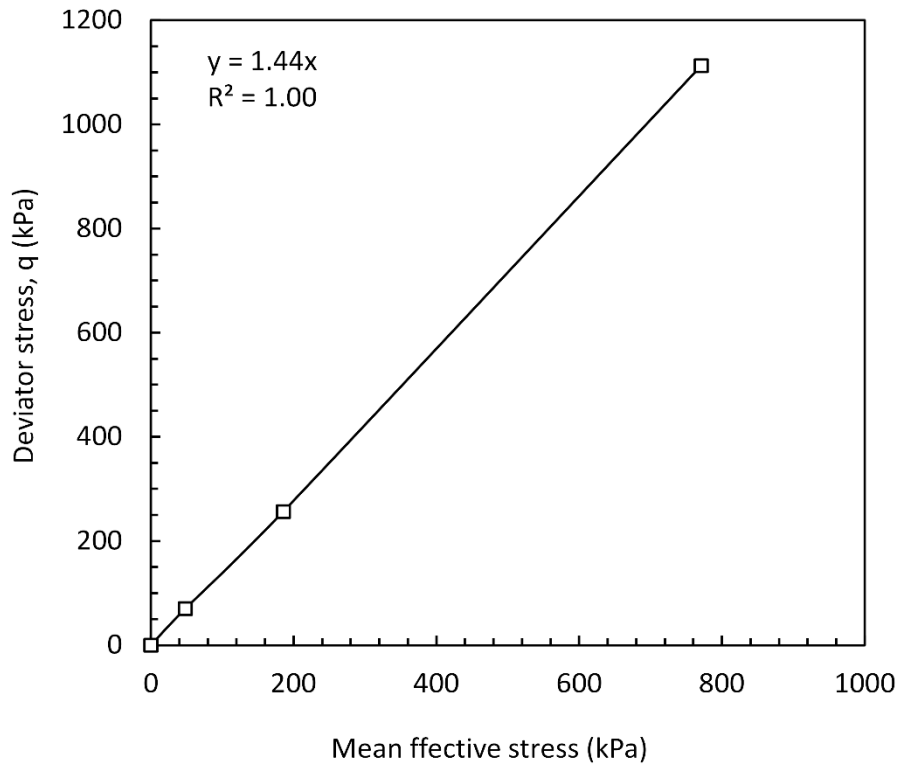
(a)
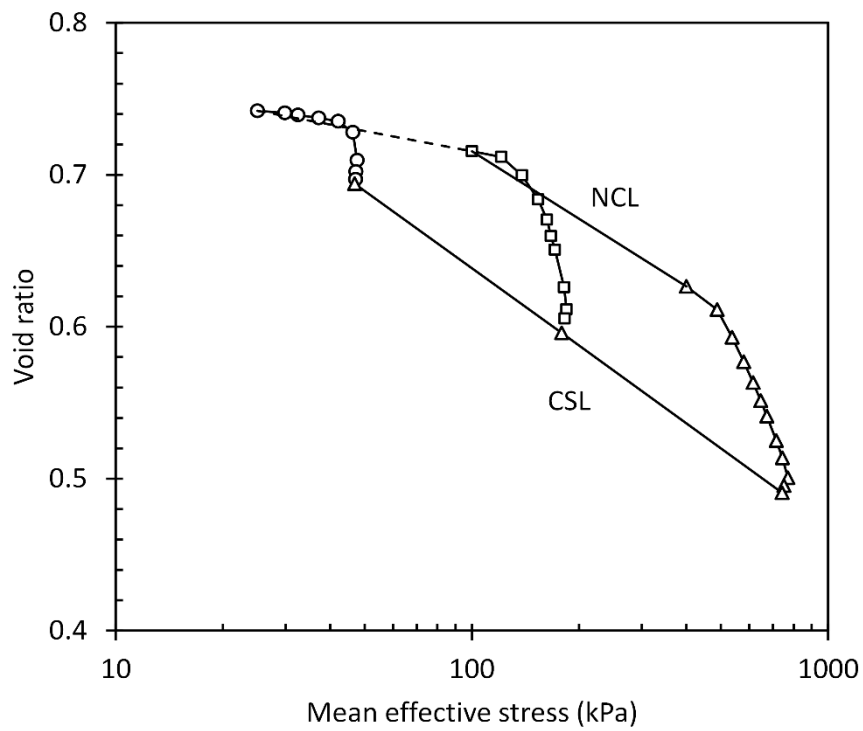
(b)

Figure 8.12 Critical state line for saturated specimens in series 1, (a) in
q - p plane; (b) in v - lnp plane.
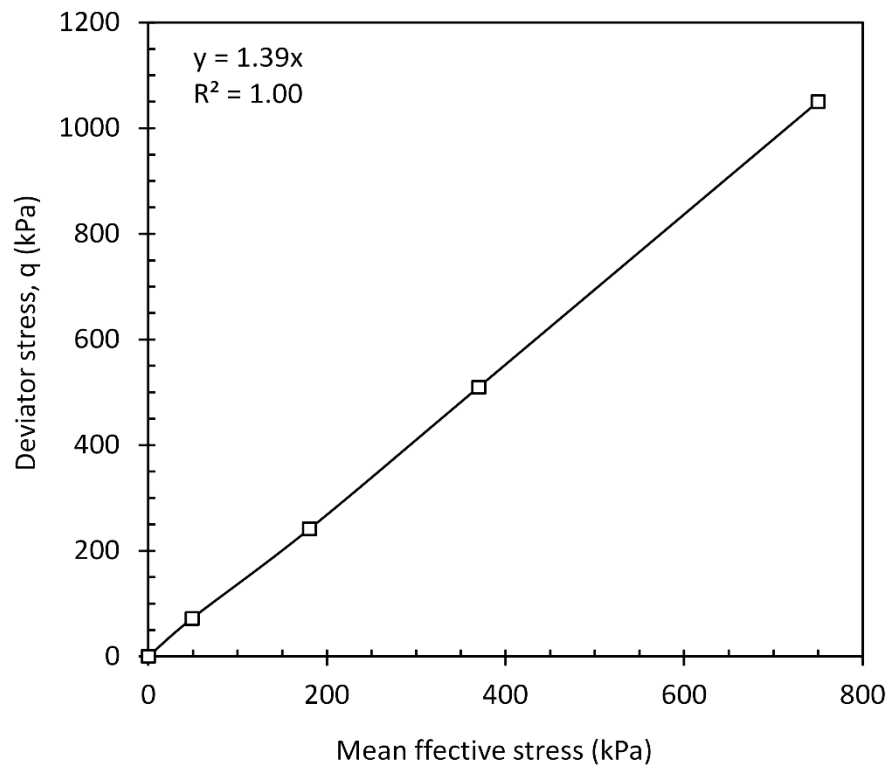
(a)
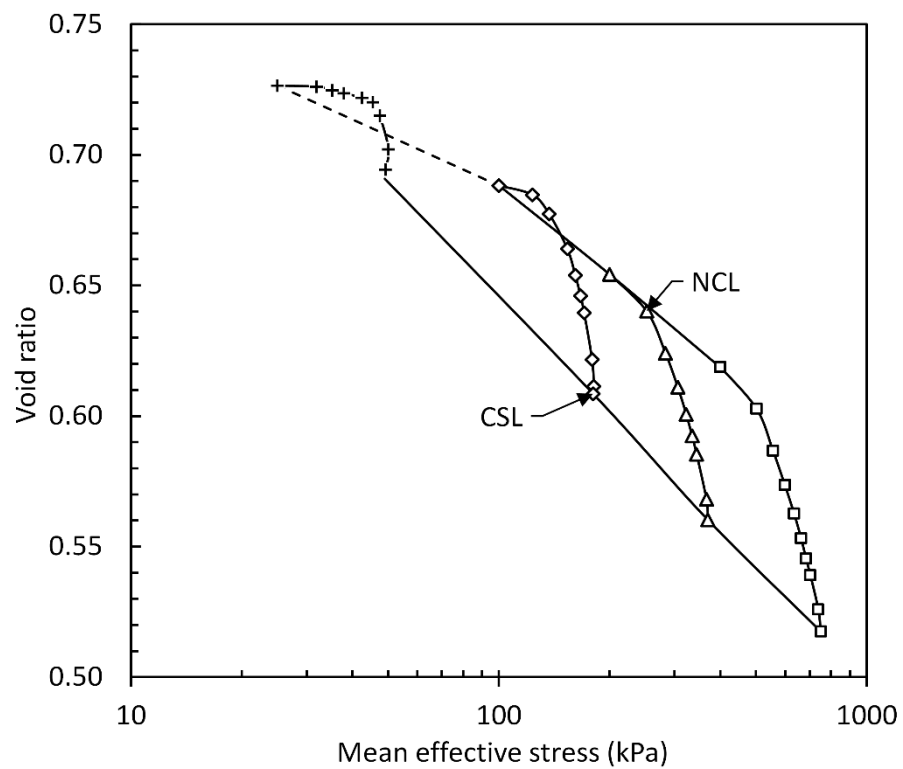
(b)

Figure 8.13 Critical state line for saturated specimens in series 2, (a) in
q - p plane; (b) in v - lnp plane.
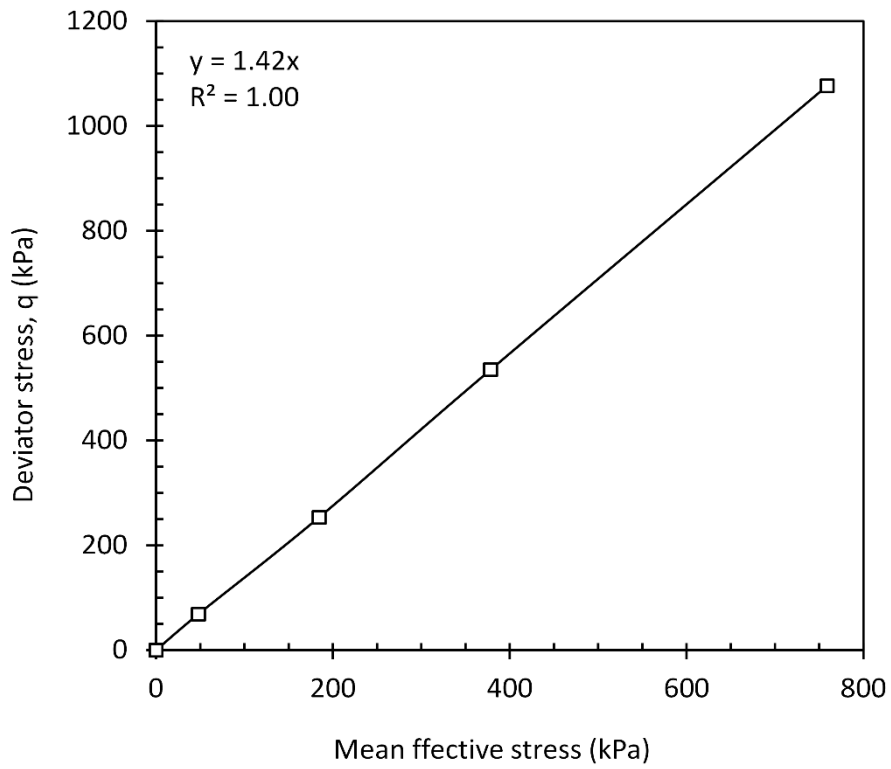
(a)
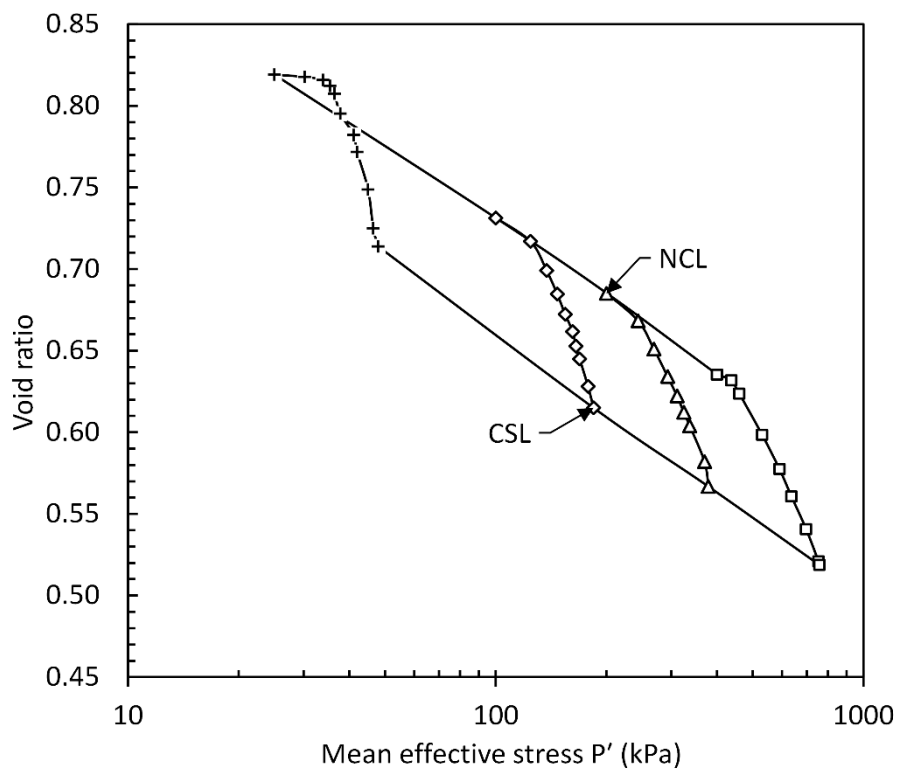
(b)

Figure 8.14 Critical state line for saturated specimens in series 3, (a) in
q - p plane; (b) in v - lnp plane.

156

8.1.2 Soil Water Characteristic Curve (SWCC)

The SWCC of the MT compacted specimen was obtained using the modified triaxial setup for both drying and wetting paths. The maximum suction is limited to 400 kPa due to the AEV of the ceramic (500 kPa). To prevent inflation of the membrane inside the triaxial cell, the SWCC was obtained at 10-kPa net stress. To obtain the SWCC specimen was first saturated. Then desired values of matric suction were applied step by step (and specimen was left to equalization under applied suction) through a drying path up to 400 kPa. Once equalization for drying path was achieved, wetting path is initiated by reducing suction to 5 kPa step by step.

The entire range of the suction was fitted using the Fredlund and Xing (1994)'s equation. Figure 8.15 shows the SWCC from experimental and the best fit from Fredlund and Xing (1996) equation. As it can be seen, hysteresis loop exists between the drying and wetting paths.

The air-entry value and the residual matric suction for drying path determined to be 18 kPa and 65 kPa, and for wetting path are 8 and 40 kPa, respectively.
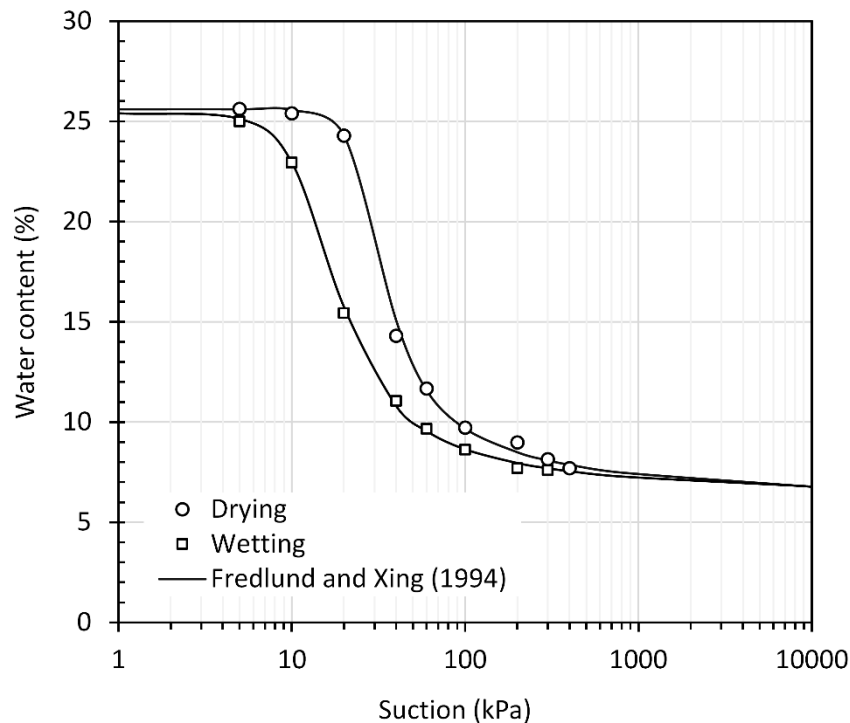
Figure 8.15 Soil water characteristic curve of Mersin silt on MT specimen.

157

8.1.3   Behavior of Unsaturated Compacted Specimens during Triaxial Tests

A total of 10 suction controlled CD triaxial tests were performed on MT compacted specimens. Following saturation of the high air entry ceramics and mounting the specimen on triaxial setup, these tests involve 3 stages:

1.   Suction *equalization*,
2.   Constant suction *Isotropic compression*,
3.   Constant suction drained *Shearing*

The sign convention for total volumetric strain is such that, the negative sign indicates compression, and positive sign indicates dilatation of the specimen; and for the volume change in the water phase, the positive sign is for water entering and the negative sign is for water exclusion from the specimen.

The adopted naming convention for MT specimens take the form of the "MT S P" where "MT" stands for specimen preparation method (i.e. moist tamped compacted specimens), "S" represents the suction value and "P" stands for the net mean stress.

In the following, the corresponding results of each stage are discussed.

8.1.3.1   Suction Equalization

First stage in triaxial testing of unsaturated soils is suction equalization. The termination criteria and procedures are discussed in section 7.2.1. The change of the water volume (with the help of DAVI) and total volume (with the method introduced in chapter 5) of the specimen during the equalization stage were monitored.

As mentioned in section 7.3.2.2, specimens were prepared with an initial water content of 10.2% that corresponds to 400-kPa suction. Therefore, wetting paths (water flows into the specimen) were followed to apply 100 and 200-kPa matric suction (see section 7.3.2.2 for followed stress paths). The state parameters of the specimen before and after the equalization stage are presented in Table 8.2. The volumetric changes of the specimens (both overall and volume of water flow) during equalization stage for each suction value (i.e. s = 100, 200 and 400 kPa) are shown in Figure 8.16 to Figure 8.18. As expected, water flows into the specimen, but the volume of water flow is very small. This can be attributed to hydraulic hysteresis

158

where irreversible changes in the water content occur during wetting and drying cycles. As it can be seen, a small amount of swelling was observed during wetting (for suction 100 and 200 kPa), which is consistent with saturation stage in saturated soil testing in series 1.

Table 8.2 State of the specimen before and after the equalization stage.

Test name	Suction (kPa)	Net mean stress (kPa)	Void ratio before	Void ratio after equalization	Degree of saturation before	Degree of saturation after equalization
MT100 25	100	25	0.72	0.73	37.8	38
MT100 100		100	0.72	0.73	37.8	39
MT100 400		400	0.72	0.74	37.8	39
MT200 25	200	25	0.72	0.73	37.8	38
MT200 100		100	0.72	0.73	37.8	38
MT200 400		400	0.72	0.74	37.8	38
MT400 25	400	25	0.72	0.73	37.8	40
MT400 100		100	0.72	0.73	37.8	40
MT400 400		400	0.72	0.72	37.8	39
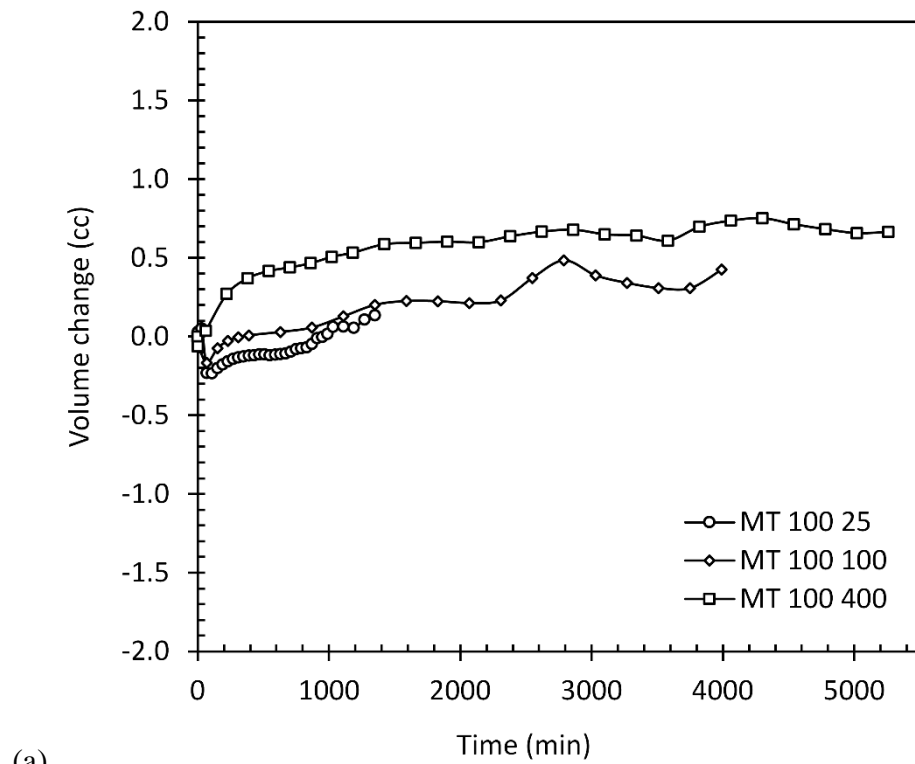
(a)
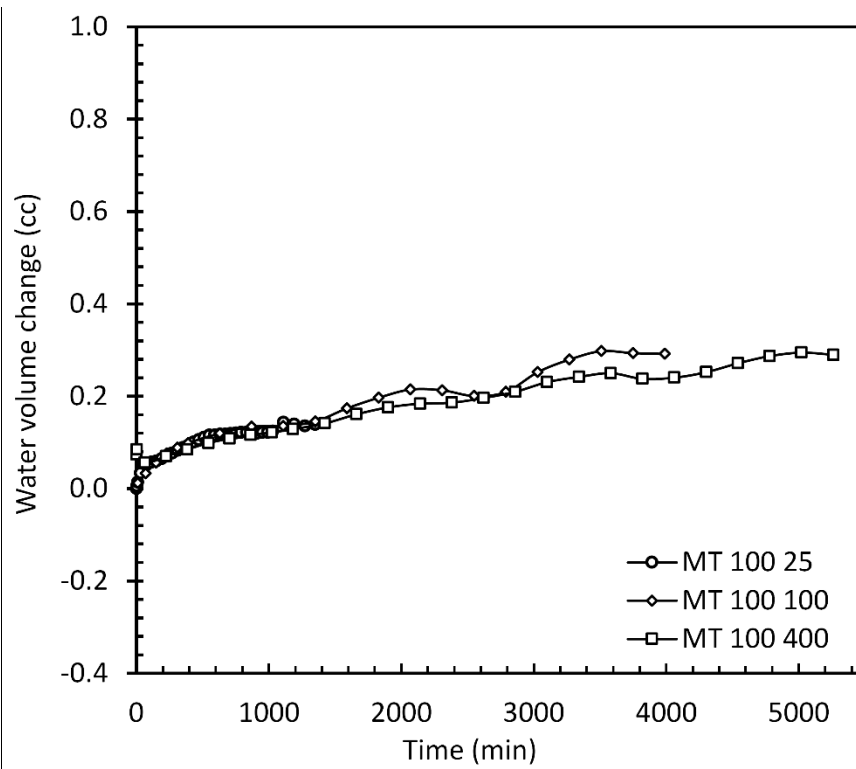
(b)

Figure 8.16 For suction = 100 kPa (a) changes in specimen volume during equalization stage (b) changes in water volume during equalization stage.
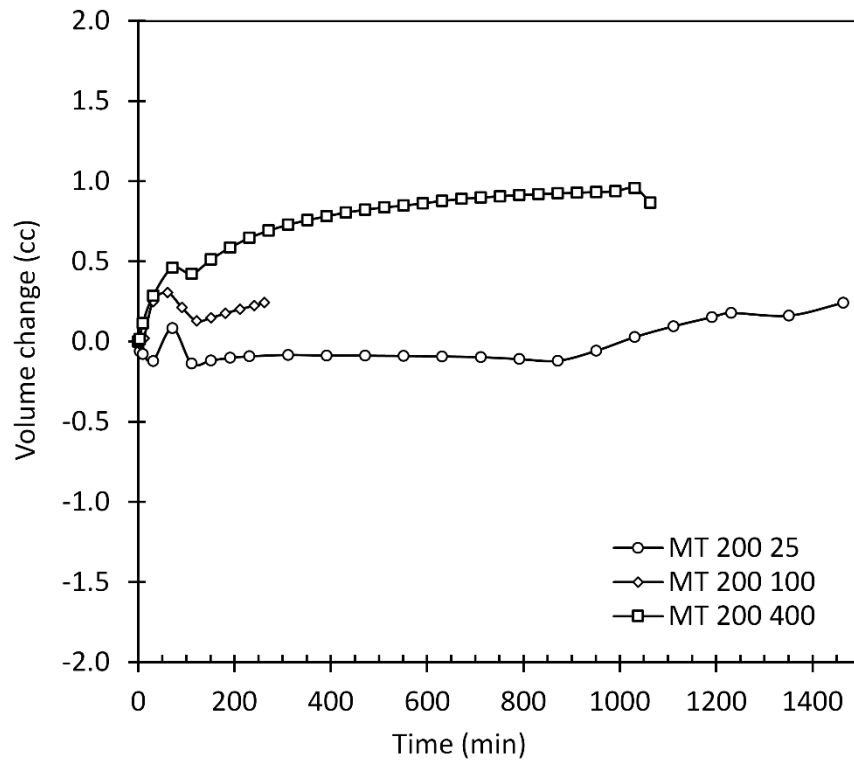
(a)
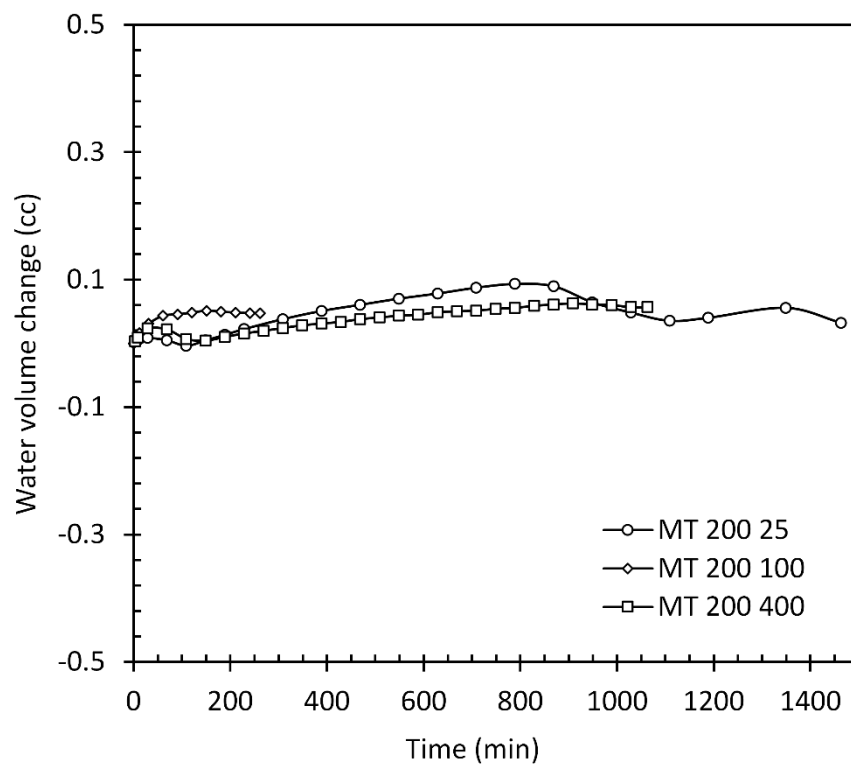
(b)

Figure 8.17 For suction = 200 kPa (a) changes in specimen volume during equalization stage (b) changes in water volume during equalization stage.
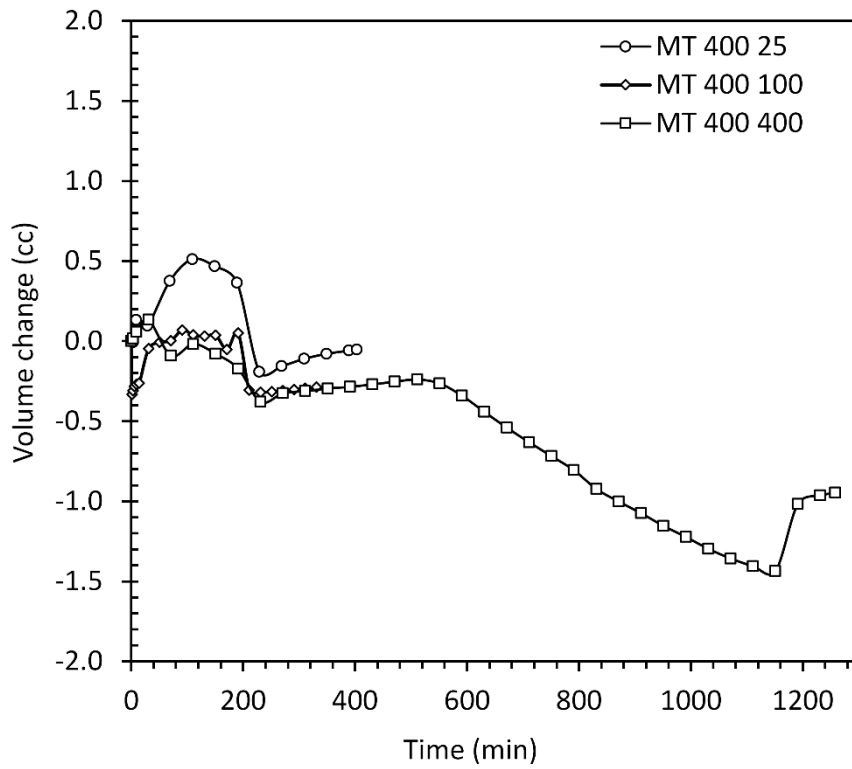
(a)
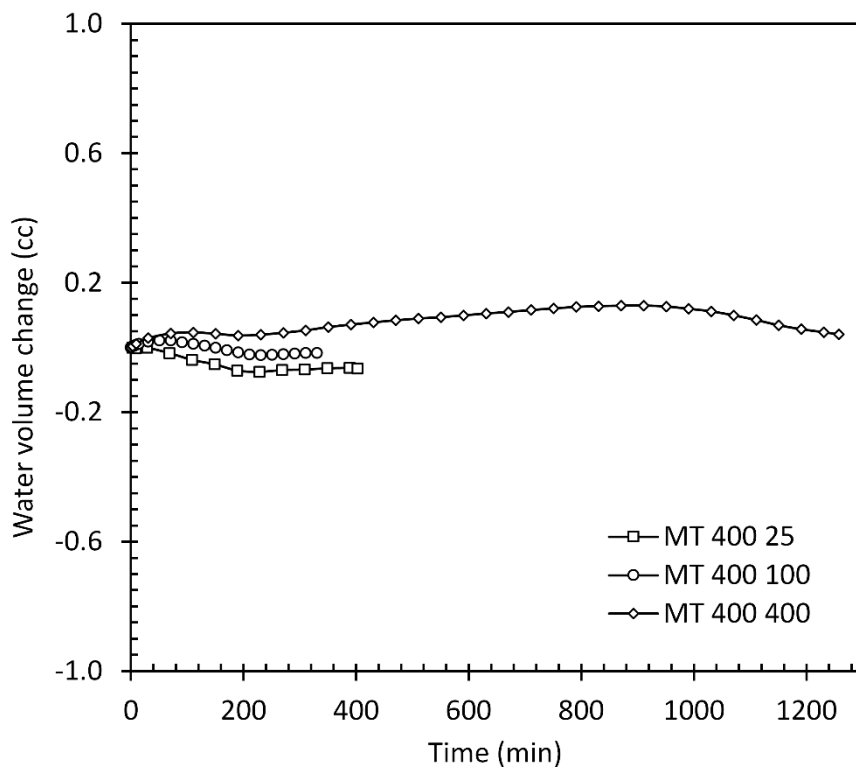
(b)

Figure 8.18 For suction = 400 kPa (a) changes in specimen volume during equalization stage (b) changes in water volume during equalization stage.

8.1.3.2 *Constant Suction Isotropic Compression*

Following equalization, specimens were isotropically compressed to a desired net mean stress at constant suction (see section 7.2.2 for detail). The variation of the void ratio, with net mean stress p, for tests at 400-kPa net mean stress (for suction values of 0, 100, 200 and 400 kPa) are presented in Figure 8.19. The void ratio prior to the compression for tests at suction values of 0, 100 and 200 kPa are higher than those at 400-kPa, due to swelling during the equalization stage.
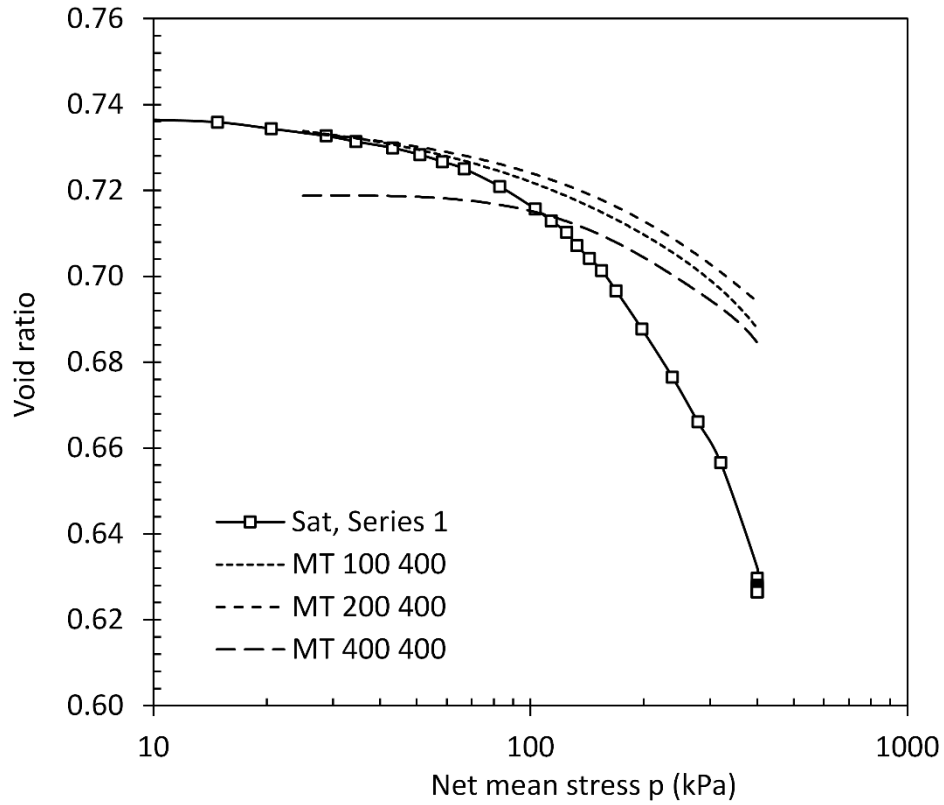
Figure 8.19 Isotropic compression curves at different suction values for MT compacted specimens.

As described in section 2.4.1.1, the elastic deformation is due to both suction, and net mean stress. Alonso, et.al. (1990) formulated the elastic variation in specific volume as below:

$$dv^e = -\kappa \frac{dp}{p} - \kappa_s \frac{ds}{s + p_{atm}} \qquad (8.1)$$

where κ is elastic constant due to net stress and κ_s is elastic constant due to suction. They assumed that κ and κ_s are soil constants and are independent of suction. The elastic section (the linear section before yield stress) of the compression curve at constant suction can be used to determine the κ. The gradient of the elastic sections in isotropic compression curves were determined as the elastic stiffness parameter κ. The elastic stiffness parameter κ, for tests at suction values of 0, 100 and 200 kPa was determined to be κ = 0.005, but this decreased to 0.002 in compression test at 400-kPa suction.

The normal compression line (NCL) for different values of the suction could be defined as a straight line after yield point in v-logp space. As discussed in section 2.4.1.2, Alonso et.al. (1990) proposed the following equation to model the NCL for different values of the suction:

$$v = N(s) - \lambda(s) \ln \frac{p}{p^c} \qquad (8.2)$$

where p^c, is the reference pressure, the N(s) is the specific volume at reference pressure and λ(s) is gradient of the NCL for a given suction. Both N(s) and λ(s) are suction dependent.

Similar to κ, the value of the λ(s) is estimated from compression curves for each value of suction. Figure 8.20 shows the variation of the λ(s) with matric suction. As it can be seen, a significant reduction in λ(s) occurs, where λ(s) decreases from 0.076 in saturated state, at a decreasing rate toward an asymptotic value, to 0.038 for 400 kPa suction.

As described in section 2.4.1.2, Alonso, et.al. (1990) proposed the Eq (2.18) to relate the variation of the λ(s) to matric suction. This equation includes two fitting parameters which were determined to be r = 0.495 and β = 0.0245 through a trial and error procedure. Using these parameters and Eq (2.18), a best line is fit onto the experimental observations and shown in Figure 8.20. This shows the variation of the

164

λ(s) with suction is in agreement with the form of equation suggested by Alonso et.al. (1990).

In all the tests, yielding ("transition from stiff to less stiff response", Wood (1991)) was occurred during isotropic compression. In this study the procedure followed by Cui and Delage (1996) was adopted to determine the yield stress. For this, two straight lines were fitted to elastic (stiff section) and plastic (less stiff section) sections of the compression curve. The intersections of these two straight line were defined as the yield stress.

The estimated values of the yield stress were used to define the loading collapse (LC) yield curve that is shown in Figure 8.21.The LC yield curve was fitted through the Eq (2.18) and Eq (2.19) proposed by Alonso, et.al. (1990).

In this equation all the parameters are determined except the fitting parameter of the p^c, which is determined to be $p^c = 92$ kPa through a trial and error procedure.
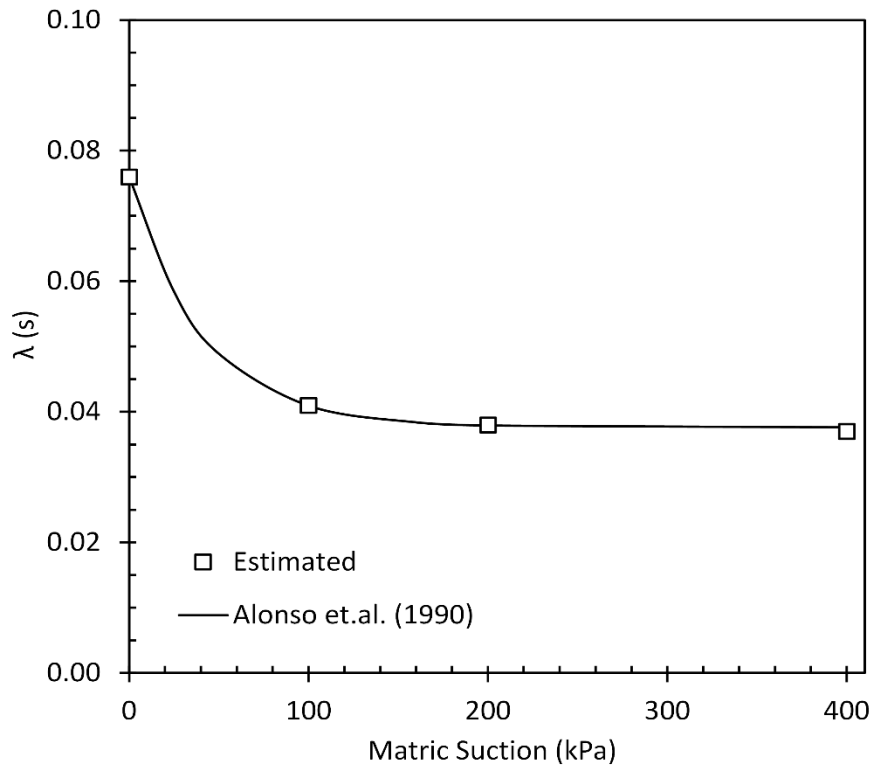
Figure 8.20 Variation of the $\lambda(s)$ values with matric suction.
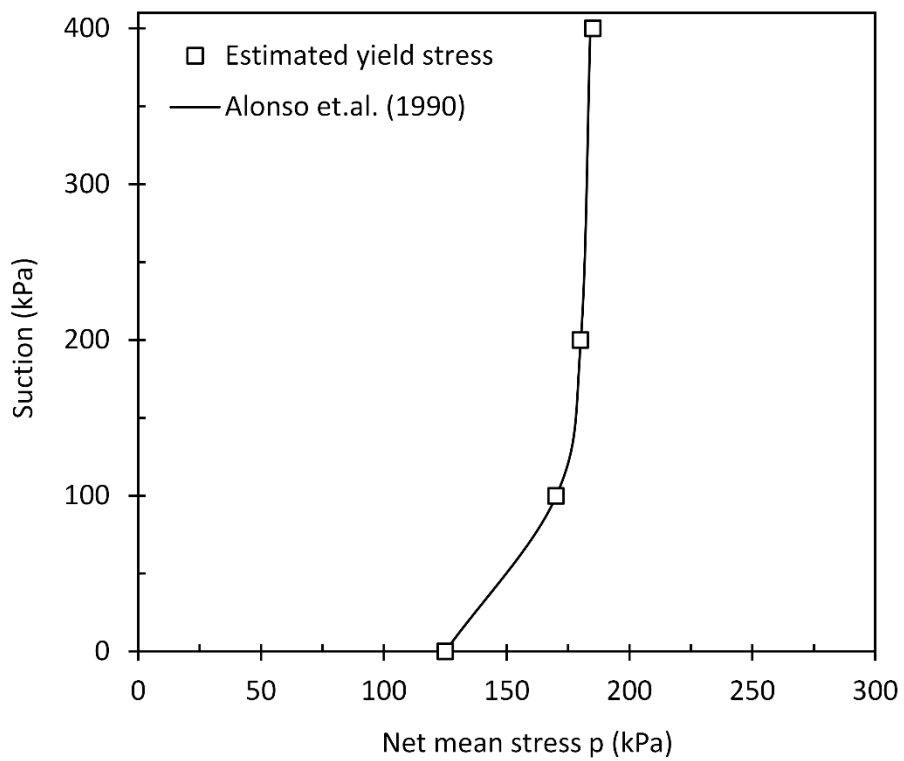
Figure 8.21 Measured and fitted loading-collapse yield curve for MT compacted specimens.

8.1.3.3 Drained Shearing at Constant Suction

Following consolidation, specimens were sheared at a constant strain rate, under constant-suction (drained condition for both air and water phase) and constant cell pressure. A total of 9 unsaturated shear tests were performed at three different values of the suction and net mean stress (i.e. suction =100, 200 and 400 kPa and net mean stress = 25, 100 and 400 kPa) (see section 7.3.2 for detail).

The test results in this study were interpreted in two ways. First, the effect of the net mean stress on stress-strain and volumetric behavior were considered. In this category, the results of the shearing stage of the triaxial tests were presented and categorized into three series, each with equal suctions and different net confining stress.

Second, effect of the suction on stress-strain and volumetric behavior of the specimens were investigated. In this category, the results of the shearing stage of the triaxial tests were presented and categorized into three series, each with equal net confining stress and different suctions.

8.1.3.4 Effect of Net-Confining Stress

Figure 8.22 (a), Figure 8.23 (a), Figure 8.24 (a), show the typical results of the triaxial tests at different net confining stresses but at the same suction. As it can be seen, most of the specimens represent a post-peak softening behavior. This becomes more pronounced at low net confining stresses, where a peak deviatoric stress is attained at lower strain. As expected, for constant values of the suction, the stiffness also increases with net confining stress.

From the stress-strain figures, it can be seen that, for a constant value of the suction, the stiffness of the specimen (modulus) and the maximum deviatoric stress increases with net confining stress.

For tests at 25-kPa net confining stress specimens reached a peak deviatoric stress, in less than 3.5% axial strain, which is followed by decrease in shear strength (strain-softening) and then gradual stabilization and a move toward critical state values. For

tests at 100-kPa net confining stress, specimen represents a behavior similar to lightly-overconsolidated specimens where reach to its maximum strength at an axial strain of about 8%, and then decreases smoothly to a critical value. For tests at 400-Kpa net confining stress, specimens represent strain-hardening behavior similar to normally consolidated specimens (the maximum strength were reached at an axial strain of about 19%). These observations are consistent with volumetric variation of the specimen (Figure 8.22 (b), Figure 8.23 (b), Figure 8.24 (b),), where specimens at 25-kPa net confining stress initially compressed and then dilation was occurred. The maximum rate of the dilation corresponds to maximum deviatoric stress. Specimen at 100-kPa net confining stress was initially compressed and then represented a smooth dilative behavior. For net confining stress of 400 kPa, specimens exhibited a completely compressive behavior.

Figure 8.22 (c), Figure 8.23 (c), Figure 8.24 (c), show the changes in water volume during shearing of three series of triaxial tests. The change in volume of the water phase of the specimens exhibit the opposite behavior to dilative behavior of the specimens. It seems that, the volume of expelled water increases with decreasing net confining stress.

The same behavior was also reported by Sivakumar (1993) and Zhan (2003), where the water content during shearing increased despite the contractive volumetric behavior. Zhan (2003) attributed this behavior to double-structure fabric.

However, in this study, the same behavior was also observed for IRS specimens (presented in section 8.2.1.3.1). It has been shown that specimens dried from slurry have a unimodal pore size (Sheng et al. 2013).

A possible explanation for this might be that, as the specimen dilates upon shearing (i.e. void ratio increases), the SWCC tends to move to the left, (i.e. water content decreases at the same suction) and therefore, water drains out of voids. The same statement applies also to the contractive behavior (i.e. as the void ratio decreases the SWCC moves to the left and water flows into the specimen).

Figure 8.22 Variations of (a) deviatoric stress, (b) volumetric strain and (c) change in volume of water during shearing at s = 100 kPa.

Figure 8.23 Variations of (a) deviatoric stress, (b) volumetric strain and (c) change in volume of water during shearing at s = 200 kPa.

(a)

(b)

(c)

Figure 8.24 Variations of (a) deviatoric stress, (b) volumetric strain and (c) change in volume of water during shearing at s = 400 kPa.

171

8.1.3.5   Effect of Suction Magnitude

25-kPa net confining pressure

Figure 8.25 (a) shows the stress-strain behavior of the specimen at net confining stress of 25 kPa with different values of suction (i.e. 100, 200 and 400 kPa) and saturated condition. The maximum shear strength is greater by about 150, 163 and 210 kPa than that of the saturated test for matric suctions of 100, 200 and 400 kPa, respectively. As it can be seen, the response of the specimens change from strain-hardening in saturated condition to strain-softening for higher values of suction. For the entire range of suction, specimens reach a peak deviator stress at low axial strain, which is followed by decrease (strain-softening) in shear strength. It then gradually stabilize and moves toward critical state values as the strain further increases.

All saturated specimens were deformed by bulging with no apparent shear plane. However, unsaturated specimens represented a distinct shear plane with bulging around shear plane. The volumetric behavior of the specimens are presented in Figure 8.25 (b). A dilative behavior was observed for all unsaturated specimens in contrast to saturated specimens which exhibit completely contractive behavior. As it can be seen, the dilatancy increases as the suction increases.

Figure 8.25 (c) presents the variation of the volume change related to water phase. As can be seen a completely opposite response with total volume change is illustrated. As the suction increases, water tends to be excluded from specimen which results in decreasing water content of the specimen. This behavior can be explained by considering SWCC shifting (either left or right depending state of the specimen) as discussed in detail in section 8.1.3.4 .
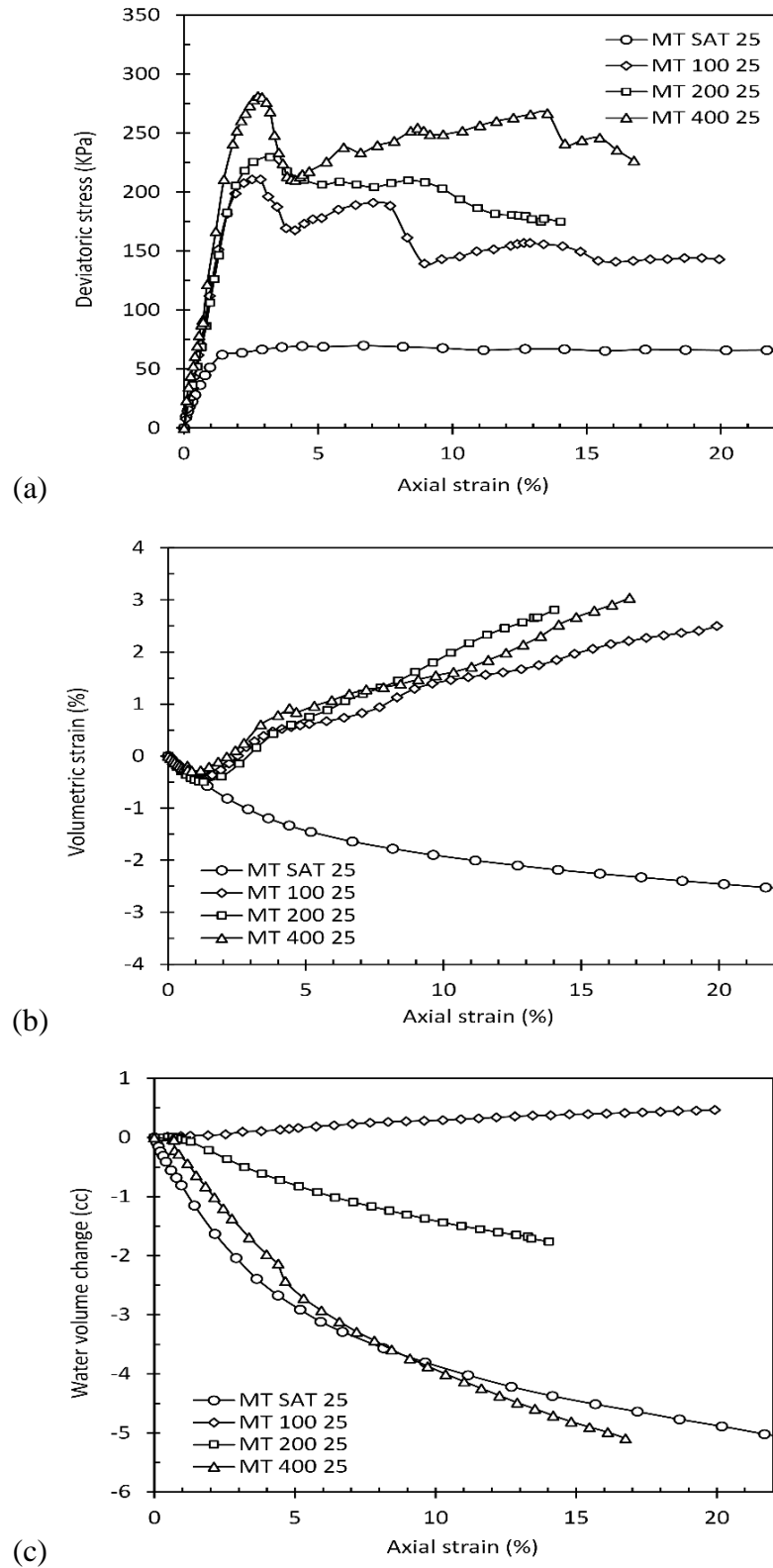
Figure 8.25 Variations of (a) deviatoric stress, (b) volumetric strain and (c) change in volume of water during drained shearing at $(\sigma_3 - u_a) = 25$ kPa.

173

100-kPa net confining pressure

The results of the shearing stage of the tests at 100-kPa net confining pressure and different values of the matric suction (i.e. 100, 200 and 400 kPa) and saturated condition are presented in Figure 8.26 (a). As before, greater shear strength and stiffness of the specimens are observed for greater matric suction. The maximum shear strength is greater by about 130, 180 and 255 kPa than that of the saturated test for matric suctions of to 100, 200 and 400 kPa, respectively. For tests at 100, 200 and 400-kPa matric suction, specimens represent behavior similar to lightly overconsolidated specimens. The specimens achieve their maximum shear strength at axial strain before 10%, and then smoothly decreases to critical value.

The volumetric behavior of the specimens are presented in Figure 8.26 (b). Unlike the saturated tests (where specimens exhibited a completely contractive behavior), specimens initially compressed and then represented a smooth gradual dilative behavior.

The variation of the volume change related to water phase also presented in Figure 8.26 (c). The same trend as before (tests at 25-kPa net confining stress) can be seen where, as the suction increases water tends to be excluded from the specimen and result in decreasing water content of the specimen. This behavior can be explained by considering SWCC shifting (either left or right depending state of the specimen) as discussed in detail in section 8.1.3.4 .
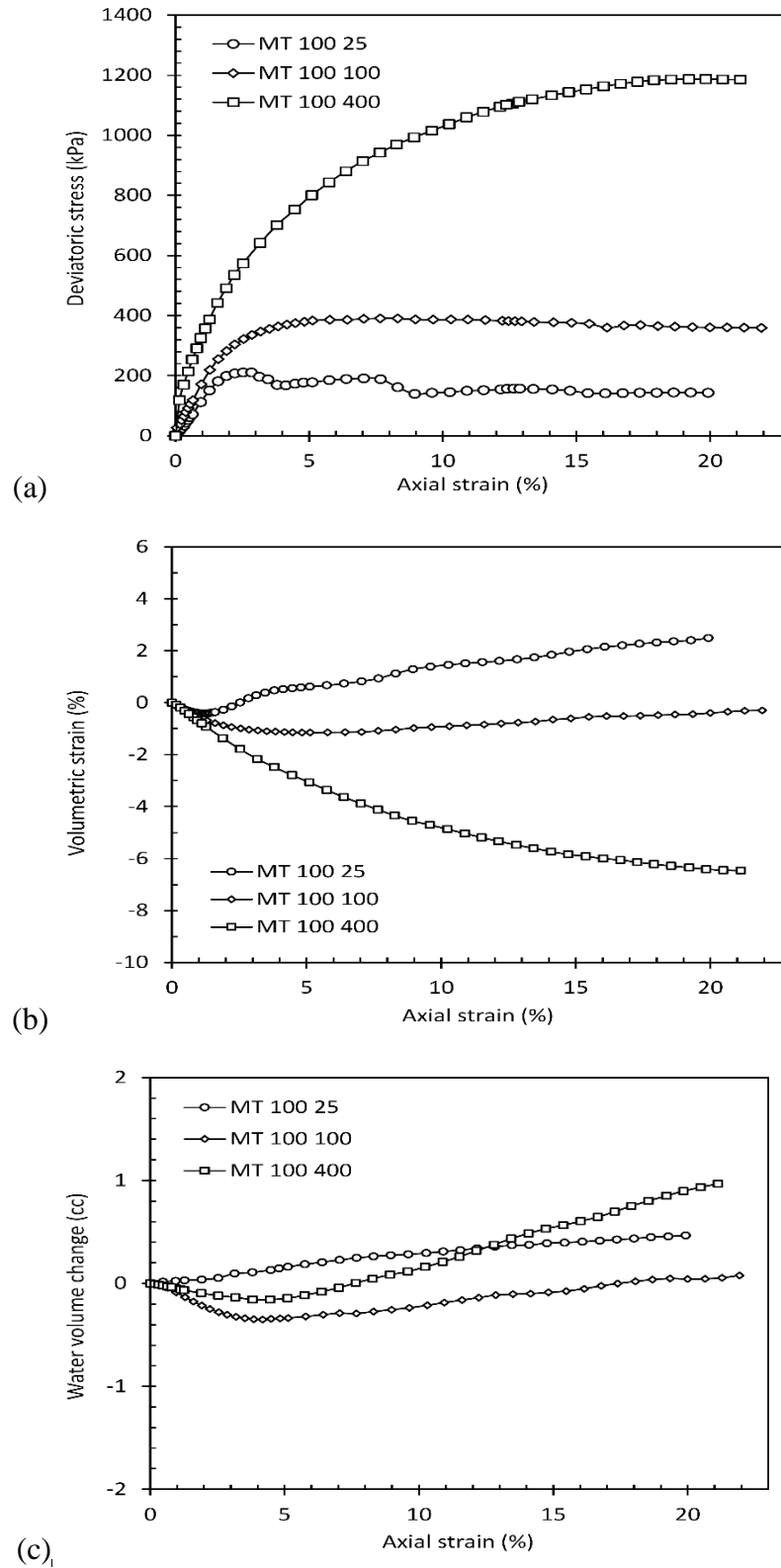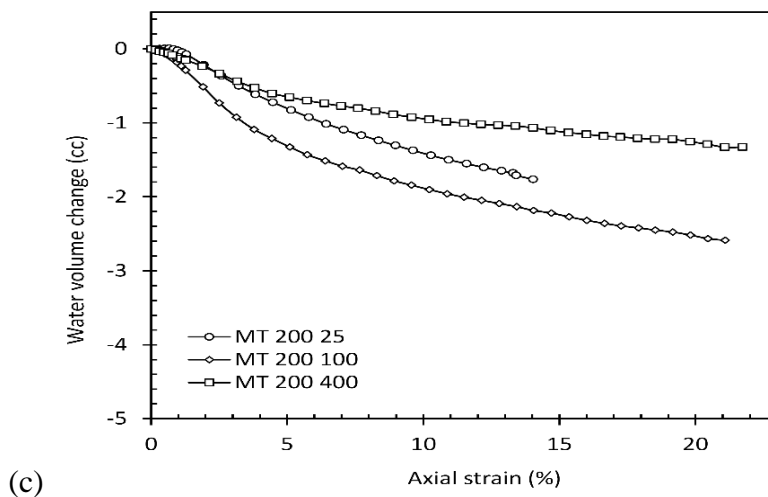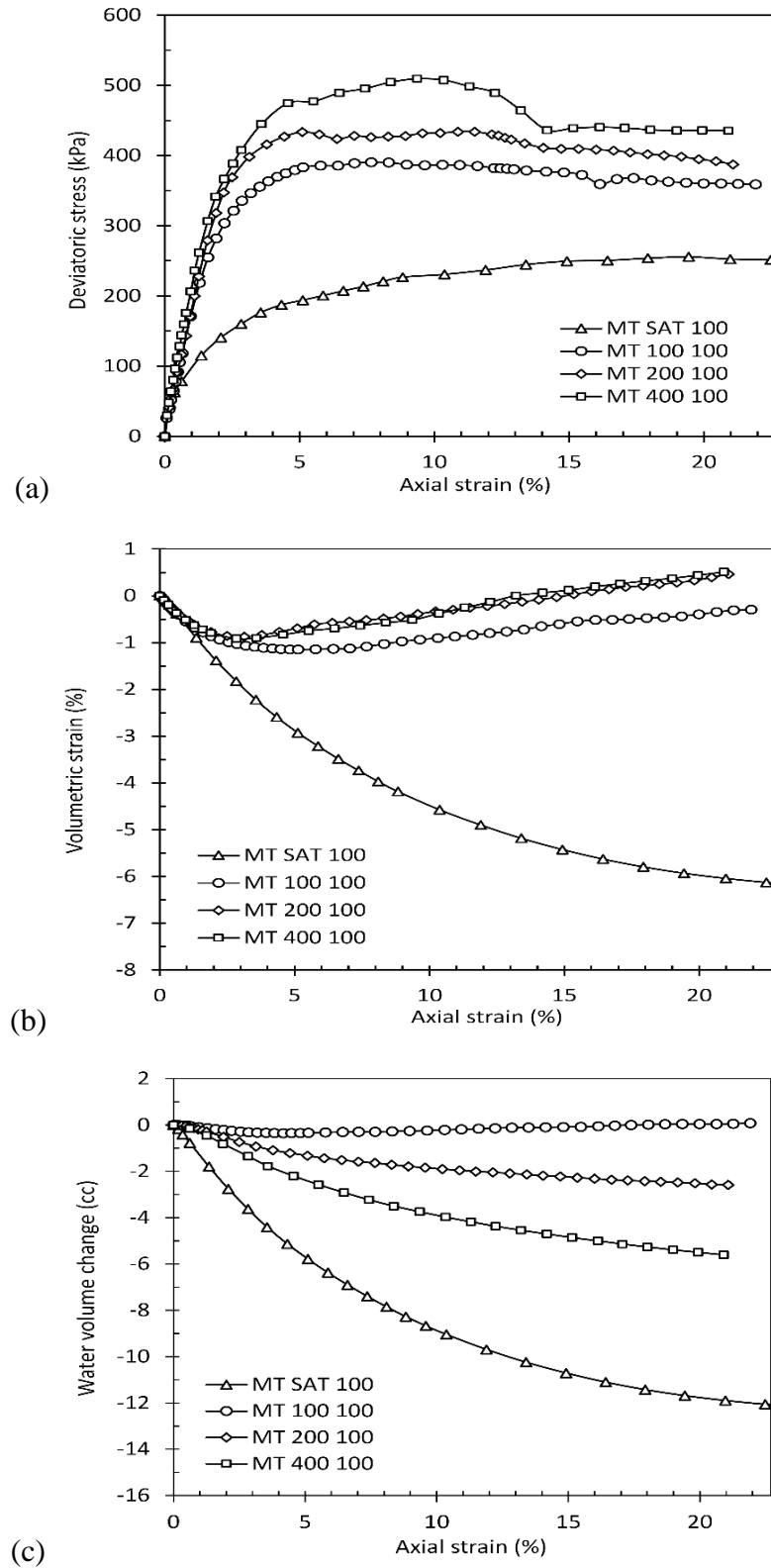
Figure 8.26 Variations of (a) deviatoric stress, (b) volumetric strain and (c) change in volume of water the during drained shearing at $(\sigma_3\text{-}u_a)$ = 100 kPa.

400-kPa net confining pressure

The results of the shearing stage of the tests at 400-kPa confining pressure and different values of the matric suction (i.e. 100, 200 and 400 kPa) and saturated condition are presented in Figure 8.27 (a). Increase in stiffness of the specimens is more evident those at 25 and 100-kPa net confining stress. As before, the maximum shear strength is greater for higher matric suction. The maximum shear strength is greater by about 75, 145 and 255 kPa than that of the saturated test for matric suctions of to 100, 200 and 400 kPa, respectively.

For the entire range of studied suctions, specimens represent a behavior similar to normally consolidated soils. In tests at 100 and 200-kPa suction, specimens with a strain-hardening behavior reach steady state after 15% axial strain. For Specimen with 400-kPa suction, the peak strength is achieved at an axial strain of about 15% and then continued with a slight reduction in deviatoric stress. The volumetric variation of the specimens are presented in Figure 8.27 (b). It can be seen that, for all values of the suctions specimens represents a contractive behavior. A monotonic trend is evident in volumetric strain of the specimen where, saturated specimen has the greatest compressive volume strain and the contractive behavior decreases as the suction increases. Figure 8.27 (c) provides the variation of the volume change with respect to water phase. The same trend as before (tests at 25and 100-kPa net confining stress) can be seen where, the trend toward the water inclusion from the specimen increases as the matric suction is increases.

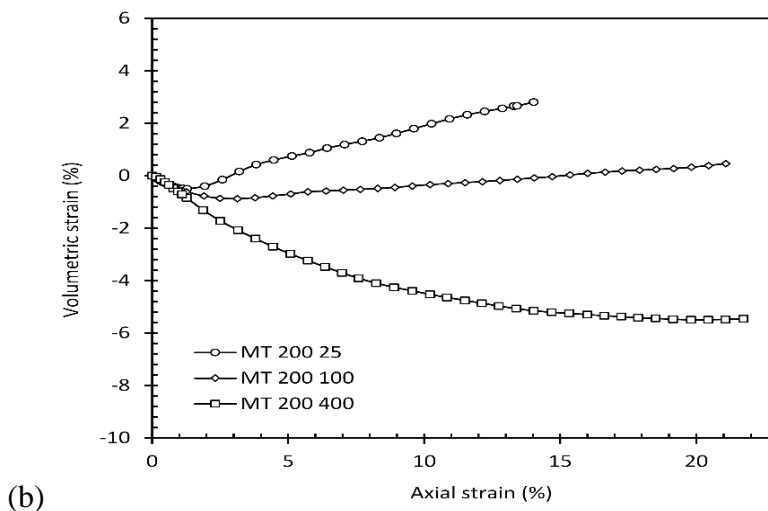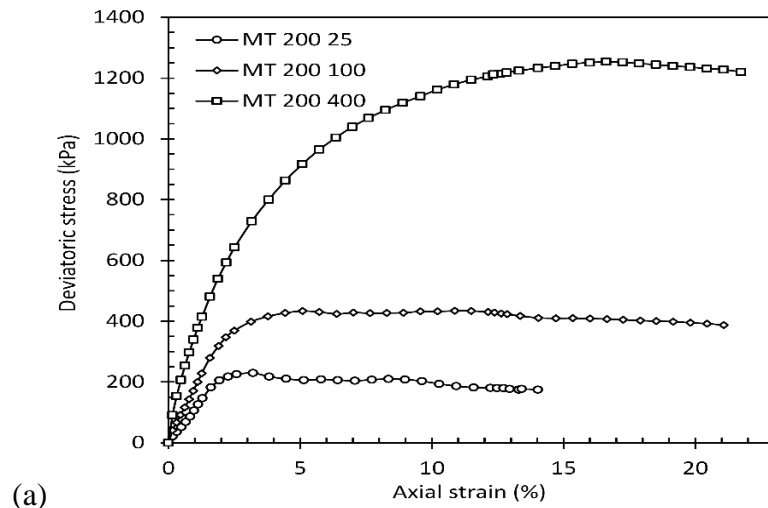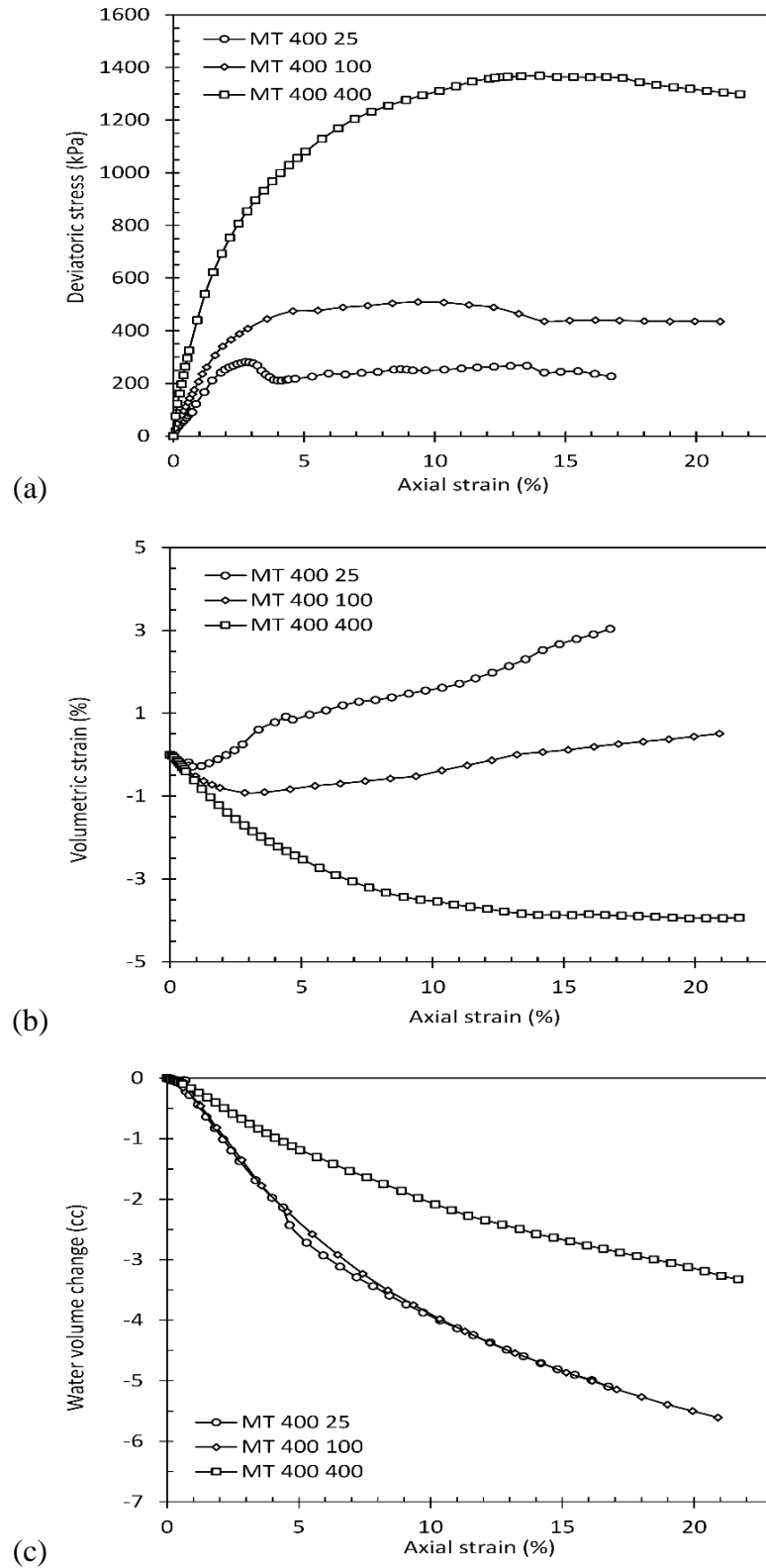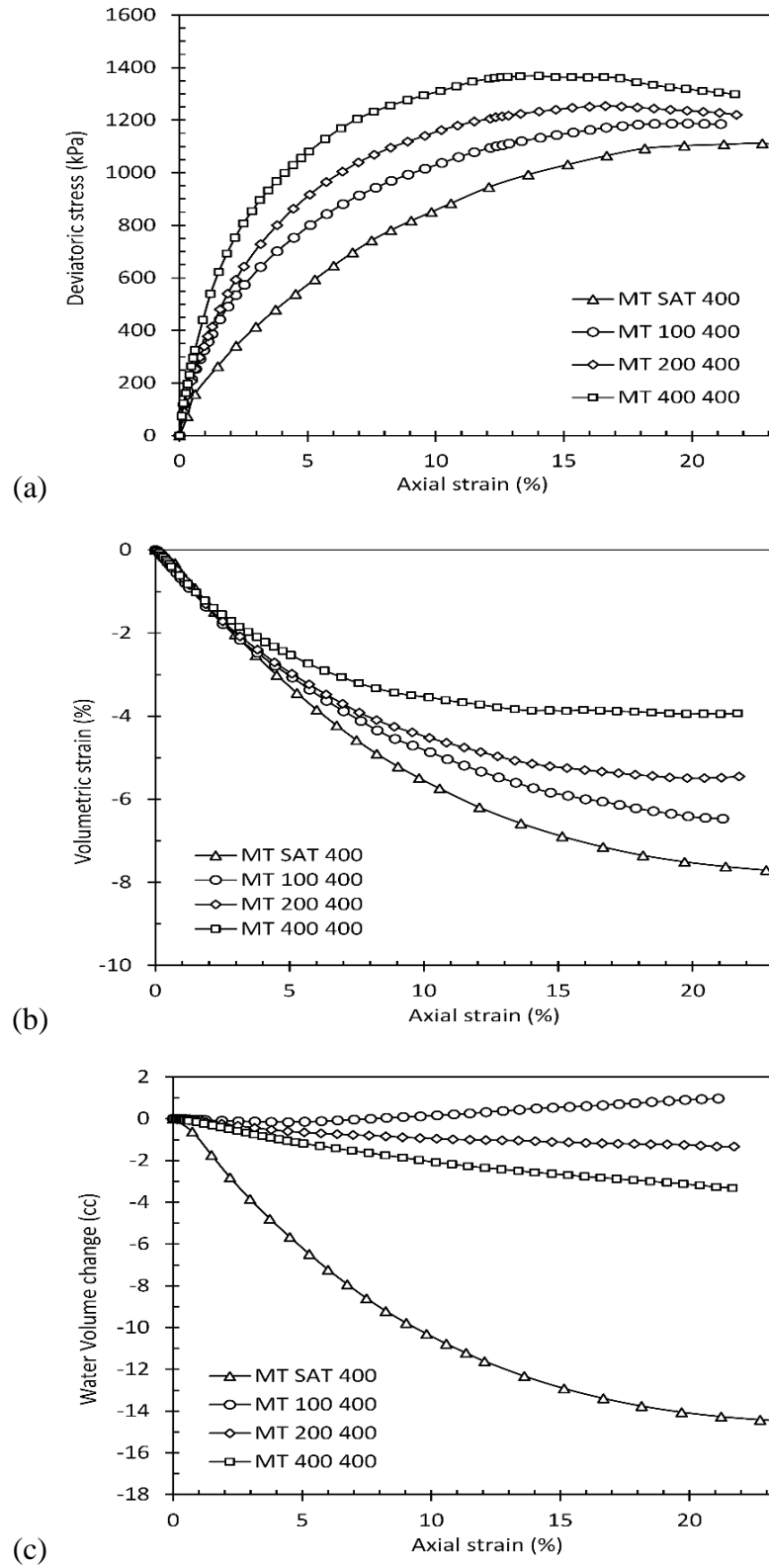Figure 8.27 Variations of (a) deviatoric stress, (b) volumetric strain and (c) change in volume of water the during drained shearing at (σ_3-u_a) = 400 kPa.

8.1.3.6 Mohr-Coulomb Failure Envelope

Figure 8.28 to Figure 8.31 illustrate the Mohr's stress circles and corresponding failure envelope (plotted at maximum shear strength) of each series of the triaxial tests (i.e. for each suction group). The shear strength parameters (i.e. friction angle and apparent cohesion intercept) were obtained from Mohr's circles failure envelope for each series of triaxial tests. The variation of the apparent shear strength (cohesion intercept) with matric suction is presented in Figure 8.32.The non-linear variation of the shear strength with matric suction is in agreement with previous studies (see chapter 3 for detail).
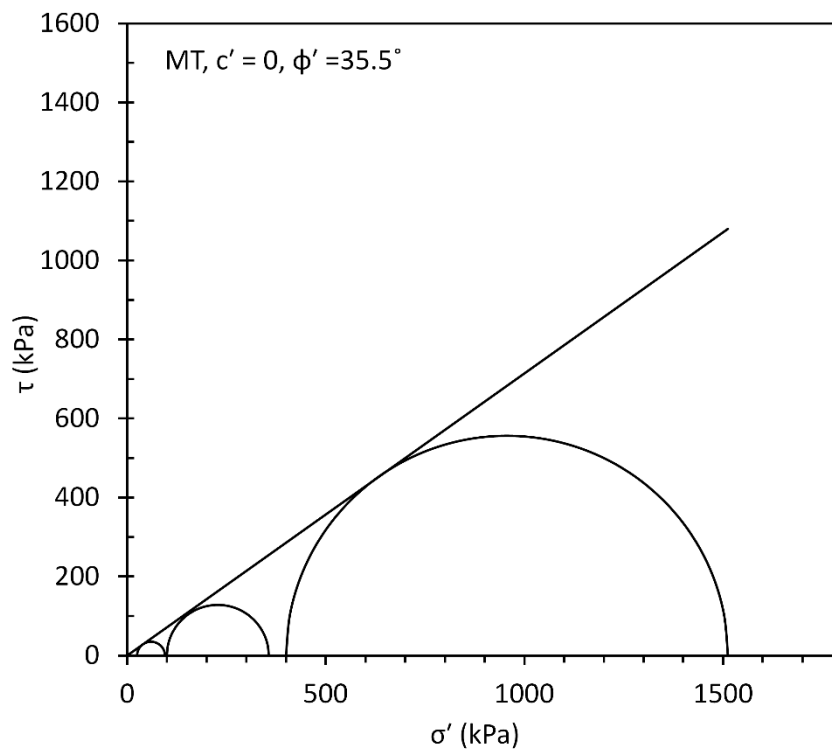
Figure 8.28 Mohr circles and cohesion intercepts for MT compacted specimen at saturated condition.
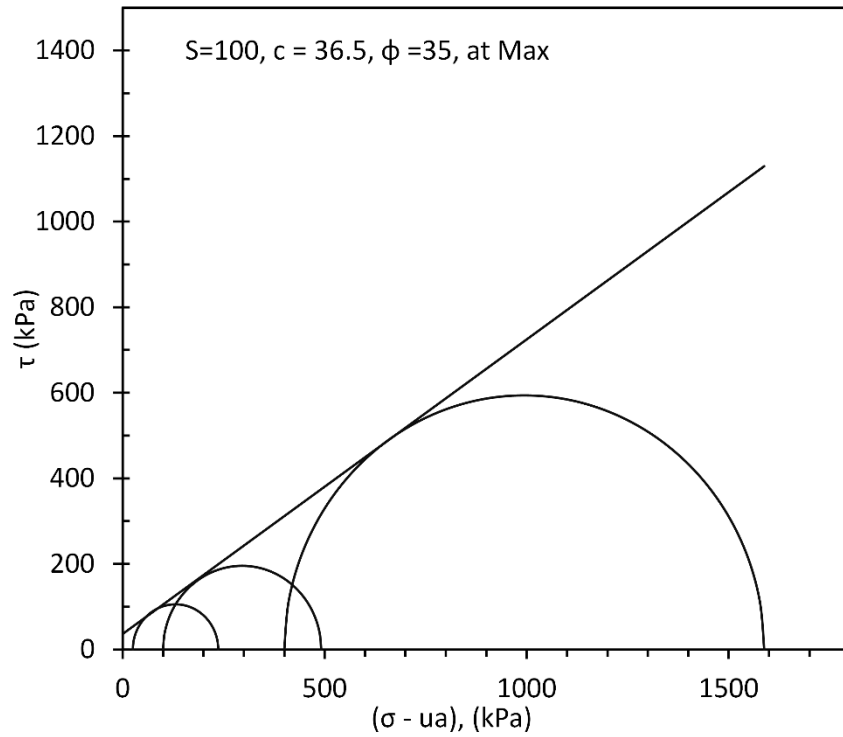
Figure 8.29 Mohr circles and cohesion intercepts for MT compacted specimen for
s = 100 kPa.
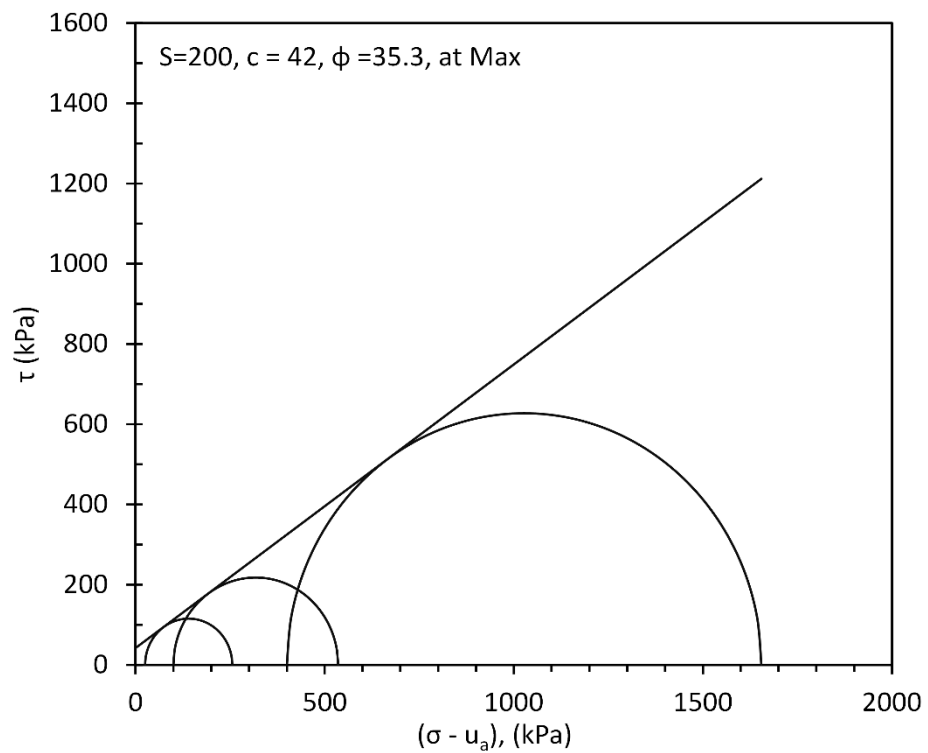
Figure 8.30 Mohr circles and cohesion intercepts for MT compacted specimen for
s = 200 kPa.

179
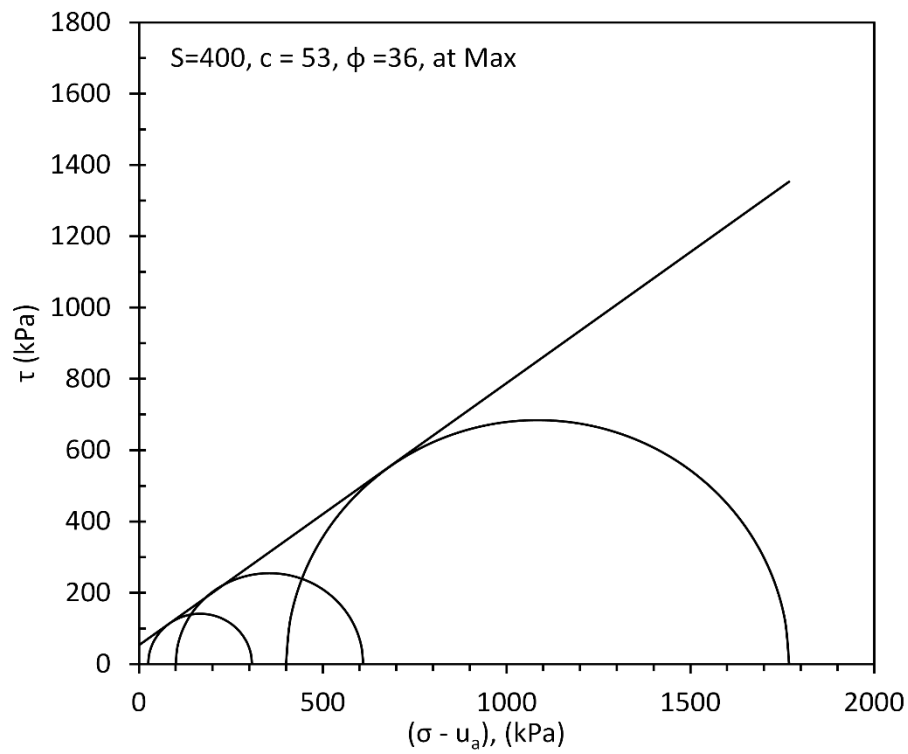
Figure 8.31 Mohr circles and cohesion intercepts for MT compacted specimen for s = 400 kPa.
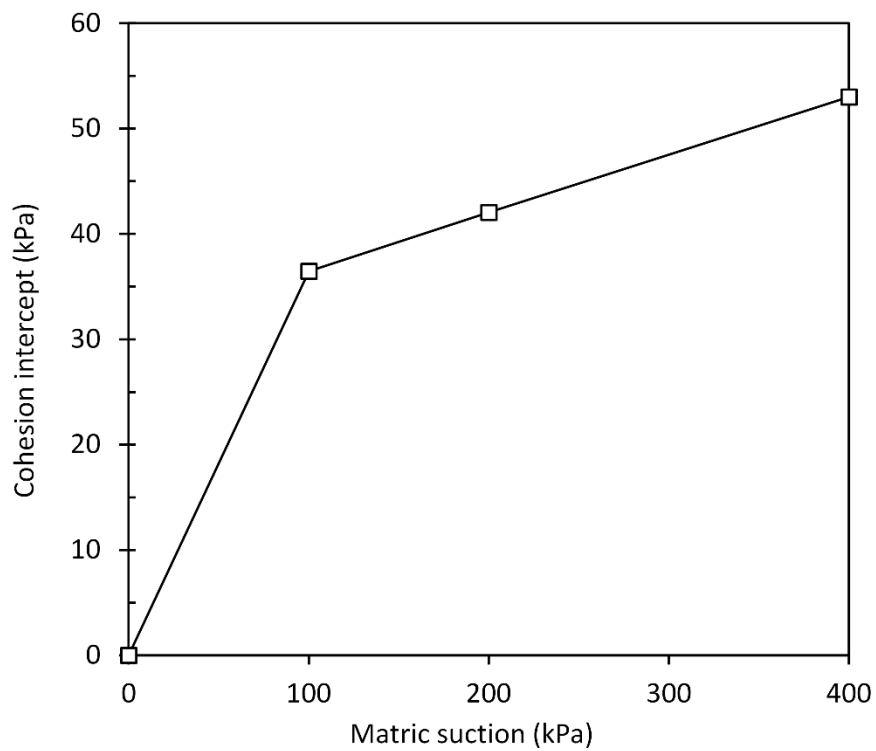
Figure 8.32 Variation of cohesion intercept with respect to matric suction.

8.1.3.7 Elasto Plastic Framework

Critical state line

As discussed in section 2.4.1.2, in BBM the slope of the critical stress (M) is assumed as a constant (independent of matric suction) but the intercept of the CSL linearly increase with suction at a rate of the k.

Wheeler and Sivakumar (1995) found a nonlinear variation for both gradient of CSL and intercept of critical state line $\mu(s)$ (increment of shear strength) with suction and modified this relationship as:

$$q = M(s)P - \mu(s) \tag{8.3}$$

where $\mu(s)$ is the intercept of critical state line at given value of suction s.

In this study, the results of constant suction triaxial tests, (where the state of the specimen were stabilized at large strain), were employed to generate the critical state line. Figure 8.33 show the critical state lines (CSL) from triaxial tests, in q-p plane for suction values of s = 0, 20, 100, 200 and 400 kPa. As it can be seen, the critical states of the each series (same matric suction) fall on a straight line. The gradient of the critical state line was determined for each series. As it can be seen, the gradient of CSL slightly varies at 400-kPa suction. To preserve the simplicity, reasonably a constant value for gradient of CSL could be considered, in consistent with the assumption presented by Alonso et al. (1990). Therefore, an average value of the M = 1.44 was adopted for the gradient of the CSL of the compacted specimens.

The intercept of critical state line $\mu(s)$, was determined for each constant suction triaxial tests and its variation with suction presented in Figure 8.34. In consistent with Wheeler and Sivakumar (1995) a nonlinear relationship between critical state line $\mu(s)$ intercept and matric suction was observed.
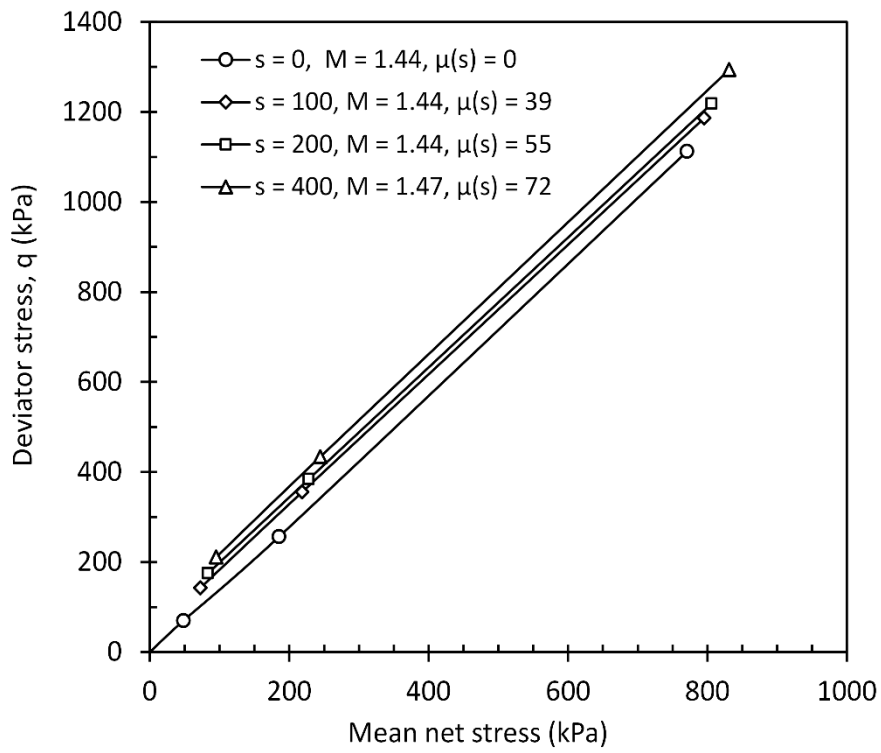
Figure 8.33 Critical state lines at different values of suctions in q - p plane.
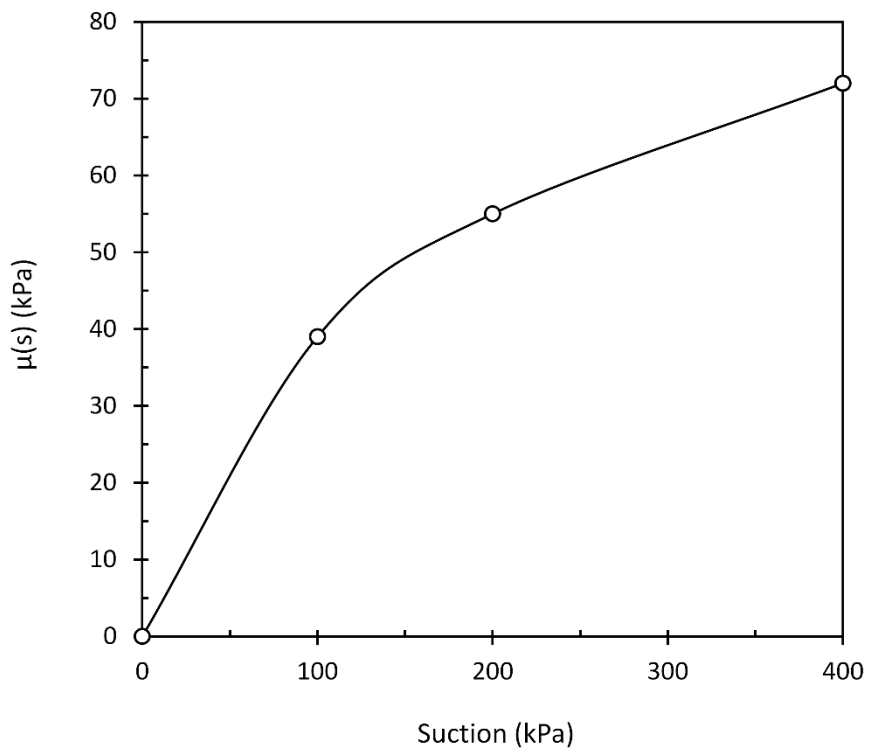
Figure 8.34 variation of the μ(s) with suction.

Determination of the yield points

In order to investigate the shape of the yield surface in the q: p plane, the yield points should be determined. The same procedure as Cui and Delage (1996) was followed to determine the yield points. It should be noted that the yield points are determinable only in specimens without yielding experience before shearing stage. In other words, the yield point were determined in specimens in which the state of the stress were inside the loading collapse (LC) yield locus at the onset of shearing. Therefore, considering Figure 8.21 the yield points were determined in tests: sat-25, sat-100, MT 100 25, MT 100 100, MT 200 25, MT 200 100, MT 400 25 and MT 400 100. For this, the plots of deviatoric stress versus axial strain (q-ε_a) and specific volume versus net mean stress (v-p) were employed.

As shown in Figure 8.35 the estimated yield values were employed to generate yield locus in q - p plane for each suction values (i.e. s= 0, 100, 200 and 400 kPa).

Cui and Delage (1996) have reported an inclined near-elliptical shape for yield locus for compacted specimens.

In this study, assuming elliptical shape of the yield loci Cui and Delage (1996) suggested for compacted specimens, inclined semi-elliptical yield curves were fitted to each series of constant suction yield points.

It can be seen that the size of the yield locus is function of the suction and expands as the suction increases. This observation is in consistent with hardening effect of the suction as included in BBM by Alonso et al. (1990). The inclination of the yield locus can be attributed to inherent anisotropic nature of the one-dimensionally compacted specimens. The yield locus appears to be symmetric about K_0 =0.45 line for all series. A constant inclination line reveals the independency of the soil anisotropy from suction, which is consistent with Cui & Delage (1996).
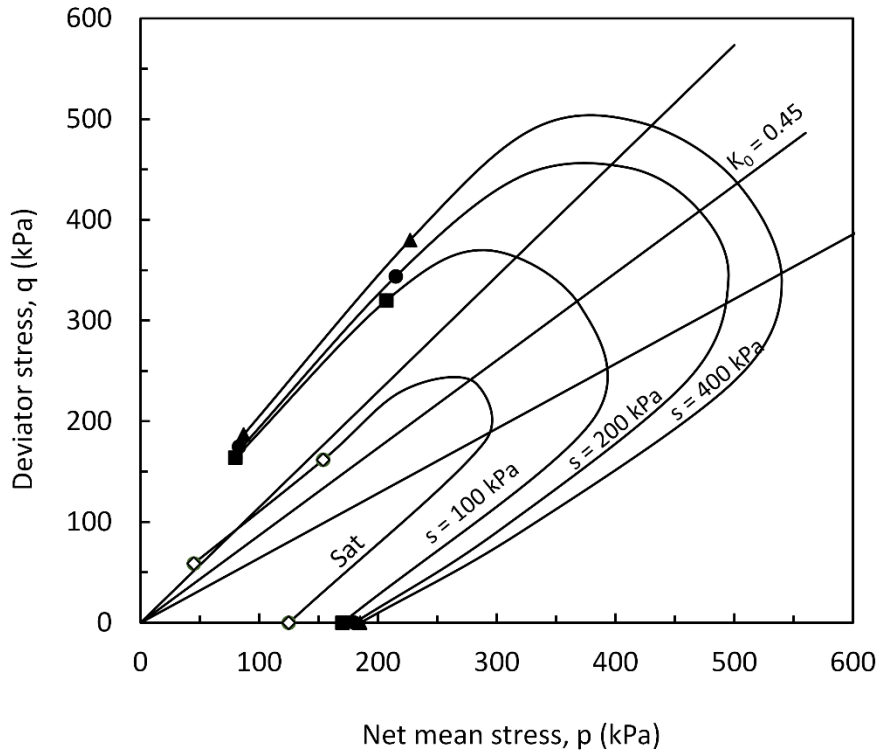
Figure 8.35 Yield curves for MT compacted specimens at different values of suction.

Shear modulus

The elastic shear modulus, G, relates the elastic component of the shear strain to the changes in deviatoric stress, q, by

$$d\varepsilon_s^e = \frac{dq}{3G}$$
(8.4)

It is assumed that plastic shear strain occurs beyond the yield locus. Therefore, the elastic parameters of the soil could be determined through the stress state of the specimen inside the yield locus where it is assumed that the response is elastic. The effect of variation of both net mean stress and suction was considered on initial shear modulus of the soil. Figure 8.36 and Figure 8.37 represents the shear modulus G (determined through the initial linear-elastic section of the deviatoric stress q, versus

184

shear strain ε_s, plots) versus net mean stress and suction. It was found that net confining stress and matric suction have considerable influence on initial shear modulus of the soil (i.e. initial shear modulus of the soil is dependent on both suction and net mean stress).

It seems that, for the range of the suction and net mean stress values employed in this study, initial shear modulus increase with suction and net mean stress.

These observations do not support the assumption of Wheeler and Sivakumar (1995) where a constant value for shear modulus, G was presumed but are in agreement with Cui (1993) and Zakaria (1994).
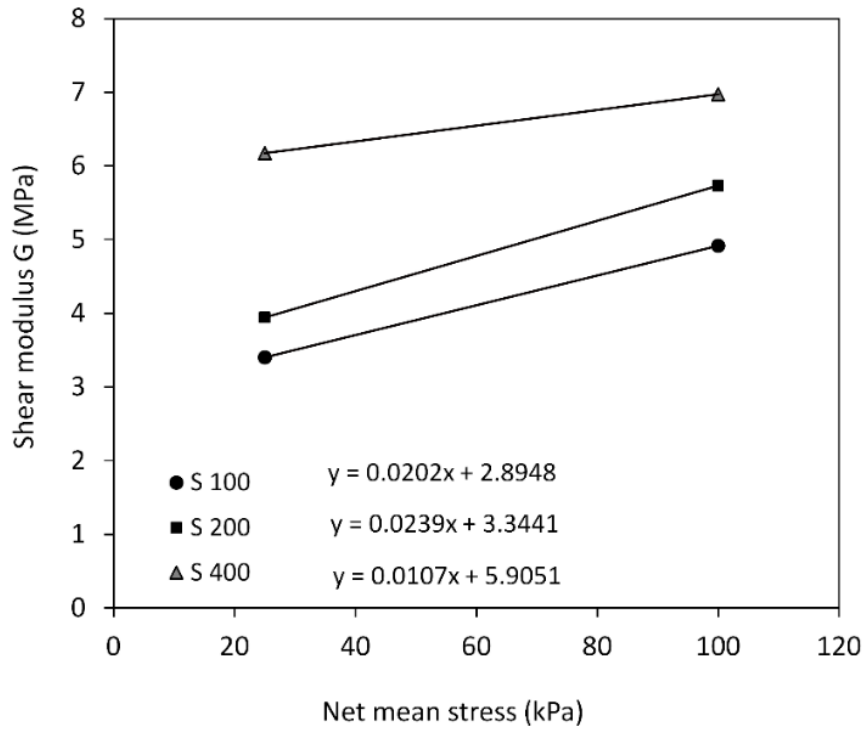
Figure 8.36 Variation of shear modulus with net mean stress
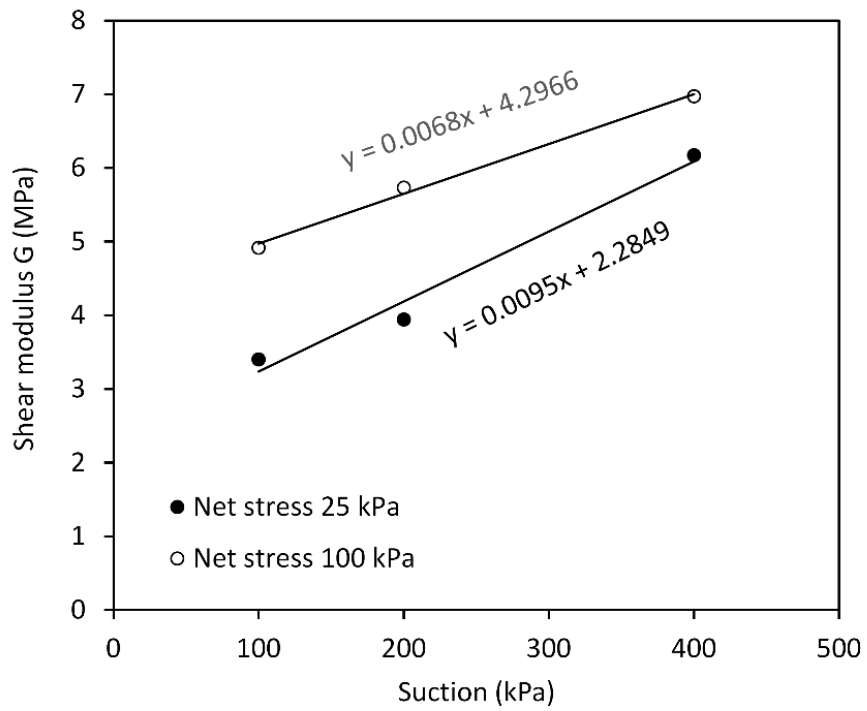
Figure 8.37 Variation of shear modulus with matric suction

186

Flow rule

The total strain increment, dε, decomposes into elastic (dε^e) and the plastic (dε^p) strain increments. In general the elastic strain increment does not get aligned with the direction of the stress increment. However, direction of the plastic strain increment does not coincide with the direction of the stress increment. Direction and magnitude of the plastic strain increment beyond the yield surface can be determined using the flow rule.

The plastic strain increment is composed of volumetric (dε$_v$^{p}) and deviatoric plastic strain (dε$_s$^{p}) increments. The volumetric and deviatoric plastic strain increments can be calculated as:

$$\delta\varepsilon_v^p = \delta\varepsilon_v - \delta\varepsilon_v^e$$

$$\delta\varepsilon_s^p = \delta\varepsilon_s - \delta\varepsilon_s^e$$

where $d\varepsilon_v$ and $d\varepsilon_s$ are total volumetric and deviatoric strain increments and $d\varepsilon_v^e$ dεve and dεse are volumetric and deviatoric elastic strain increments.

The volumetric and deviatoric plastic strain increments were calculated to identify the direction of plastic strain increment. For this, the plot of the deviatoric stress against shear strain was employed to calculate the deviatoric plastic strain increments, and the plot of the mean net stress versus volumetric strain were used to calculate volumetric plastic strain increment. The plastic strain increment vectors were determined and superimposed on related yield locus in q: p planes along with dε$_s$^{p}:dε$_v$^{p} (Figure 8.38).

Inspection of the Figure 8.38 reveals that the plastic strain increment vectors are not perpendicular to yield locus therefore, it could be recognized that the associate flow rule is not satisfied.
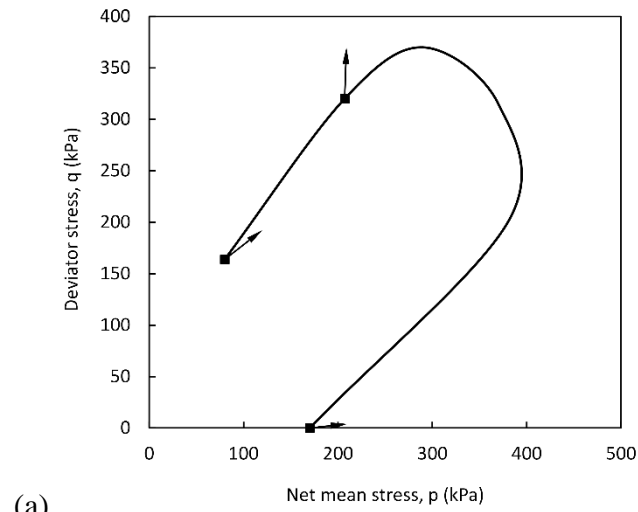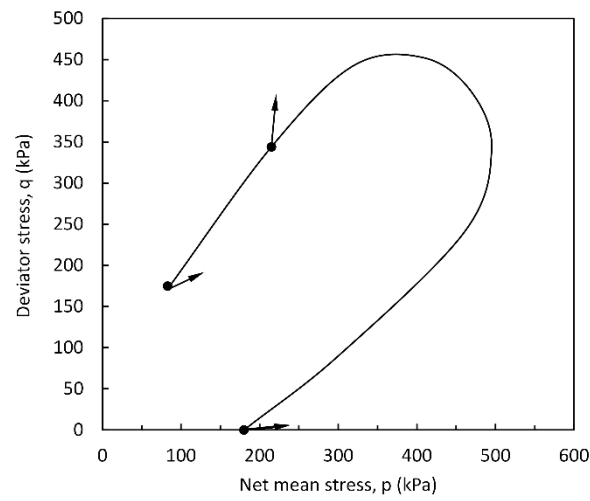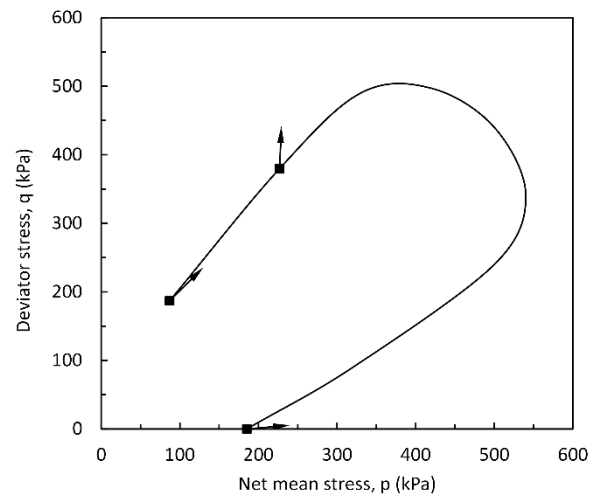
Figure 8.38 Measured yield points and plastic strain increment directions and
fitted yield curve at a) s = 100 kPa, b) s = 200 kPa, c) s = 400 kPa

188

8.2   Behavior of the Isotropically Reconstituted Specimens from the Slurry

A total of 31 consolidated-drained triaxial tests were performed on isotropically reconstituted specimens from the slurry (IRS). This involve 11 conventional consolidated-drained tests on saturated specimens and 20 unsaturated suction-controlled CD triaxial tests. The testing program is presented in chapter 7. Saturated Tests

Three series of conventional consolidated drained triaxial tests were performed on specimens isotropically reconstituted from the slurry (IRS) and one-dimensionally reconstituted from slurry (ORS).

- Series 1 includes CD test on IRS specimens at four effective confining stress of 25, 100, 200, and 400 kPa.
- Series 2 includes CD test on IRS specimens with loading-unloading.
- Series 3 includes CD test on ORS specimens at three effective confining stress of 100, 200, and 400 kPa.

Series 1 and 3 are compared in chapter 6, where the effect of the preparation method on soil response was investigated. Therefore, in this section, the results of only series 1 and 2 will be discussed.

Similar to CD tests on moist tamped compacted specimens, each test involves three stages: saturation, consolidation and shearing stage.

Saturation
Despite preparing specimens from the slurry, air bubbles could be entrapped in the slurry. Therefore, specimens were back-pressure saturated to drive all air bubbles into solution and ensure full saturation.

Isotropic consolidation
Following saturation, the consolidation stage was initiated by elevating the cell pressure at a rate of the 20 kPa/min. In series 1, specimens were consolidated at four effective confining stress (i.e. 25, 100, 200 and 400 kPa). Variation of the specific volume with effective stress for 400 kPa effective stress is shown in Figure 8.39.

In addition, one isotropic step-loading consolidation test was carried out on an IRS specimen. Variation of the specific volume with effective stress during isotropic consolidation is shown in Figure 8.39. The yield point from ramp loading and step loading was determined to be 80 and 25 kPa, respectively. The difference between the results of step loading and continuous loading was also reported by Cui and Delage (1996).

The elastic constant κ (slope of the unloading or swelling line) and plastic constant λ (slope of the virgin compression line) are determined to be $\kappa = 0.002$, and $\lambda = 0.066$ from continuous loading and $\kappa = 0.002$, and $\lambda = 0.052$ from step loading.
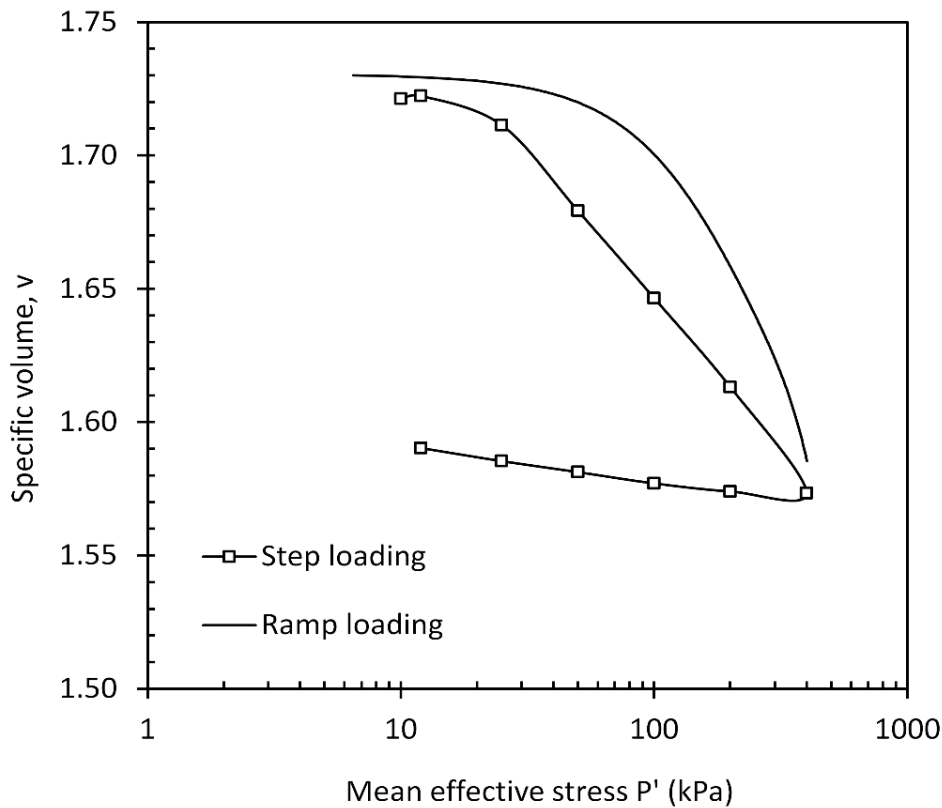
Figure 8.39 Isotropic consolidation curve for saturated IRS specimen with ramp and step loading.

In tests series 2, specimens were first consolidated to 400-kPa, then unloaded to a 200, 100 or 25 kPa to yield an OCR = 2, 4 or 16, respectively.

Shearing Stage

Following consolidation, specimens were sheared at constant confining pressure. Figure 8.40 shows the stress-strain and volumetric response of tests in series 1. Figure 8.41 compares the stress-strain and volumetric response of series 1 (normally consolidated) and series 2 (overconsolidated). In series 1, the strength increases with strain at a decreasing rate up to axial strain of about 15%, followed by moderate amount of softening. In series 2, specimens reach a peak strength, at a lower axial strain, followed by a marked strain-softening.

In series 1, for the entire range of the confining pressure, a contractive behavior followed by a less pronounced amount of dilation. In series 2, specimens with OCR = 4, 16 illustrated contractive behavior followed by considerable amount of dilation. The dilatancy is less pronounced for specimen with OCR = 2.

For a given effective pressure, both series 1 and 2 approach to critical state values.
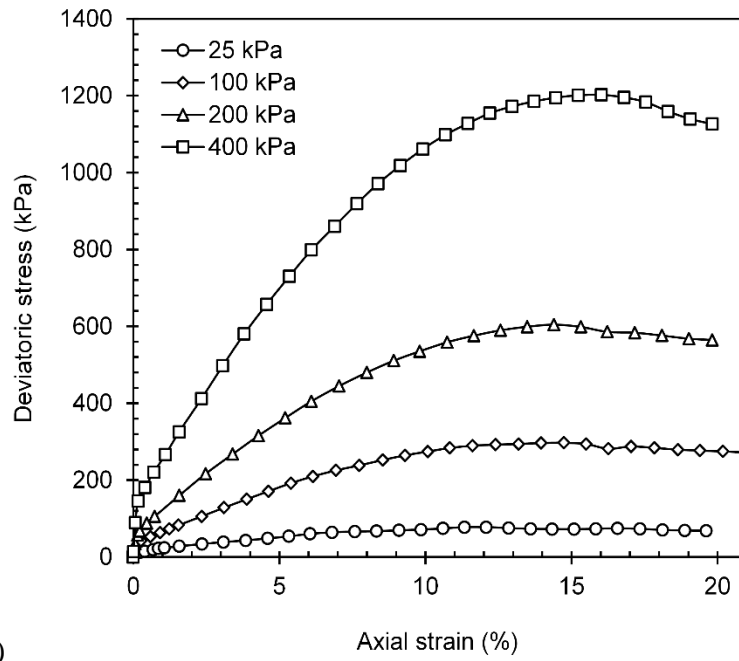
(a)
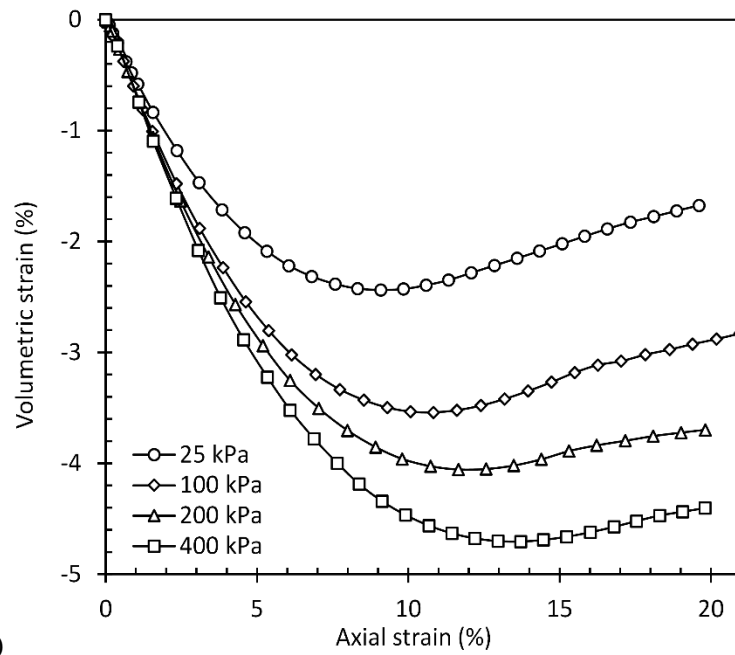
(b)

Figure 8.40 Results from triaxial tests on saturated IRS specimen for different σ′₃ values, (a) stress-strain (b) volumetric strain-axial strain.
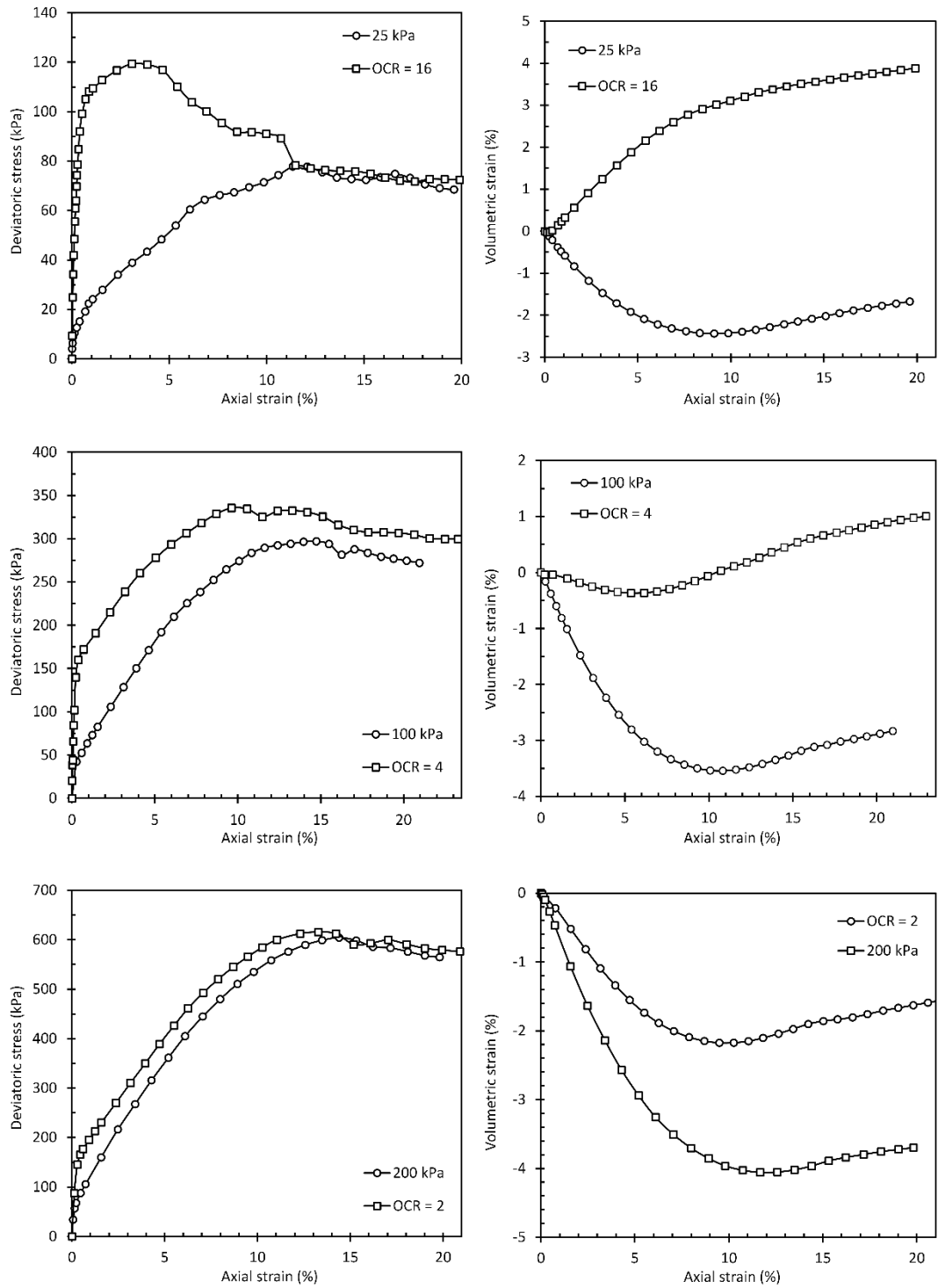
Figure 8.41 Comparison of Triaxial Stress-Strain Curves and volumetric behavior for series 1 (normally consolidated) and series 2 (overconsolidated) a) $\sigma'_3 = 25$ kPa, (b) $\sigma'_3 = 100$ kPa, (c) $\sigma'_3 = 200$ kPa.

8.2.1 Behavior of Unsaturated IRS Specimens from Triaxial Tests

A total of 20 constant-suction consolidated-drained (CS-CD or simply CD) tests were performed on isotropically reconstituted specimens from the slurry (IRS). A CD test includes three stages:

1. Suction *equalization*,
2. Constant suction *Isotropic compression*,
3. Constant suction drained *Shearing*

What follows is a description of the results of the each stage for series 1 and series 2**Suction Equalization**

As a first stage, specimens were subjected to given values of suction through drying path. Suction equalization was performed under a 25-kPa net confining stress. The changes in water volume and volume of the specimen during the equalization stage were monitored.

As specimens are prepared from the slurry, the desired suction values were achieved through a drying path. Figure 8.42 and Figure 8.43 present the variation in specimen volume and water volume during equalization stage for each suction value (i.e. s = 100, 200 and 400 kPa). In all tests, as expected, water is expelled from the specimen and water content decreases as suction increases.

It can also be seen that, for applied suction values, specimens exhibit a considerable amount of volumetric compression before reaching the equilibrium.
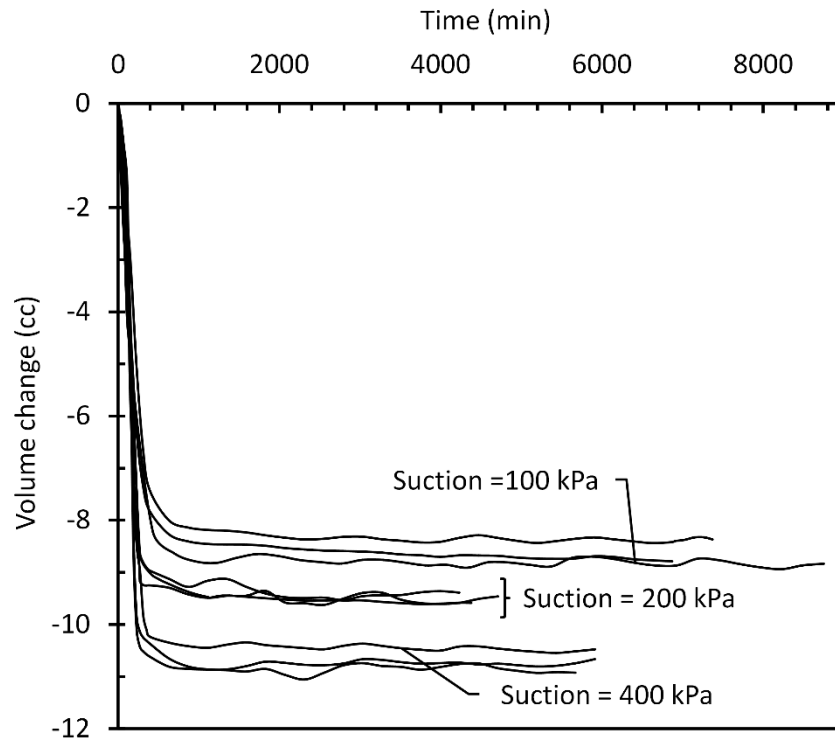
Figure 8.42 Variation in specimen volume during equalization stage.
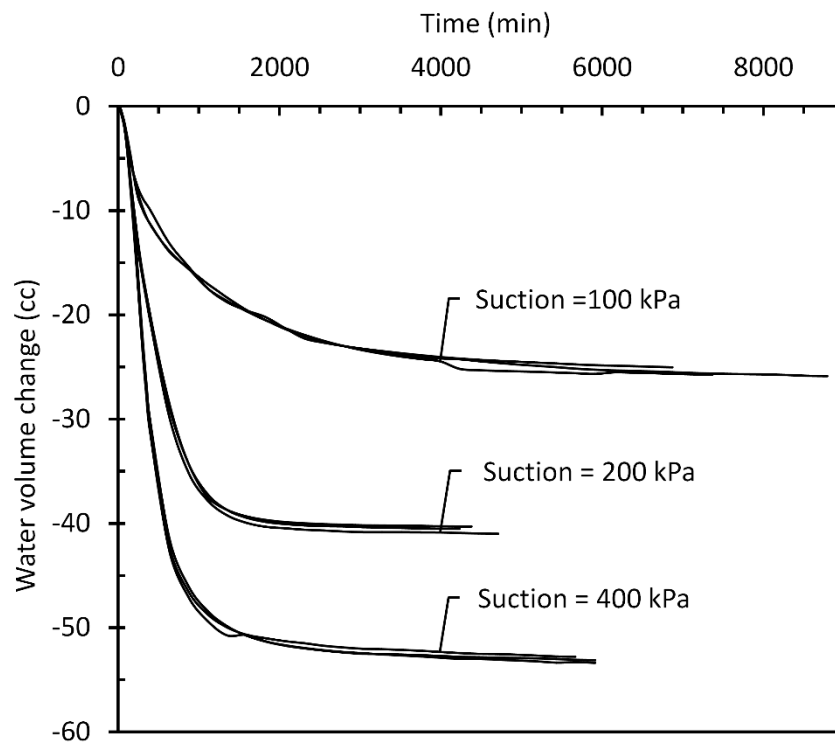
Figure 8.43 Variation in water volume during equalization stage.

8.2.1.2 Constant Suction Isotropic Compression

Following equalization, specimens were isotropically compressed (at constant suction) to the desired value of the net-confining stress. More details of the testing procedures for the compression stage are given in section 7.2.2. In this stage specimen were subjected to 25, 100 and 400 kPa net stress. Since the suction equalization was carried out under 25-kPa net stress, therefore, for those the shear stage was initiated after suction equalization stage. The variation of the specific volume v, with net mean stress p, for 400-kPa net stress (for suction values of 20, 100, 200 and 400 kPa) are presented in Figure 8.44.
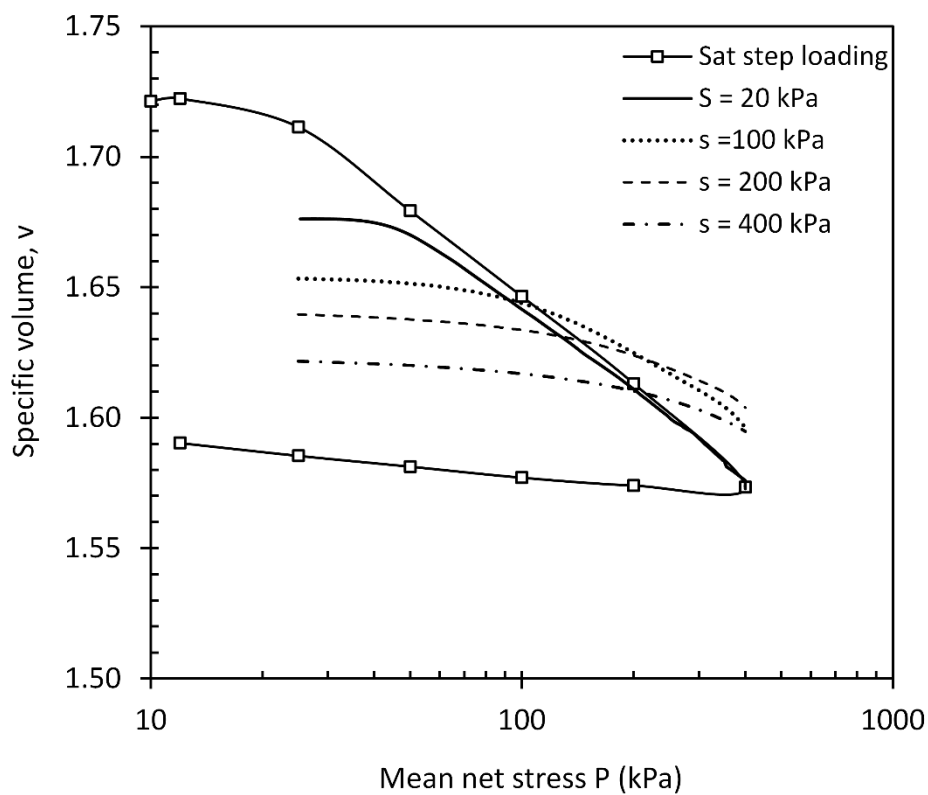
Figure 8.44 Isotropic compression curves at different suction values for IRS specimens.

In all the tests (under 400-kPa net stress), yielding was observed during isotropic compression.

The elastic stiffness parameter, κ, is determined to be 0.002 for all the tests. This is in agreement with the assumption of the suction independency of the κ.

The slope of the normal compression curve λ(s) were also estimated from compression curves for each values of suction. Figure 8.45 shows the variation of the λ(s) with matric suction. As it can be seen, the slope of the normal compression curve λ(s) decreases from 0.066 in saturated state, at a decreasing rate toward an asymptotic value, to 0.033 for 400-kPa suction. This is in agreement with Alonso, et.al. (1990) (BBM).
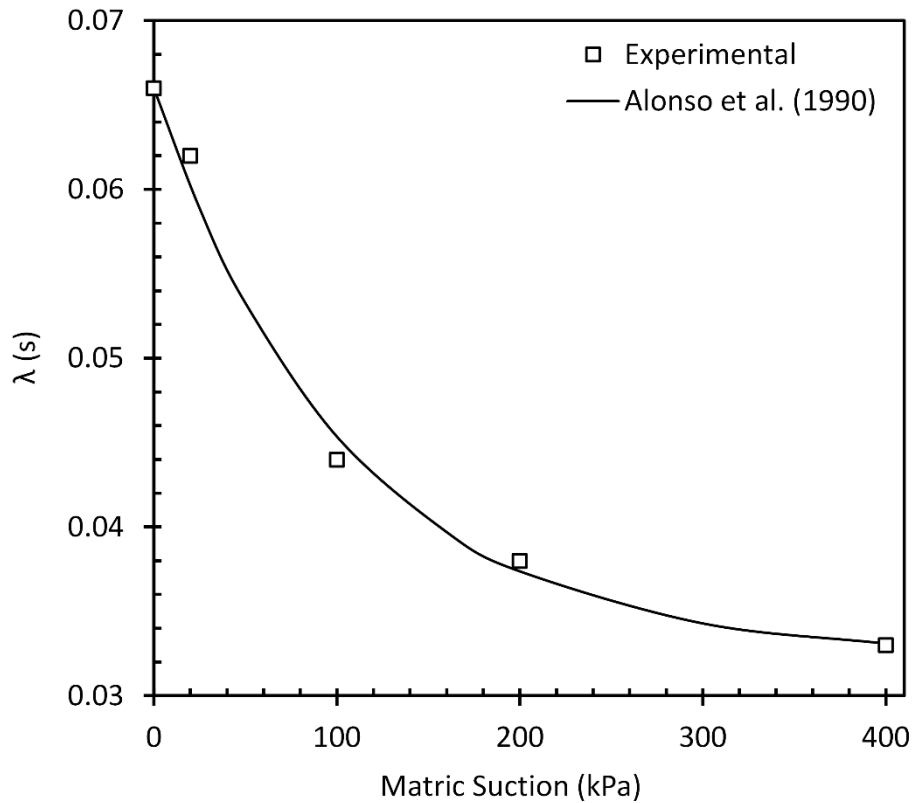
Figure 8.45 Variation of the λ(s) values with matric suction.

The nonlinear variation of the λ(s), with suction is fitted by equation 2.18. This equation includes two fitting parameters which are determined through a trial and error procedure as r = 0.49 and β = 0.0095.

The yield stresses are estimated from compression curves for each values of suction. These values used to define the loading collapse (LC) yield curve in s – p plane (Figure 8.46). The yield points in unsaturated condition are determined through the results of the compression tests with ramp loading tests. Therefore, for the sake of

consistency, the yield stress with ramp loading in saturated condition was adopted in LC yield curve. As it can be seen in Figure 8.46, the yield stress, increases from 80 kPa at saturated state at a decreasing rate to 200 kPa when matric suction increased to 400 kPa.

The LC yield curve was fitted through the equation 2.18 and 2.19 proposed by Alonso, et.al. (1990). The fitting parameter is determined to be $p^c = 32$ kPa through a trial and error procedure.
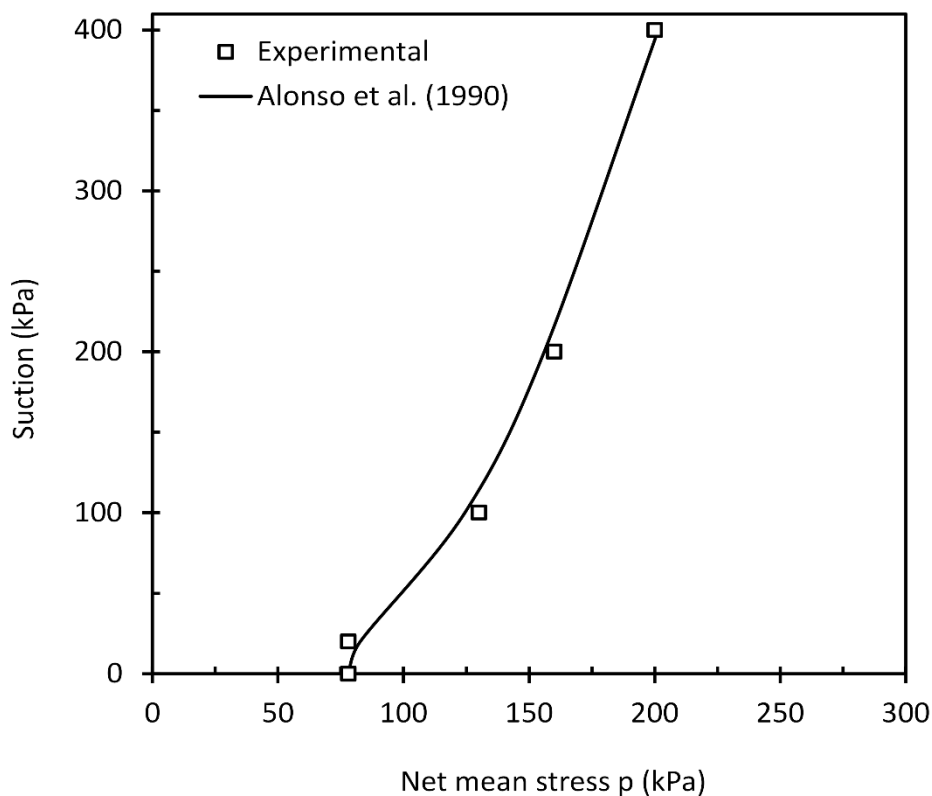
Figure 8.46 Measured and fitted loading-collapse yield curve for IRS specimens.

8.2.1.3 Constant Suction Drained Shearing Stage

A total of 10 constant-suction consolidated drained triaxial test were conducted at constant values of suction (s = 20, 100, 200 and 400 kPa). For each values of suction, triaxial tests were conducted at three net-confining pressures (i.e. 25, 100 and 400 kPa), except for test at 20-kPa suction in which only one test was performed at 400-kPa net stress.

Similar to compacted specimens, the results of the tests were interpreted in two ways. Section 8.2.1.3.1, investigates the effect of net confining stress on the mechanical response of the specimens and section 8.2.1.3.2, investigates the impact of the suction on the mechanical response of the specimens.

8.2.1.3.1 *Effect of Net-Confining Stress*

Figure 8.47 (a), Figure 8.48 (a) and Figure 8.49 (a) show the typical results of the triaxial tests at different net confining stresses but at the same suction. As it can be seen, most of the specimens represent a post-peak softening behavior. This becomes more pronounced at low net confining stresses, where a peak deviatoric stress is attained at lower strain. As expected, for constant values of the suction, the stiffness also increases with net confining stress.

Figure 8.47 (b), Figure 8.48 (b) and Figure 8.49 (b) show the changes in volumetric strain during shearing from three sets of triaxial tests. For net confining stress of 25 and 100 kPa specimens show an initial contraction in volume followed by dilation. However, for net confining stress of 400 kPa specimens exhibited a compressive behavior. In other words, the dilatancy decreases with increasing net confining stress. The maximum rate of the dilation correspond to maximum deviatoric stress. Eventually, at larger strains all specimens tend towards critical state, which is in agreement with the stress-strain behavior.

Figure 8.47 (c), Figure 8.48 (c) and Figure 8.49 (c) show the changes in water volume during shearing of the three sets of triaxial tests. In all the cases, the water was drained out from the specimen during shearing stage, which is inconsistent with dilative behavior of the specimens. It seems that, the volume of expelled water increases with decreasing the net confining stress. This behavior can be explained by considering SWCC shifting (either left or right depending state of the specimen) as discussed in detail in section 8.1.3.4 .

Figure 8.47 Variations of (a) deviatoric stress, (b) volumetric strain and (c) change in volume of water during drained shearing at s = 100 kPa.

Figure 8.48 Variations of (a) deviatoric stress, (b) volumetric strain and (c) change in volume of water during drained shearing at s = 200 kPa.

Figure 8.49 Variations of (a) deviatoric stress, (b) volumetric strain and (c) change in volume of water during drained shearing at s = 400 kPa

8.2.1.3.2 Effect of Suction Magnitude

Tests at 25-kPa net confining pressure

Figure 8.50 (a) shows the stress-strain behavior of the specimen at net confining stress of 25 kPa with different values of suction (i.e. 0, 100, 200 and 400 kPa). As before, greater shear strength and stiffness of the specimens are observed for higher matric suction. The maximum shear strength is greater by about 242, 332 and 477 kPa than that of the saturated test for matric suctions of to 100, 200 and 400 kPa, respectively.

As it can be seen, the response of the specimens change from strain-hardening in saturated condition to strain-softening at higher suction values. For the entire range of the suction, specimens with a rapid increase in shear strength, reach a peak value, at low axial strain, followed by a marked drop in strength. Finally, shear strength were stabilized and moves toward critical state values. For tests at suctions of 100, 200 and 400-kPa the peak deviatoric stress is attained at 5, 7 and 10% axial strain, respectively.

The volumetric behavior of the specimens are presented in Figure 8.50 (b). For all values of the suction (greater than zero), specimens were initially contracted and then dilated. As it can be seen, the dilatancy is increases as the suction increases.

Figure 8.50 (c) shows the changes in water volume during shearing stage. In all the unsaturated tests, the water was drained out from the specimen during shearing stage. It seems that, the volume of expelled water decreases as the suction increases.
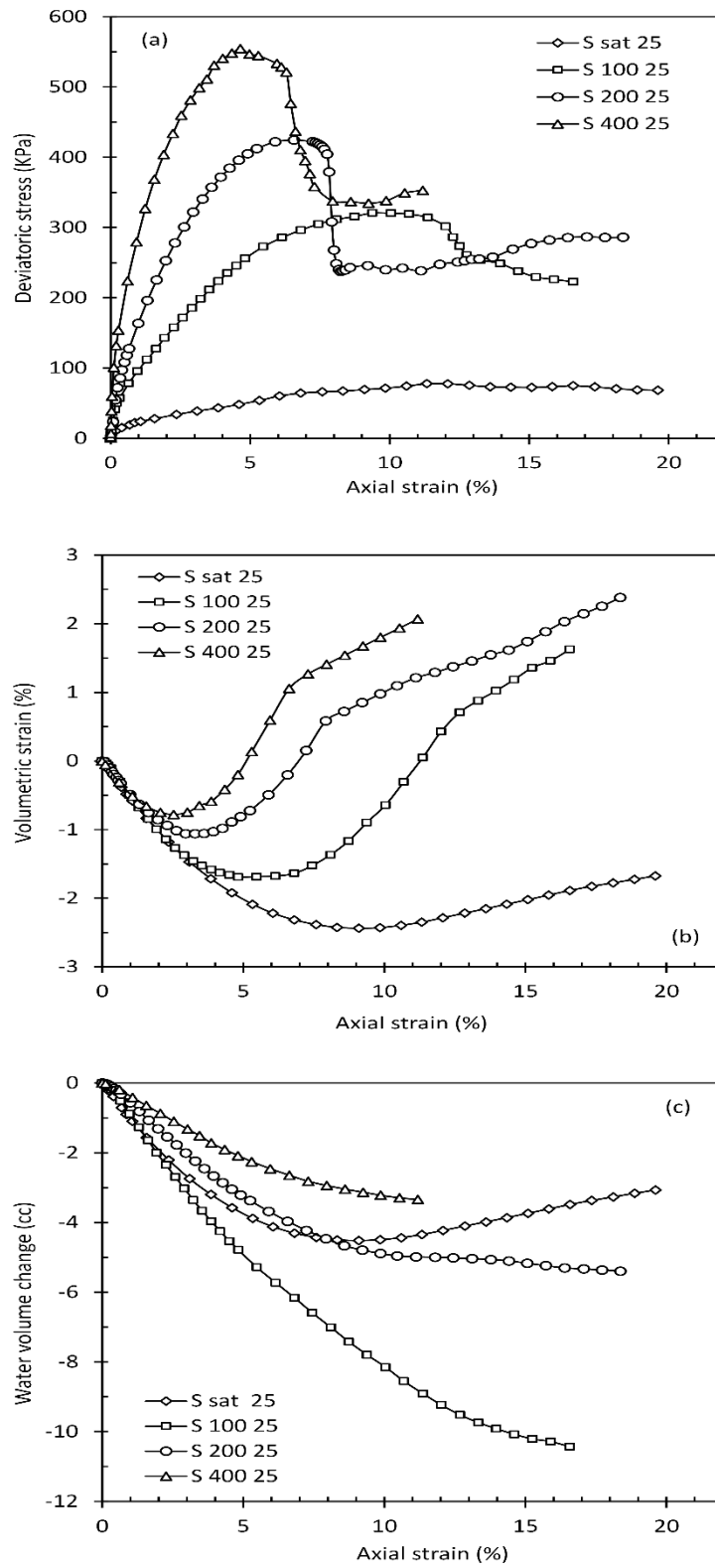
Figure 8.50 Variations of (a) deviatoric stress, (b) volumetric strain and (c) change in volume of water during drained shearing at $(\sigma_3-u_a) = 25$ kPa.

100-kPa confining pressure

The results of the tests at 100-kPa net confining pressure for different values of the matric suction (i.e. 0, 100, 200 and 400 kPa) are shown in Figure 8.51 (a). The general response is similar to those at net stress of 25 kPa, where the initial stiffness and maximum deviatoric stress is grater for higher suction values. The maximum shear strength is greater by about 233, 373 and 473 kPa than that of the saturated test for matric suctions of to 100, 200 and 400 kPa, respectively. For suctions above 100 kPa, a pronounced peak strength is observed at a lower axial strain. The specimens achieve to their maximum strength at axial strain of about at 15, 14, 10 and 8%, for suction values of 0, 100, 200 and 400 kPa, respectively. Eventually, shear strength moves toward the critical state.

The volume strain of the specimens are presented in Figure 8.51 (b). For the entire range of the suctions, volumetric contraction followed by dilation.

The variation of the volume change related to water phase are shown in Figure 8.51 (c). The results show almost the same trend as the tests at 25-kPa net confining stress. The water tends to be excluded from the specimen (and result in decreasing water content) as the suction increases.
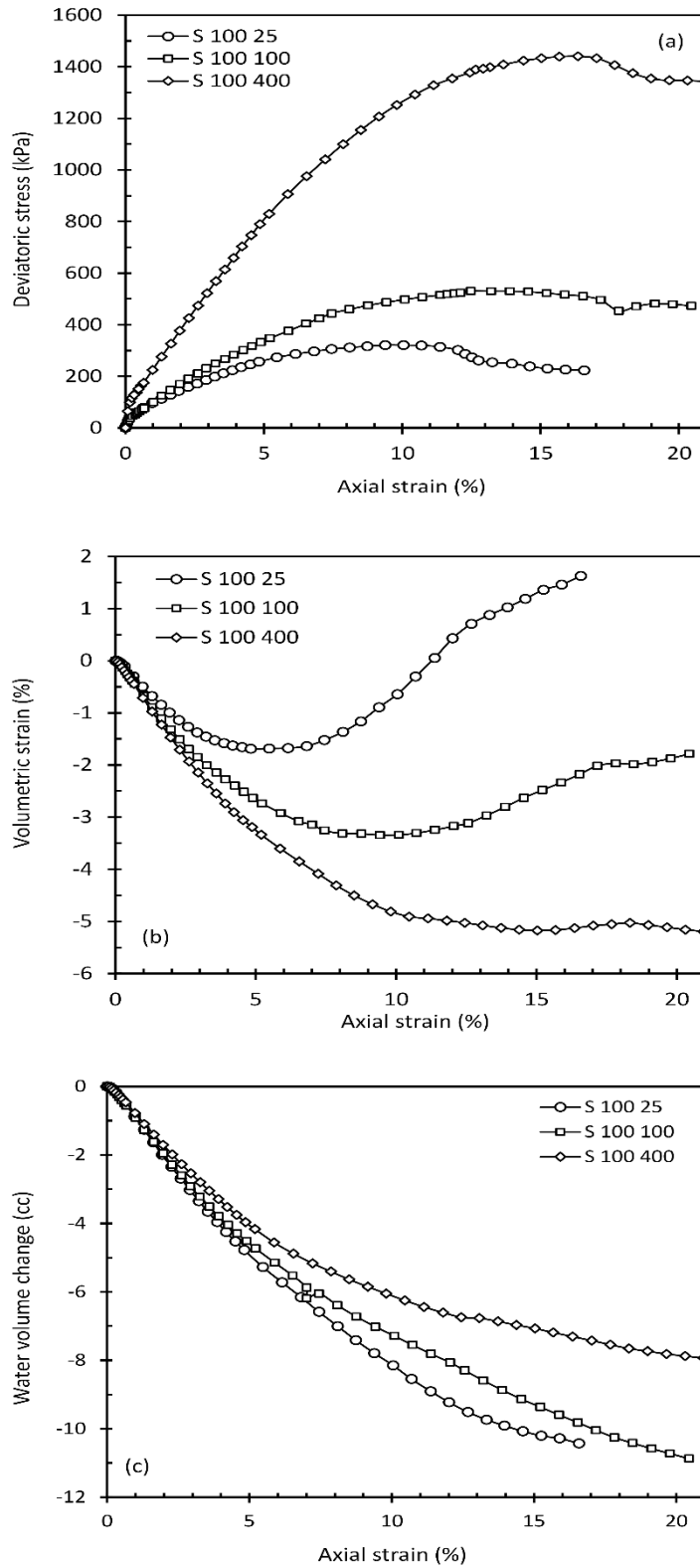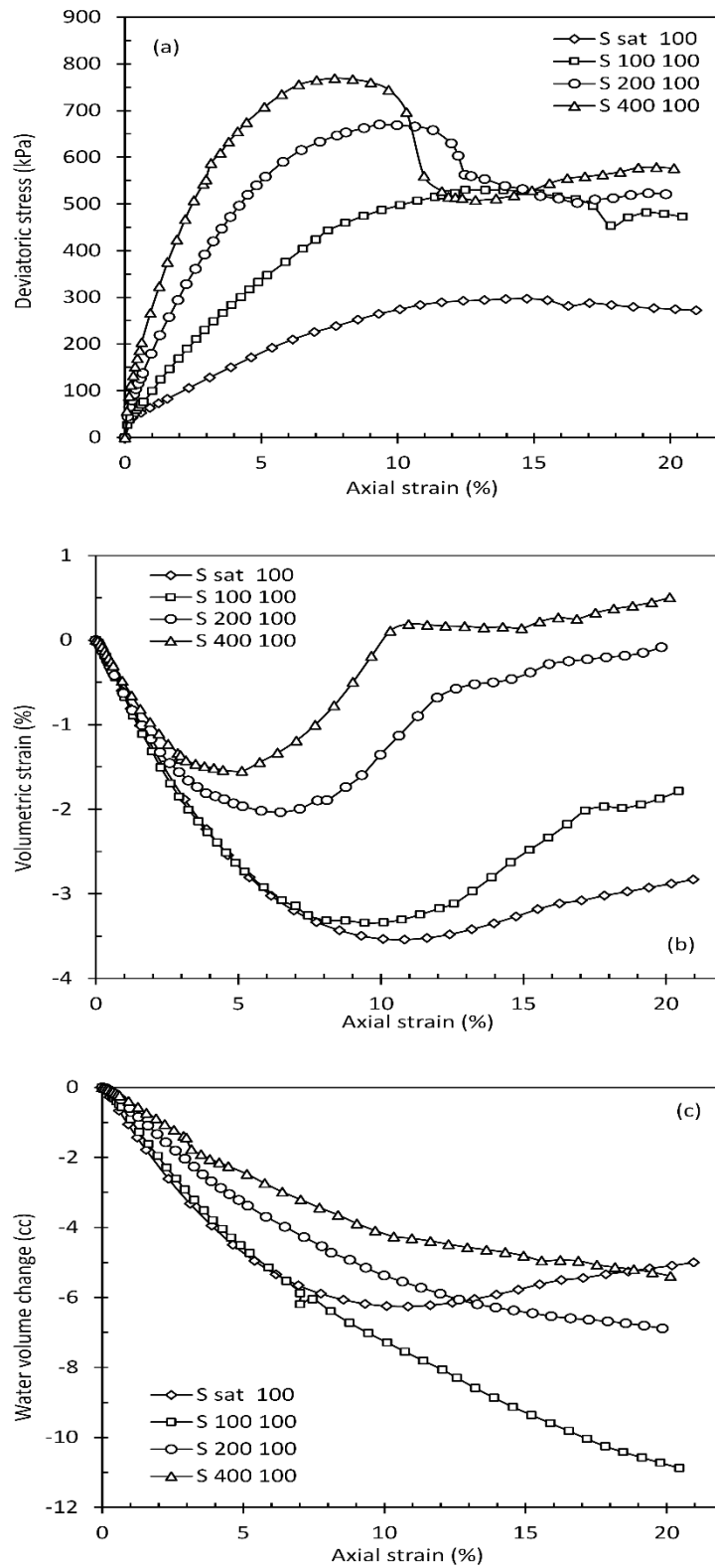
Figure 8.51 Variations of (a) deviatoric stress, (b) volumetric strain and (c) change in volume of water during drained shearing at $(\sigma_3 - u_a) = 100$ kPa

206

400-kPa confining pressure

The results of the tests at 400-kPa net confining pressure and different values of the matric suction (i.e. 0, 20, 100, 200 and 400 kPa) are presented in Figure 8.52 (a). Increase in stiffness and shear strength is similar to those at net confining stress of 25, and 100 kPa. In this series, the peak values and softening from the peak values become less pronounced. The maximum shear strength is greater by about 236, 358 and 446 kPa than that of the saturated test for matric suctions of to 100, 200 and 400 kPa, respectively. Specimens in all values of the suctions represents behavior similar to normally consolidated soils.

The volumetric behavior of the specimens are presented in Figure 8.52 (b). It can be seen that, for the entire range of the suctions a contractive behavior was observed. A consistent trend exists in volumetric behavior, where the contraction decreases as the suction increases.

Figure 8.52 (c) shows changes in water volume during shearing. The same trend as tests at 25 and 100-kPa net confining stress was observed, were, the water is drained out from the specimens. The amount of drained water is greater at lower suction values.
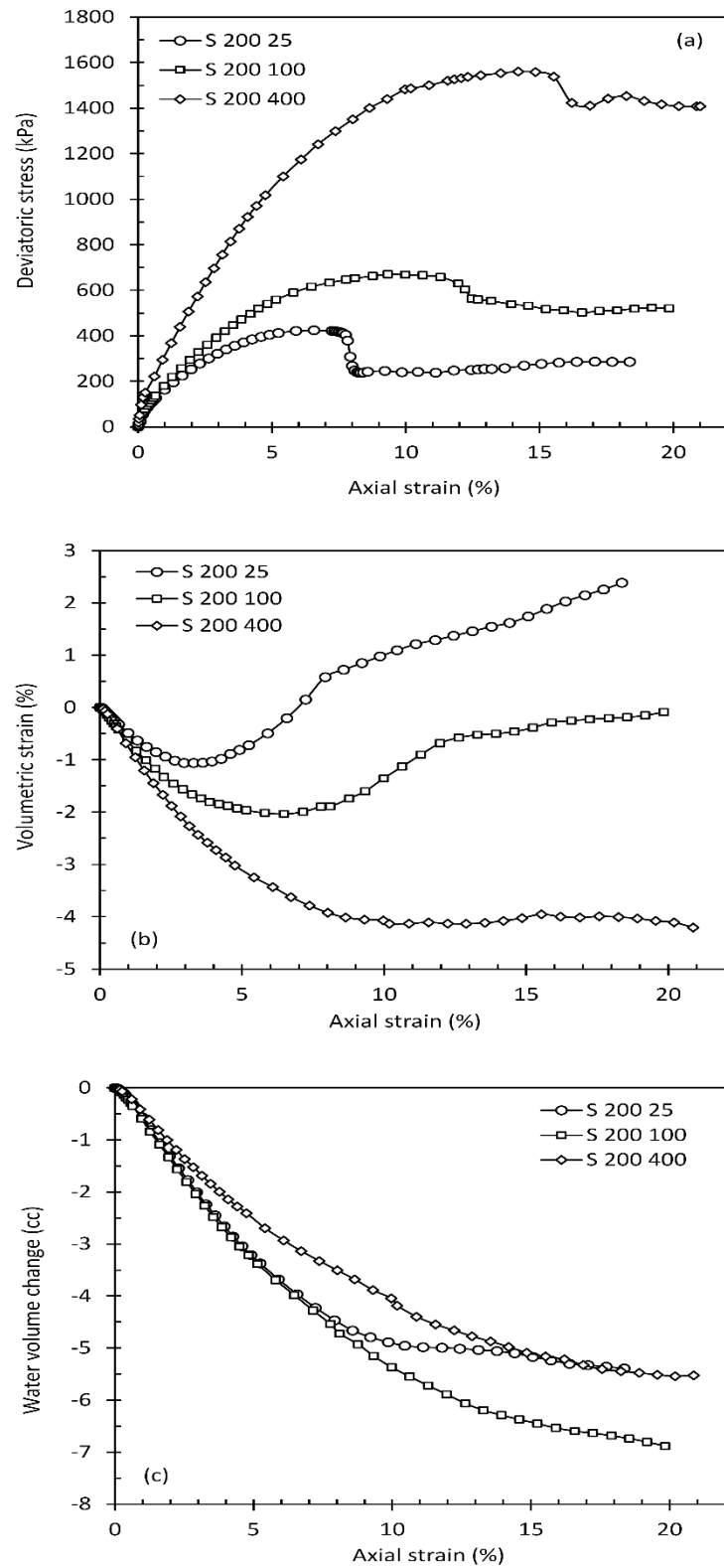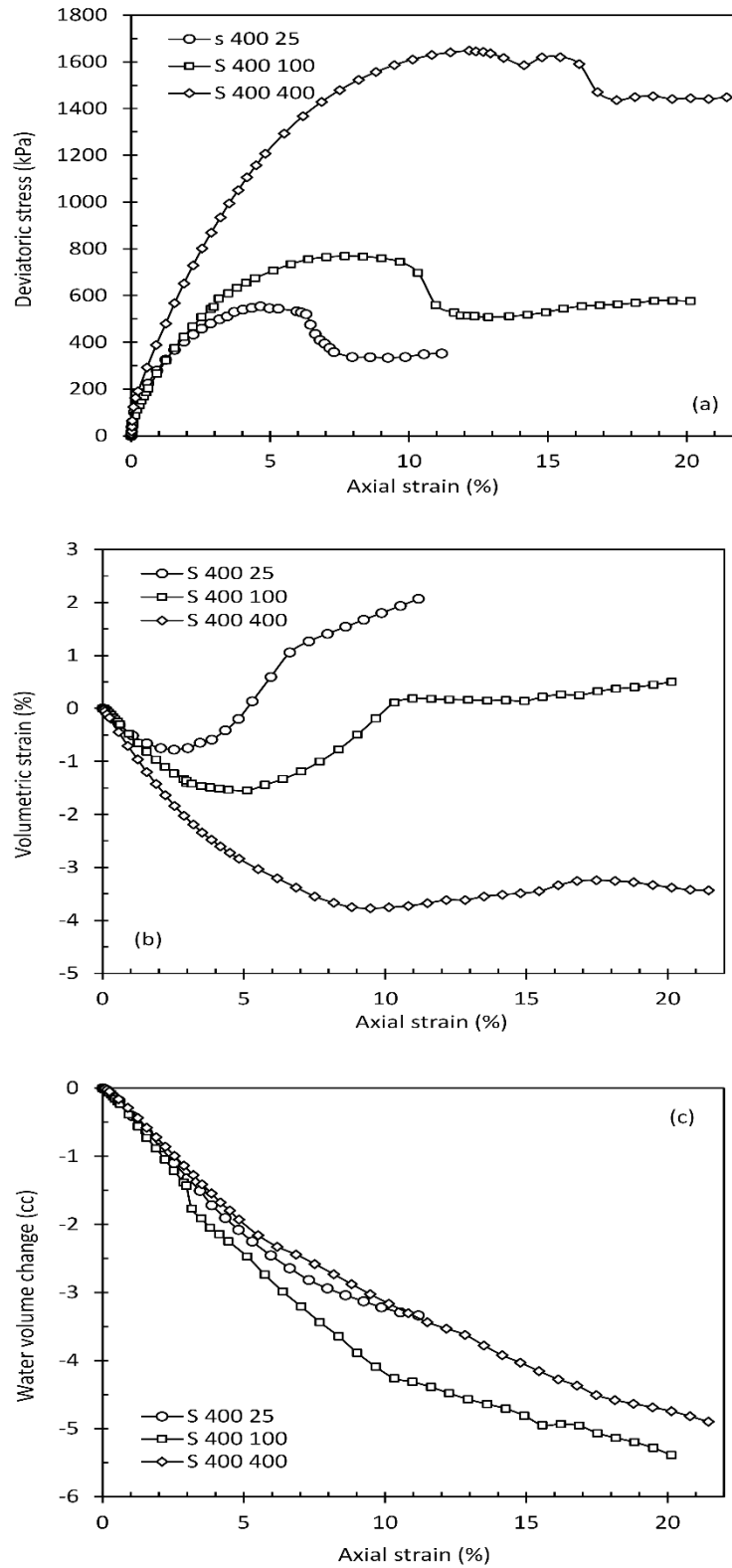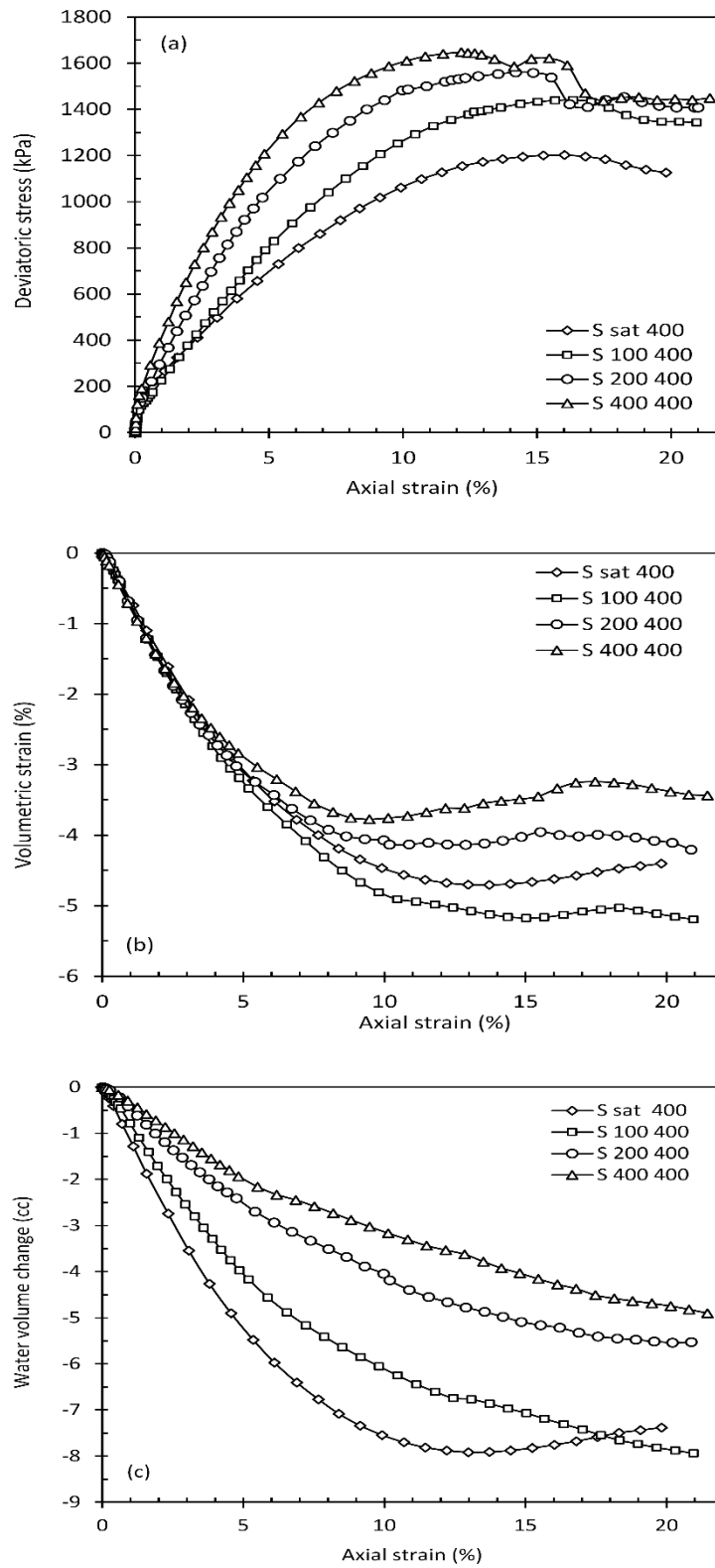
Figure 8.52 Variations of (a) deviatoric stress, (b) volumetric strain and (c) change in volume of water the during drained shearing at (σ3-ua) = 400 kPa.

8.2.1.4 Mohr-Coulomb Failure Envelope

Figure 8.53 to Figure 8.57 illustrate the Mohr's stress circles and corresponding failure envelope (plotted at maximum shear strength) of each set of the triaxial tests (i.e. for each suction). The shear strength parameters (i.e. friction angle and apparent cohesion intercept) were obtained from Mohr's circles failure envelope for each series of triaxial tests. Failure envelope for the single test at 20-kPa suction was plotted by assuming a same angle of internal friction with saturated tests. The variation of the shear strength (cohesion intercept) with matric suction are presented in Figure 8.58. The non-linear variation of the shear strength with matric suction is evident, which is consistent with previous studies (discussed in Chapter 3).
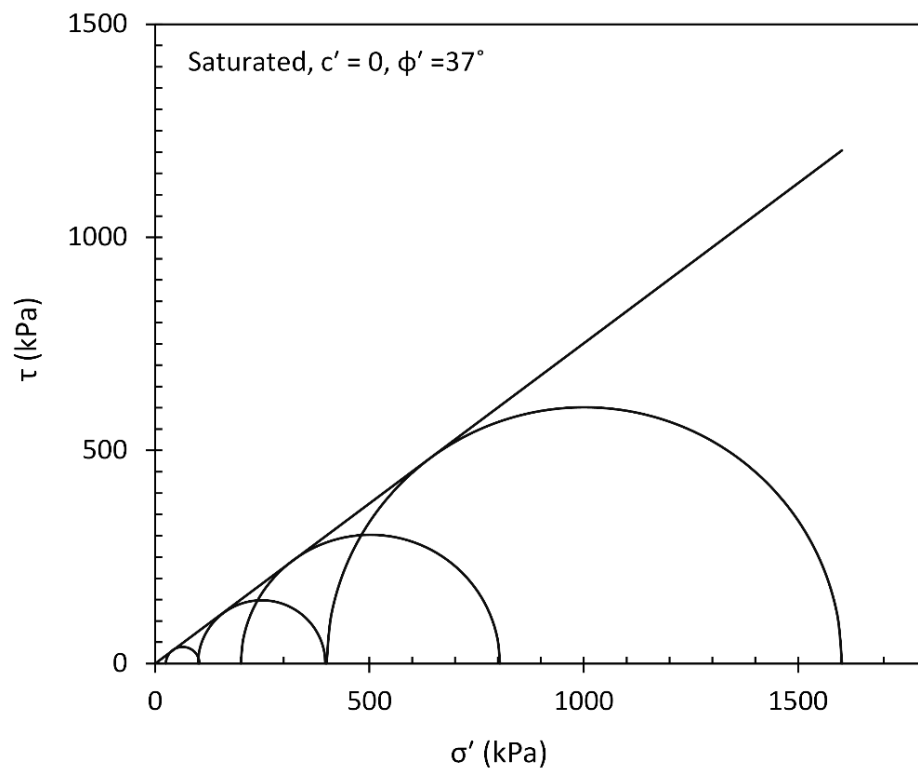
Figure 8.53 Mohr circles and cohesion intercepts for IRS specimen at saturated condition.

209
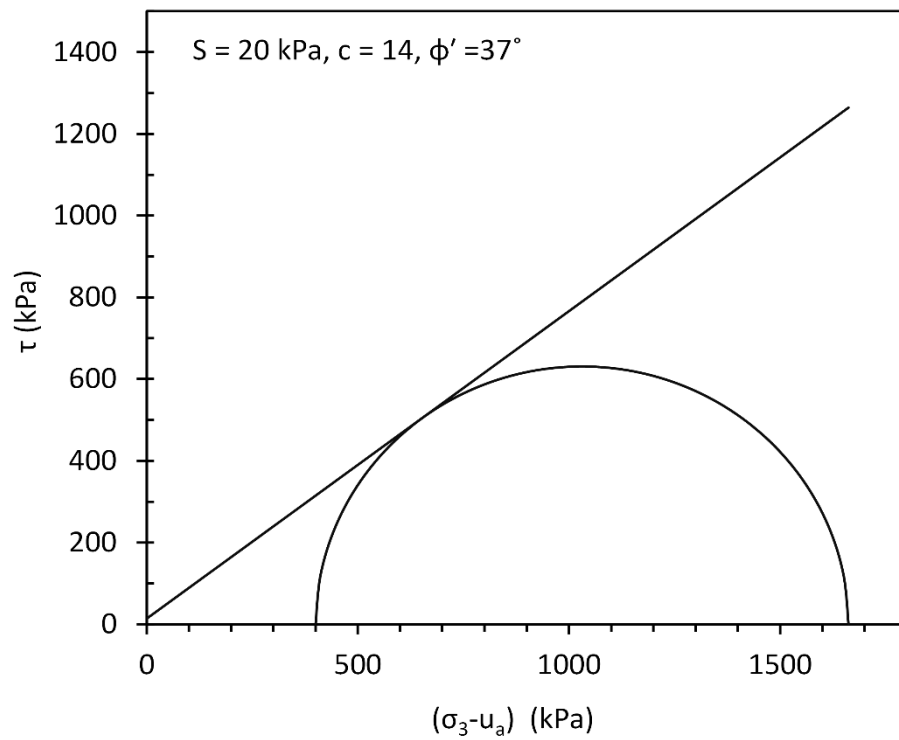
Figure 8.54 Mohr circles and cohesion intercepts for IRS specimen at suction of 20 kPa
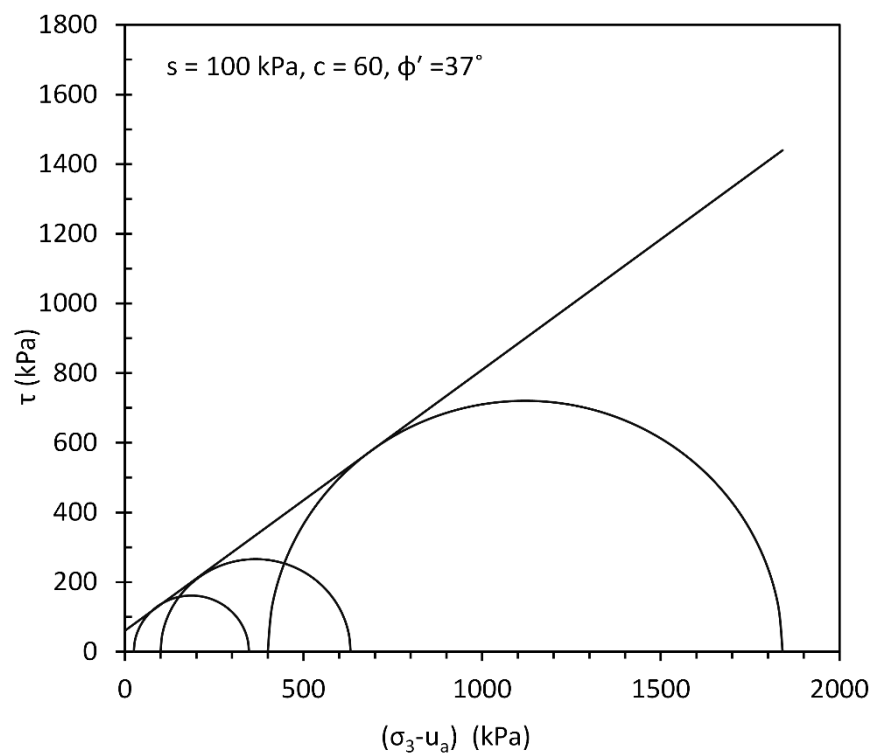
Figure 8.55 Mohr circles and cohesion intercepts for IRS specimen at suction of 100 kPa

210
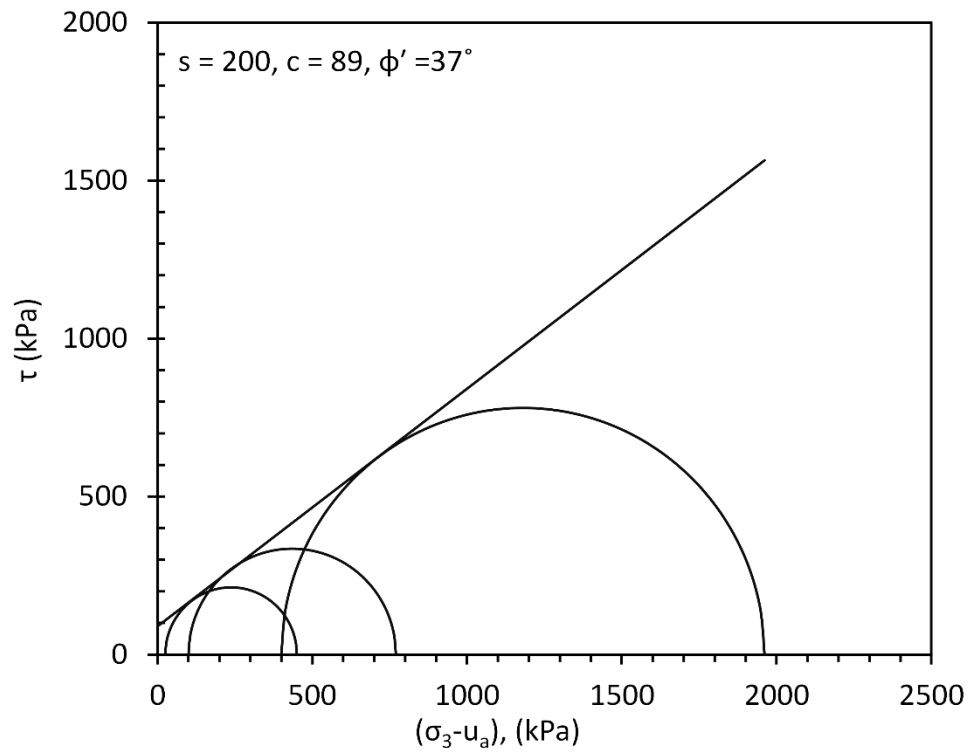
Figure 8.56 Mohr circles and cohesion intercepts for IRS specimen at suction of
200 kPa
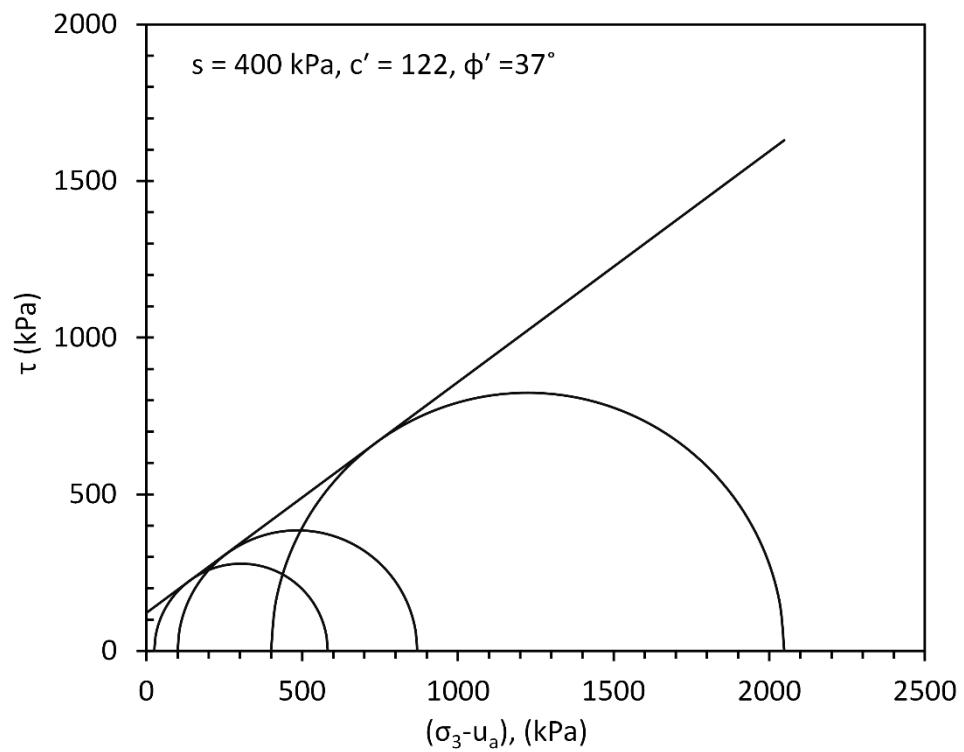
Figure 8.57 Mohr circles and cohesion intercepts for IRS specimen at suction of
400 kPa.
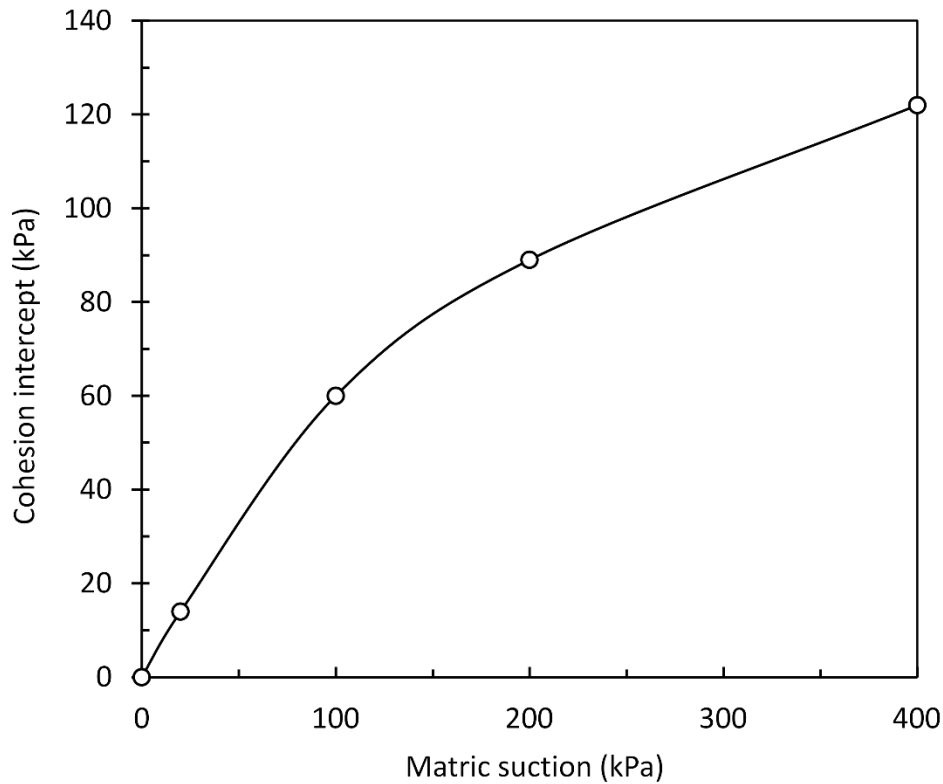
Figure 8.58 Variation of cohesion intercept with respect to matric suction.

8.2.1.5 Elasto Plastic Framework

8.2.1.5.1 Critical state line

Figure 8.59 show the critical state lines (CSL) from triaxial tests, in q-p plane for suction values of s = 0, 100, 200 and 400 kPa. As it can be seen Figure 8.59, the critical states of the each series (same matric suction) fall on a straight line. The gradient of the critical state line was determined for each series. Consistent with the assumption presented by Alonso et al. (1990), the gradient of the critical state lines appears to be a constant value independent of the suction, where it is determined to be M = 1.45 for saturated condition and M = 1.48 for suction values of 100, 200 and 400 kPa.

212
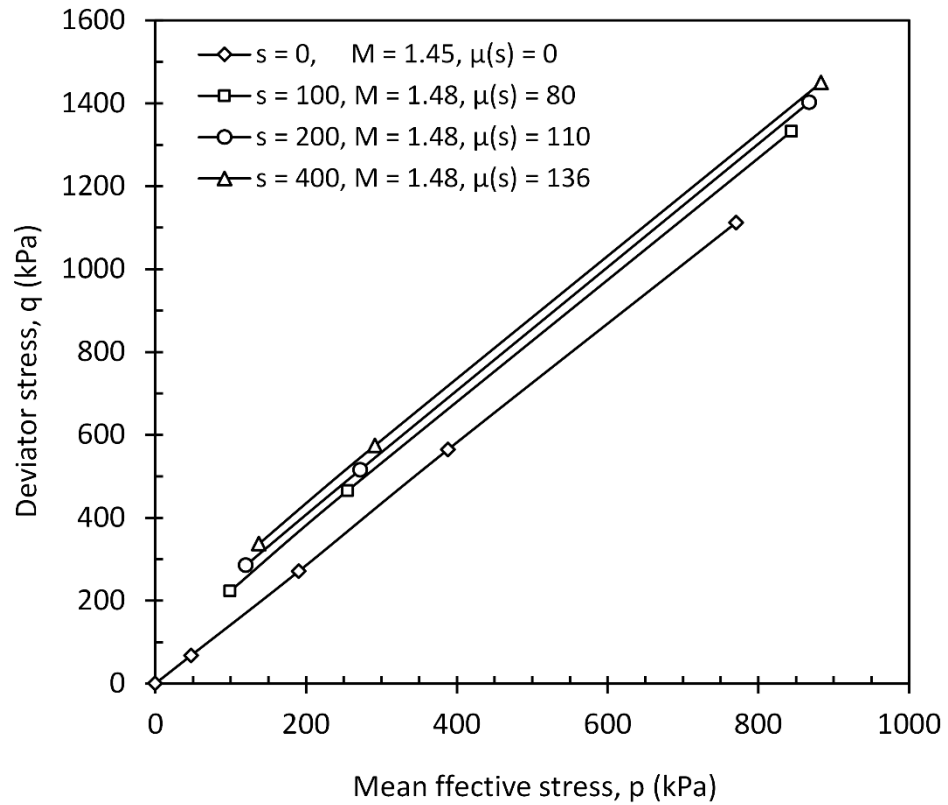
Figure 8.59 Critical state lines at different values of suctions in q - p plane.

The q-intercept of critical state line, $\mu(s)$, are determined for each constant suction triaxial tests and its variation with suction is presented in Figure 8.60. Consistent with Wheeler and Sivakumar (1995), a nonlinear relationship between critical state line $\mu(s)$ intercept and matric suction is observed, where the intercept increase with suction at a decreasing rate.

213
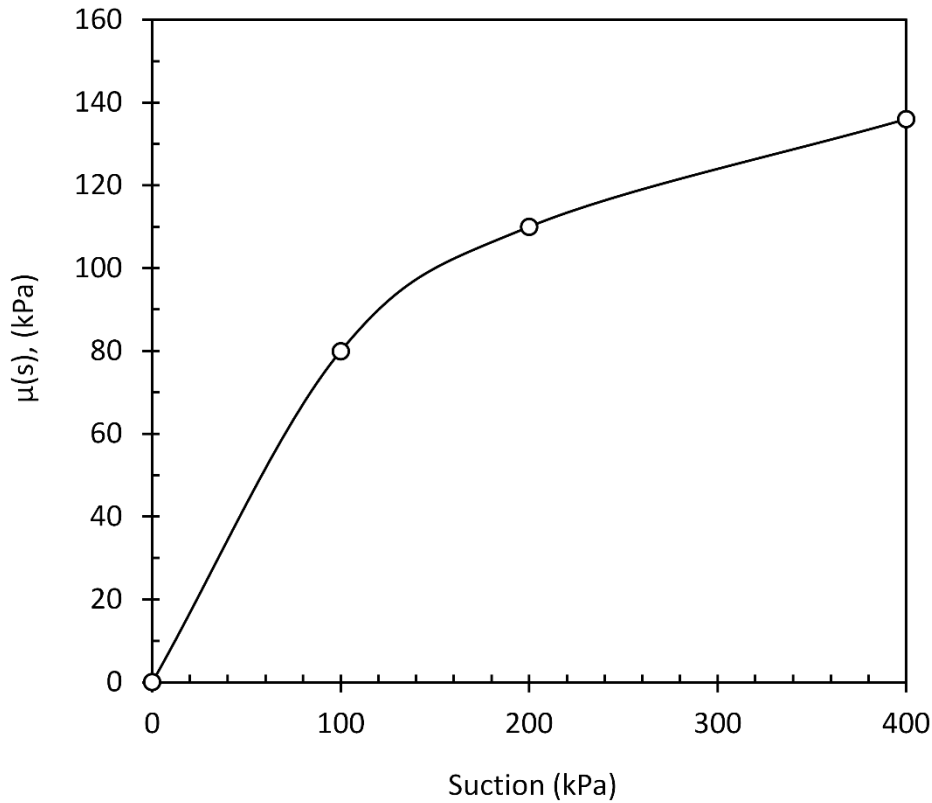
Figure 8.60 variation of the μ(s) with suction.

8.2.1.5.2 *Yield surface*

Yield points were determined for both saturated and unsaturated triaxial tests results. Yield points in saturated condition were determined through results of tests with loading and unloading path (overconsolidated). As shown in Figure 8.61 to Figure 8.64, the estimated yield values were employed to generate yield locus in q - p plane for each suction values (i.e. s= 0, 100, 200 and 400 kPa). An elliptical yield surface with the axis of net mean stress as the major axis were fitted successfully to yield points. This is in agreement with modified Cam-Clay model and BBM for both saturated and unsaturated condition. Figure 8.65 shows the summary of the yield curves for unsaturated conditions. It can be seen that, the size of the yield locus is function of the suction and larger for grater suction values. This observation is consistent with hardening effect of matric suction as included in BBM by Alonso et al. (1990).

214
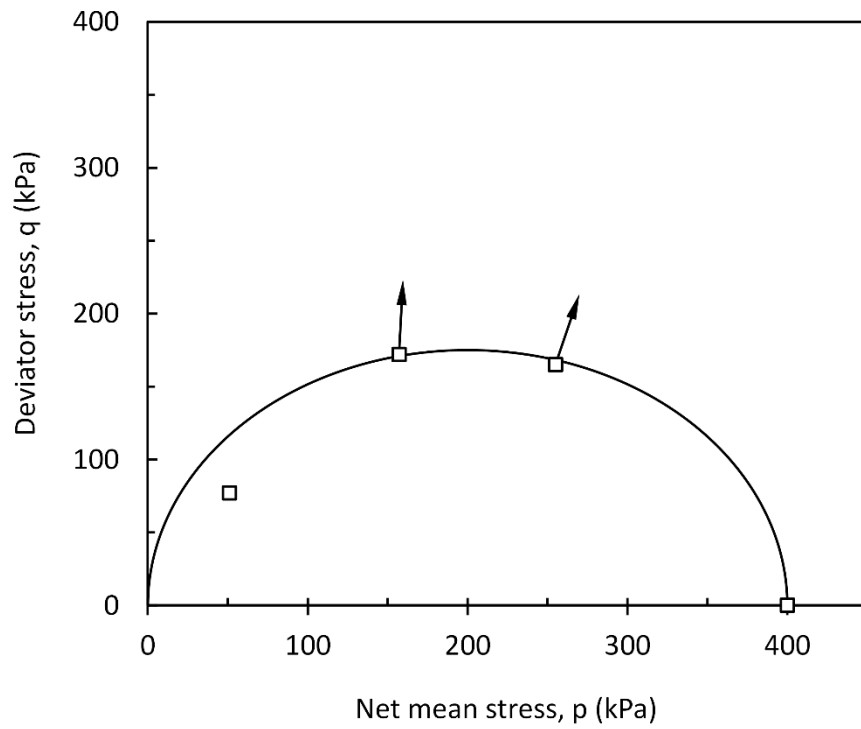
Figure 8.61 Measured yield points and fitted yield curve at s = 0 kPa, and plastic strain increment directions
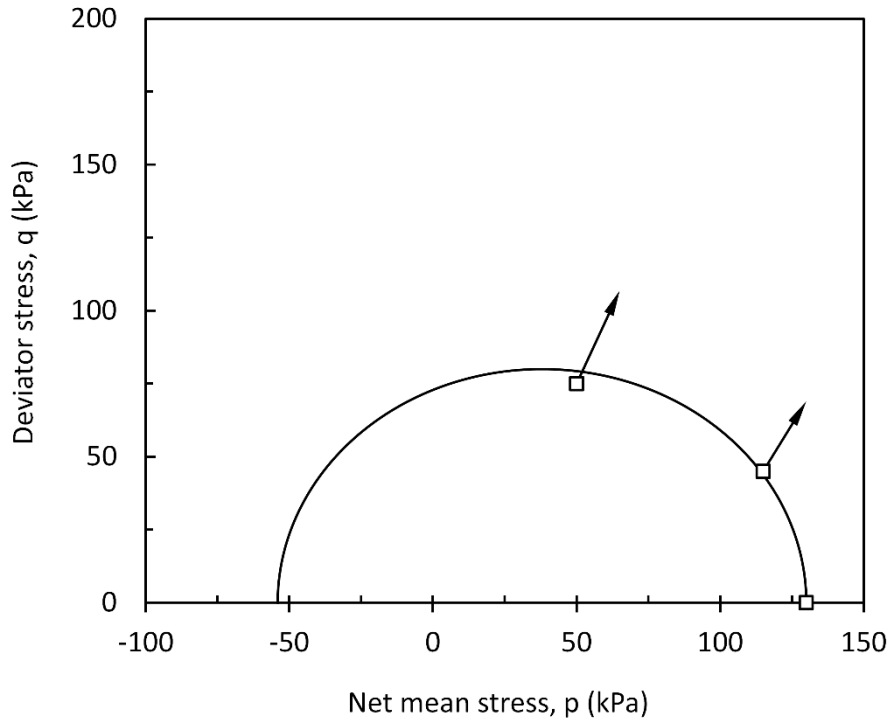
Figure 8.62 Measured yield points and fitted yield curve at s = 100 kPa, and plastic strain increment directions.
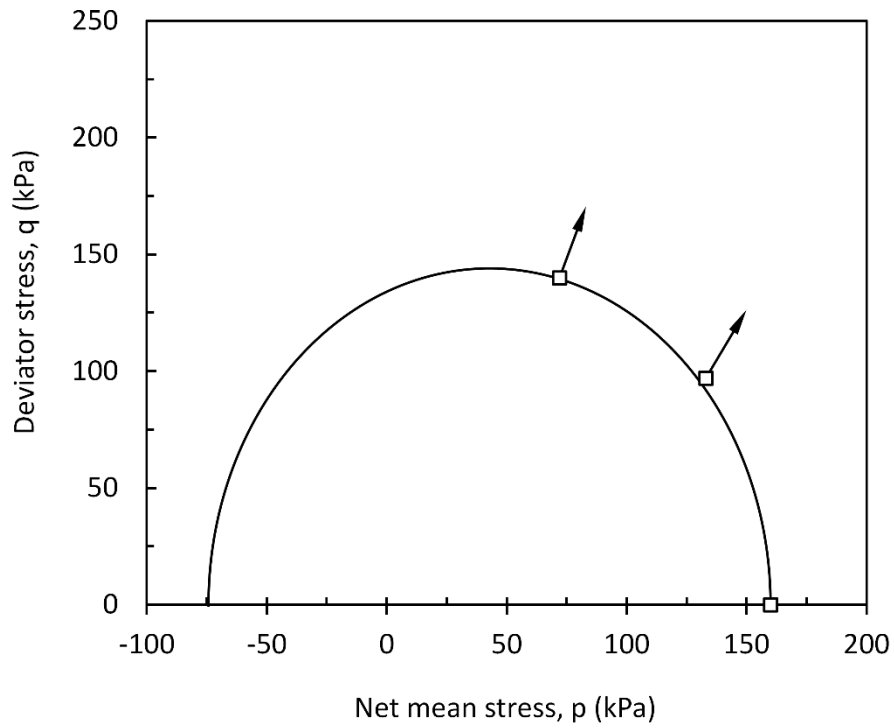
Figure 8.63 Measured yield points and fitted yield curve at s = 200 kPa, and
plastic strain increment directions
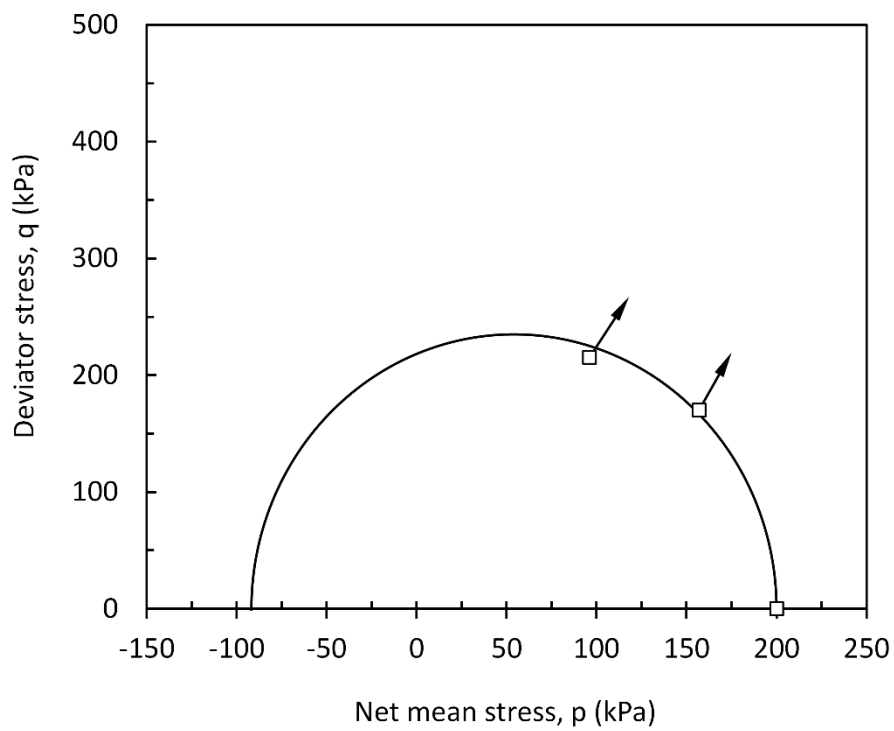
Figure 8.64 Measured yield points and fitted yield curve at s = 400 kPa, and
plastic strain increment directions
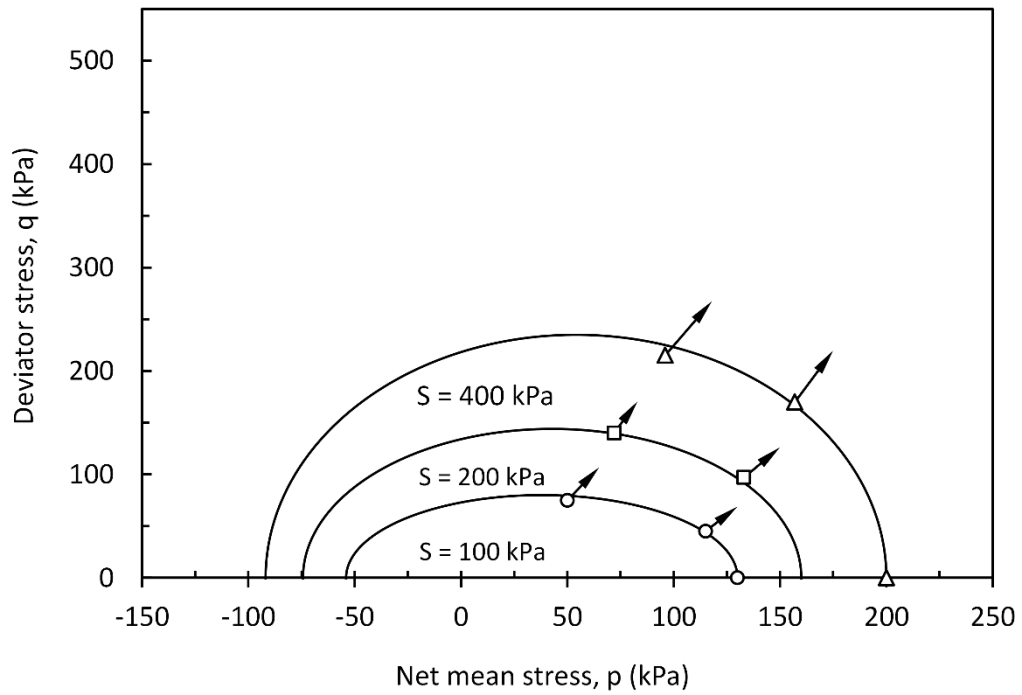
Figure 8.65 Yield curves for IRS specimens at different values of suction.

8.2.1.5.3 Flow rule

The volumetric and deviatoric plastic strain increments were calculated to identify the direction of plastic strain increment. The plastic strain increment vectors were determined and superimposed on related yield locus in the q-p plane with the slope of $d\varepsilon_s^p$: $d\varepsilon_v^p$ (Figure 8.61 to Figure 8.64). Inspection of the figures reveals that the plastic strain increment vectors are perpendicular to yield locus. Therefore, the associate flow rule is satisfied.

8.2.1.5.4 Shear modulus,

The shear modulus (G), were determined through the initial linear-elastic section of the deviatoric stress q, versus shear strain ε_s, plots.

Variation of the shear modulus versus net mean stress and suction are shown in Figure 8.66 and Figure 8.67. It is observed that, the initial shear modulus increases with suction and net mean stress. These observations do not support the assumption of Wheeler and Sivakumar (1995) where a constant value for shear modulus, were presumed.

217
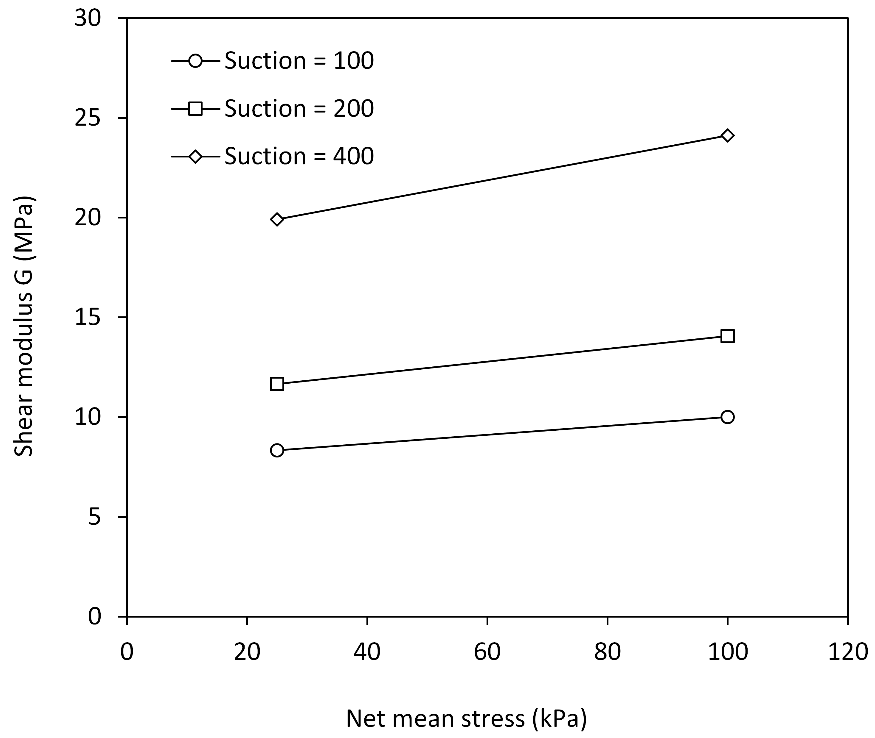
Figure 8.66 Variation of shear modulus with net mean stress.
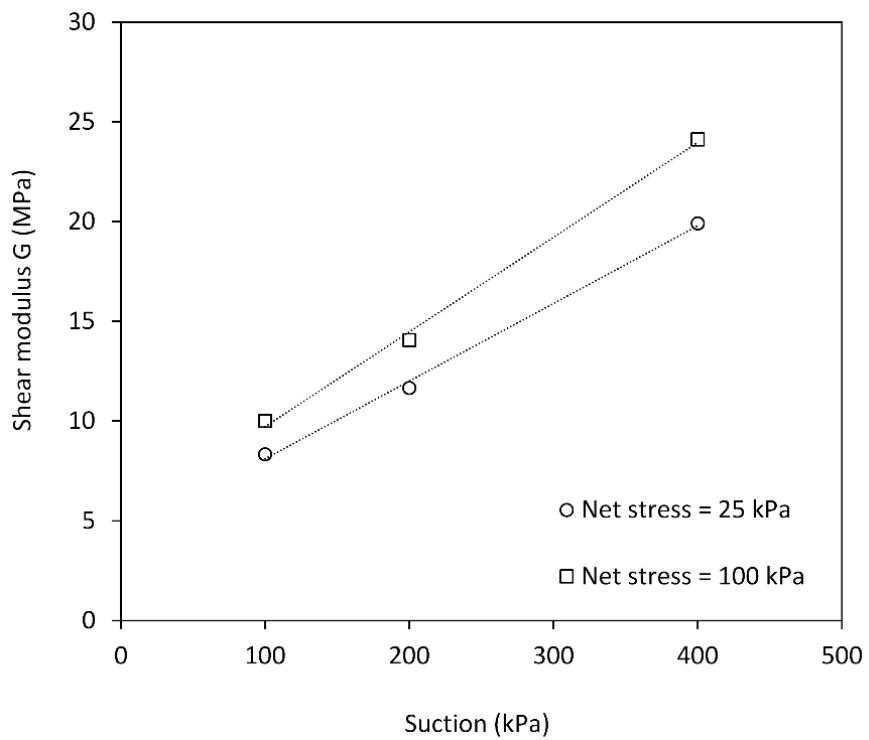
Figure 8.67 Variation of shear modulus with suction.

218

8.2.2 Behavior of Unsaturated IRS Specimens with Precedent drying-wetting

This Series 2 (see section 7.3.1.2 for test program) involves nine suction controlled CD test on IRS specimens with drying-wetting. The adopted naming convention for these series take the form of the "S D-W, P" where "S" stands for specimen preparation method (i.e. slurry), "D" represents the suction on the drying path, "W" represents the suction on the wetting path and "p" stands for the net mean stress.

8.2.2.1 Suction Equalization

Similar to that of series 1, at net mean stress of 25 kPa, specimens were brought to a suction of 400 kPa for equalization following a drying path. Once the equalization is achieved, following wetting path, suction is reduced to 0, 100, and 200 kPa for equalization. The changes in water volume and volume of the specimen during the equalization stage were monitored.

Figure 8.68 and Figure 8.69 present the variation in specimen volume and water volume during equalization stage for drying and wetting. In all tests, as expected, on the drying path water is drained out of the specimen, as suction increases. Water flows into the specimen, as suction decreases, on the wetting path. However, it should be noted the amounts of water that flow into the specimen are considerably less than those drained out during drying. This is because of the hysteresis of the SWCC where for a given suction the water content on the wetting curve is less than that of the drying curve. It can also be seen, specimens undergo permanent volumetric compression while drying, and there is a small elastic recovery of this volume change during the wetting stage.

The permanent volumetric compression during the drying process can be explained by the suction increase (SI) yield curves proposed by Alonso et al. (1990), where plastic volumetric strains occur when crossing the SI yield boundary (see section 2.4).

As the specimens were prepared from slurry (saturated condition), they had never previously been subjected to suction stress. Therefore, for specimen prepared from the slurry, application of even small amounts of suction can cause additional plastic volumetric strains.

219
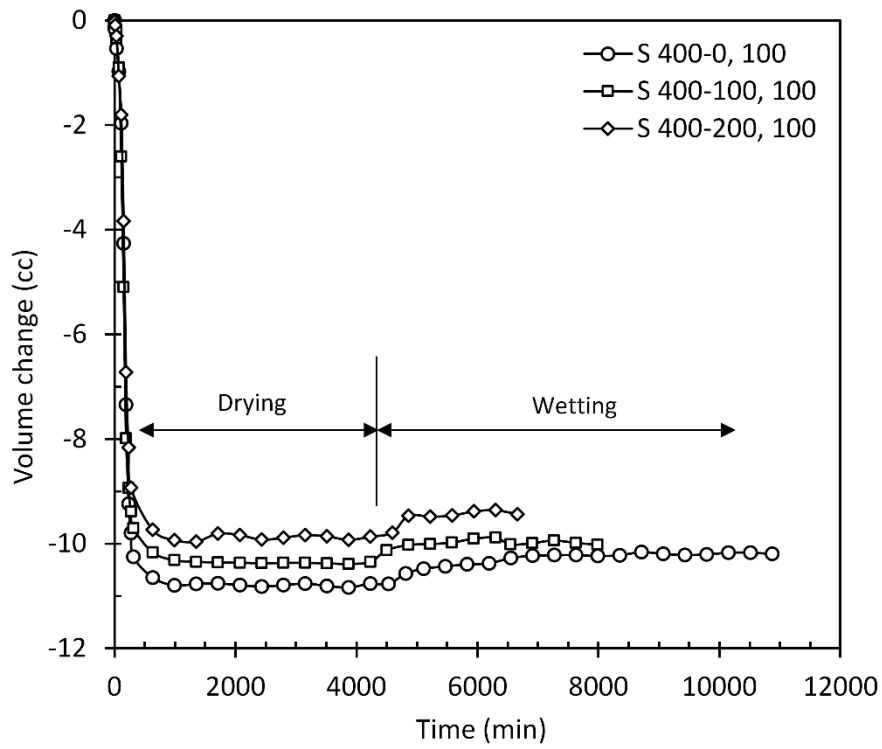
Figure 8.68 Variation in specimen volume during drying-wetting.
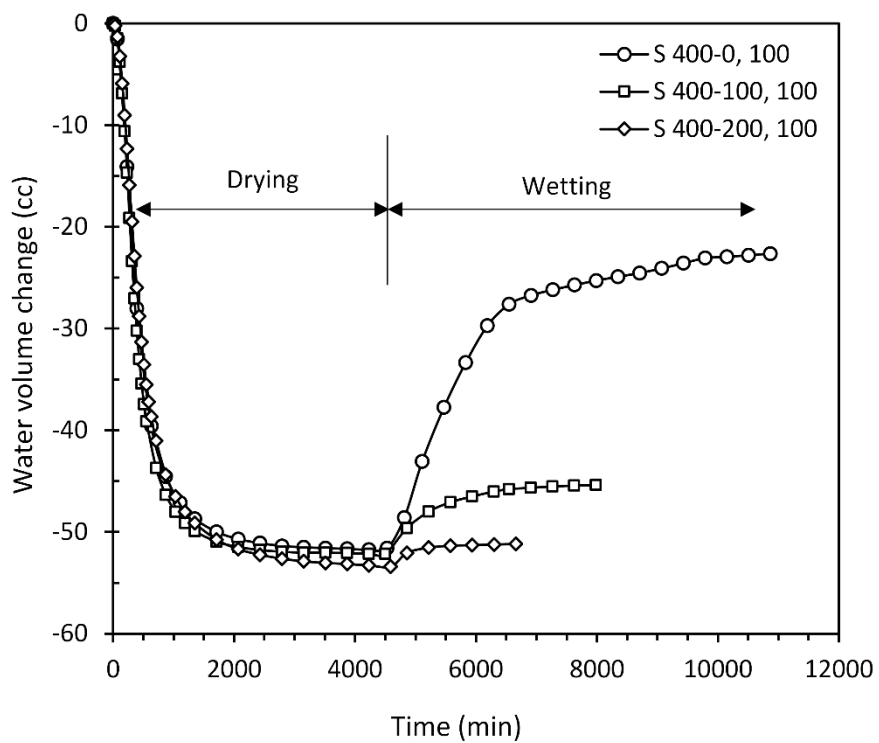
Figure 8.69 Variation in water volume during drying-wetting.

220

8.2.2.2 Isotropic Compression at Constant Suction

Following equalization in wetting stage, specimens were isotropically compressed (at constant suction) to the desired value of the net-confining stress. At this stage specimens were subjected to 25, 100 or 400 kPa net stress. The variation of the void ratio (e) with net mean stress p, for 400-kPa net stress (for suction values of 20, 100, 200 and 400 kPa) are presented in Figure 8.70. As it can be seen in Figure 8.70, yielding (preconsolidation) was observed during isotropic compression.
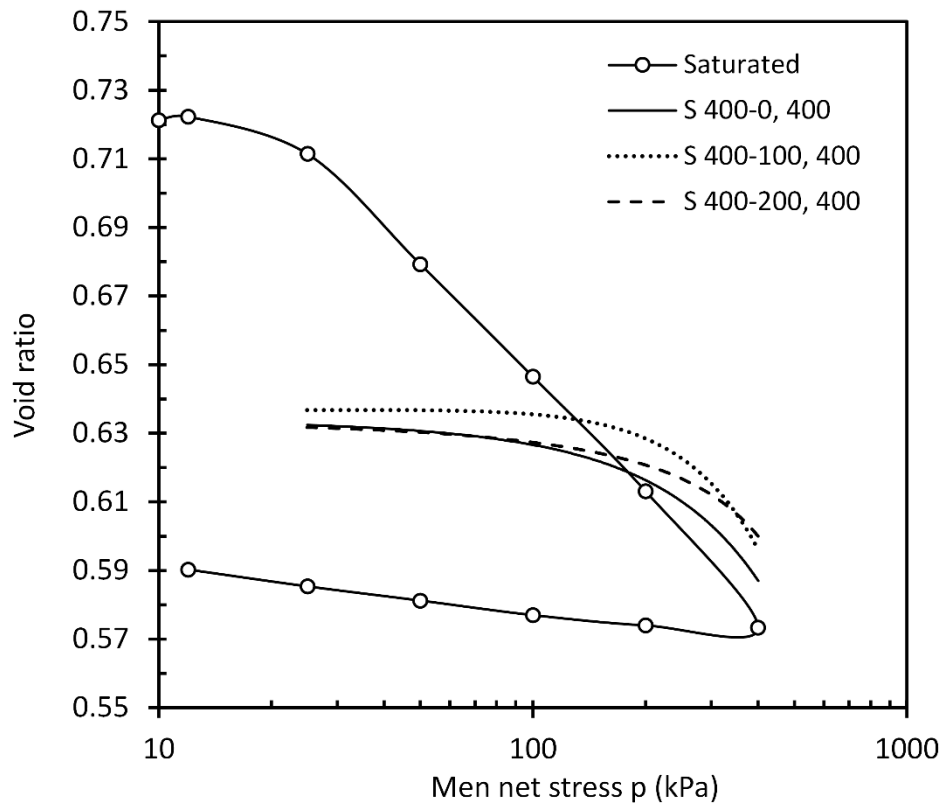
Figure 8.70 Isotropic compression curves at different suction values after wetting for IRS specimens.

The yield stresses are estimated from compression curves for each values of suction. These values used to define the loading collapse (LC) yield curve in s – p plane (Figure 8.71). As it can be seen in Figure 8.71, the yield stress increases from 200 kPa at zero suction, at a decreasing rate, to 245 kPa when matric suction is 200 kPa.
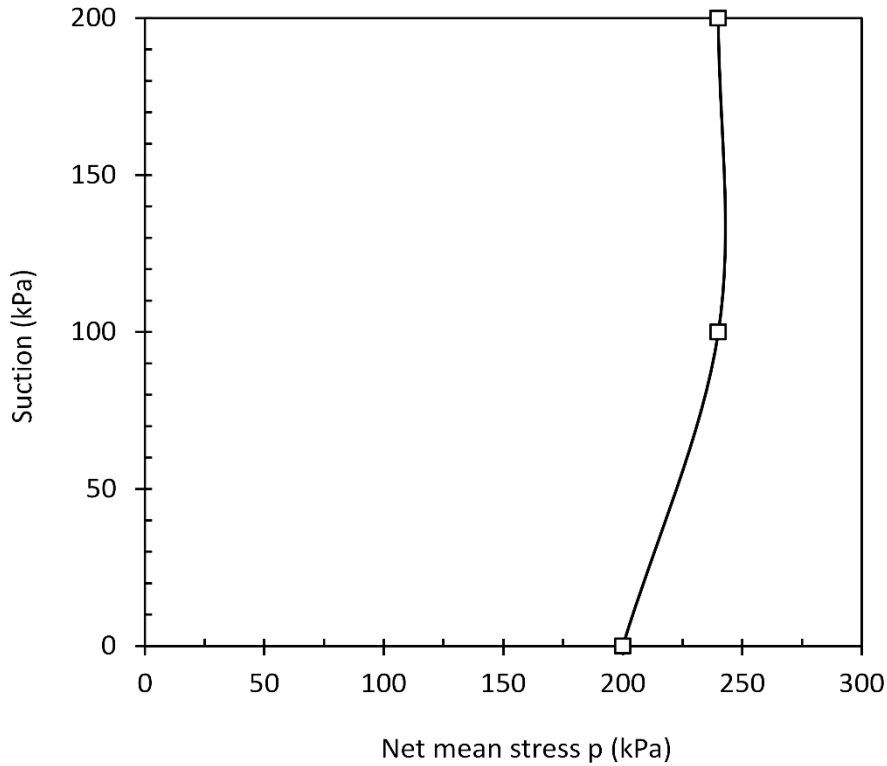
Figure 8.71 The loading-collapse yield curve for IRS specimens in wetting path.

8.2.2.3 Constant Suction Drained Shearing Stage

Figure 8.72 (a), Figure 8.73 (a) and Figure 8.74 (a) show the typical results of the triaxial tests at different values of suction but at the same net confining stresses. For the entire range of the suction, the stiffness and maximum shear strength is larger at higher suction values. Specimens exhibit a strain-softening behavior. This becomes more pronounced at low net confining stresses, where a peak deviatoric stress is attained at lower strains. The response of the specimens change from moderate strain-hardening in specimens with zero suction (wetted from 400-kPa suction) to severe strain-softening for the final suction of 200 kPa.

Figure 8.72 (b), Figure 8.73 (b) and Figure 8.74 (b) show the corresponding volumetric strain during shearing. Similar to series 1, for net confining stress of 25 and 100 kPa specimens show an initial contraction in volume followed by dilation. For net confining stress of 400 kPa specimen exhibited a compressive behavior.

Figure 8.72 (c), Figure 8.73 (c) and Figure 8.74 (c) show the changes in water volume during shearing. It seems that, water tends to flow into the specimen at smaller suction values.

222
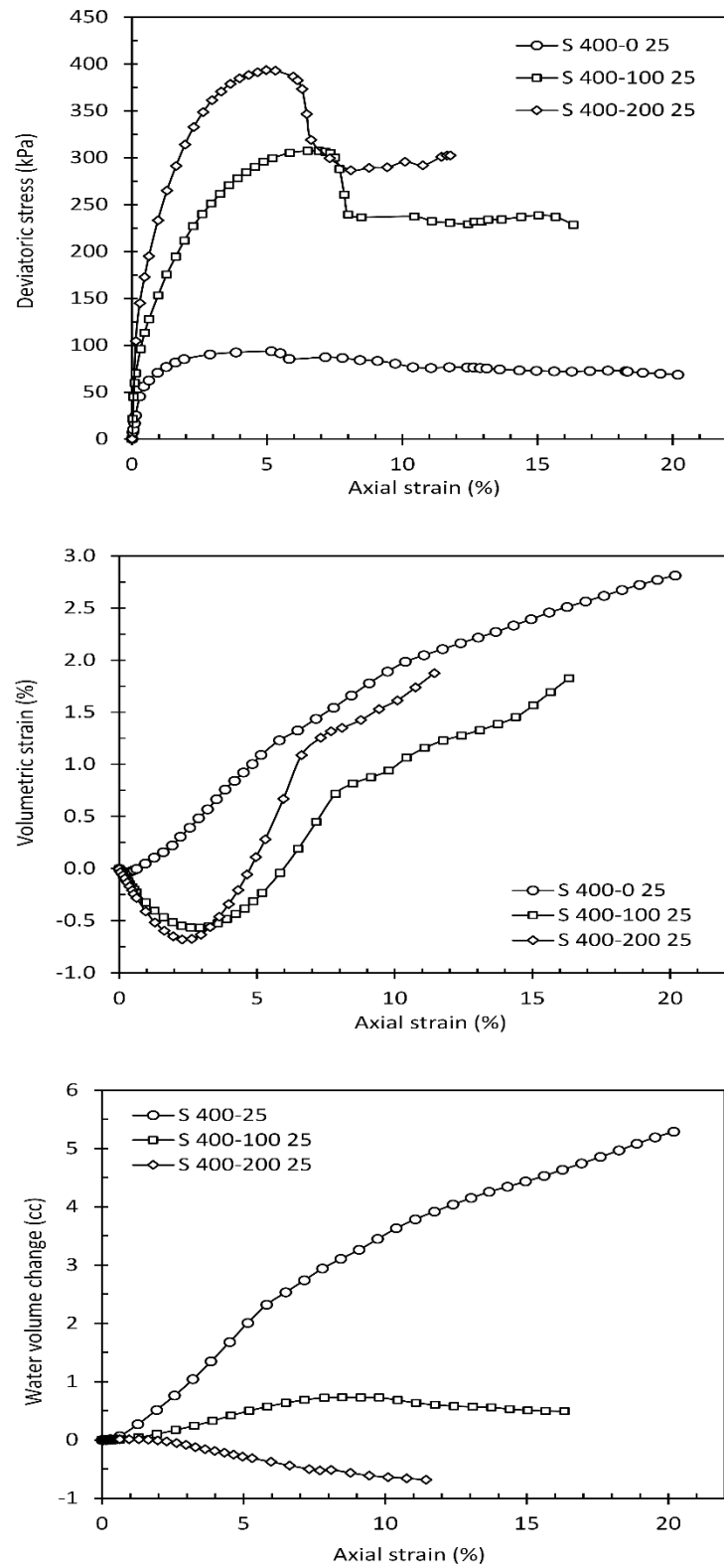
Figure 8.72 Variations of (a) deviatoric stress, (b) volumetric strain and (c) change in volume of water during drained shearing at $(\sigma_3 - u_a) = 25$ kPa

223
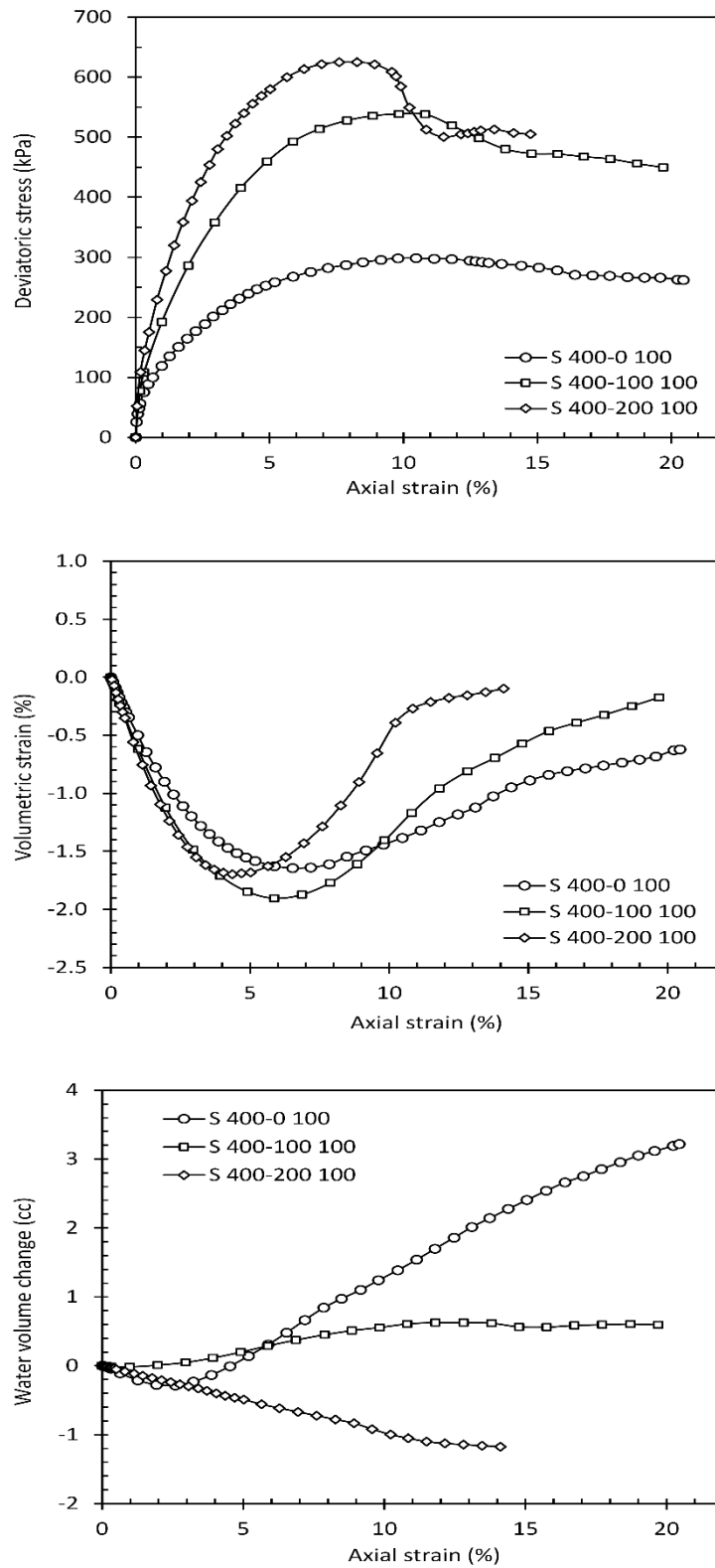
Figure 8.73 Variations of (a) deviatoric stress, (b) volumetric strain and (c) change in volume of water during drained shearing at $(\sigma_3\text{-}u_a) = 100$ kPa.
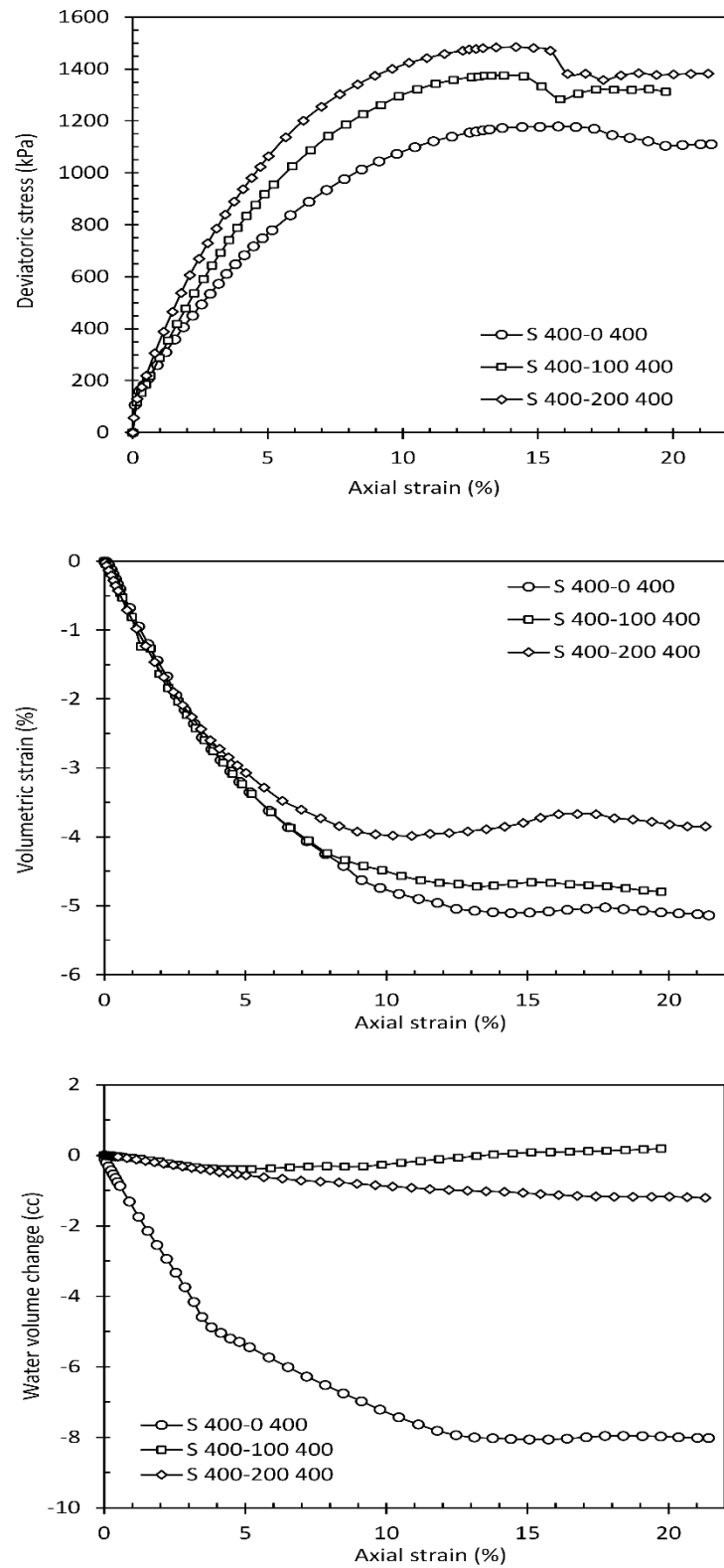
Figure 8.74 Variations of (a) deviatoric stress, (b) volumetric strain and (c) change in volume of water during drained shearing at $(\sigma_3 - u_a) = 400$ kPa.

8.2.2.4 Mohr-Coulomb Failure Envelope

Figure 8.75 to Figure 8.77 illustrate Mohr's stress circles and corresponding failure envelopes (plotted at maximum shear strength) for each suction group. The shear strength parameters (i.e. friction angle and apparent cohesion intercept) were obtained from these failure envelopes for each set of triaxial tests. The variation of the cohesion intercept (apparent cohesion) with matric suction is presented in Figure 8.78. The non-linear variation of the shear strength with matric suction is evident, which is consistent with previous studies.

The friction angle was determined to be 36°, that appears to be independent of suction in wetting path.
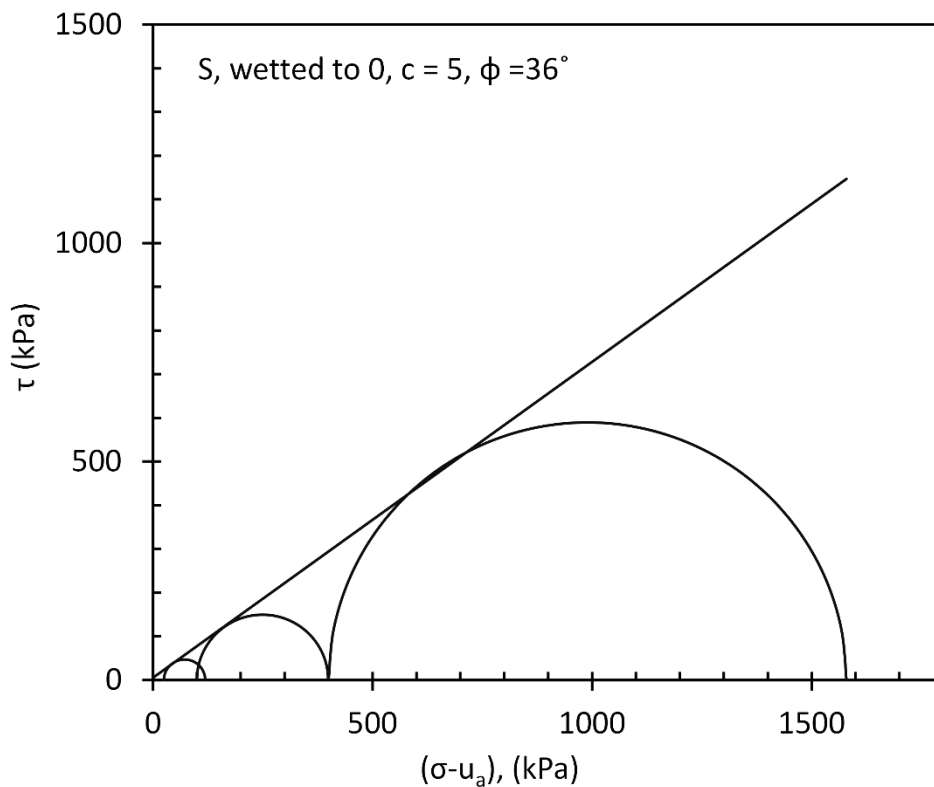
Figure 8.75 Mohr circles and cohesion intercepts of specimens wetted to zero suction.
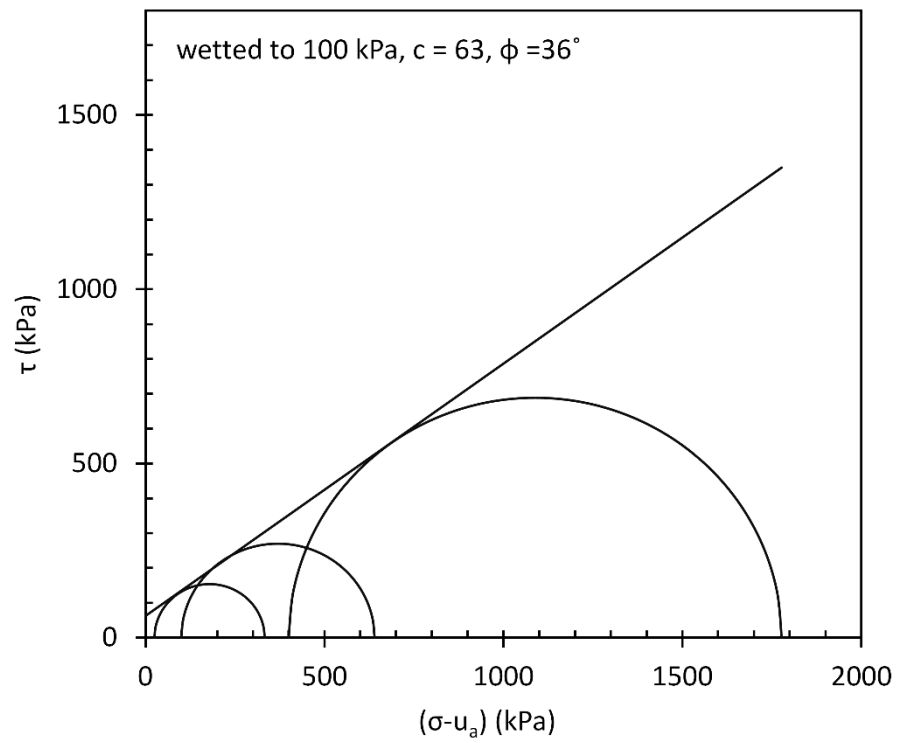
Figure 8.76 Mohr circles and cohesion intercepts of specimens wetted to 100 kPa suction.
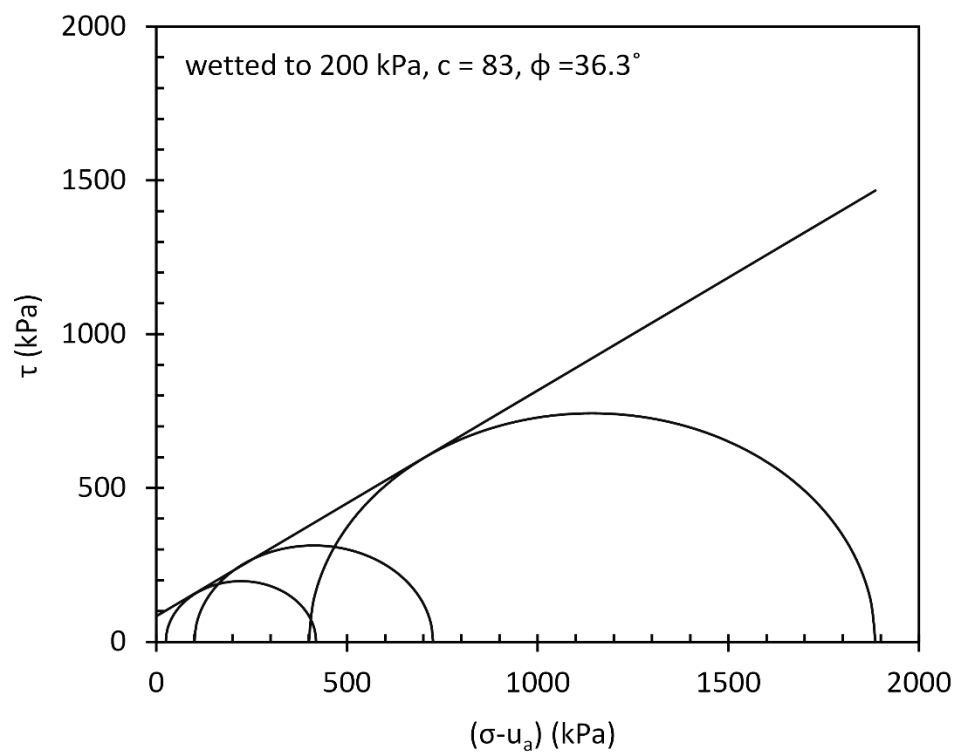
Figure 8.77 Mohr circles and cohesion intercepts of specimens wetted to 200 kPa suction.

227
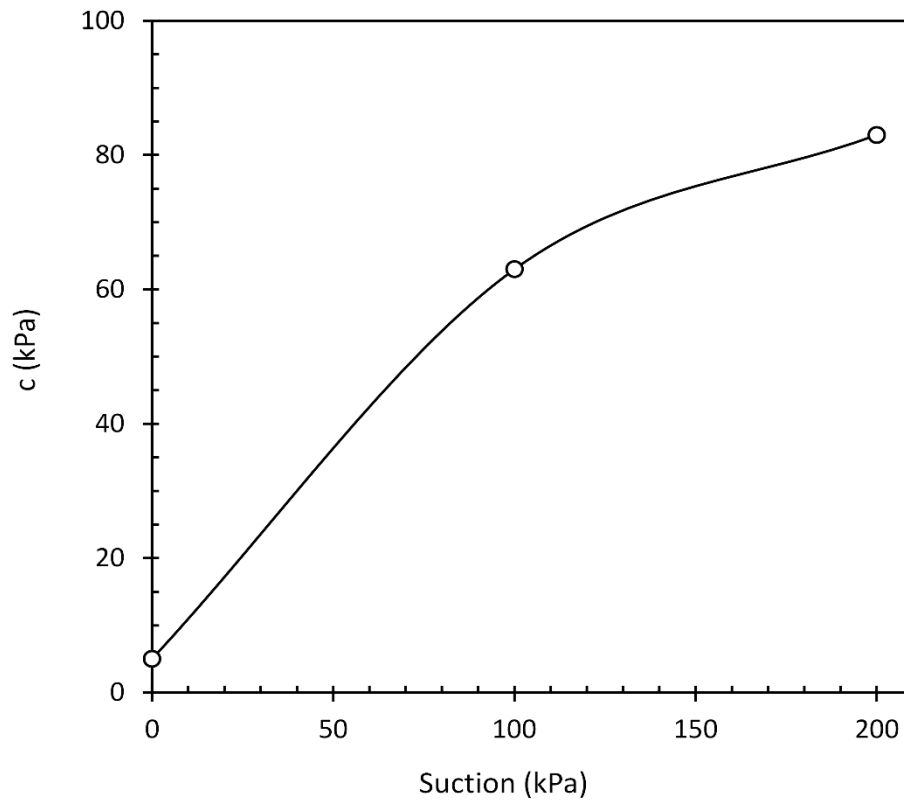
Figure 8.78 Variation of cohesion intercept with respect to matric suction in wetting path.

8.3.2.1. *Critical State Line in q-p Plan*

The critical state lines (CSL) from triaxial tests, in q-p plane (for suction values wetted to 0, 100, 200 kPa from the initial value of 400 kPa) are shown in Figure 8.79. The critical states of the each series (same matric suction) fall on a straight line. The gradient of the critical state line was determined for each series. The gradient of the CSL was determined to be M = 1.44 for specimens wetted to zero suction and M = 1.47 for wetting to 100 and 200 kPa suction.

Nonlinear variation of intercept of critical state line $\mu(s)$ with suction is shown in Figure 8.80.
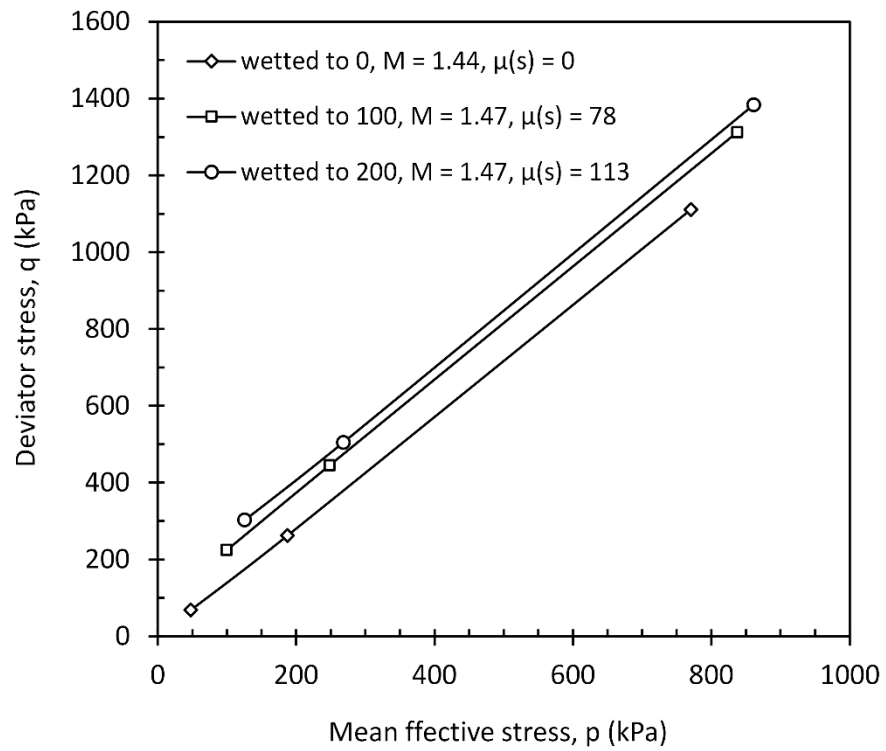
Figure 8.79 Critical state lines for wetting path in q - p plane for IRS specimen with drying and wetting.
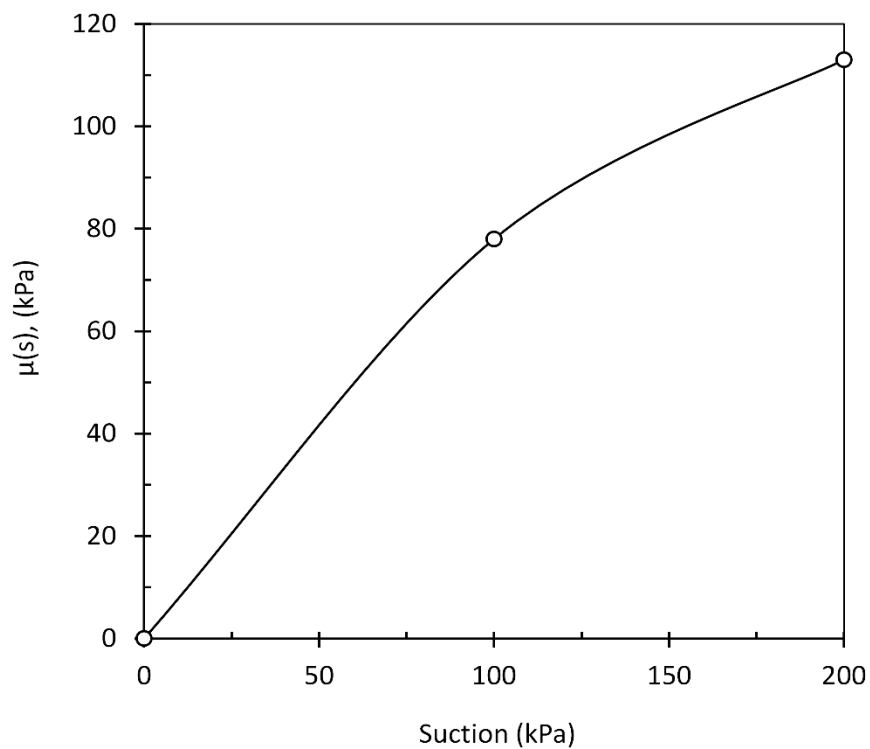
Figure 8.80 Variation of the μ(s) with suction for IRS specimen with drying and wetting.

229

8.2.2.5 Yield Surface

Yield points were determined for both unsaturated triaxial tests results. As shown in Figure 8.81 and Figure 8.82, the estimated yield values were used to generate yield locus in q - p plane for suction values wetted to 100 and 200 kPa. An elliptical yield surface with the axis of net mean stress as the major axis were fitted successfully to yield points. Figure 8.83 shows the summary of the yield curves for unsaturated conditions. The size of the yield locus is function of the suction (larger for grater suction values).
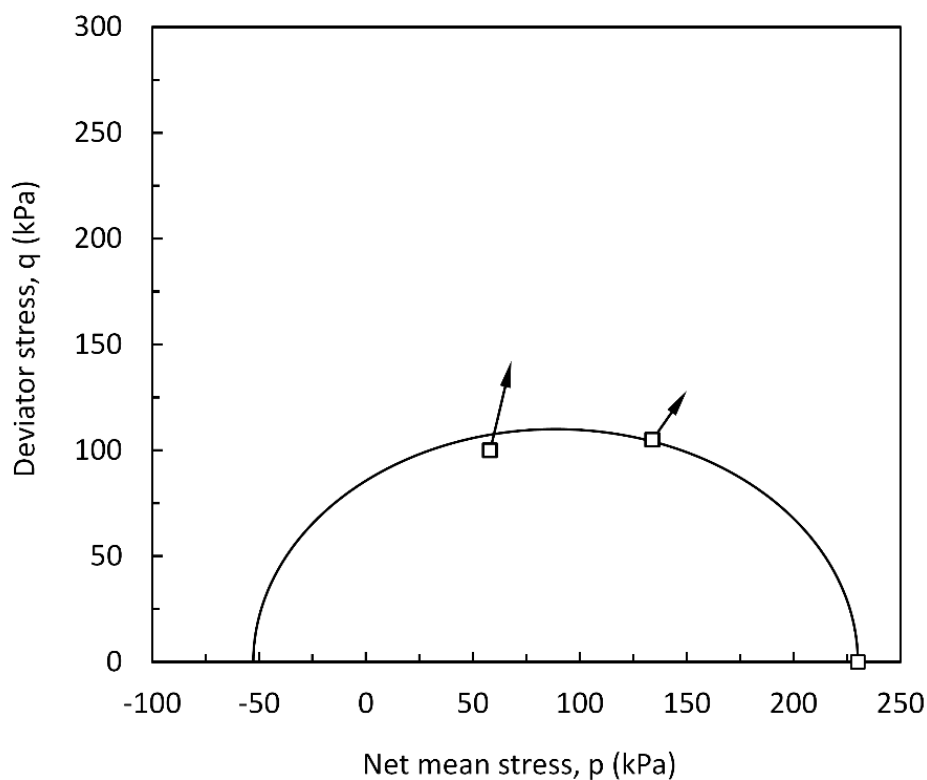
Figure 8.81 Measured yield points and fitted yield curve at suction wetted to 100-kPa and plastic strain increment directions.
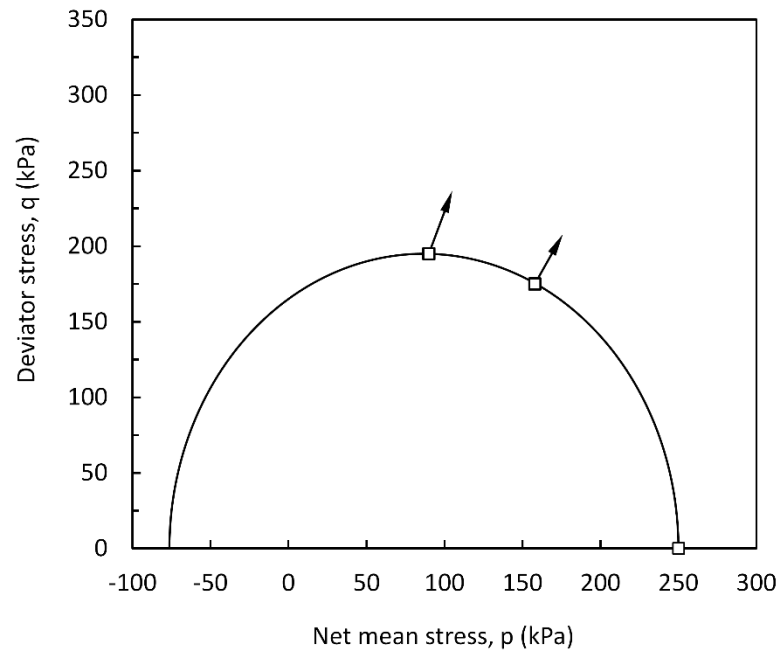
Figure 8.82 Measured yield points and fitted yield curve at suction wetted to 200-kPa and plastic strain increment directions.
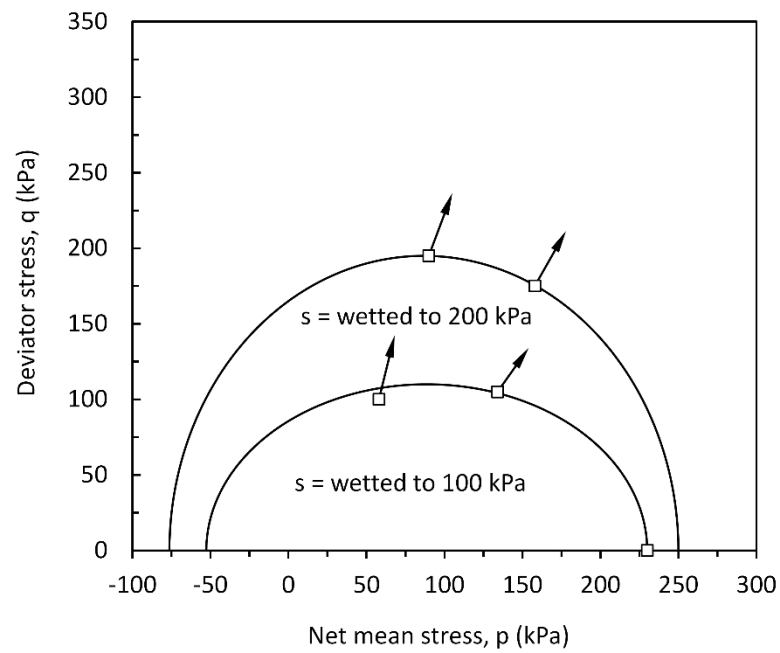
Figure 8.83 Yield curves for IRS specimens at different values of suction in wetting path.

8.2.2.6 Flow Rule

The volumetric and deviatoric plastic strain increments were calculated to identify the direction of plastic strain increment. The plastic strain increment vectors were determined and superimposed on related yield locus in q-p plane with the slope of $d\varepsilon_s^p : d\varepsilon_v^p$ (Figure 8.81 and Figure 8.82).

CHAPTER 9

COMPARISON AND DISCUSSION

This chapter compares and discusses saturated and unsaturated triaxial tests result (presented in chapter 8) performed on specimens with different preparation and suction history. The proposed shear strength equation is verified through the laboratory test results presented in chapter eight. In addition, validity of the equation is investigated regarding shear strength test results of five soil published in the literature and compared with predicted values of equations summarized in Table 3.1.

9.1 Comparing Behavior of Saturated Specimens by Different Preparation Methods

The effects of preparation methods on strength and volumetric behavior of saturated specimens are investigated. For this, three sets of consolidated drained (CD) triaxial tests were performed on the saturated specimens prepared by three distinctive preparation methods: a) isotropically reconstituted from slurry (IRS), b) one-dimensionally reconstituted from slurry (ORS) and c) moist tamping with under-compaction (MT) specimens.

9.1.1 Volume Changes during Consolidation

Figure 9.1 compares the changes in volume of the specimens during consolidation stage. The effect of preparation method on volume change of the specimens is obvious. For a given confining pressure, the change in volume of the MT specimens is considerably less than the two other methods. In other words, MT specimens are less compressible in comparison to IRS and ORS.
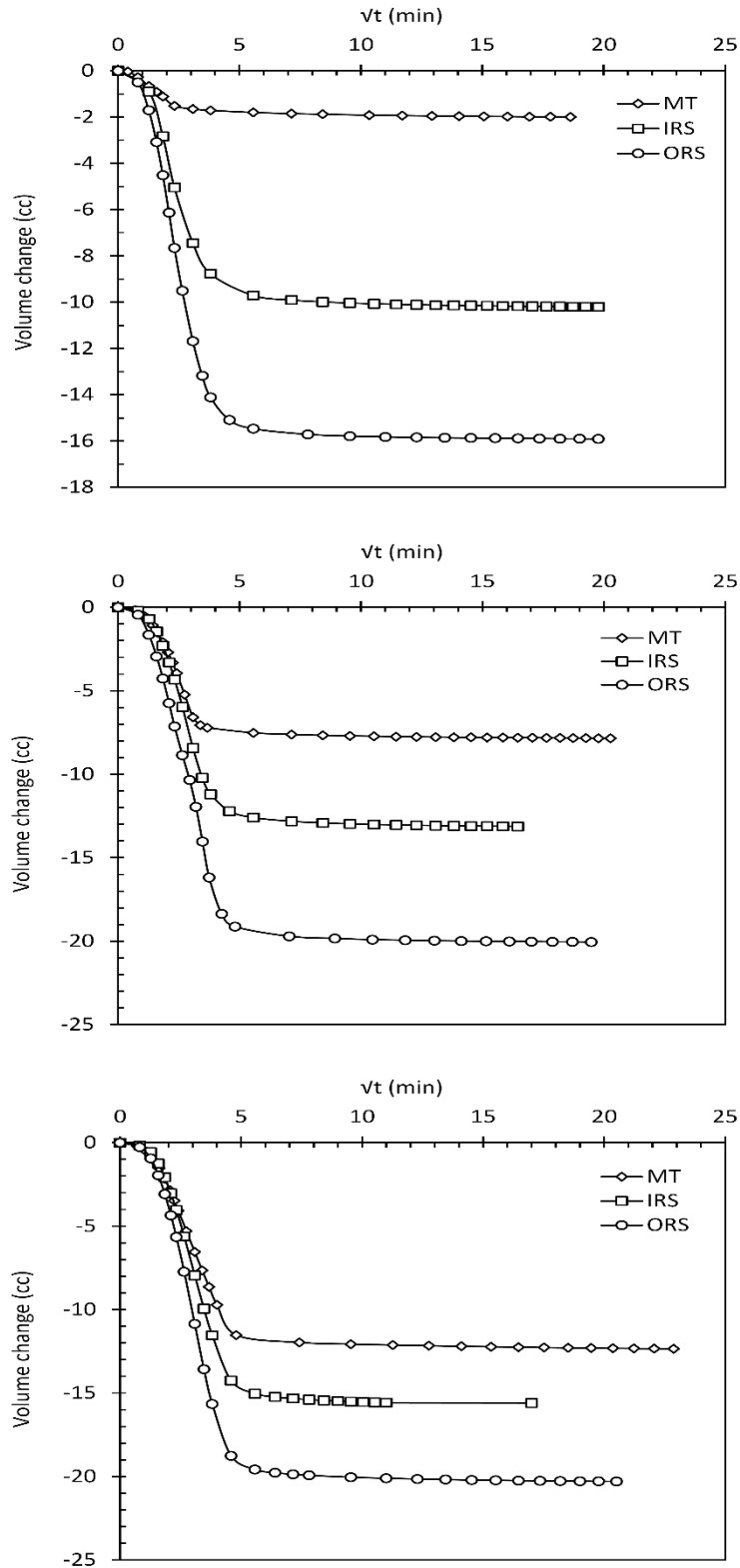
Figure 9.1 Comparison of volumetric behavior during consolidation at different
confining pressure. a) 100-kPa, b) 200-kPa c) 400-kPa

9.1.2 *Drained Stress-Strain Behavior*

Figure 9.2(a) to Figure 9.4(a) illustrate the variation of the deviatoric stress versus axial strain of IRS, ORS and MT for three confining pressures of 100, 200, and 400 kPa. MT specimens, for the whole range of the confining pressures, exhibit strain-hardening behavior (similar to normal consolidated soils) up to axial strain about 15% and then gradually flatted. However, specimens of IRS and ORS represent a smooth post-peak softening behavior.

The developed shear strength of the specimen prepared with MT technique is almost 20 to 25% less than the two other methods. For specimen prepared from IRS and ORS the difference in maximum shear strength (2 to 4%) is less tangible. It seems that ORS specimens attain the peak stress at lower strains, showing greater stiffness.

Figure 9.2(b) to Figure 9.4(b) show the variation of the volumetric strain versus axial strain. Inspection of the figures reveal a contractive behavior of the MT specimens for entire range of the confining pressure. However, both IRS and ORS indicate contraction behavior is followed by a slight dilation.

ORS specimens start to dilate at lower strains (i.e. axial strain of 8, 10, and 12% for confining stress of 100, 200 and 400 KPa respectively) compared to IRS specimens (10, 12, and 14% for confining stress of 100, 200 and 400 KPa respectively).
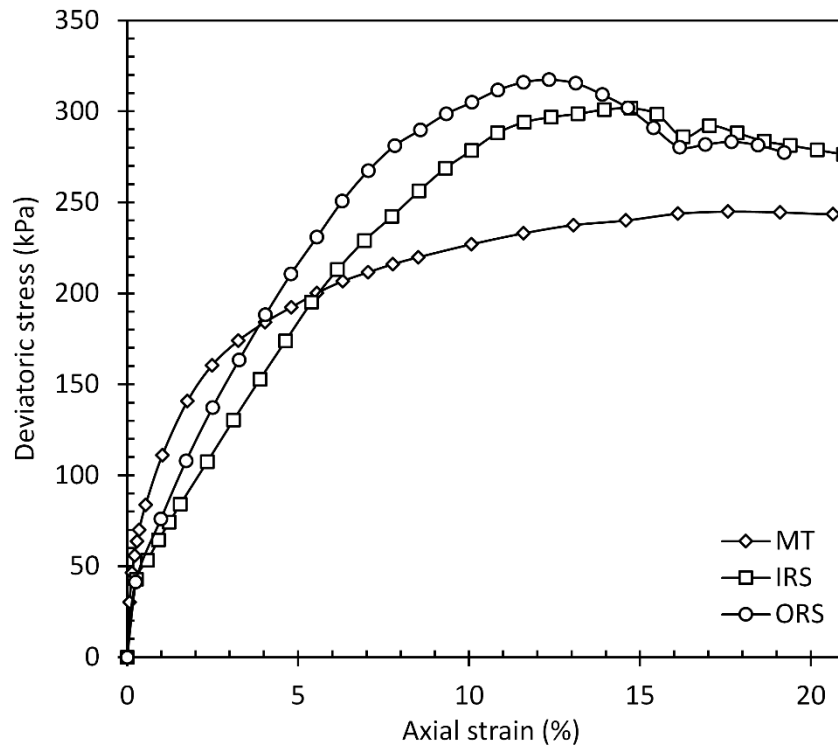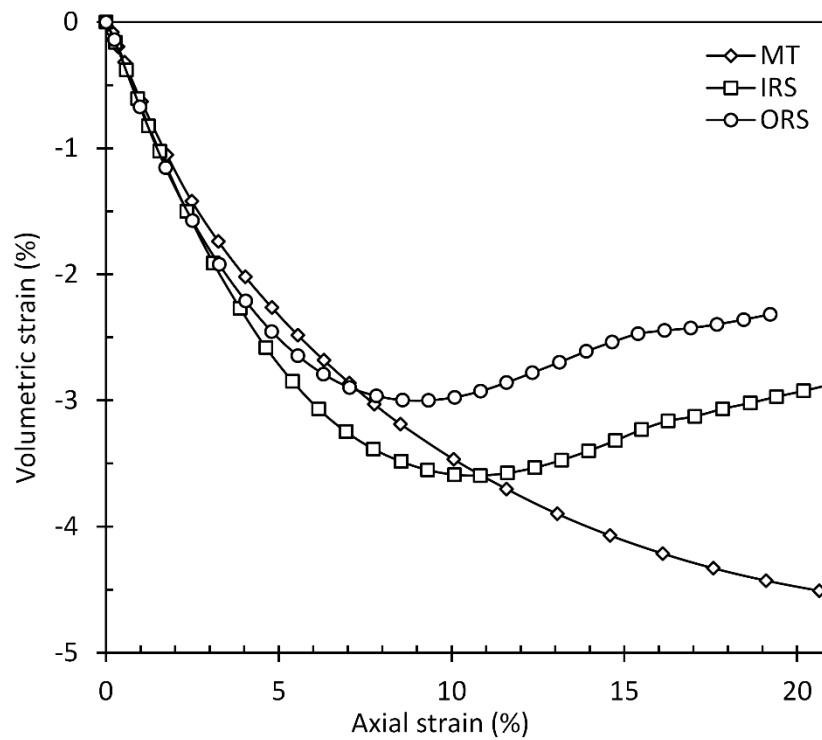
Figure 9.2 (a) Comparison of stress-strain response at 100-kPa confining pressure, (b) Comparison of volumetric change behavior at 100-kPa confining pressure.
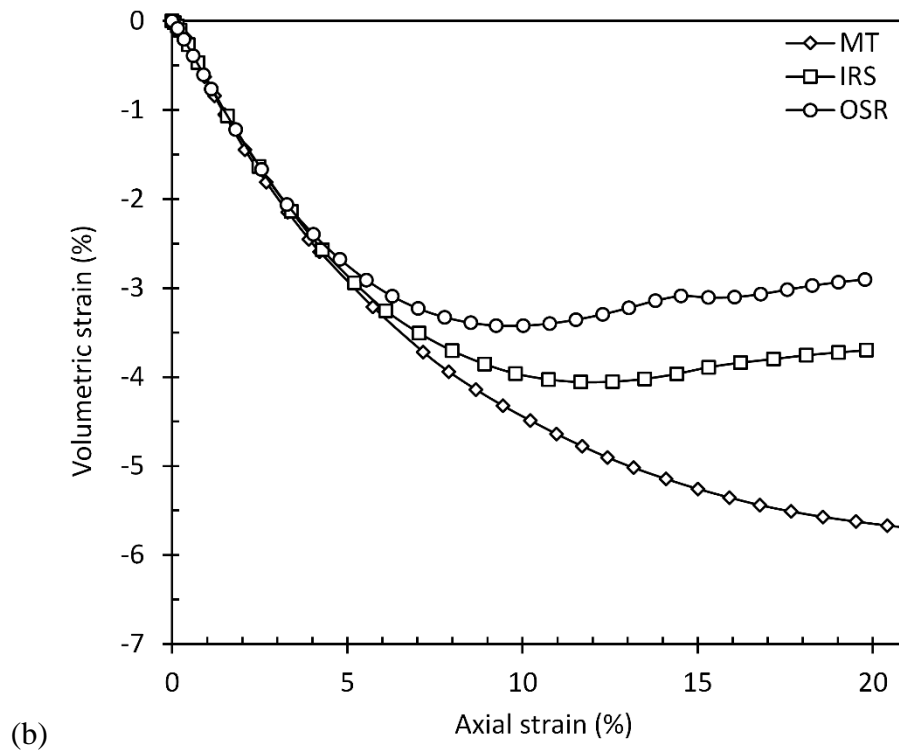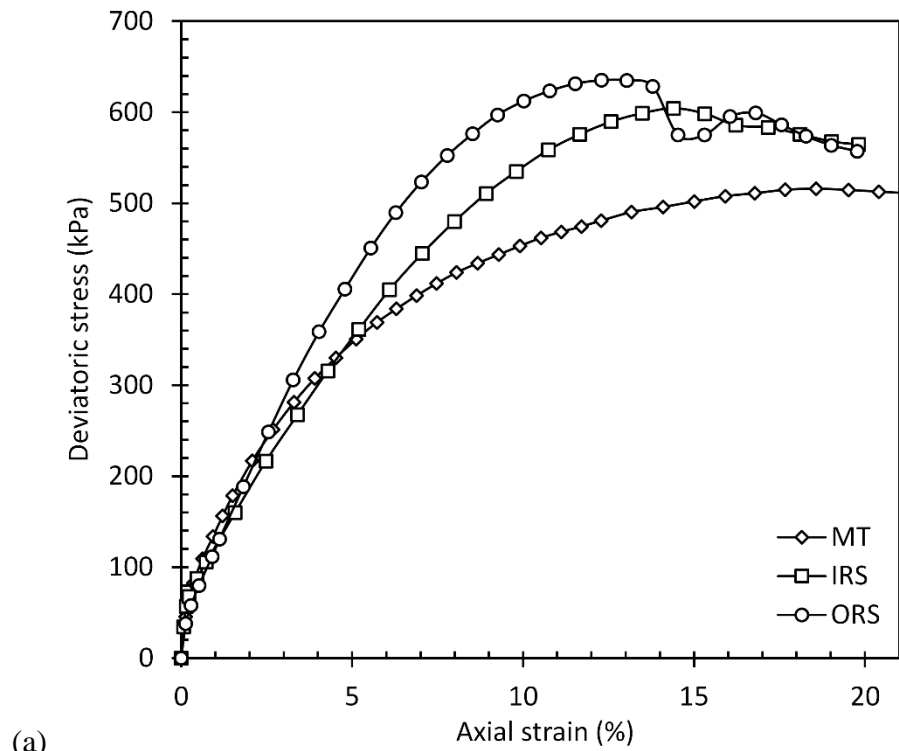
Figure 9.3 (a) comparison of stress-strain response at 200-kPa confining pressure, (b) comparison of volumetric change behavior at 200-kPa confining pressure.
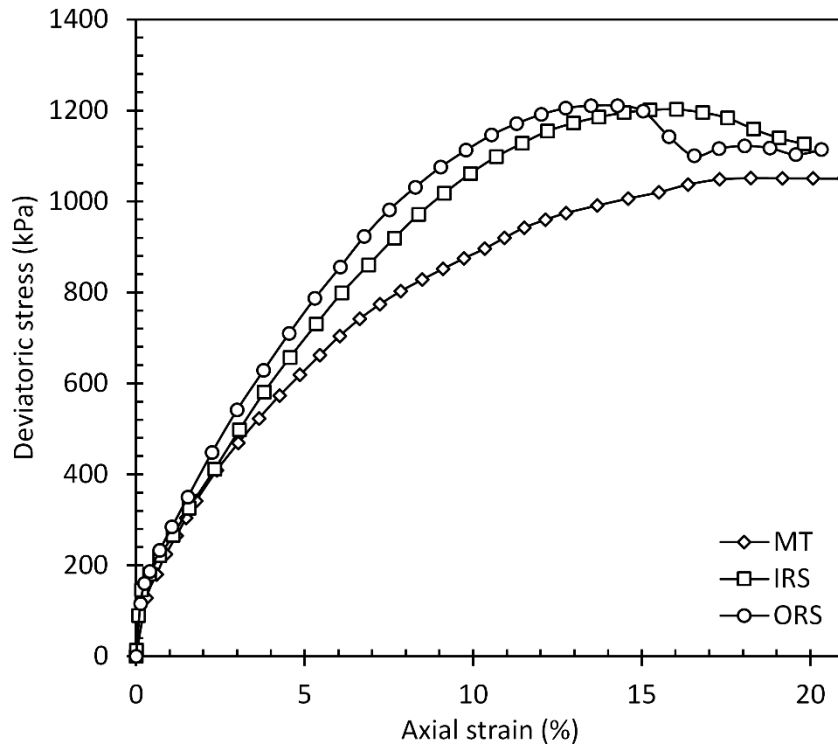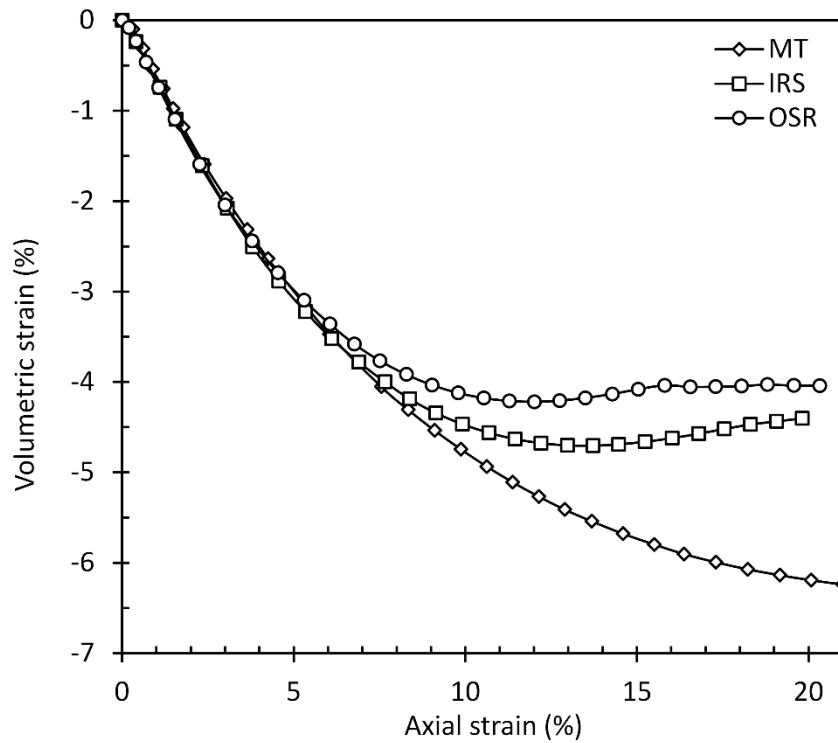
Figure 9.4(a) comparison of stress-strain response at 400-kPa confining pressure,
(b) comparison of volumetric change behavior at 400-kPa confining pressure.

238

9.2 Comparison of Soil-water characteristic curves (SWCC)

Figure 9.5 compares the SWCCs in drying and wetting paths on MT compacted and IRS specimens. It can be seen that there are apparent differences between the SWCCs. The AEV of IRS specimen is considerably larger than that of MT compacted specimen.

For a given suction, IRS specimen retains more water as compared with the MT compacted specimen. A hysteresis loop exists between the drying and wetting curves for two types of the specimen. However, the size of the hysteresis loop is larger in the case IRS specimens. In addition, despite the same starting point, the endpoints of the SWCCs in wetting front are different for both IRS and MT specimens. The difference (between the starting point and endpoint) becomes more pronounced for IRS specimen.

It should be noted that both IRS and MT specimen are prepared at the same void ratio but with different preparation procedure. Therefore, the different behavior may arise from the different structure. It has been demonstrated that compacted specimens with initial water content of less than optimum involve large pore space between clods of soils (double-structure) (Vanapalli et al. 1999). However, specimens dried from the slurry have a uniform pore-size distribution (Sheng et al. 2013). Therefore, large pore space in compacted specimens (ink bottle analogy) will be desaturated at lower suction values. Accordingly, the MT specimen has air-entry value lower than that of IRS specimen. The larger size of the hysteresis loop and the higher difference between the starting point and endpoint in IRS specimen are attributed to uniform pore-size distribution.
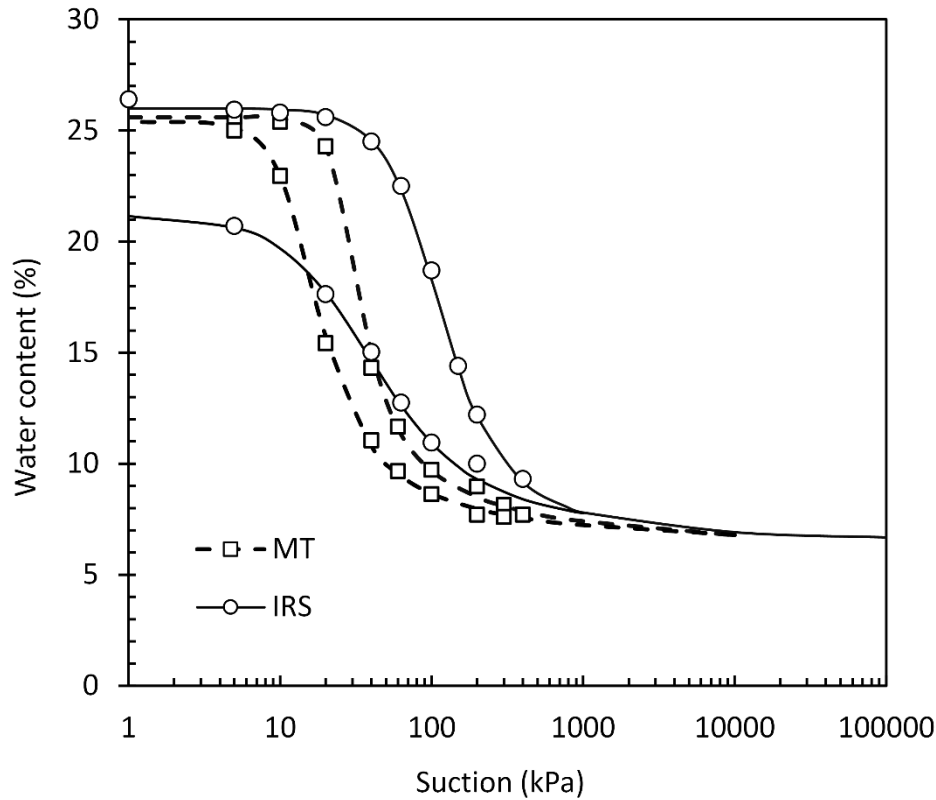
Figure 9.5 Comparison of SWCC of MT and IRS specimens.

9.3 Comparison of the loading collapse yield loci of the unsaturated soil with different preparation method and suction history

Figure 9.6 compares the LC yield loci, in the p-s plane, for MT compacted specimens and IRS specimens (in drying and wetting paths). It can be seen that the initial location of the LC locus (i.e. yield stress for saturated condition) in MT specimen is located at the right side of the IRS specimen. This can be attributed to the greater compaction pressure in MT specimen during preparation. The results show that the yield stresses in MT specimens increases nonlinearly at a decreasing rate up to 100 kPa and then approximately remain constant. However, the yield stresses in IRS specimens increases with a higher rate where the yield stress in 400-kPa suction is greater than that of MT specimen. Therefore, it can be said that the influence of suction on expanding LC yield locus in MT specimen is not as significant as that of IRS specimens.

240

Subsequent wetting causes plastic compression in the specimen and consequently shifts the LC yield locus to a new position shown in Figure 9.6. It can be seen that the yield stresses at different suctions in wetting path are higher than those in the drying path. Therefore, it can be concluded that the additional wetting results in further expansion of the loading collapse yield locus.
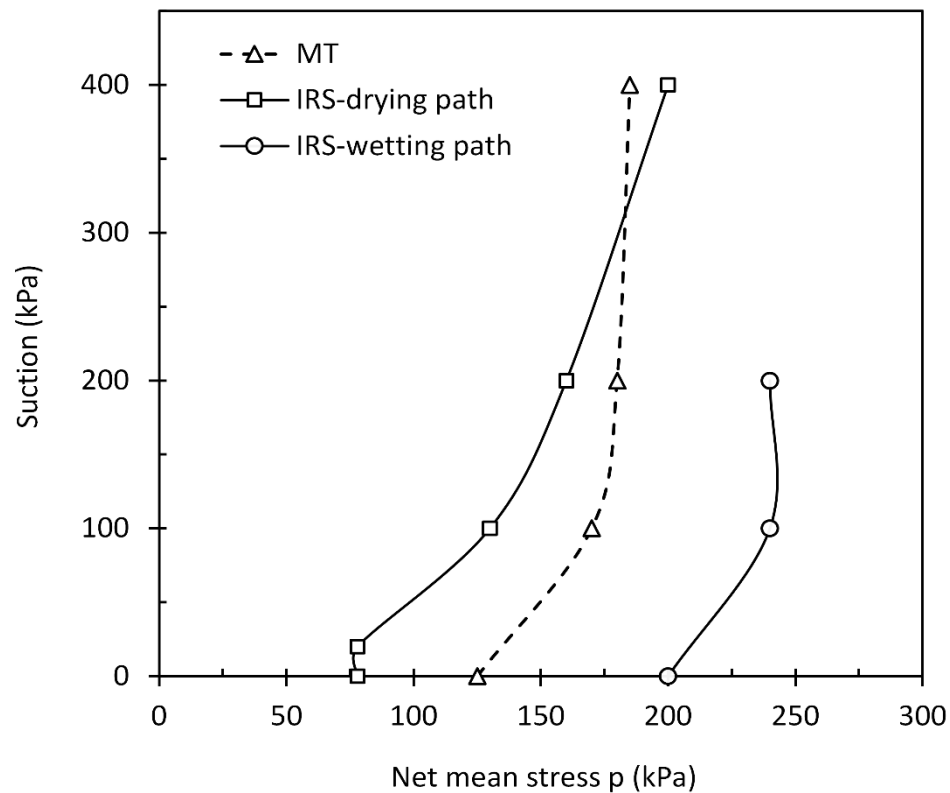
Figure 9.6 Comparison of the Loading–collapse (LC) yield loci for MT compacted specimens and IRS specimens (in drying and wetting paths).

9.4 Comparison of shear behavior of the unsaturated soil with different preparation method and suction history

The suction controlled triaxial test results of isotropically reconstituted specimens from slurry (IRS) compared to those of moist tamped compacted (MT) specimens subjected to the identical values of suction. It should be noted that in tests on IRS specimens, the same suction values were achieved with two different approaches (i.e. applying desired values of suction through drying path (IRS-D) or applying first a

400-kPa suction through drying path and then wetting to the desired suction (IRS-W).

The stress-strain and volumetric behavior of specimens is shown in Figure 9.7 to Figure 9.18. In the following, the effects of preparation method and suction history on shear strength, stiffens, total and water volume change are discussed.

9.4.1 *Maximum and critical state shear strength*

A comparison of the results reveals that IRS-D specimens (i.e. IRS through drying path) for suction values greater than zero have a higher maximum shear strength than those of IRS-W (i.e. IRS through wetting path) and MT specimens. For zero suction, IRS-W specimens exhibit higher shear strength than those of IRS-D and MT specimens. This can be explained by the fact that, specimens which are wetted to zero suction are not fully saturated (there are air pockets within the specimen that are not completely dissolved), and accordingly, represent higher shear strength. The difference (at zero suction) becomes less pronounced for greater net confining stress, where the stress-strain curve approximately coincides for net confining stress of 400 kPa.

In all cases, IRS-W and IRS-D exhibit strain-softening behavior that is more noticeable at greater suction and lower net confining stress. MT compacted specimens, exhibit an obvious strain-softening behavior at only net confining stress of 25 kPa, and in most of the cases represent approximately strain hardening behavior.

There are two likely causes for the hardening behavior of the MT specimens. Firstly, as presented in Chapter 8, MT compacted specimens, for the same void ratio, have greater preconsolidation pressure. Second, compacted specimens have bimodal pore size distribution (Sheng et al. 2013); therefore, during shearing specimens represent hardening behavior as the large pores tend to contract.

In all cases, IRS-W reaches a peak deviatoric stress at lower axial strain than those of IRS-D. For tests at greater suction and net mean stress, this becomes less pronounced. However, for net confining stress of 25 kPa MT specimens reach to peak deviatoric stress at lower axial strain than those of IRS-D and IRS-W.

Inspection of the figures for IRS-D and IRS-W reveals that regardless of the suction history, specimens beyond the peak value tend to approach to critical state values at large strains. However, it seems that, MT compacted specimens, for non-zero suctions values, do not converge to the same critical state (under a same suction and net confining stress) of IRS-D and IRS-W specimens.

9.4.2 Stiffness

The results indicate that, for lower values of the suctions, IRS-W and MT specimens have approximately the same stiffness greater than that for IRS-D. For the greater suction values this becomes less pronounced, so that the stiffness of the IRS-D becomes greater for suction of 400 kPa and at net confining stress of 25 kPa.

These behaviors can be explained by the fact that, the initial suction in MT specimens (after compaction) is 400 kPa; therefore, a wetting path similar to those of IRS-W is followed to achieve suction values of the zero, 100 and 200 kPa.

9.4.3 Volumetric behavior with respect to total volume and water volume

For zero suction and net confining stress of 25 kPa, both IRS-D and MT specimens represent a contractive behavior. However, IRS-W specimens, from the beginning of the test exhibit a marked dilative behavior. The behavior of the IRS-W change from dilative to contractive behavior for higher net confining stress. Change in volume of the water (for all) is consistent with total volume change (i.e. water drains out for contractive behavior and flows into the specimen for dilative behavior).

It can be seen from the figures that the dilatancy increases for greater values of suction and decreases for grater values of net confining stress. For the entire range of the suction (used in this study), generally, the dilative behavior is more pronounced for IRS-W compared to those in IRS-D and MT specimens.

For the entire range of the suction, for IRS-D water drains out of the specimens.

Interestingly, similar to stiffness, IRS-W and MT specimens represent approximately similar behavior with respect to total and water volume change.
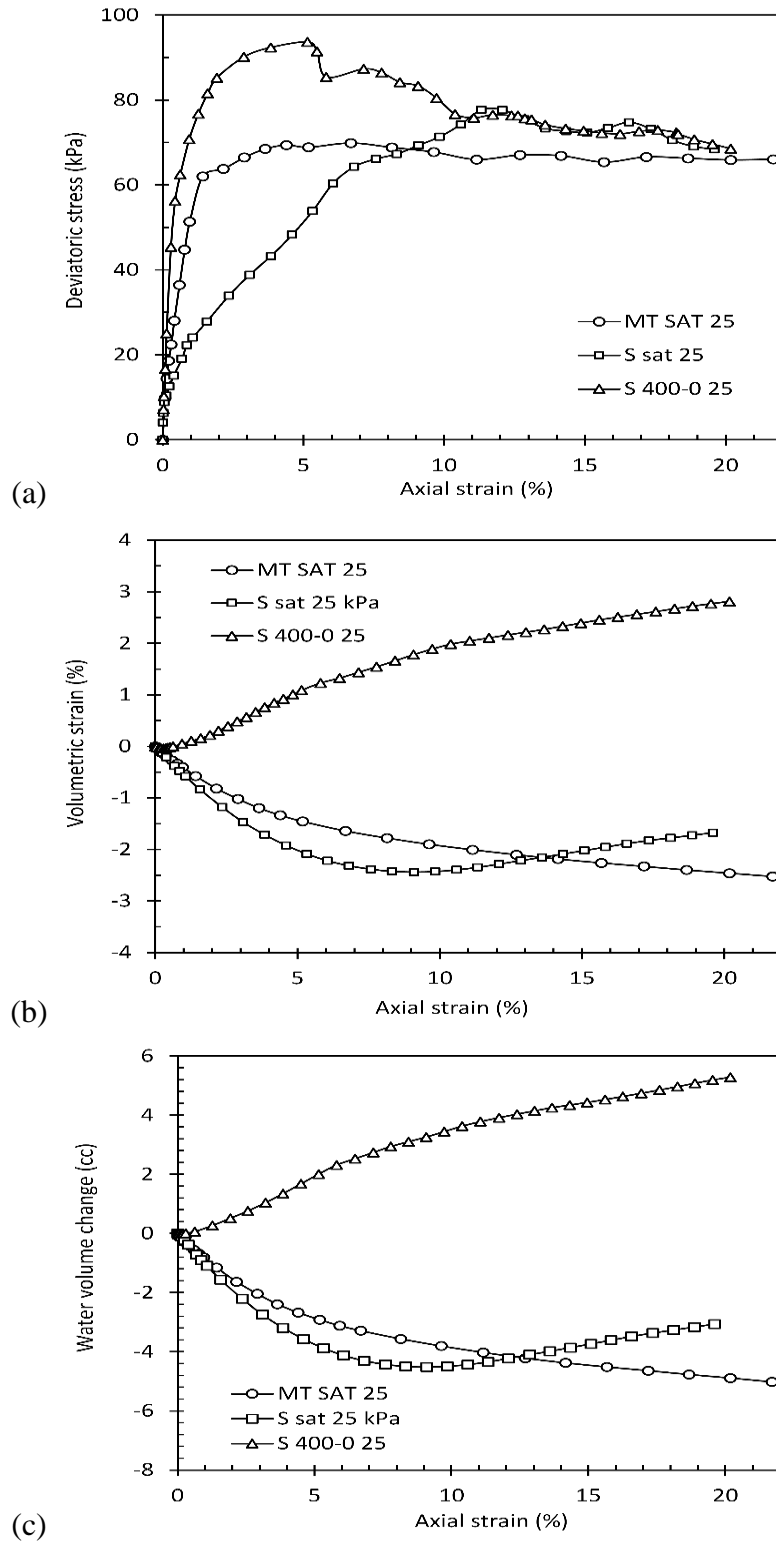
Figure 9.7 Variations of (a) deviatoric stress, (b) volumetric strain and (c) change
in volume of water during shearing at s = 0 and $(\sigma_3 - u_a)$ = 25 kPa.
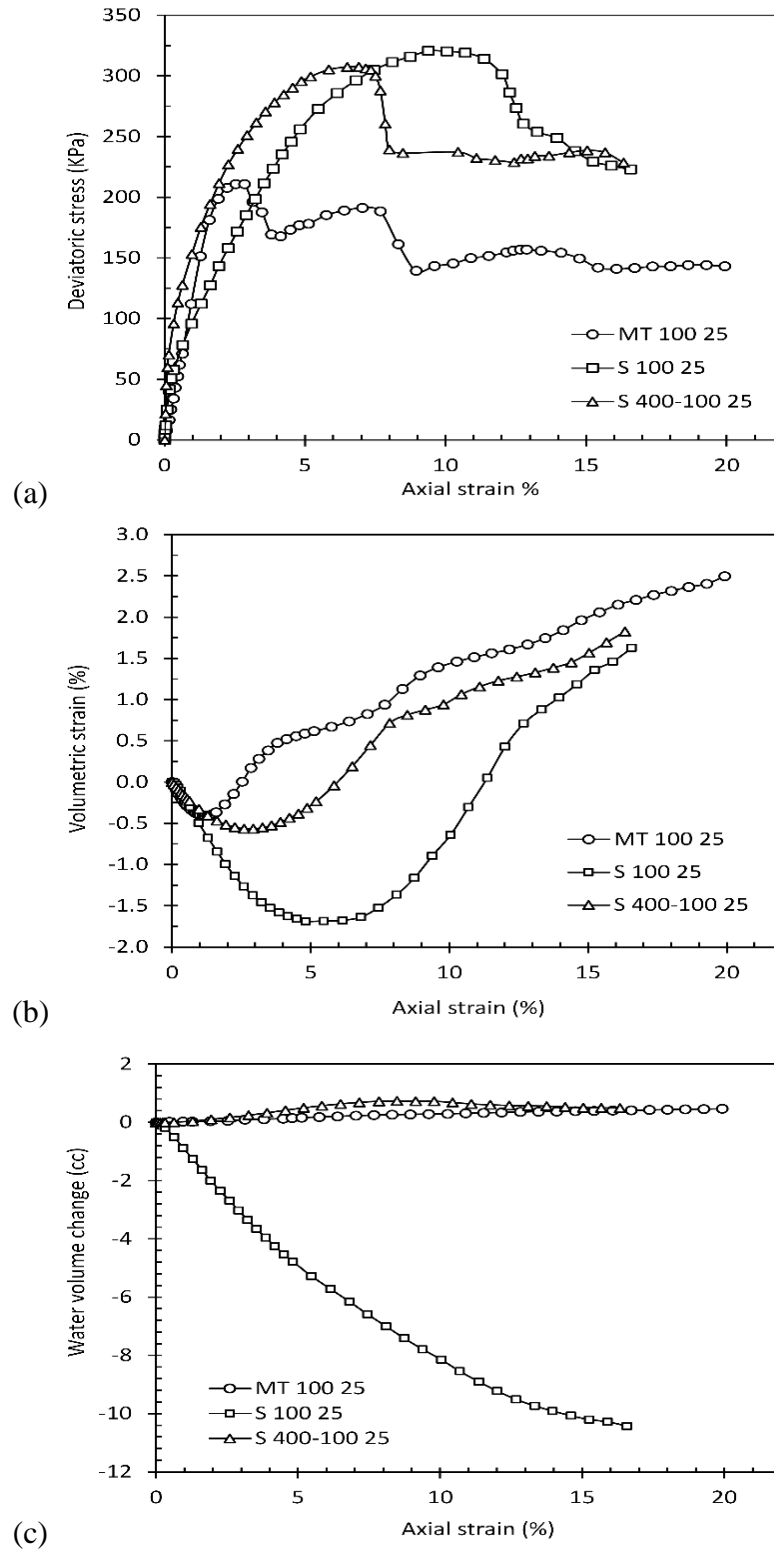
Figure 9.8 Variations of (a) deviatoric stress, (b) volumetric strain and (c) change in volume of water during shearing at s = 100 and (σ_3-u_a) = 25 kPa.

245

(a)

(b)

(c)
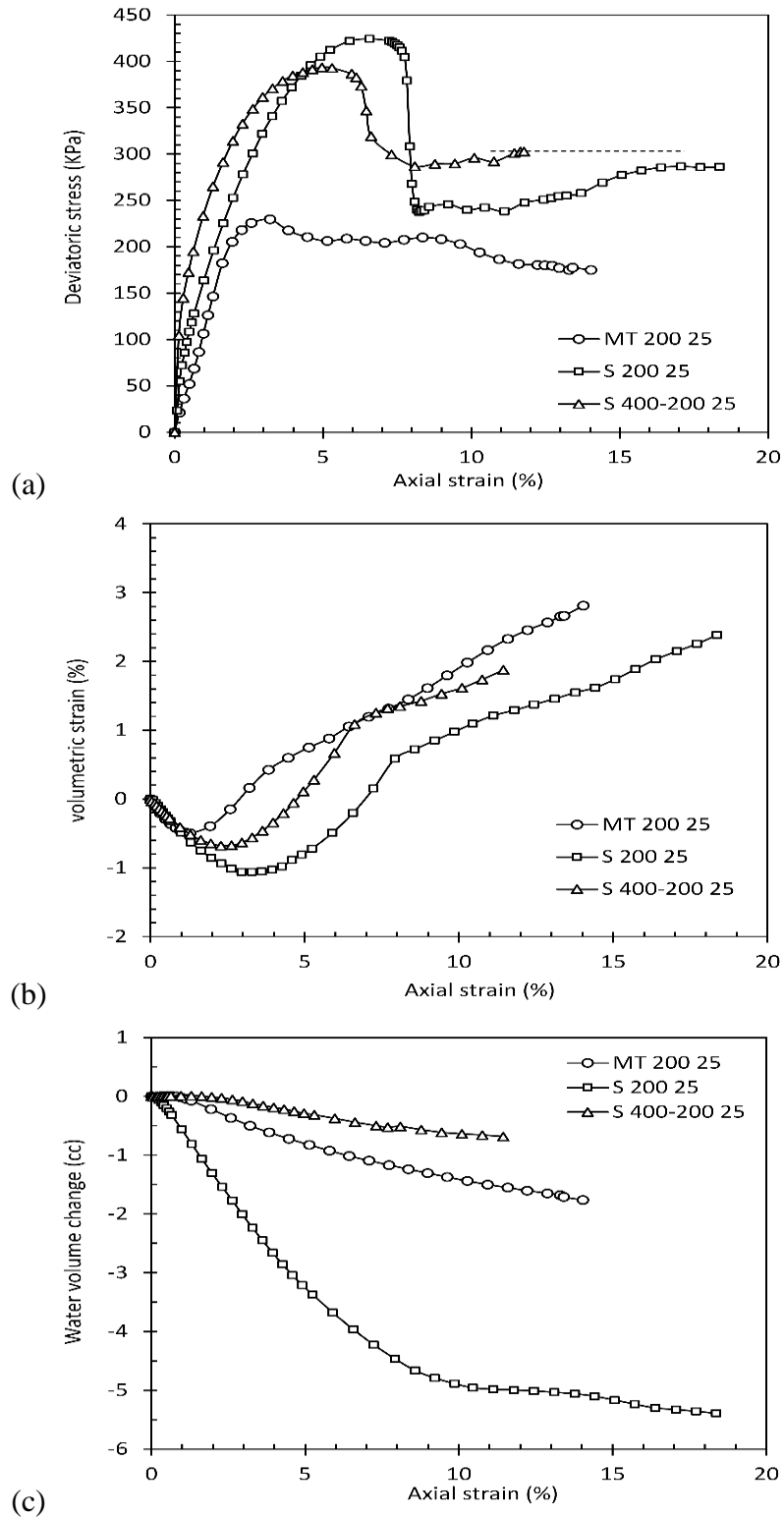
Figure 9.9 Variations of (a) deviatoric stress, (b) volumetric strain and (c) change in volume of water during shearing at s = 200 and $(\sigma_3 - u_a) = 25$ kPa.

246

(a)

(b)

(c)
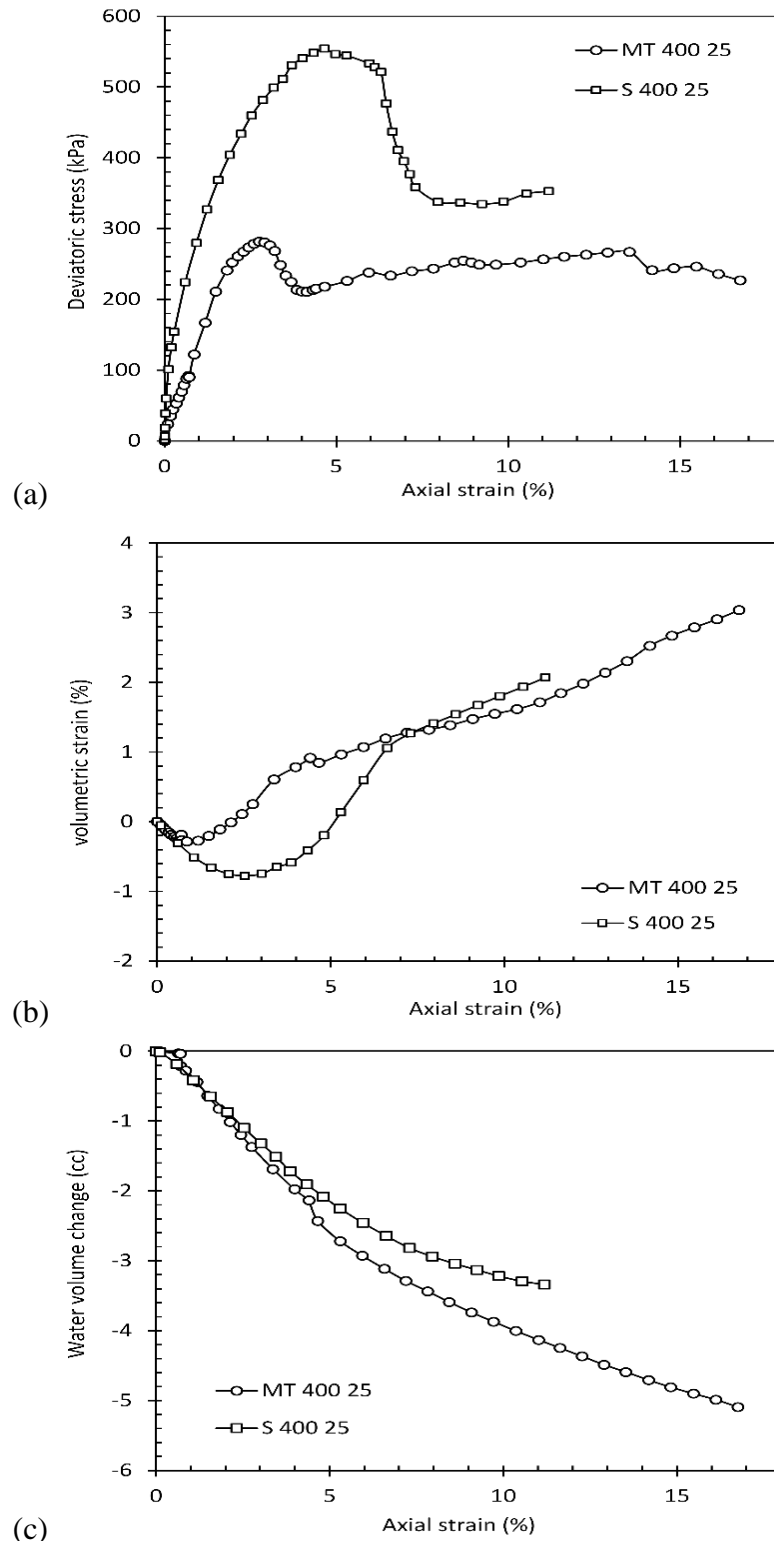
Figure 9.10 Variations of (a) deviatoric stress, (b) volumetric strain and (c) change in volume of water during shearing at s = 400 and $(\sigma_3 - u_a)$ = 25 kPa.
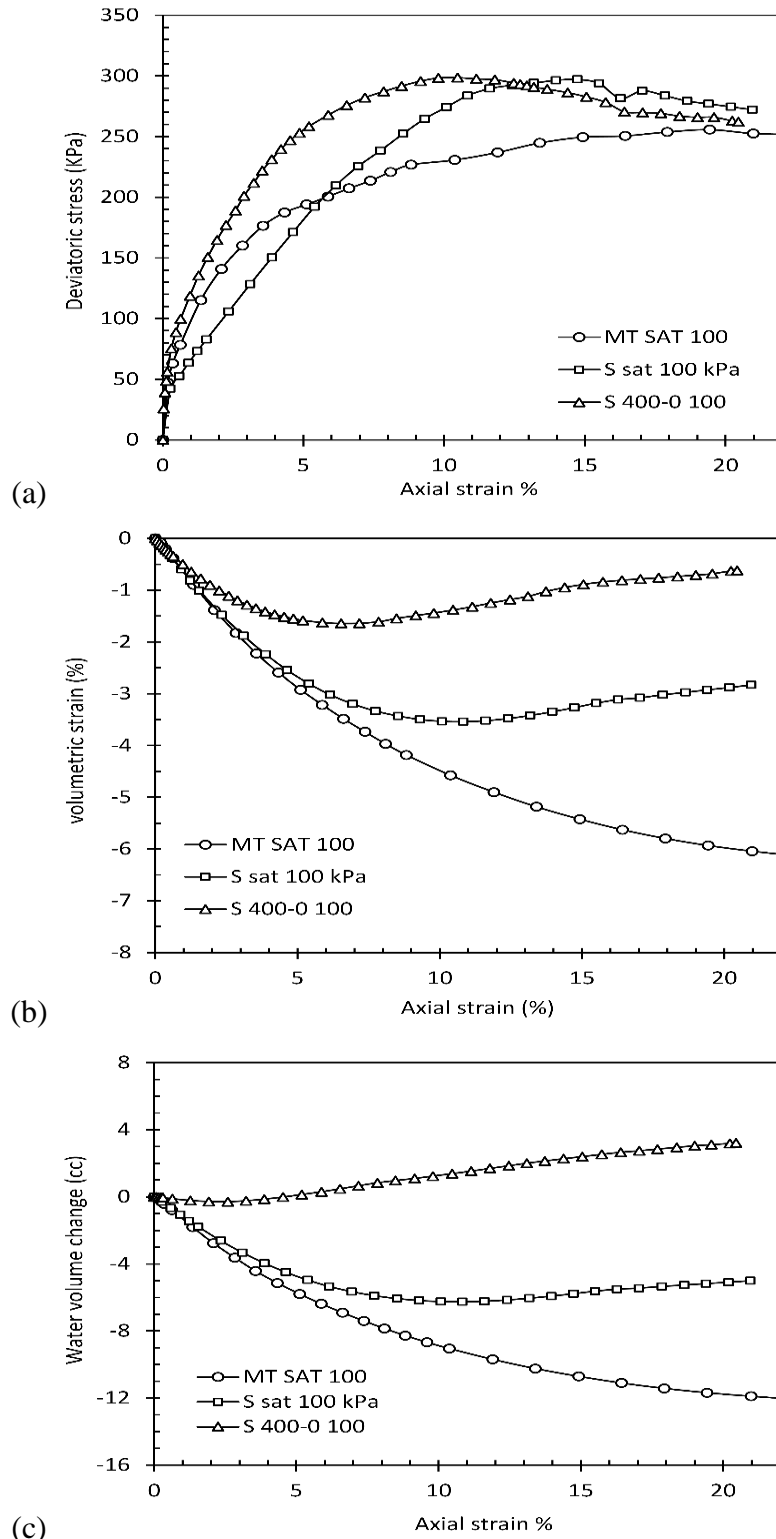
Figure 9.11 Variations of (a) deviatoric stress, (b) volumetric strain and (c) change in volume of water during shearing at s = 0 and $(\sigma_3 - u_a) = 100$ kPa.

(a)

(b)

(c)
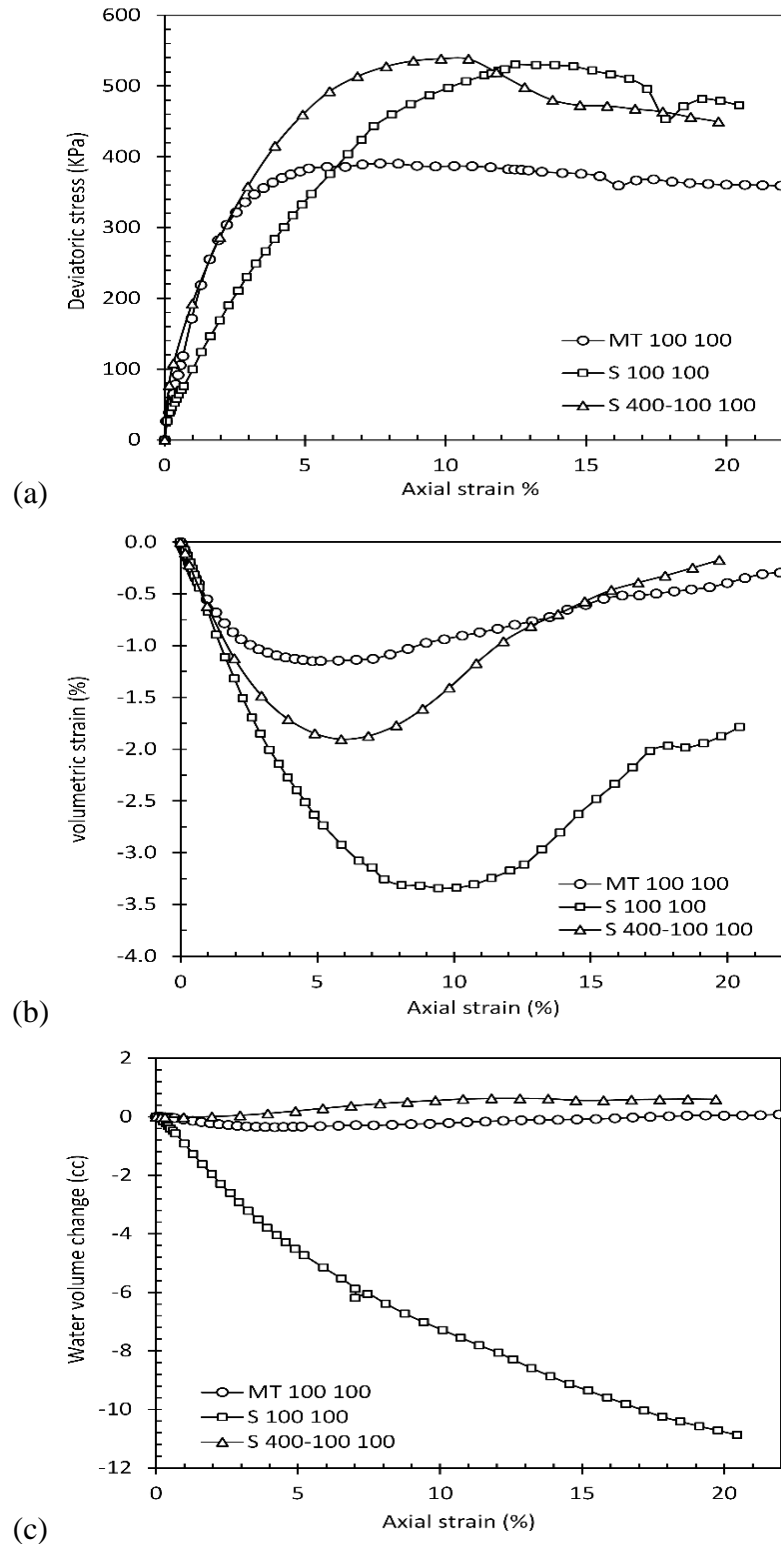
Figure 9.12 Variations of (a) deviatoric stress, (b) volumetric strain and (c) change in volume of water during shearing at s = 100 and (σ_3-u_a) = 100 kPa.
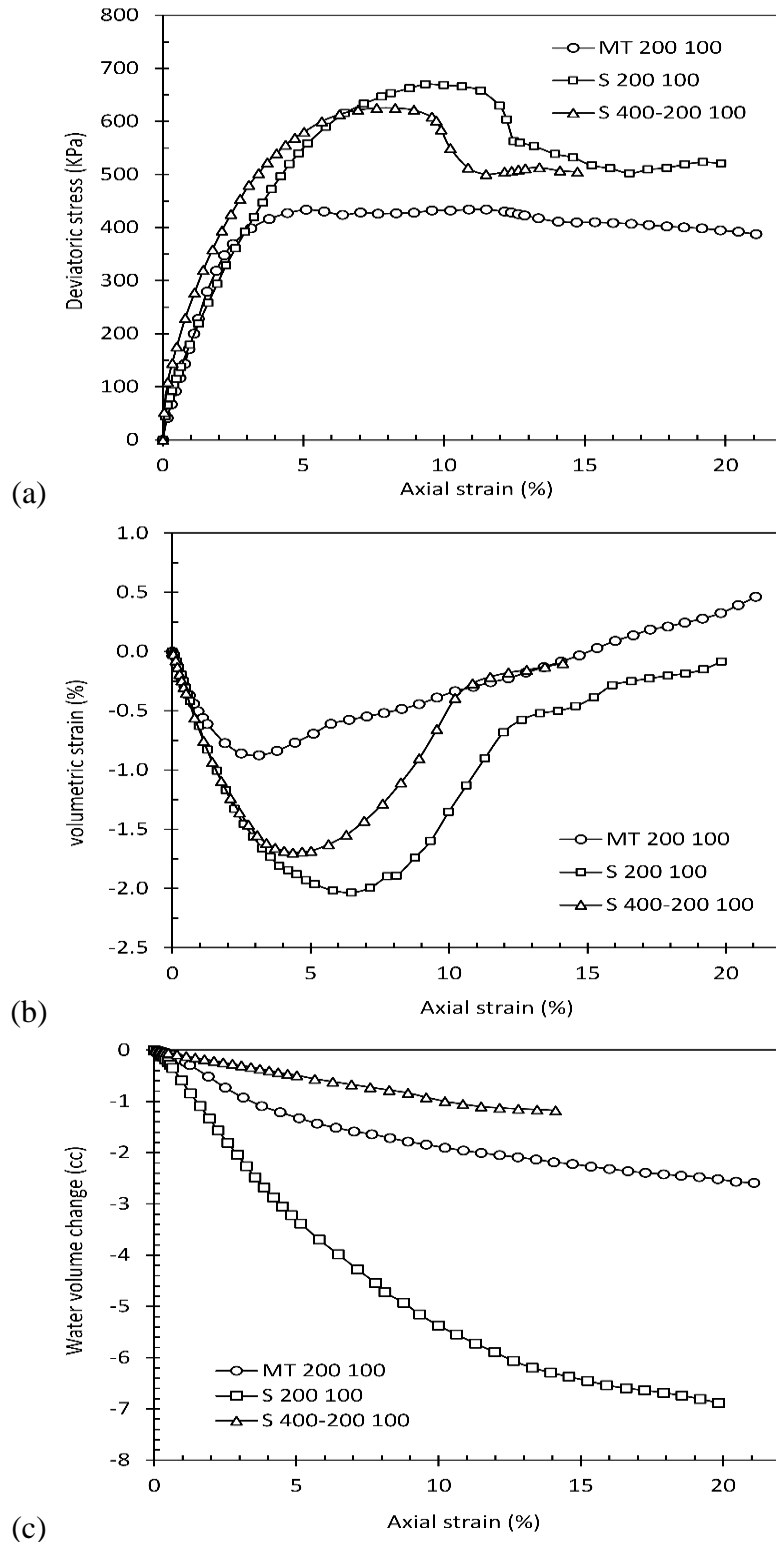
Figure 9.13 Variations of (a) deviatoric stress, (b) volumetric strain and (c) change in volume of water during shearing at s = 200 and $(\sigma_3 - u_a) = 100$ kPa.

(a)

(b)

(c)
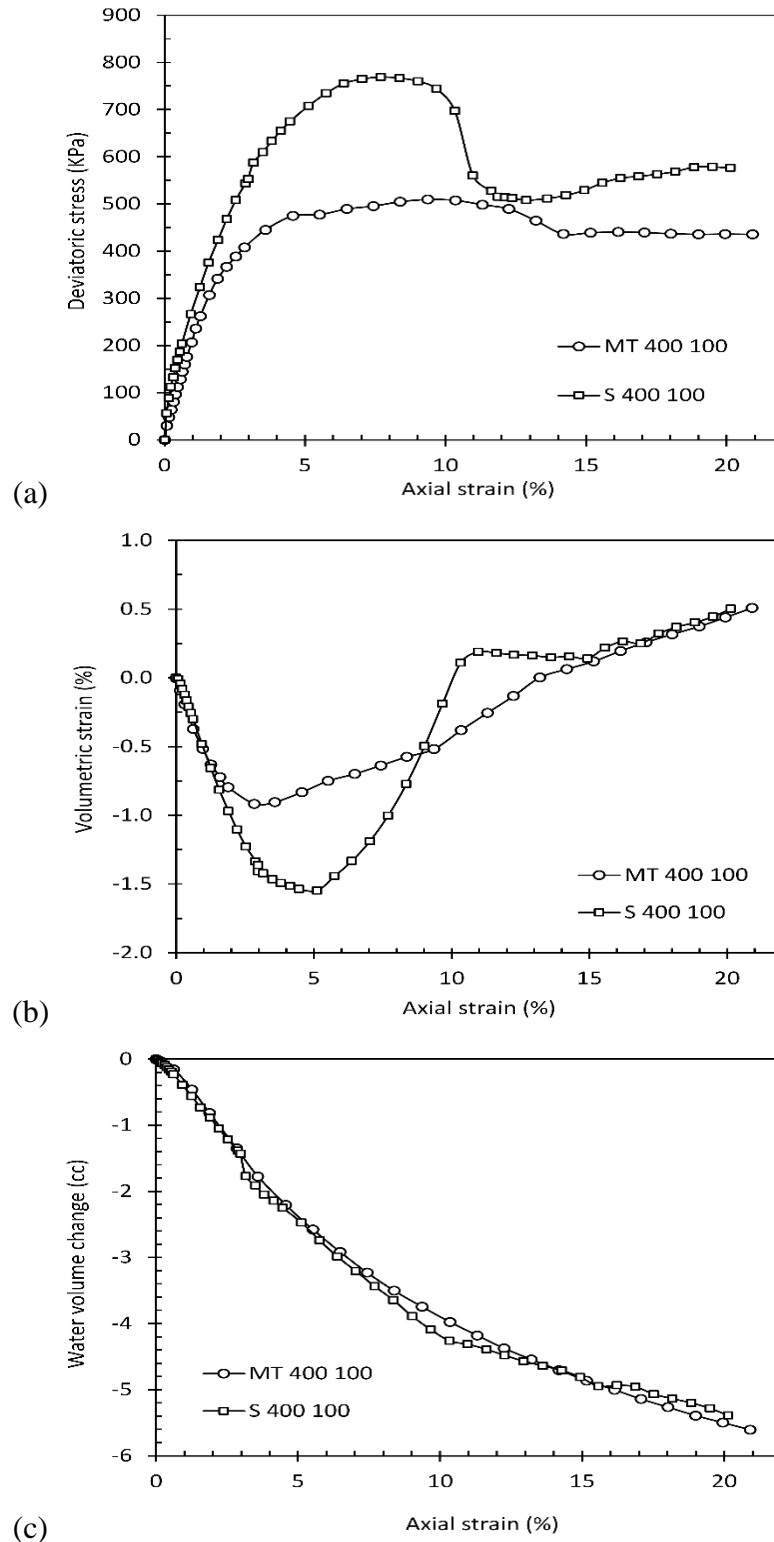
Figure 9.14 Variations of (a) deviatoric stress, (b) volumetric strain and (c) change in volume of water during shearing at s = 400 and (σ_3-u_a) = 100 kPa.

251
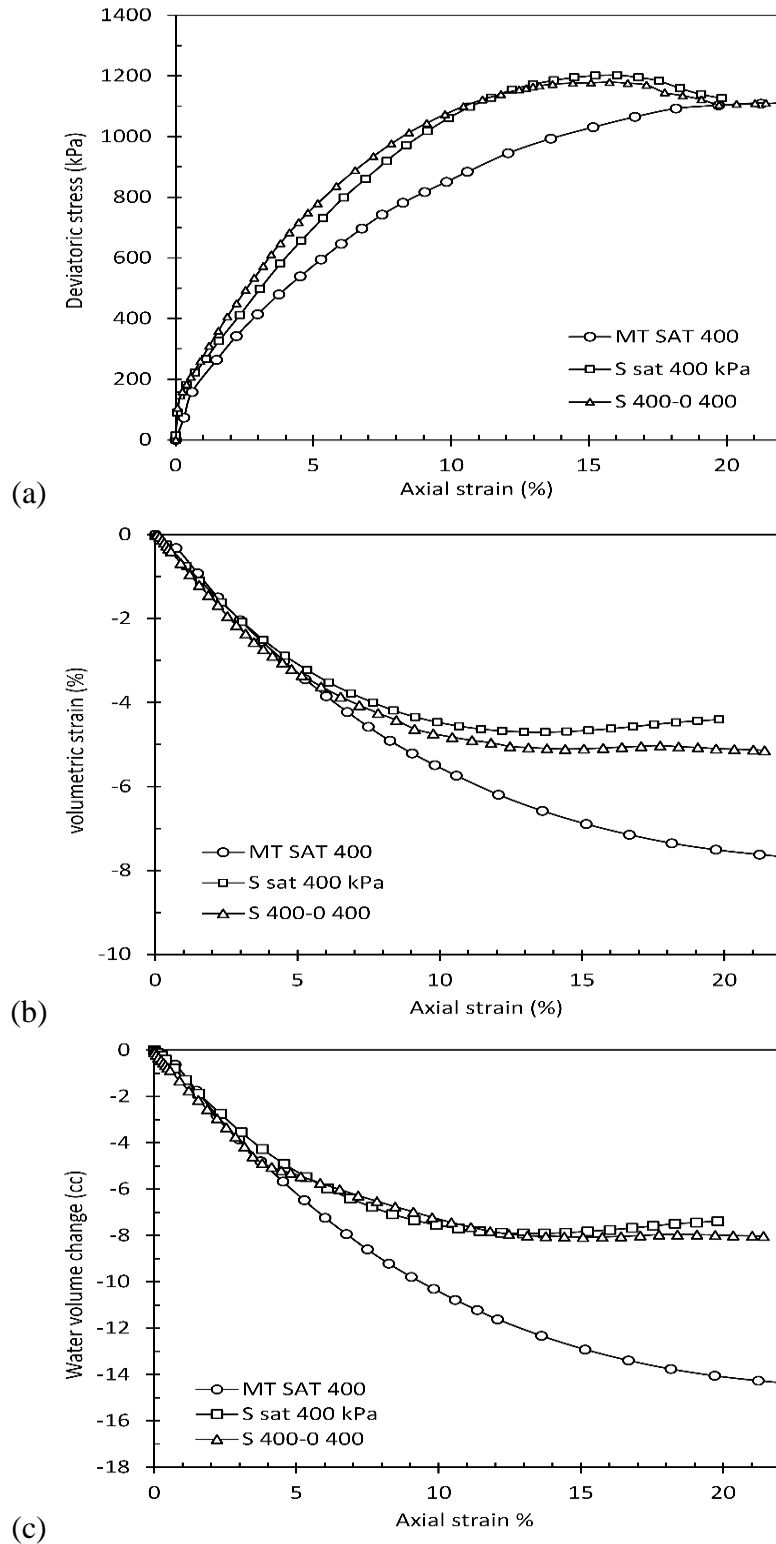
Figure 9.15 Variations of (a) deviatoric stress, (b) volumetric strain and (c) change in volume of water during shearing at s = 0 and (σ_3-u_a) = 400 kPa.

(a)

(b)

(c)
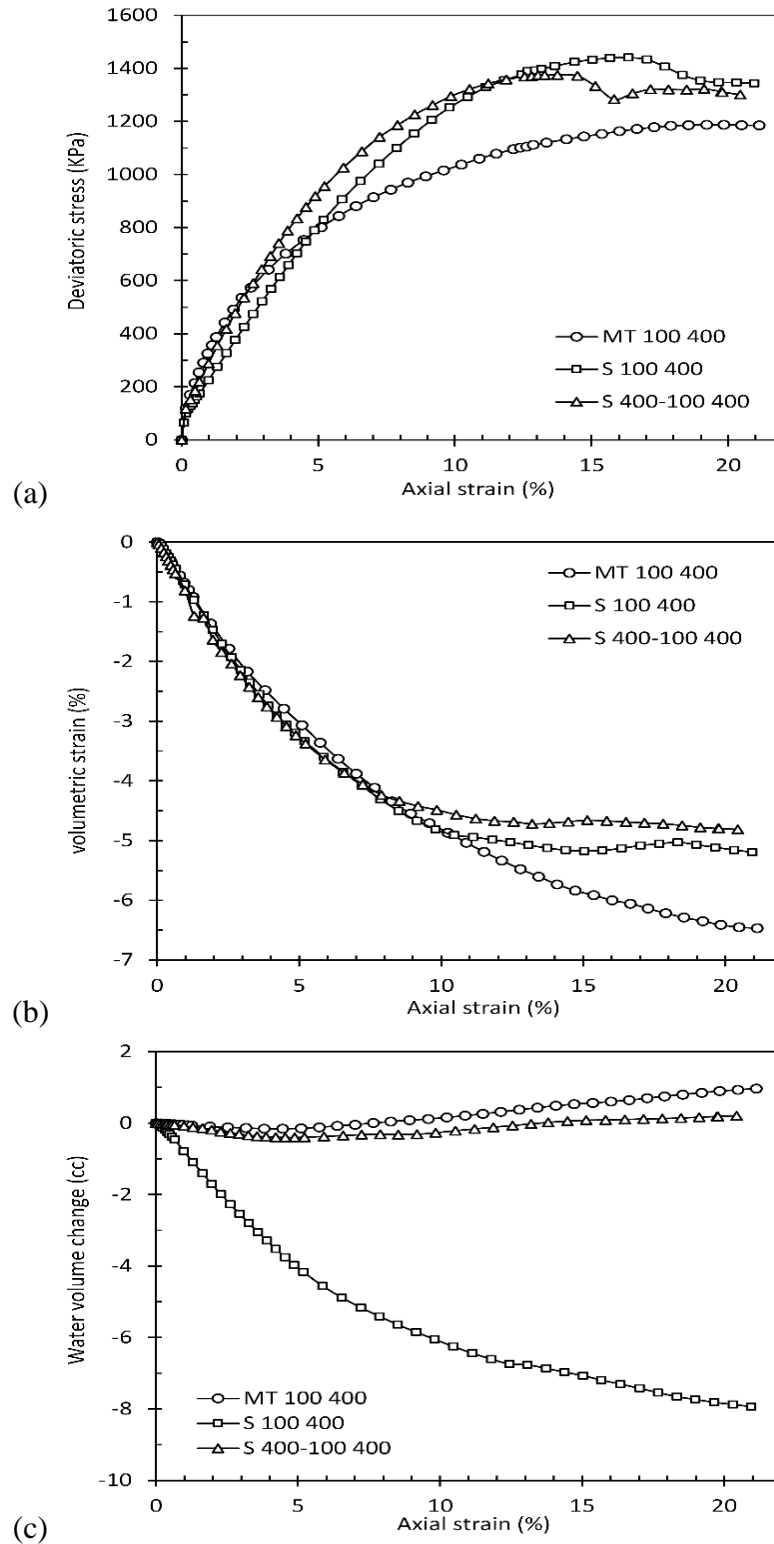
Figure 9.16 Variations of (a) deviatoric stress, (b) volumetric strain and (c) change in volume of water during shearing at s = 100 and (σ_3-u_a) = 400 kPa.

(a)

(b)

(c)
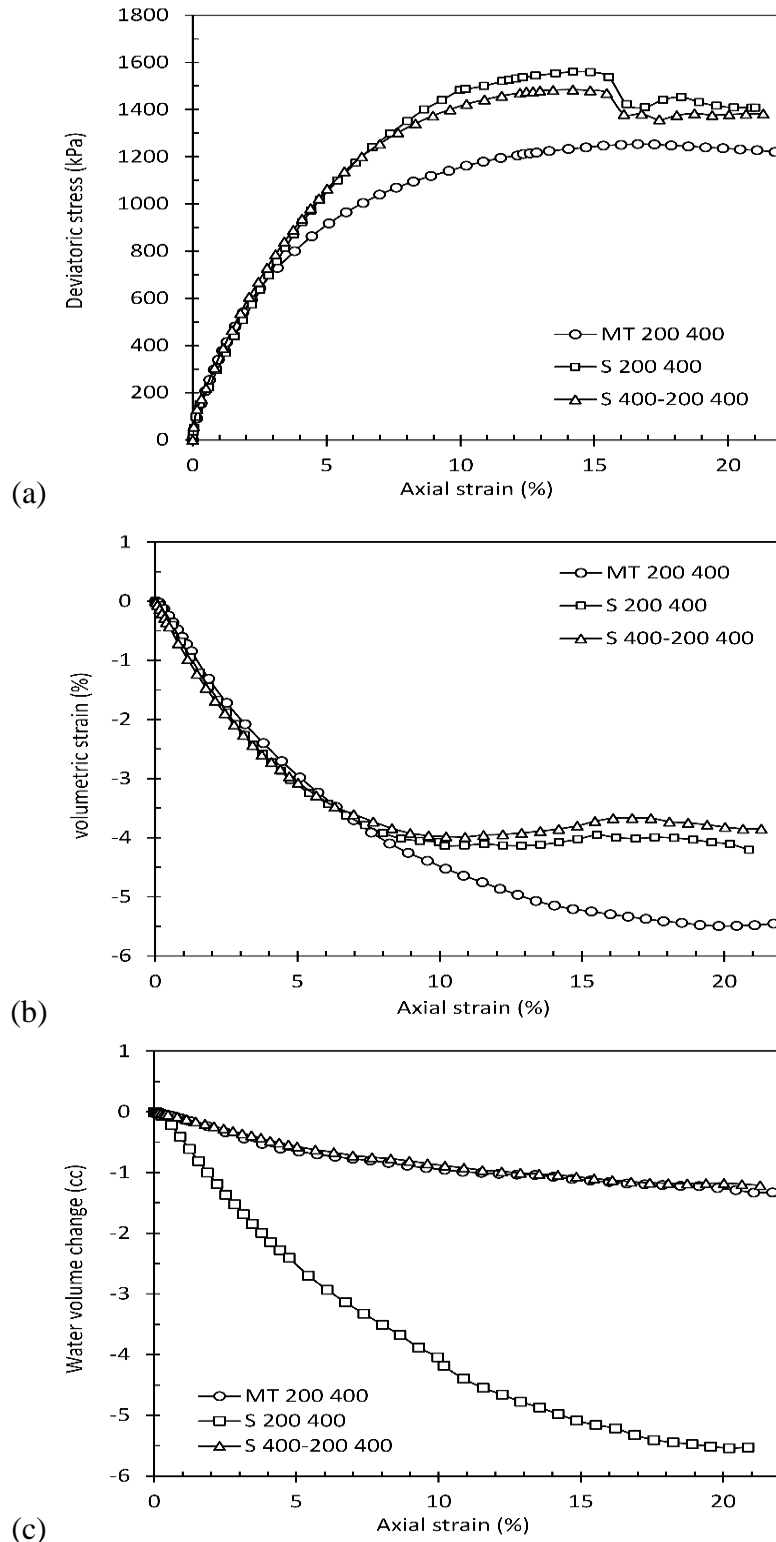
Figure 9.17 Variations of (a) deviatoric stress, (b) volumetric strain and (c) change in volume of water during shearing at s = 200 and $(\sigma_3 - u_a) = 400$ kPa.

254
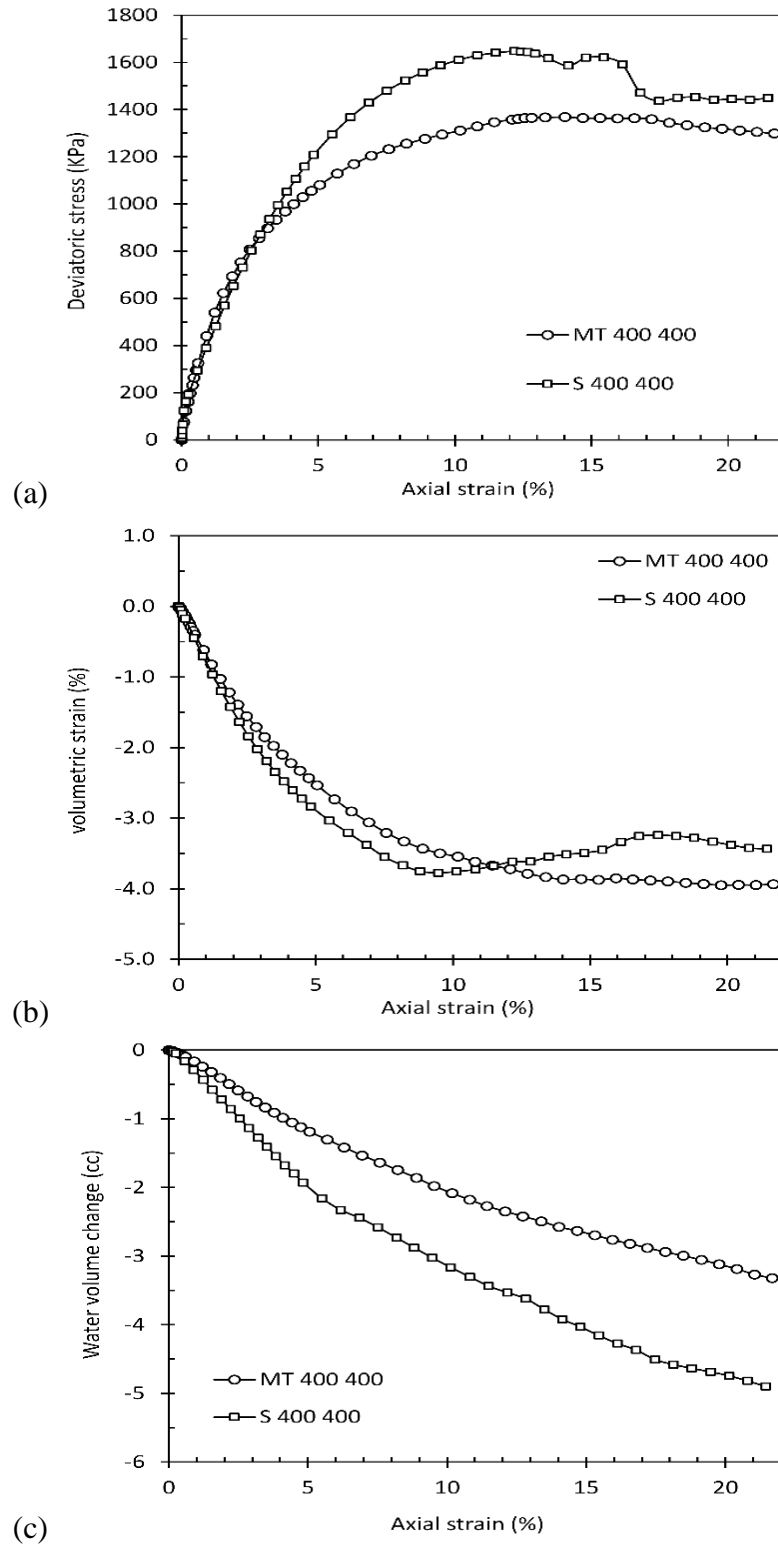
Figure 9.18 Variations of (a) deviatoric stress, (b) volumetric strain and (c) change in volume of water during shearing at s = 400 and (σ_3-u_a) = 400 kPa.

255

9.5   Comparison of Yield Surface of the unsaturated soil with different preparation method and suction history

Yield locus in q-p plane for each suction value were determined for both MT compacted specimens and IRS, from saturated and unsaturated triaxial tests results (Chapter 8). For MT compacted specimens, inclined semi-elliptical yield curves were fitted to each series of constant suction yield points (Figure 8.35). The inclination of the yield locus can be attributed to inherent anisotropic nature of the one-dimensionally compacted specimens. The yield locus appears to be symmetric about K0 =0.45 line for all series. A constant inclination line reveals the independency of the soil anisotropy from suction, which is consistent with Cui and Delage (1996). For IRS specimens, an elliptical yield surface with the axis of net mean stress as the major axis were fitted successfully to yield points (Figure 8.65). This is in agreement with modified Cam-Clay model and BBM for both saturated and unsaturated condition. For both MT and IRS, it was shown that, the size of the yield locus is suction dependent and expands as the suction increases. This observation is consistent with hardening effect of the suction as included in BBM by Alonso et al. (1990).

For a given suction, MT specimens have a larger yield locus compared to IRS specimens. The higher yield stress in MT specimen can be attributed to the pre-compression due to compaction.

Figure 9.19 and Figure 9.20 compare the yield loci, in the q - p plane, for a given suction with different suction history (i.e. drying or drying-wetting).

It is apparent that during drying-wetting the shape (elliptical) and the center of the yield loci remain unchanged (independent of suction history). However, the size of the yield locus changes with suction history, where specimens with drying-wetting have larger yield locus.
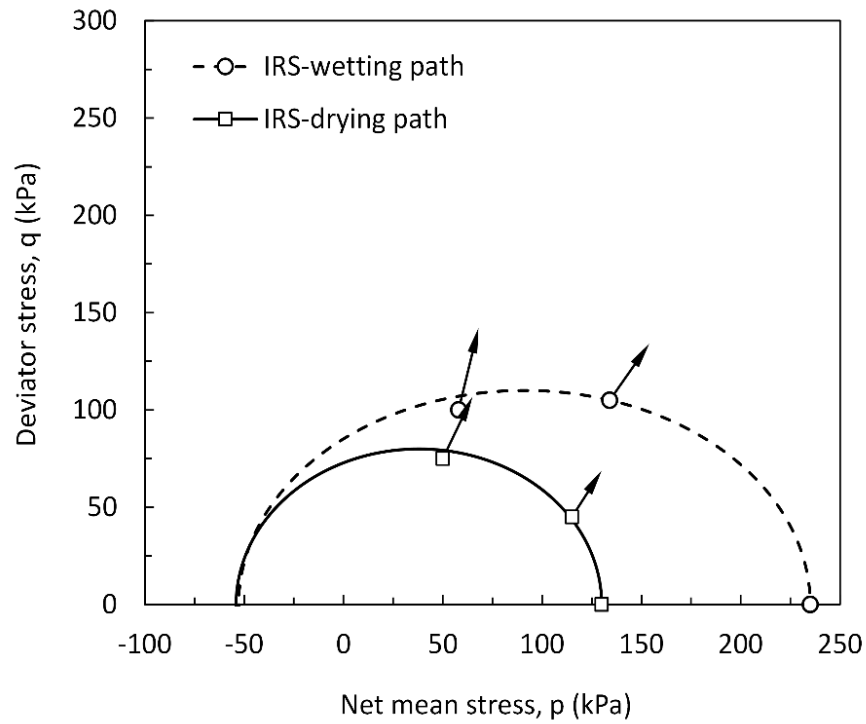
Figure 9.19 Effects of suction history on the yield locus of specimens at suction of 100 kPa.
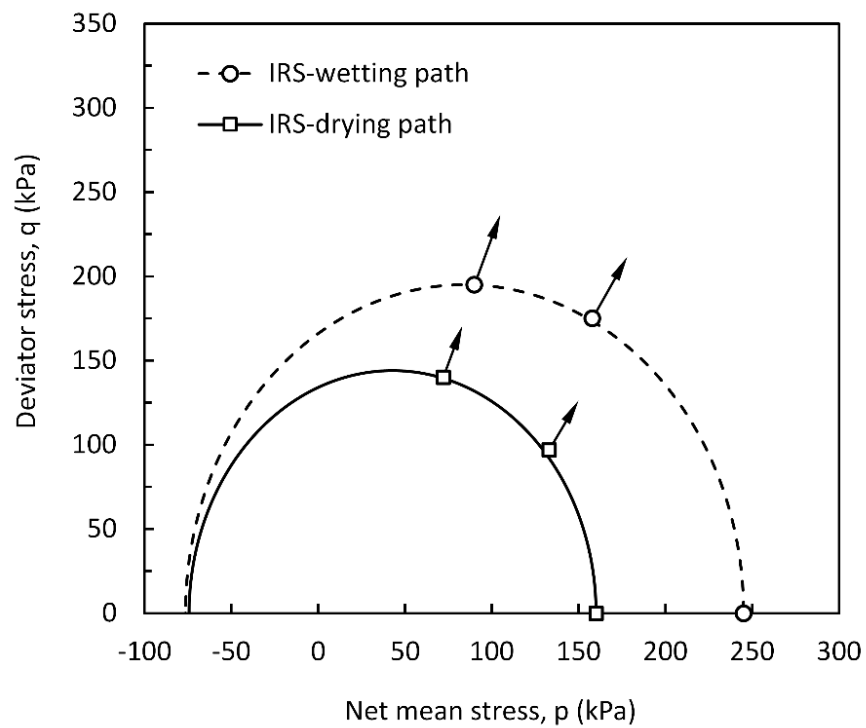
Figure 9.20 Effects of suction history on the yield locus of specimens at suction of 200 kPa.

257

9.6 Evaluation of the Proposed Shear Strength Equations

The performance of the proposed equation (presented in chapter 3) was investigated through laboratory tests conducted on IRS-D and results of five other published studies. In addition, shear strengths were compared between proposed method and the other selected equations (summarized in Table 3.1).

The equation is evaluated using three statistical criteria. The first criterion is the Nash-Sutcliffe efficiency (NSE) (Nash & Sutcliffe, 1970). This criterion reveals the effectiveness of the measured versus predicted curve to the 1:1 line. NSE varies from $-\infty$ to 1.0 with the value of 1 revealing the best prediction:

$$\text{NSE} = 1 - \left[\frac{\sum_{i=1}^{n}(E_i - P_i)^2}{\sum_{i=1}^{n}(E_i - \bar{E})^2}\right] \tag{9.1}$$

Where E_i is the experimental measurement of the ith data, P_i is the predicted value of the ith of data and $\bar{E}$ is the mean of the experimental measurements. NSE does not measure the tendency of the prediction regarding under-or overestimation. For this, the Percent Bias (PBIAS) criterion selected to measure the average tendency of the predicted values (under-or overestimating) against experimental measurement. Positive values of PBIAS express an underestimation tendency, and negative values reveal an overestimation tendency of the predictions. The optimum value is zero indicating a good prediction.

$$\text{PBAIS} = \left[\frac{\sum_{i=1}^{n}(E_i - P_i) \times 100}{\sum_{i=1}^{n}(E_i)}\right] \tag{9.2}$$

Mean relative error (MRE), as defined by Eq (9.3), is the last criterion selected to evaluate the performance of the proposed equation.

$$\text{MRE} = \frac{1}{n}\sum_{i=1}^{n}\left|\frac{E_i - P_i}{E_i}\right| \times 100 \tag{9.3}$$

The smaller values of the MRE indicate the better prediction of the model.

In this study, performance is considered satisfactory for NSE > 0.70, PBIAS ± 25% and, MRE < 10.

9.6.1   Saturated Shear Strength Parameter

Saturated shear strength parameters (i.e., effective cohesion c´, and effective angle of internal friction $\phi´$) are determined in chapter 8 (for effective internal friction angle $\phi´$ =37° and for effective cohesion c´=0 were determined).

9.6.2   Soil Water Characteristic Curve (SWCC)

The SWCC of the testing soil was obtained using the modified triaxial setup. The maximum suction is limited to 400 kPa due to the AEV of the ceramic (500 kPa). To prevent inflation of the membrane inside the triaxial cell, the SWCC was obtained at 10-kPa net stress. The entire range of the suction was fitted using the Fredlund and Xing (1994)'s equation. Figure 9.21 shows the SWCC from experimental and the best fit from Fredlund and Xing (1996) equation. The air-entry value and the residual water content determined to be 35 kPa and 8% respectively. The transition value ψ_t, introduced in this study, determined (following the procedure described in Chapter 3) to be 170 kPa (Figure 9.22).
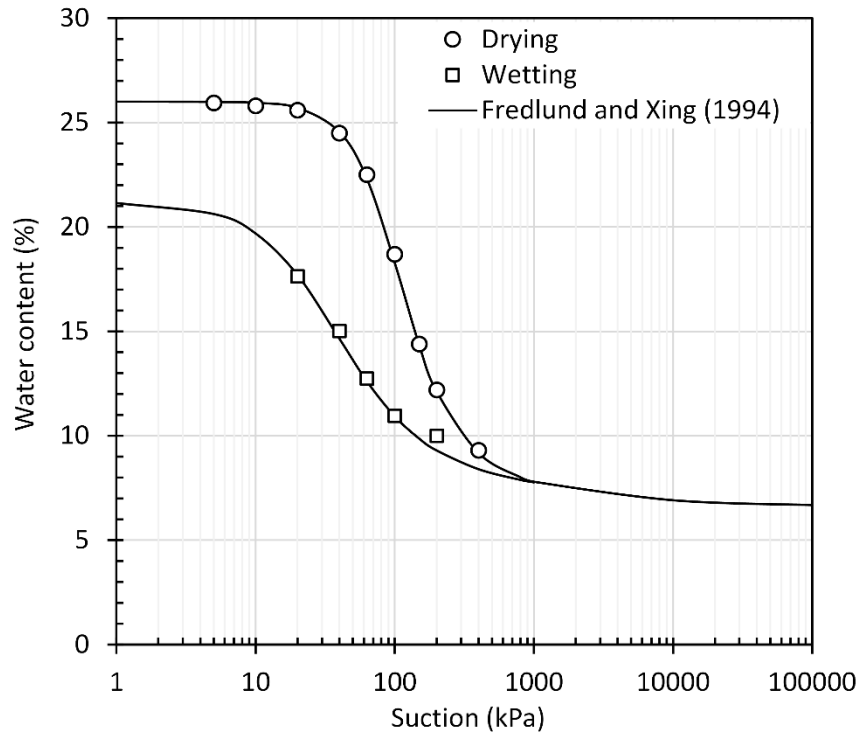
Figure 9.21 Soil water characteristic curve of Mersin silt on IRS.
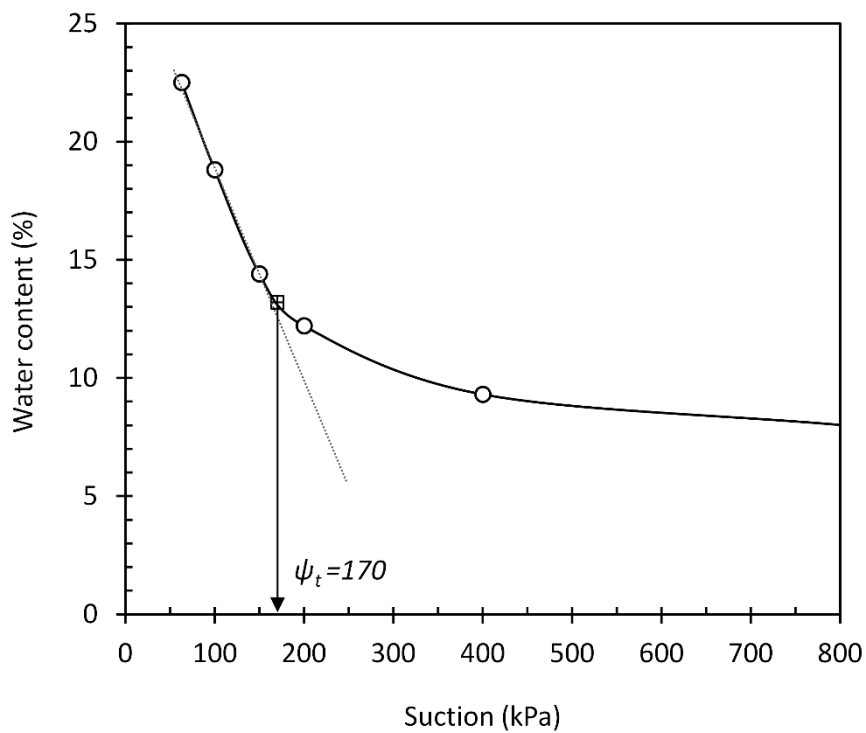
Figure 9.22 SWCC of Mersin silt in arithmetic scale and graphical representation of transition value, ψ_t.

9.6.3 Unsaturated Shear Strength Parameter

As mentioned in chapter 7, a total of 10 constant-suction consolidated drained triaxial tests were performed on IRS specimens at constant matric suctions of 20, 100, 200 and 400 kPa. For each suction, triaxial tests were conducted at three net confining pressures (i.e. 25, 100 and 400 kPa), except for test at 20-kPa suction in which only one test was performed at 400-kPa net stress.

The shear strength parameters (i.e. friction angle and apparent cohesion intercept) for each series are determined in chapter 8.

9.6.4 Comparison of Proposed Equation Predictions with Test Results

The shear strength due to suction was estimated using the proposed equation and three constant parameters (saturated shear strength parameters ($c' = 0$ and $\phi' = 37°$) and the transition value ($\psi_t = 170$ kPa). Comparisons between predicted values and experimental measurement are shown in Figure 9.23. The comparison reveals a successful agreement between the measured and estimated results.

Comparisons are also made between the predicted values of the proposed equation and those equations summarized in Table 3.1 (Figure 9.23). The predictions of the equations are evaluated quantitatively using the statistical measures (i.e. NSE, PBIAS and MRE) and are summarized in the "this study" column of Table 9.1. It can be seen that the prediction values for proposed equation are more accurate compared to other equations.
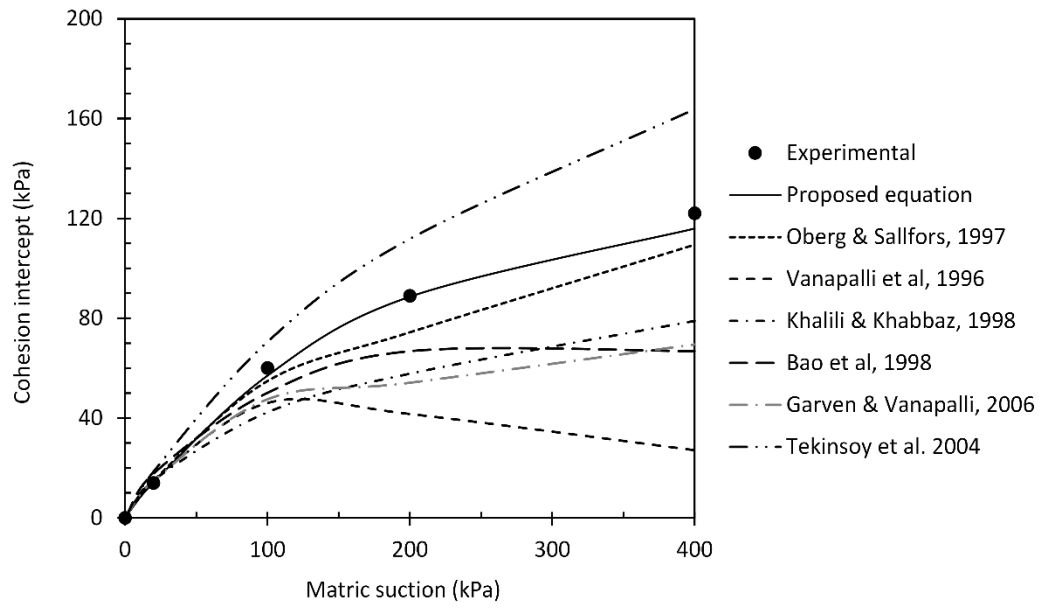
Figure 9.23 Comparisons between experimental measurement and predicted values.

Table 9.1 Summary of the Comparisons between the Proposed Equations and the Various Published Equations.

References	Criteria	This study	Selected soils				
			Escario and Juca (1989)	Vanapalli et al.1996a	Miao et al. (2002)	Trinh Minh Thu	Kayadelen et al 2007
Proposed equation	MRE	3.01	3.55	5.51	4.41	9.84	3.54
	PBIAS	3.4	-1.8	5.6	4.5	3.5	2.5
	NSE	0.99	0.99	0.94	0.97	0.96	0.99
Oberg and Sallfors, 1997	MRE	10.5	30.3	29.7	6.9	30.7	16.1
	PBIAS	11.7	-33.6	-36.5	-3.8	31.1	-17.4
	NSE	0.95	0.60	0.78	0.98	0.49	0.85
Vanapalli et al, 1996	MRE	40.1	3.0	11.4	6.5	92.3	14.3
	PBIAS	57.4	-1.3	8.9	5.5	97.4	-14.9
	NSE	-0.82	0.98	0.97	0.99	-0.44	0.87
Khalili and Khabbaz, 1998	MRE	26.9	15.5	41.1	45.7	28.0	23.4
	PBIAS	33.5	15.9	47.6	49.1	27.5	26.4
	NSE	0.45	0.69	-0.20	-0.20	0.63	0.07
Bao et al, 1998	MRE	28.4	54.9	9.9	25.4	103.3	15.8
	PBIAS	30.9	-61.0	11.2	27.6	109.9	-18.9
	NSE	0.27	0.42	0.91	0.53	-0.41	0.85
Garven and Vanapalli, 2006	MRE	27.2	26.9	8.8	15.5	68.5	7.3
	PBIAS	36.5	28.9	4.9	15.9	70.5	4.0
	NSE	0.22	0.01	0.99	0.88	-0.37	0.99
Tekinsoy et al. 2004	MRE	27.4	42.4	11.3	4.3	25.7	9.9
	PBIAS	-29.4	-45.4	-6.7	3.9	-28.0	-8.9
	NSE	0.88	0.53	0.98	0.99	0.80	0.97

9.6.5 *Comparison of Proposed Equation Predictions with Published Data in Literature*

Comparisons are performed between the predicted values of the proposed equation and the experimental data published in literature. For this, experimental results from Escario and Juca (1989), Vanapalli (1994), Miao et al. (2002), Thu (2006) and Kayadelen et al. (2007) are selected to be analyzed. The input parameters of the equations were extracted and presented in Table 9.2. All the parameters, like air entry value and residual suction, are reported in the original study or adopted from the literature. The only exception is the transition value, proposed in this study, which is determined through the SWCC of each soil.

Table 9.2 Detail of soils data used for analysis.

Parameters	Escario and Juca (1989)	Vanapalli (1994)	Miao et al. (2002)	Thu. (2006)	Kayadelen et al. (2007)
Classification	CL	CL	CH	MH	CH
c' (kPa)	41	0	32	0	14.82
ϕ' (°)	39.5	23	21.3	32	21.9
LL	32	36	58.3	51	77
PI	15	19	31.8	15	45
Air entry value	30	30	25	47	40
Residual suction	12000	3000	1500	200	285000
Transition value	150	220	240	190	240

Escario and Juca (1989) performed a series of suction controlled direct shear tests on three different soils. Two of which, Madrid gray clay and Guadalix red clay (Red clay), presented a non-constant effective friction angle (i.e. dependent on matric suction). The Madrid clayey sand was selected to be analyzed, as a constant friction angle with suction is reported. The air entry value of 30 kPa and a residual suction of the 12000 kPa are adopted from Vanapalli and Fredlund (2000). As shown in Figure 3.4, the transition value of the 150 kPa is determined through the soil water characteristic curve. Figure 9.24 compares the predicted values of the proposed equations and selected equations with experimental measurement. The results of statistical evaluation are summarized in Table 9.1. An acceptable agreement between the predicted and measured values is evident. For proposed equation a mean relative error (MRE) of 3.55, PBIAS of -1.8% and NSE of 0.99 indicates a satisfactory prediction.

Figure 9.24 Comparisons between experimental data and model predictions of Madrid clayey sand Escario and Juca 1989.

Vanapalli (1994) performed a series of suction-controlled multistage direct shear tests on Indian Head till. Statically compacted specimens were prepared at three different water contents (i.e. dry of optimum, optimum and wet of optimum water content). The test results of the specimens prepared at optimum water content are selected for comparison. The average saturated shear strength parameters are reported as $\phi' = 23°$ and c' = 0. The SWCC is obtained using the pressure plate apparatus. The transition value of $\psi_t = 220$ kPa is determined through the SWCC. Figure 9.25 compares the experimental measures of the cohesion intercept with predicted values of the proposed equation and the selected equations. For proposed equation a mean relative error (MRE) of 5.51, PBIAS of -5.6%, and NSE of 0.94 indicates a satisfactory prediction.
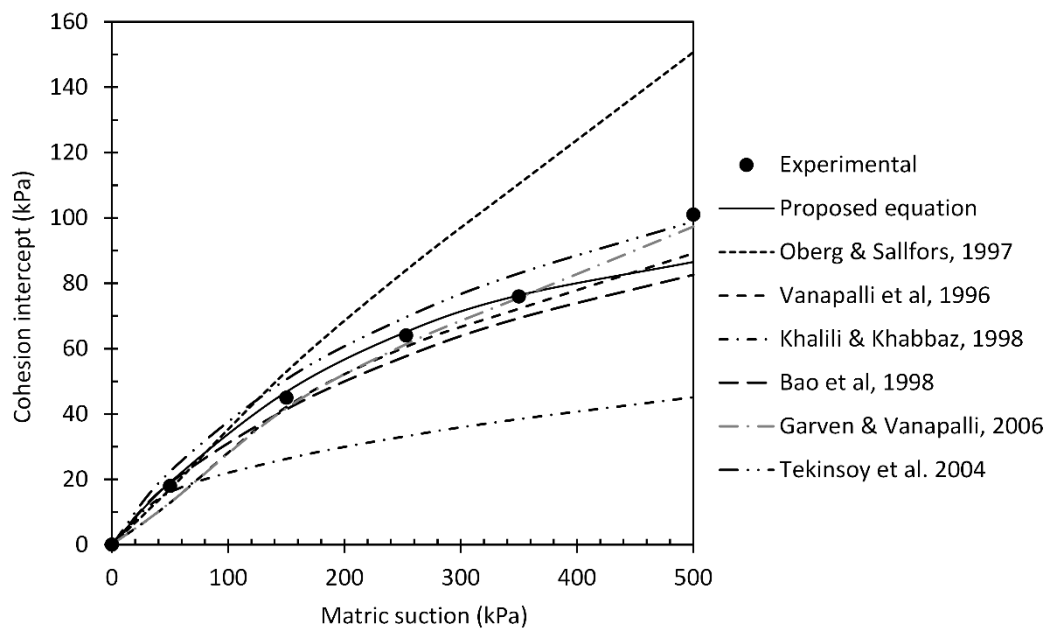
Figure 9.25 Comparisons between experimental data and model predictions of Vanapalli (1994).

Miao et al. (2002) studied the characteristics of the Nanyang expansive soil in its unsaturated state. They used a pressure plate with and without pre-load exerting on the specimen to obtain the SWCCs of the soil. They reported superiority of the pre-loaded specimen in reflecting the soil property of expansive soil. Therefore, in this study the SWCC with preloaded specimen is used, to determine the transition value

of the soil. They used a modified triaxial setup to perform series of constant suction CD tests on the statically compacted specimen with dry density of the 1.5 g/cm³, and the initial water content of the 17%. Figure 9.26 compares the experimental measurements of the cohesion intercepts and predicted values using the proposed equation and selected equations. The results of the statistical analysis are presented in Table 3.1. For proposed equation a mean relative error (MRE) of 4.41, PBIAS of 4.5%, and NSE of 0.97 indicates a satisfactory prediction.
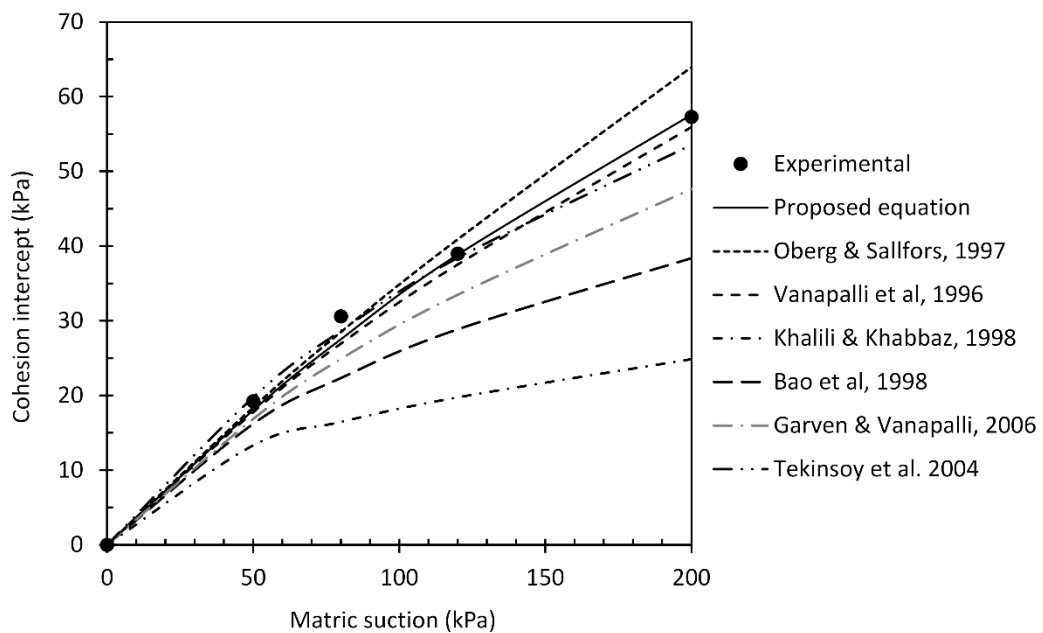
Figure 9.26 Comparisons between experimental data and model predictions of Miao et al. (2002).

Thu (2006) performed a series of suction controlled CD triaxial tests to obtain the shear strength of the statically compacted coarse kaolin. The SWCC of the specimen also was determined through the same modified triaxial setup. The AEV of 47 kPa and residual suction value of 200 kPa is reported in the original study, and the identical value adopted in this study (it seems the residual suction may be higher than this value). Table 9.2 provides the input parameters of the equations. Comparison of the experimental measurements and the predicted values of the proposed equation and the selected equations are presented in Figure 9.27. For proposed equation a mean relative error (MRE) of 9.84, PBIAS of 3.5%, and NSE of 0.96 indicates a satisfactory prediction.
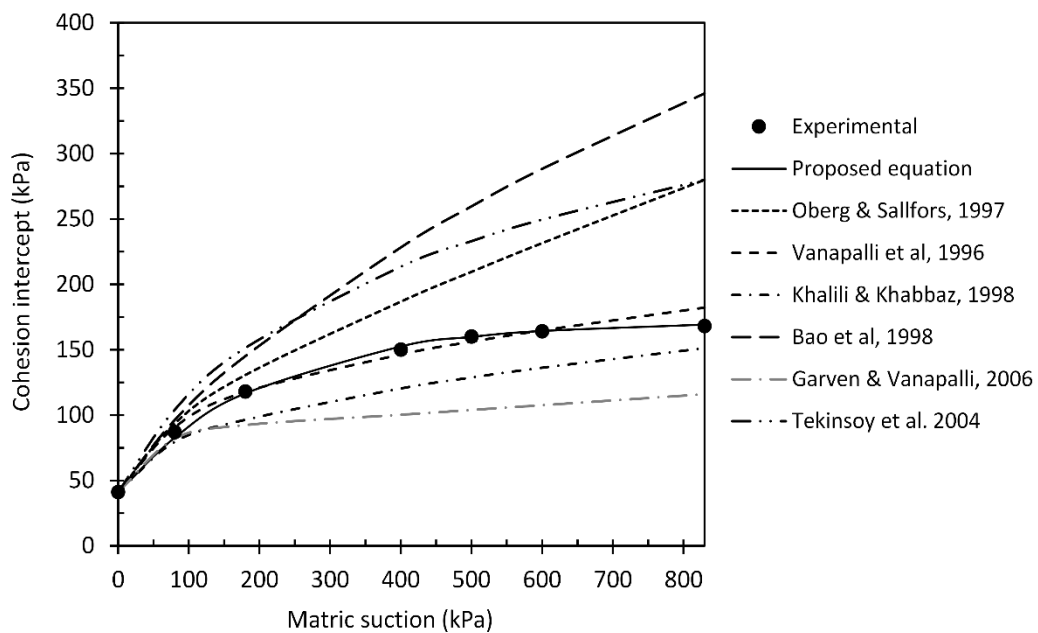
267
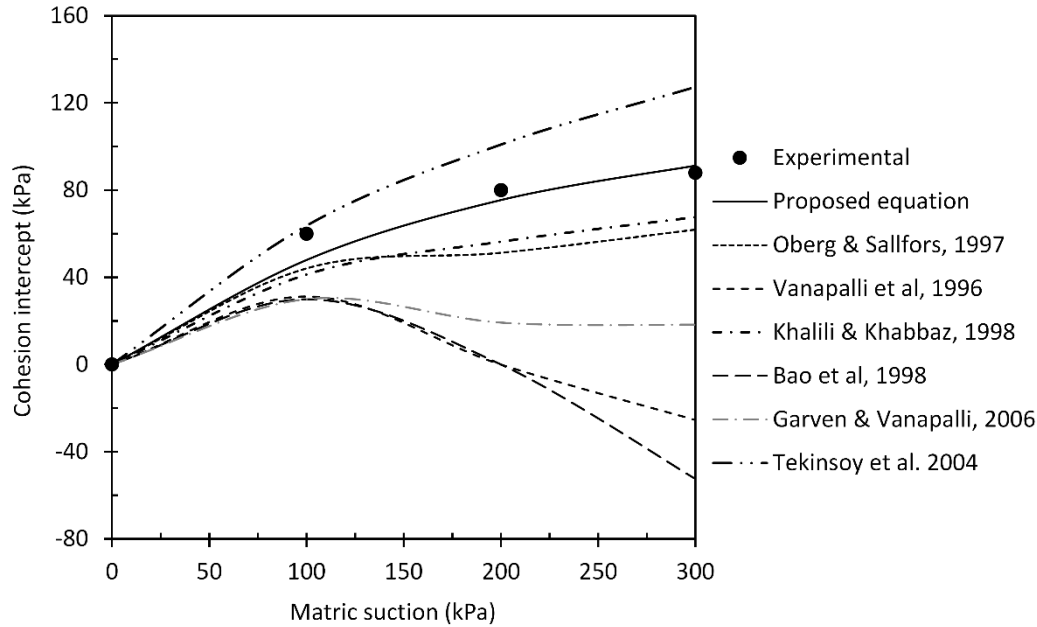
Figure 9.27 Comparisons between experimental data and model predictions of Thu (2006).

Kayadelen et al. (2007) performed a series of suction controlled triaxial tests on residual clay. They employed pressure plate to obtain the SWCC of the soil. They used the Fredlund and Xing (1996) fitting equation to obtain the entire of the SWCC. The AEV and the residual suction adopted from the reported value and presented in Table 9.2. The statistical analysis results are presented in Table 9.1. The transition value equal to 240 kPa is determined through the reported SWCC.

9.6.6 Sensitivity Analysis

As explained, the proposed equation involves three parameters (i.e. ϕ', c' and ψ_t). A graphical procedure is introduced to determine the third parameter, ψ_t. Although the introduced procedure is completely clear, different values for ψ_t may be reported due to approximate nature of the graphical methods. Therefore, parameter sensitivity analysis is carried out to measure the amount of variability of the transition value. It is performed by changing the transition value, one at a time, while holding the other two parameters (i.e. c' and ϕ') fixed. The MRE was determined for each new transition value. The performance of the equation is considered as satisfactory for transition value with MRE < 10.

268

It was observed that, variation in the range of ±50 kPa in transition value provides satisfactory prediction (for the selected data) so that MRE be in the acceptable range.

CHAPTER 10

CONCLUSIONS AND RECOMMENDATIONS

This research can be divided into three main parts: a) Developing and modifying testing setup and procedures to perform tests on both saturated and unsaturated soils test b) theoretical study and c) performing laboratory tests on both reconstituted specimens from slurry and moist-tamped compacted specimens. This chapter presents the achievements and conclusions drawn from each part

Key Achievements:

• Developed a novel volume-change measurement technique in triaxial testing of unsaturated soil by monitoring cell fluid volume based on viscoelastic behavior of the test setup.

• Developed a new procedure for preparation of specimens isotropically reconstituted from the slurry for use in both saturated and unsaturated soil testing.

• Performed a comprehensive laboratory-based study on both saturated and unsaturated specimens reconstituted from slurry and compacted specimens with drying-wetting cycles.

• Proposed an equation to predict shear strength of unsaturated soils.

10.1 New Shear Strength Equation

A prediction type exponential equation (Eq 3.23) is developed to predict the shear strength of the unsaturated soil. Equation involves three constant parameters, two of which are effective shear strength parameters (i.e. ϕ' and c' can be determined through conventional saturated shear strength tests). The third parameter is the ultimate cohesion, c''_{max}, introduced in this study, which is determined through SWCC. The proposed equation was validated against test results of the five types of soils published in the literature as well as through laboratory tests conducted in this

271

study and summarized in 10.3. Comparison on prediction of shear strength was performed between proposed equation and six other published shear strength equations. For the six sets of test results, the proposed equation was found to predict the shear strengths accurately.

10.2 Equipment and procedures development

Developing testing setup and procedures involves a) modifying triaxial setup to axis translation technique (to control matric suction), b) developing volume-change measurement techniques and c) developing a procedure to prepare isotropically reconstituted specimens from slurry for use in both saturated and unsaturated soil testing. Note that this is the first unsaturated triaxial setup of Turkey with both suction control and volume change measurement capability, to the author's knowledge.

10.2.1 Volume Change Measurement

In this study, a novel and inexpensive procedure, that assumes viscoelastic constitutive model for triaxial system, is developed for the measurement of unsaturated soil volume change. Calibration procedure to obtain viscoelastic model (Burgers model) parameters is explained in detail. The proposed method could potentially be embedded into triaxial software to monitor the real time volume change of both saturated and unsaturated soil testing without any modification in triaxial testing setup for volume measurement purpose. The performance of the presented method is verified through comparing measurements of volume change of saturated soil specimens (assuming conventional pore water volume measurements as true values). The maximum absolute error in volume measurement during consolidation and shear stages (for specimen of 5-cm diameter and 10-cm height) was between 0.09 - 0.32 cm^3, in which these corresponded to volumetric strain values of about 10^{-3} on average. In addition, to verify repeatability of the measurements of volume changes of unsaturated soil specimens, suction controlled tests were performed and repeated three times for suctions of 100 and 400 kPa.

Evaluation of the test results confirms the successful application of the proposed method in volume change measurement, where the accuracy of the method is found to be at least as good as the other methods reported in the literature. Moreover, this

is cost-effective and easier to implement in a conventional triaxial setup, once the algorithm is developed and calibrated for the setup.

This is the use of single cell fluid variation for volume measurement that reports the best accuracy in the world literature.

10.2.2 Suction Control

In this study, axis translation technique with double drainage (to reduce the length of the drainage to half and therefore to reduce the testing time) is employed to control and induce soil suction in triaxial testing of unsaturated soils. For this purpose, a triaxial base and top cap and pedestal with new features were developed. The pedestal and top cap include a peripheral annular coarse porous metal (for pore air pressure) and higher air entry ceramic at center (for pore water pressure).

A diffused air volume indicator (DAVI) was developed to flush and measure the volume of the diffused air.

10.2.3 Specimen Preparation Method

In this study, a new slurry preparation procedure for testing both saturated and unsaturated soils is developed, to produce isotropic and homogenous specimens with simple stress history. After preparation, Specimen was divided to five horizontal slices, the uniformity of the specimen, regarding void radio and particle segregation, was verified by measuring the water content and grain size distribution of each slice.

The repeatability of the proposed method in preparing identical specimens was verified for both saturated and unsaturated soil testing. The strength and volume change behavior of specimens prepared by the introduced method are compared with those of compacted specimens, as well as one-dimensionally reconstituted slurry specimens, as part of the consolidated drained (CD) triaxial test results summarized in section 10.3.

10.3 Laboratory Tests

A comprehensive laboratory-based study has been carried out, with modified triaxial setup, to investigate the effects of matric suction and suction history (drying- wetting) as well as net mean stress on shear strength of moist-tamped compacted specimens

and specimens isotropically reconstituted from slurry. A total of 51 triaxial tests (20 saturated and 31 unsaturated) were performed on low-plastic silt from Mersin. On average, each suction-controlled triaxial tests lasts 20 days to complete.

The main conclusions made from the laboratory work are listed as follows:

10.3.1 Equalization Stage

- During suction equalization stage (drying paths), irreversible volumetric compression was observed for IRS specimens. This can be explained by the suction increase (SI) yield curves proposed by Alonso et al. (1990), where plastic volumetric strains occurs when crossing the SI yield curve. As the specimens prepared from slurry (saturated condition), they had never been previously subjected to suction stress. Therefore, for specimen prepared from the slurry, application of even small amounts of suction can cause additional plastic volumetric strains.

10.3.2 Isotropic Compression

- The gradient of the post-yield compression curve $\lambda(s)$ was determined from isotropic compression curves for each value of suction. It was found to be suction dependent, where it becomes exponentially smaller for greater suction values.

- The results of isotropic compression indicated that the yield stress (Pre-consolidation pressure) increases nonlinearly at a decreasing rate as suction increases.

10.3.3 Shearing

- The results show that the shear strength of a soil increases nonlinearly at a decreasing rate toward an asymptotic value as suction increases. This is modeled in the proposed strength equations by c''_{max}.

  For a constant value of the suction, the stiffness of the specimen (modulus) and the maximum deviatoric stress increases with net confining stress, as it is the case for saturated soils.

- The response of the specimens change from strain-hardening in saturated condition to strain-softening as suction increases.
  For the same net confining stress, specimens with higher suction values reach to a peak deviatoric stress at lower axial strain.
- All the saturated MT compacted specimens failed by bulging (with no shear plane) however, unsaturated MT compacted specimens represented a distinct shear plane with bulging around shear plane. For IRS specimens shear plane was observed for both saturated and unsaturated tests.
- For the range of the suction and net mean stress values employed in this study, it was found that the initial shear modulus increases with suction and net mean stress. These observations do not support the assumption of Wheeler and Sivakumar (1995), where a constant value for shear modulus, G were presumed.
- In general, it is found that volumetric deformation (total volume change) became more dilative as the suction increases.
- The change in volume of the water phase of the specimens exhibit the opposite behavior to total volume change. As the most specimens dilated, their water content decreased. This behavior was explained by considering shifting SWCC (either left or right depending state of the specimen).
  It seems that, the volume of the expelled water increases at lower suction values.

10.3.4 Effects of Wetting Drying

- In this study, stiffness and maximum shear strength is found to be dependent on the direction of the suction path (whether wetting or drying) where specimens exhibit higher shear strength and stiffness for a given suction through drying paths than those on the wetting paths. However, that shear strength in critical state is found to be independent of the direction of the suction path, where for a given net confining stress and suction (through drying or wetting paths) specimen approaches a critical state.
- For the entire range of suction, it was found that specimens on the wetting path reach a peak deviatoric stress at lower axial strain than those at the same

suction and net confining stress on the drying path (i.e. modulus in wetting is greater than modulus in drying).

- During shearing, for a given net confining stress and suction, specimens on the wetting path exhibit more dilative behavior than those on the drying path.

10.3.5 Elasto Plastic Model Comparison

The laboratory test results were also interpreted under elasto-plastic framework for unsaturated soils and following conclusions were drawn:

- The critical state lines were generated through the results of the constant suction triaxial tests. The gradient of the critical state line, M, was determined for each test series. Consistent with Alonso et al. (1990), the gradient of the critical state lines was found to be a constant value and independent of the suction.

- The intercept of critical state line, $\mu(s)$, were determined for each constant suction triaxial tests. In consistent with Wheeler and Sivakumar (1995) a nonlinear relationship between critical state line intercept $\mu(s)$ and matric suction were observed.

- Yield points were determined for both MT compacted specimens and IRS, from saturated and unsaturated triaxial tests results. The estimated yield values were employed to generate yield locus in q-p plane for each suction value. For MT compacted specimens, inclined semi-elliptical yield curves were fitted to each series of constant suction yield points. The inclination of the yield locus can be attributed to inherent anisotropic nature of the one-dimensionally compacted specimens. The yield locus appears to be symmetric about $K_0 = 0.45$ line for all series. A constant inclination line reveals the independency of the soil anisotropy from suction, which is consistent with Cui and Delage (1996). For IRS specimens, an elliptical yield surface with the axis of net mean stress as the major axis were fitted successfully to yield points. This is in agreement with modified Cam-Clay model and BBM for both saturated and unsaturated condition.

276

- For both MT and IRS, it was shown that, the size of the yield locus is suction dependent and expands as the suction increases. This observation is consistent with hardening effect of the suction as included in BBM by Alonso et al. (1990).

- The volumetric and deviatoric plastic strain increments were calculated to examine the flow rule. It was found that, for MT compacted specimens the associated flow rule (normality) was not satisfied (i.e. the plastic strain increment vectors were not perpendicular to yield locus). However, for IRS specimens, the plastic strain increment vectors were found to be approximately perpendicular to the yield locus.

10.4 Recommendation for further research

- This work is a comprehensive study, however, all the findings and results are based on the laboratory tests on low-plastic (non-plastic) silt. Therefore, the conclusions of this research might need verification for other soil types.

- In this study, the SWCC, shear strength, and volumetric behavior of the specimens along the single cycle of drying and wetting path were investigated. Therefore, further study are necessary to investigate the effect of the drying and wetting with several cycles.

- An attempt should be made to capture some aspects of unsaturated soil behavior by conventional tests (i.e. unconfined compression test, triaxial shear test, oedometer etc.) with minimal or no modification.

- In this study, the Axis translation technique was used to apply and control given values of matric suction (in this research the applied maximum suction was limited to 400 kPa). However, this technique is suitable for cohesionless soils with low range of the suction. However, in the case of finer soils (i.e. clays), unsaturated soil specimens may be subjected to high suction values. Therefore, new test setups should be developed to control and apply the high range of suction values.

- In this study, a novel procedure is developed to measure the total volume change of the saturated and unsaturated soils in triaxial testing. The principle of the proposed method is based on cell fluid volume measurements. It is

277

recommended to compare the volume change measurements of the developed method against the measurements of the additional techniques, like local transducers, inner cell or laser techniques.

REFERENCES

Ahmadi-Naghadeh, R., and Toker, N. K. (2012). Volume change measurement in triaxial testing of unsaturated soils. In *3 rd International Conference on New Developments in Soil Mechanics and Geotechnical Engineering,* (Vol. c, pp. 627–634). Nicosia: Near East University.

Aitchinson, G. D. (1965). Moisture equilibria and moisture changes in soils beneath covered areas. In *Engineering concepts of moisture equilibria and moisture changes in soils* (pp. 7–22). Australia: Butterworths.

Alonso, E. E., Gens, A., and Hight, D. W. (1987). Special problem soils. General report. In *Proceedings of the 9th European conference on soil mechanics and foundation engineering* (pp. 1087–1146).

Alonso, E. E., Gens, A., and Josa, A. (1990). A constitutive model for partially saturated soils. *Géotechnique*, *40*(3), 405–430.

Bao, C., Gong, B., & Zhan, L. (1998). Properties of unsaturated soils and slope stability of expansive soils. In *Proc., 2nd Int. Conf. on Unsaturated Soils (UNSAT 98),* (pp. 71–98).

Becker, T., & Meißner, H. (2002). Direct suction measurement in cyclic triaxial test devices. In *Proc. of 3rd Int. Conf. on Unsaturated Soils* (pp. 459–462). Recife, Brasil.

Bishop, A. (1959). The principle of effective stress. *Teknisk Ukeblad*, *106*(39), 859–863.

Bishop, A. W., and Blight, G. E. (1963). Some aspects of effective stress in saturated and partly saturated soils. *Géotechnique*, *13*(3), 177–197.

Bishop, A. W., and Donald, I. B. (1961). The experimental study of partly saturated soil in the triaxial apparatus. In *5th International Conference on Soil Mechanics and Foundation Engineering* (pp. 13–21). Paris.

Brooks, R. H., and Corey, A. T. (1964). *Hydraulic properties of porous media. Hydrology Paper, No. 3, Colorado State Univ., Fort Collins, Colo.*

Brutsaert, W. (1967). Some methods of calculating unsaturated permeability. *Trans. ASAE*, *10*(3), 400–404.

Burgers, J. M. (1935). *First and Second Report on Viscosity and Plasticity*. Academy of Sciences at Amsterdam, the Netherlands.

Carraro, J. A. H., and Prezzi, M. (2007). A new slurry-based method of preparation of specimens of sand containing fines. *Geotech. Test. J*, *31*(1), 1–11.

Castro, G., Poulos, S. J., France, J. W., and Enos, J. L. (1982). *Liquefaction induced by cyclic loading*. *Report to National Science Foundation*. Washington, DC.

Chiu, C. (2001). *Behaviour of unsaturated loosely compacted weathered materials*. Hong Kong University of Science and Technology.

Clayton, C. R., Khatrush, S., Bica, A. V., and Siddique, A. (1989). The Use of hall effect semiconductors in geotechnical instrumentation. *Geotechnical Testing Journal*, *12*(1), 69.

Conciani, W., Herrmann, P. S., and Soares, M. M. (1996). The time domain reflectometry to study matrix suction. In *Proceedings of the First International Conference on Unsaturated Soils (Unsat 95), Volume 3* (pp. 1481–1486). Paris.

Costa-Filho, L. (1985). Measurement of axial strains in triaxial tests on london clay. *Geotechnical Testing Journal*, *8*(1), 3–13.

Croney, D. (1952). The movement and distribution of water in soils. *Géotechnique*, *3*(1), 1–16.

Cui, Y. J. (1993). *Etude Du Comportement D'un Limon Compacte Non Sature, Et De*

Sa Modelisation Dans Un Cadre Elasto-Plastique. Ph.D. Thesis, Ecole Nationale des Ponts et Chaussees.

Cui, Y. J., and Delage, P. (1996). Yielding and plastic behaviour of an unsaturated compacted silt. *Géotechnique*, *46*(2), 291–311.

Cunningham, M. R., Ridley, A. M., Dineen, K., and Burland, J. J. (2003). The mechanical behaviour of a reconstituted unsaturated silty clay. *Géotechnique*, *53*(2), 183–194.

Donahue, J. L. (2007). *The Liquefaction Susceptibility, Resistance, and Response of Silty and Clayey Soils*. Ph.D. Thesis , University of California, Berkeley.

Emery, J. J., Liam Finn, W. D., and Lee, K. W. (1973). Uniformity of saturated sand specimens. In *Evaluation of Relative Density and its Role in Geotechnical Projects Involving Cohesionless Soils, ASTM STP 523, American Society for Testing and Materials* (pp. 182–194).

Escario, V., and Juca, J. F. T. (1989). Strength and deformation of partly saturated soils. In *Proceedings of the 12th international conference on soil mechanics and foundation engineering* (pp. 43–46). Rio De Janeiro.

Findley, W., Lai, J. S., and Onaran, K. (1976). *Creep and relaxation of nonlinear viscoelastic materials*. North Holland, Amsterdam.

Fredlund, D., and Xing, A. (1994). Equations for the soil-water characteristic curve. *Canadian Geotechnical Journal*, *31*(4), 521–532.

Fredlund, D. G. (1975). A Diffused Air Volume Indicator for Unsaturated Soils. *Canadian Geotechnical Journal*, *12*(4), 533–539.

Fredlund, D. G. (2006). Unsaturated soil mechanics in engineering practice. *Journal of geotechnical and geoenvironmental engineering, 132*(3), 286–321.

Fredlund, D. G., and Morgenstern, N. R. (1976). Constitutive relations for volume change in unsaturated soils. *Canadian Geotechnical Journal*, *13*(3), 261–276.

Fredlund, D. G., and Morgenstern, N. R. (1977). Stress state variables for saturated and unsaturated soils. *Journal of Geotechnical Division*, *103*(GT5), 447–466.

Fredlund, D. G., & Rahardjo, H. (1993). *Soil mechanics for unsaturated soils*. New York: John Wiley and Sons Inc.

Fredlund, D. G., Rahardjo, H., and Fredlund, M. D. (2012). *Unsaturated Soil Mechanics in Engineering Practice*. Hoboken, NJ, USA: John Wiley & Sons, Inc.

Fredlund, D. G., Xing, A., Fredlund, M. D., and Barbour, S. L. (1995). The relationship of the unsaturated soil shear to the soil-water characteristic curve. *Canadian Geotechnical Journal*, *33*(3), 440–448.

Frost, J. D., and Park, J. Y. (2003). A critical assessment of the moist tamping technique. *Geotechnical Testing Journal*, *26*(1), 57–70.

Gan, J. K. M., Fredlund, D. G., and Rahardjo, H. (1988). Determination of the shear strength parameters of an unsaturated soil using the direct shear test. *Canadian Geotechnical Journal*, *25*(3), 500–510.

Gardner, W. R. (1958). Some steady-state solutions of the unsaturated moisture flow equation with application to evaporation from a water table. *Soil Science*, *85*(4), 228–232.

Garven, E. A., and Vanapalli, S. K. (2006). Evaluation of empirical procedures for predicting the shear strength of unsaturated soils. In *Unsaturated Soils 2006* (pp. 2570–2581). Reston, VA: American Society of Civil Engineers.

Germaine, J. T., and Germaine, A. V. (2009). *Geotechnical Laboratory Measurements for Engineers*. *Geotechnical Laboratory Measurements for Engineers*. Hoboken, NJ, USA: John Wiley & Sons.

Gilbert, P. A., & Marcuson, W. F. (1988). Density variation in specimens subjected to cyclic and monotonic loads. *Journal of Geotechnical Engineering*, *114*(1), 1–20.

Haines, W. B. (1930). Studies in the physical properties of soil. The hysteresis effect in capillary properties, and the modes of moisture distribution associated therewith. *The Journal of Agricultural Science*, *20*(01), 97–116.

Hilf, J. W. (1956). An investigation of pore-water pressure in compacted cohesive soils. Ph.D. Thesis. Technical Memo No. 654, United Stated Bureau of Reclamation, Denver.

Ho, D., and Fredlund, D. (1982). A multistage triaxial test for unsaturated soil. *Geotechnical Testing Journal, 5*(1), 18–25.

Hoyos, L. R., Laloui, L., and Vassallo, R. (2008). Mechanical testing in unsaturated soils. *Geotechnical and Geological Engineering*, *26*(6), 675–689.

Hyde, A. F. L., Higuchi, T., and Yasuhara, K. (2006). Liquefaction, cyclic mobility, and failure of silt. *Journal of Geotechnical and Geoenvironmental Engineering*, *132*(6), 716–735.

Irgens, F. (2008). *Continuum Mechanics*. Berlin, Heidelberg: Springer Berlin Heidelberg.

Ishihara, K., Sodekawa, M., and Tanaka, Y. (1978). Effects of overconsolidation on liquefaction characteristics of sands containing fines. *Dynamic Geotechnical Testing, ASTM STP 654*.

Izadi, A. M., Luna, R., and Stephenson, R. W. (2008). Liquefaction behavior of mississippi river silts. In *Geotechnical Earthquake Engineering and Soil Dynamics* (pp. 1–10). Reston, VA: American Society of Civil Engineers.

Jennings, J. E. B., and Burland, J. B. (1962). Limitations to the use of effective stresses in partly saturated soils. *Géotechnique*, *12*(2), 125–144.

Josa, A. (1988). *Un modelo elastoplastico para suelos no saturados*. Ph.D. Thesis, Universitat Politècnica de Catalunya.

Josa, A., Alonso, E. E., Lloret, A., and Gens, A. (1987). Stress-strain behavior of

partially saturated soils. In *Proc. 9th ECSMFE* (pp. 561–564).

Jotisankasa, A., Coop, M., and Ridley, A. (2007). The development of a suction control system for a triaxial apparatus. *Geotechnical Testing Journal*, *30*(1), 1–7.

Kayadelen, C., Tekinsoy, M. a, and Taşkıran, T. (2007). Influence of matric suction on shear strength behavior of a residual clayey soil. *Environmental Geology*, *53*(4), 891–901.

Kelvin, S. (1875). *Elasticity*. (E. Britannica, Ed.) (9th editio).

Khalili, N., and Khabbaz, M. (1998). A unique relationship of chi for the determination of the shear strength of unsaturated soils. *Geotechnique*, *48*(5), 681–687.

Klotz, E., and Coop, M. (2002). On the identification of critical state lines for sands. *Geotechnical Testing Journal*, *25*(3), 288–301.

Kuerbis, R., and Vaid, Y. P. (1988). Sand sample preparation-the slurry deposition method. *Soils and Foundations*.

Ladd, R. (1978). Preparing test specimens using undercompaction. *Geotechnical Testing Journal*, *1*(1), 16–23.

Lambe W. T. (1951). *Soil Testing for Engineers*. New York: John Wiley and Sons Inc.

Laudahn, A., Sosna, K., & Boháč, J. (2005). A simple method for air volume change measurement in triaxial tests. *Geotechnical Testing Journal*, *28*(3), 313–318.

Lee, H. C., and Wray, W. K. (1995). Techniques to evaluate soil suction- a vital unsaturated soil variable. In *Proceedings of the 1st International conference on Unsaturated soils* (pp. 615 – 622). Paris.

Lu, N., and Likos, W. J. (2004). *Unsaturated soil mechanics*. John Wiley and Sons Inc., New Jersey.

Macari, E., Parker, J., and Costes, N. (1997). Measurement of volume changes in triaxial tests using digital imaging techniques. *Geotechnical Testing Journal*, *20*(1), 103–109.

Mandeville, D., and Penumadu, D. (2004). True triaxial testing system for clay with proportional-integral-differential (PID) Control. *Geotechnical Testing Journal*, *27*(2), 134–144.

Matyas, E. L., and Radhakrishna, H. S. (1968). Volume change characteristics of partially saturated soils. *Géotechnique*, *18*(4), 432–448.

Maxwell, J. (1868). On the dynamical theory of gases. *Philosophical Magazine*, *35*, 129–145.

Miao, L., Liu, S., and Lai, Y. (2002). Research of soil–water characteristics and shear strength features of Nanyang expansive soil. *Engineering Geology*, *65*(4), 261–267.

Miller, E. E., and Miller, R. D. (1956). Physical theory for capillary flow phenomena. *Journal of Applied Physics*, *27*(1956), 324–332.

Mualem, Y. (1984). A modified dependent-domain theory of hysteresis. *Soil Science*, *137*(5), 283–291.

Nash, J. E., and Sutcliffe, J. V. (1970). River flow forecasting through conceptual models part I - A discussion of principles. *Journal of Hydrology*, *10*(3), 282–290.

Ng, C. W. ., Zhan, L. T., and Cui, Y. J. (2002). A new simple system for measuring volume changes in unsaturated soils. *Canadian Geotechnical Journal*, *39*(3), 757–764.

Öberg, A., and Sällfors, G. (1997). Determination of shear strength parameters of unsaturated silts and sands based on the water retention curve. *Geotechnical Testing Journal*, *20*(1), 40.

Oloo, S. Y., and Fredlund, D. G. (1996). A method for determination of ϕ b for statically compacted soils. *Canadian Geotechnical Journal*, *33*(2), 272–280.

Rad, N. S., and Tumay, M. T. (1987). Factors affecting sand specimen preparation by raining. *Geotechnical Testing Journal*, *10*(1), 31–37.

Rampino, C., Mancuso, C., & Vinale, F. (1999). Laboratory testing on an unsaturated soil: equipment, procedures, and first experimental results. *Canadian Geotechnical Journal*, *36*(1), 1–12.

Romero, E., Facio, J. A., Lloret, A., Gens, A., Alonso, E. E., and Publicat Comm Of Xiv, I. (1997). A new suction and temperature controlled triaxial apparatus. *Proceedings of the Fourteenth International Conference on Soil Mechanics and Foundation Engineering, Vol 1: Technical Papers*. Hamburg.

Rumpf, H. (1962). The strength of granules and agglomerates. In *Agglomeration* (pp. 379–418). New York.

Salgado, R., Bandini, P., and Karim, A. (2000). Shear Strength and Stiffness of Silty Sand. *Journal of Geotechnical and Geoenvironmental Engineering*, *126*(5), 451–462.

Sharma, R. (1998). *Mechanical behaviour on unsaturated highly expansive clays*. Ph.D. Thesis, University of Oxford, UK.

Sheeran, D. E., and Krizek, R. J. (1971). Preparation of homogenous soil samples by slurry consolidation. *Journal of Materials*, *6*(2), 356–373.

Shen, J., and Kushwaha, R. L. (1998). *Soil-machine interactions: a finite element perspective*. New York: M. Dekker.

Sheng, D. C., Zhang, S., and Yu, Z. W. (2013). Unanswered questions in unsaturated soil mechanics. *Science China Technological Sciences*, *56*(5), 1257–1272.

Sheng, D., Fredlund, D. G., and Gens, A. (2008). A new modelling approach for unsaturated soils using independent stress variables. *Canadian Geotechnical*

Journal, *45*(4), 511–534.

Sivakumar, R., Sivakumar, V., Blatz, J., and Vimalan, J. (2006). Twin-Cell stress path apparatus for testing unsaturated soils. *Geotechnical Testing Journal*, *29*(2), 175–179.

Sivakumar, V. (1993). *A critical state framework for unsaturated soils*. Ph.D. Thesis, University of Sheffield, UK.

Tastan, E. O., and Carraro, J. A. H. (2013). A new slurry-based method of preparation of hollow cylinder specimens of clean and silty sands. *Geotechnical Testing Journal*, *36*(6), 1–12.

Tekinsoy, M. ., Kayadelen, C., Keskin, M. ., and Söylemez, M. (2004). An equation for predicting shear strength envelope with respect to matric suction. *Computers and Geotechnics*, *31*(7), 589–593.

Terzaghi, K. (1925). Erdbaumechanik auf Bodenphsikalischer Grundlage.

Thomas, S. (1987). *The consolidation behaviour of gassy soil*. Ph.D. Thesis, The University of Oxford.

Thu, T. M. (2006). *Shear strength and volume change relationship for an unsaturated soil*. Ph.D. Thesis, Nanyang Technological University.

Toker, N. K. (2007). *Modeling the relation between suction, effective stress and shear strength in partially saturated granular media*. Ph.D. Thesis, Massachusetts Institute of Technology.

Uchaipichat, A., Khalili, N., and Zargarbashi, S. (2011). A temperature controlled triaxial apparatus for testing unsaturated soils. *Geotechnical Testing Journal*, *34*(5), 1–8.

Vaid, Y. P., and Negussey, D. (1988). Preparation of reconstituted sand specimens. In *Advanced Triaxial Testing of Soil and Rock, ASTM STP 9* (pp. 405–417).

Vaid, Y. P., and Sivathayalan, S. (2000). Fundamental factors affecting liquefaction

susceptibility of sands. *Canadian Geotechnical Journal*, *37*(3), 592–606.

Vaid, Y. P., Sivathayalan, S., and Stedman, D. (1999). Influence of specimen-reconstituting method on the undrained response of sand. *Geotechnical Testing Journal*, *22*(3), 187–195.

Van der Waals, J. D. (1979). The thermodynamic theory of capillarity under the hypothesis of a continuous variation of density. *Journal of Statistical Physics*, *20*(2), 200–244.

Van Genuchten, M. T. (1980). A Closed-form equation for predicting the hydraulic conductivity of unsaturated soils. *Soil Science Society of America Journal*, *44*(5), 892–898.

Vanapalli, S. (1994). *Simple test procedures and their interpretation in evaluating the shear strength of an unsaturated soil*. Ph.D. Thesis, University of Saskatchewan.

Vanapalli, S. K., and Fredlund, D. G. (2000). Comparison of different procedures to predict unsaturated soil shear strength. In *Advances in Unsaturated Geotechnics* (pp. 195–209). Reston, VA: American Society of Civil Engineers.

Vanapalli, S. K., Fredlund, D. G., Pufahl, D. E., and Clifton, A. W. (1996). Model for the prediction of shear strength with respect to soil suction. *Canadian Geotechnical Journal*, *33*(3), 379–392.

Voigt, W. (1892). Ueber innere Reibung fester Körper, insbesondere der Metalle. *Annalen Der Physik Und Chemie*, *283*(12), 671–693.

Wang, S., Luna, R., and Stephenson, R. W. (2011). A Slurry consolidation approach to reconstitute low-plasticity silt specimens for laboratory triaxial testing. *Geotechnical Testing Journal*, *34*(4), 288–296.

Wheeler, S. J. (1988). The undrained shear strength of soils containing large gas bubbles. *Géotechnique*, *38*(3), 399–413.

White, N. F., Duke, H. R., Sunada, D. K., and Corey, A. T. (1970). Physics of desaturation in porous materials. *Journal of the Irrigation and Drainage Division*, *96*(2), 165–191.

Wong, J.-C., Rahardjo, H., Toll, D. G., aand Leong, E.-C. (2001). Modified triaxial apparatus for shearing-infiltration test. *Geotechnical Testing Journal*, *24*(4), 370–380.

Wood, D. M. (1991). *Soil Behaviour and Critical State Soil Mechanics*. Cambridge: Cambridge University Press.

Zakaria, I. (1994). *Yielding of unsaturated soil.* Ph.D. thesis, University of Sheffield, UK.

Zhan, L. (2003). *Field and laboratory study of an unsaturated expansive soil associated with rain-induced slope instability*. Ph.D. thesis, Hong Kong University of Science and Technology.

APPENDIX A

SOIL PROPERTIES OF QUARTZ AND M100 SILTS

The Atterberg limits and specific gravity tests were performed to determine the index properties of the soil samples. The SWCC of the soil samples for compacted specimens were obtained from pressure plate test. The testing results are presented in Table A.1 and A.2 and Figures A.1- A.4.

TABLE A.1 Summary of index properties of the quartz.

Soil properties	Description/value
Liquid Limit	NA
Plastic Limit	NA
Plasticity Index, IP	NA
Specific Gravity Gs	2.67
Maximum dry density (g/cm3)	1.6
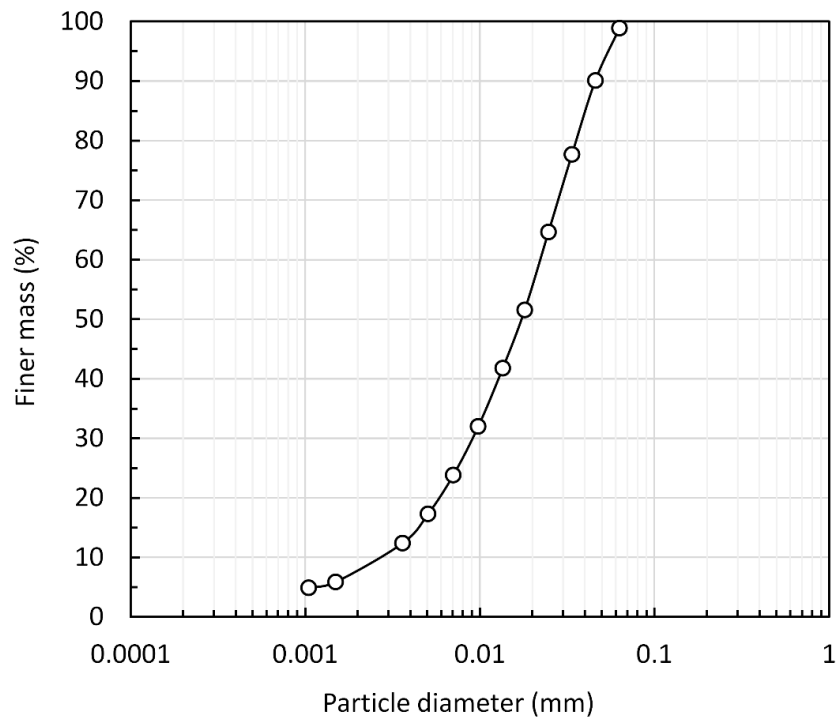
Figure A.1 Grain size distribution of quartz silt.
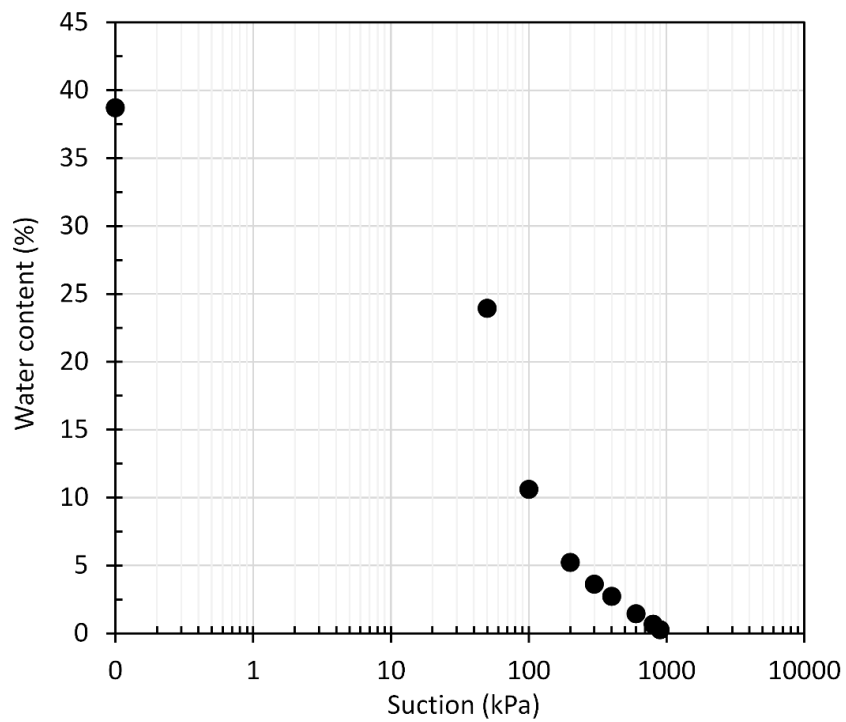
Figure A.2 Soil water characteristic curve of quartz silt from pressure plate test.

TABLE A.2 Summary of index properties of the M100.

Soil properties	Description/value
Liquid Limit	28.8 %
Plastic Limit	21.6 %
Plasticity Index, IP	7.1
USCS classification	ML
Specific Gravity Gs	2.36
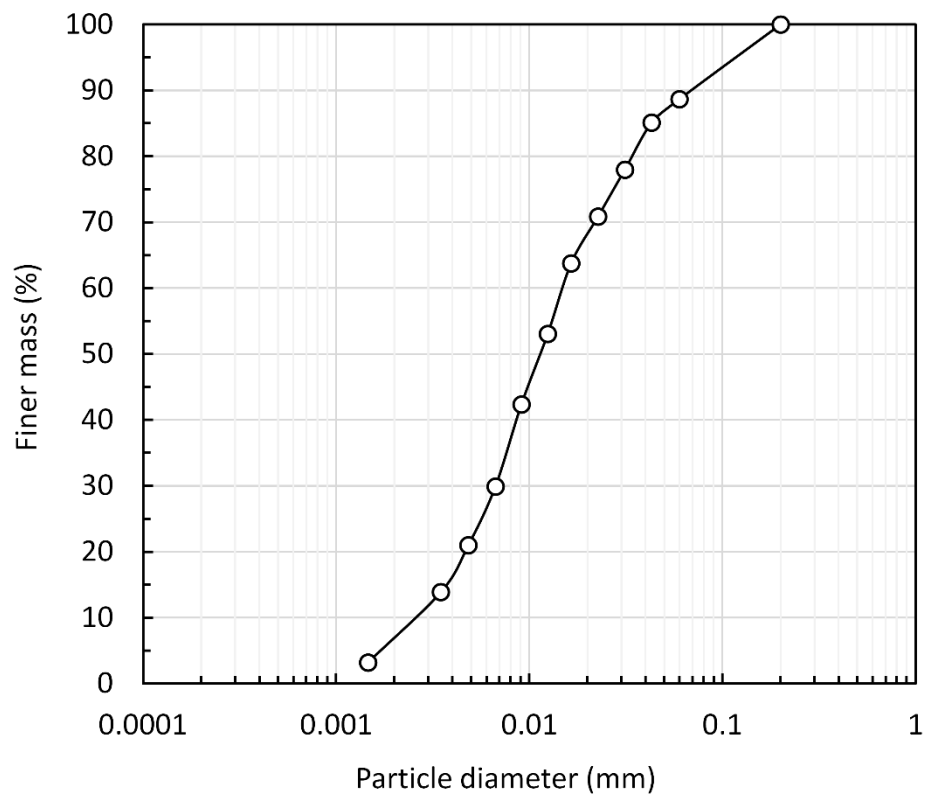
Figure A.3 Grain size distribution of M100 silt.
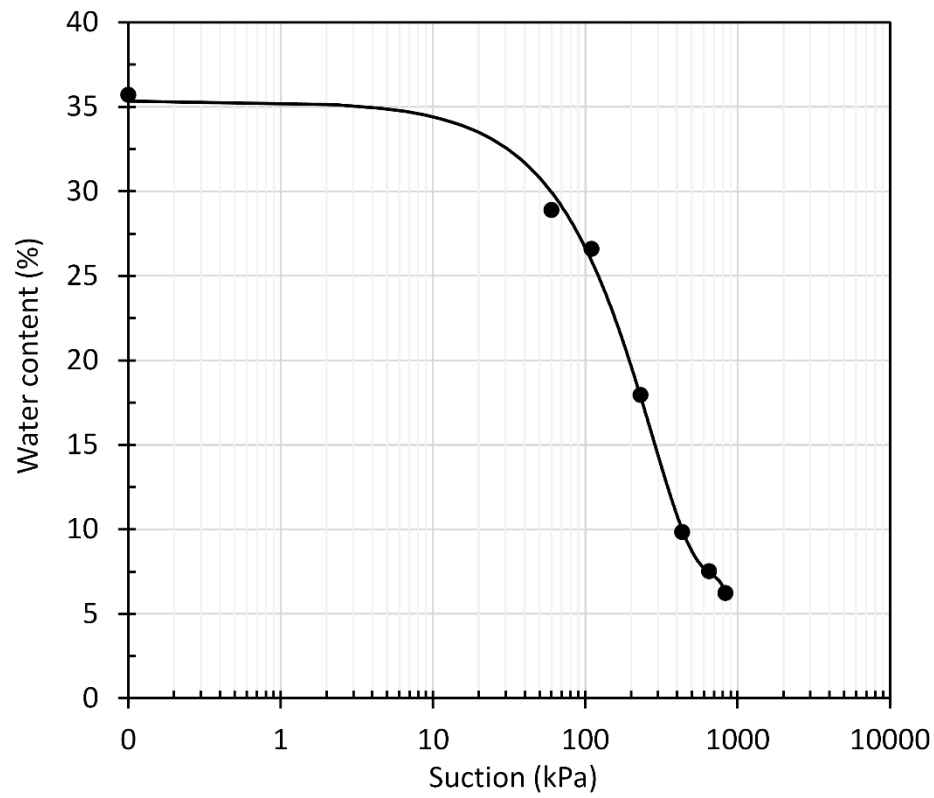
Figure A.4 Soil water characteristic curve of M100 silt from pressure plate test.

APPENDIX B

CALIBRATION OF TRANSDUCERS

Calibration of Volume Change Transducer

The volume change transducer was calibrated using the flow track. The calibration was performed for the entire capacity of the volume change transducer, which is 80-ml. a linear calibration between the output voltage and the volume change adopted. The calibration curve is shown in Figures B.1.
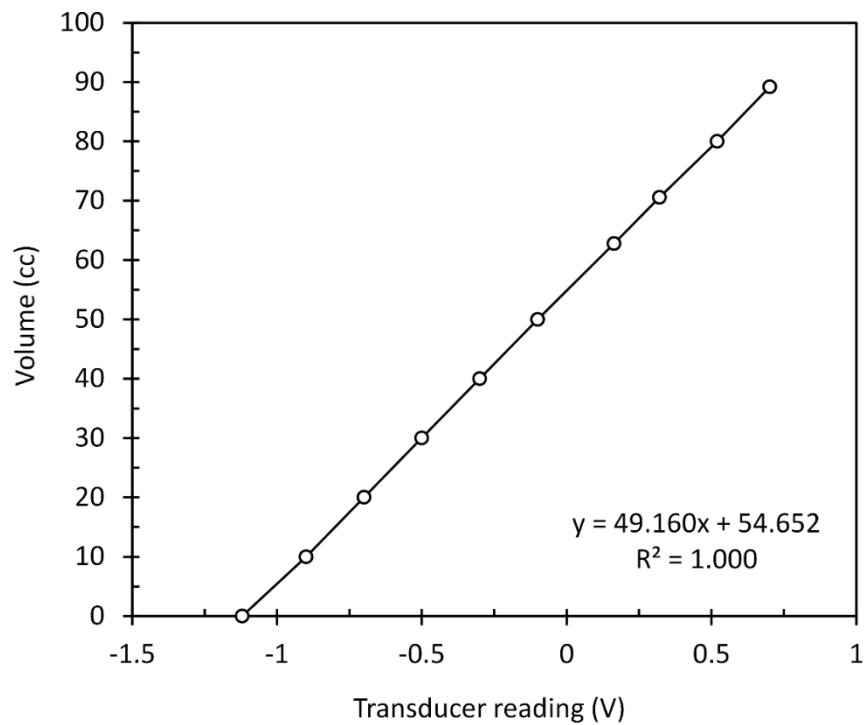
Figure B.1 Calibration curve for the volume change transducer.

Calibration of pressure transducers

The pressure transducers, for monitoring the applied pore air pressure and air pressure in DAVI, were calibrated using flow track. A linear calibration equation for transducers adopted. The calibration curves are shown in Figures B.2 and B.3.
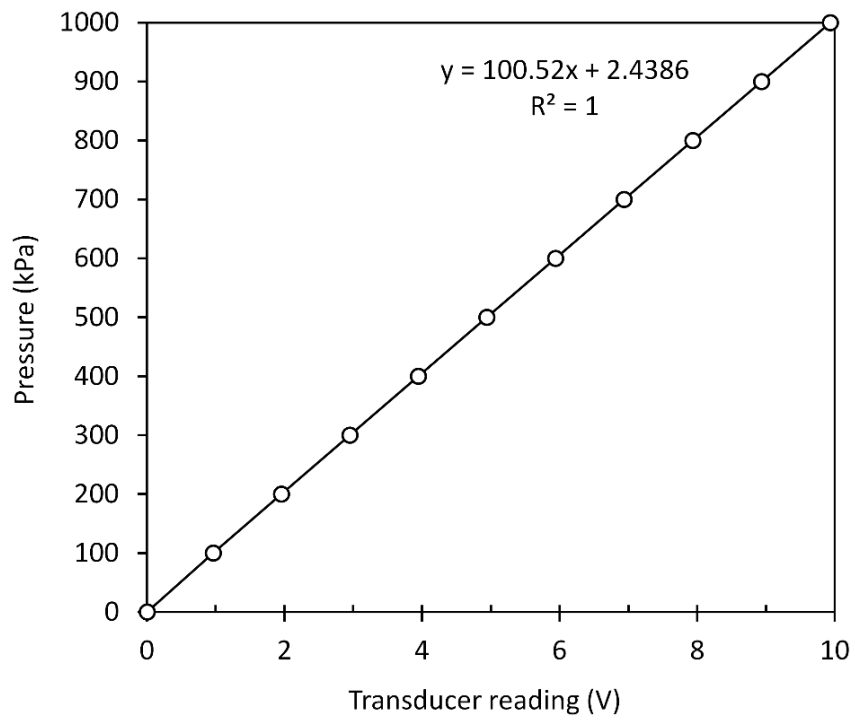
Figure B.2 Calibration curve for the air pressure transducers.
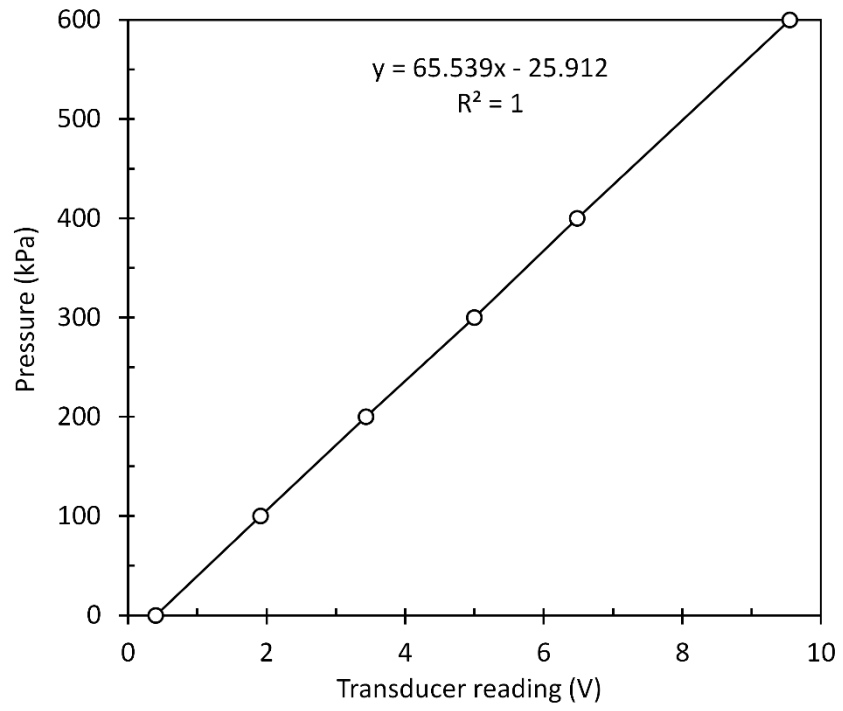
Figure B.3 Calibration curve for the air pressure transducers in DAVI.

FAILURE MODES OF SPECIMENS AT THE END OF THE TESTS

Saturated tests

Figures C.1 Failure mode of IRS specimen at saturated condition, $\sigma'_3 = 25$ kPa.

Figures C.2 Failure mode of IRS specimen at saturated condition, $\sigma'_3 = 100$ kPa.

Figures C.3 Failure mode of IRS specimen at saturated condition, $\sigma'_3 = 200$ kPa.

Figures C.4 Failure mode of IRS specimen at saturated condition, $\sigma'_3 = 400$ kPa.

Figures C.5 Failure mode of IRS specimen at saturated condition with loading-unloading, $\sigma'_3 = 400\text{-}200$ kPa (OCR = 2).
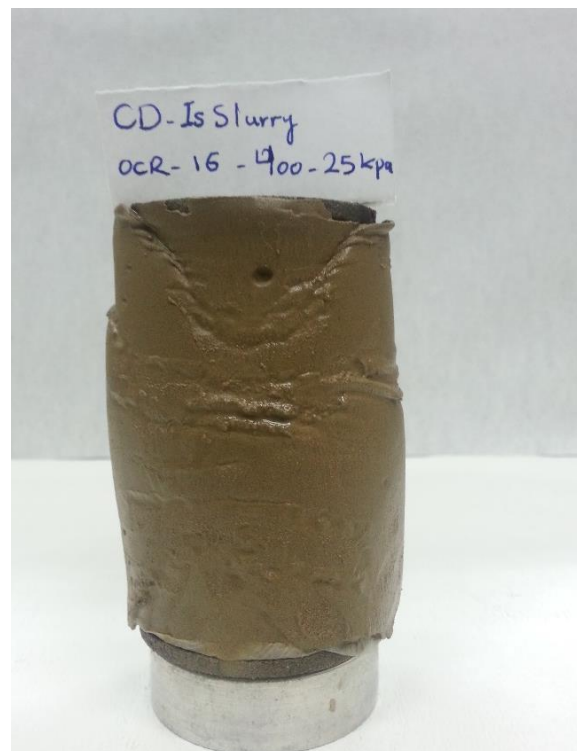
Figures C.6 Failure mode of IRS specimen at saturated condition with loading-unloading, $\sigma'_3 = 400\text{-}25$ kPa (OCR = 16).

Figures C.7 Failure mode of ORS specimen at saturated condition, $\sigma'_3 = 100$ kPa.
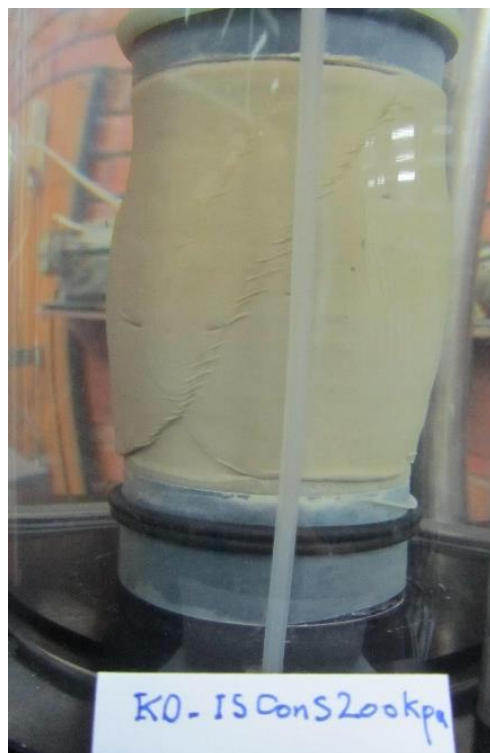
Figures C.8 Failure mode of ORS specimen at saturated condition, $\sigma'_3 = 200$ kPa.

Figures C.9 Failure mode of ORS specimen at saturated condition, $\sigma'_3 = 400$ kPa.

Figures C.10 Failure mode of MT specimen at saturated condition
(w% = 10.2, e = 0.72), $\sigma'_3 = 25$ kPa.

Figures C.11 Failure mode of MT specimen at saturated condition
(w% = 10.2, e = 0.72), σ′₃ = 100 kPa.

Figures C.12 Failure mode of MT specimen at saturated condition
(w% = 10.2, e = 0.72), σ′₃ = 400 kPa.

Figures C.13 Failure mode of MT specimen at saturated condition
(w% = 17.5, e = 0.72), σ'_3 = 25 kPa.

Figures C.14 Failure mode of MT specimen at saturated condition
(w% = 17.5, e = 0.72), σ'_3 = 100 kPa.

Figures C.15 Failure mode of MT specimen at saturated condition
(w% = 17.5, e = 0.72), σ′$_3$ = 200 kPa.

Figures C.16 Failure mode of MT specimen at saturated condition
(w% = 17.5, e = 0.72), σ′$_3$ = 400 kPa.

Figures C.17 Failure mode of MT specimen at saturated condition
(w% = 17.5, e = 0.82), σ′₃ = 25 kPa.

Figures C.18 Failure mode of MT specimen at saturated condition
(w% = 17.5, e = 0.82), σ′₃ = 100 kPa.

Figures C.19 Failure mode of MT specimen at saturated condition
(w% = 17.5, e = 0.82), σ′₃ = 200 kPa.
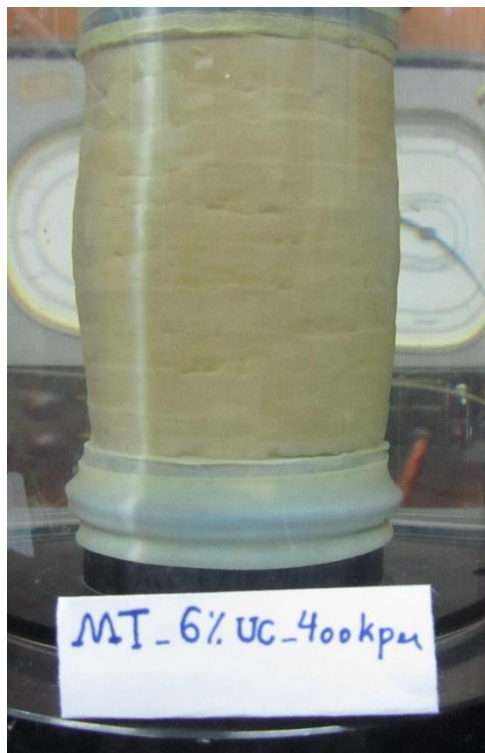
Figures C.20 Failure mode of MT specimen at saturated condition
(w% = 17.5, e = 0.82), σ′₃ = 400 kPa.
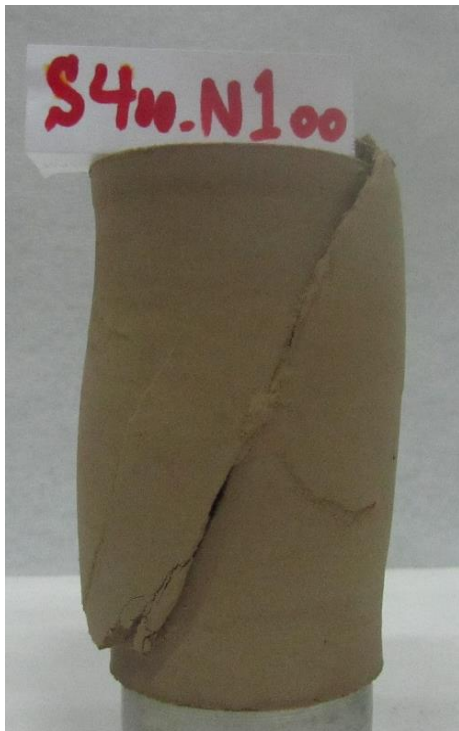
Unsaturated tests on IRS specimens.
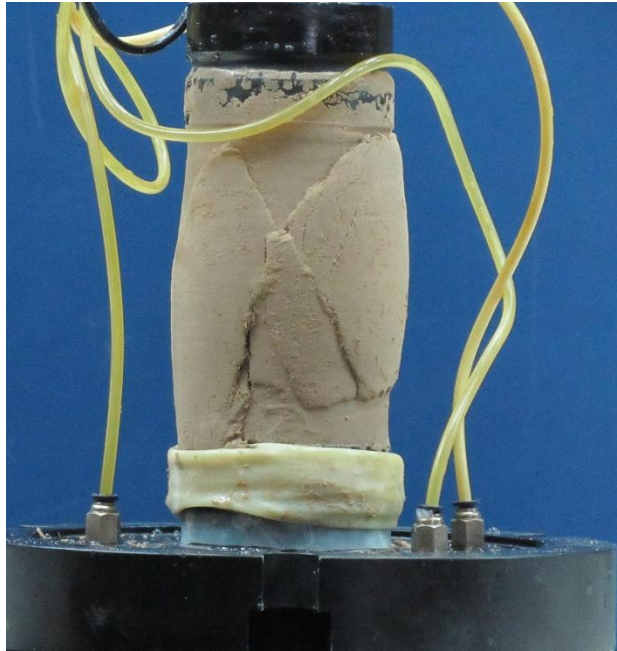
Figures C.21 Failure mode of IRS specimen at unsaturated condition s = 100 kPa,
$(\sigma_3 - u_a) = 25$ kPa
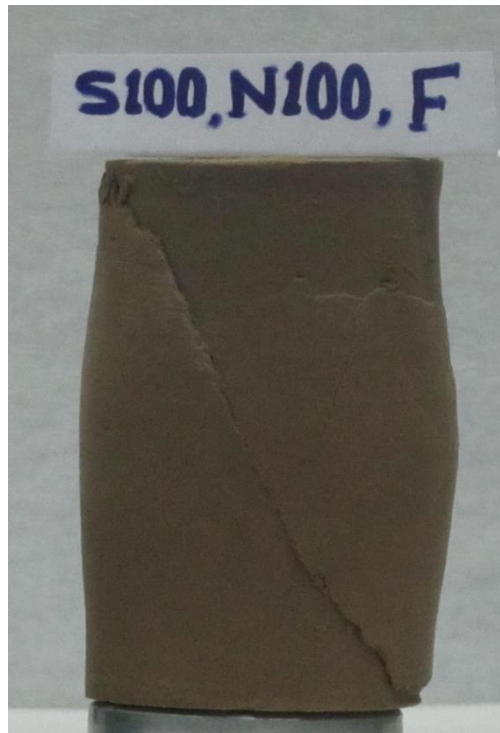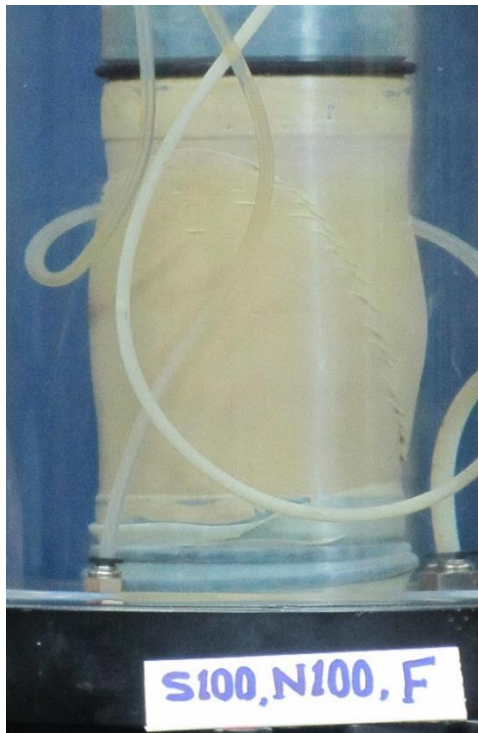
Figures C.22 Failure mode of IRS specimen at unsaturated condition s = 100 kPa,
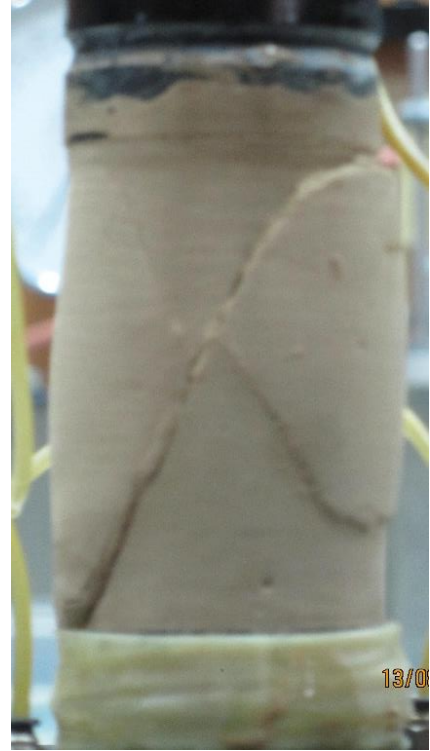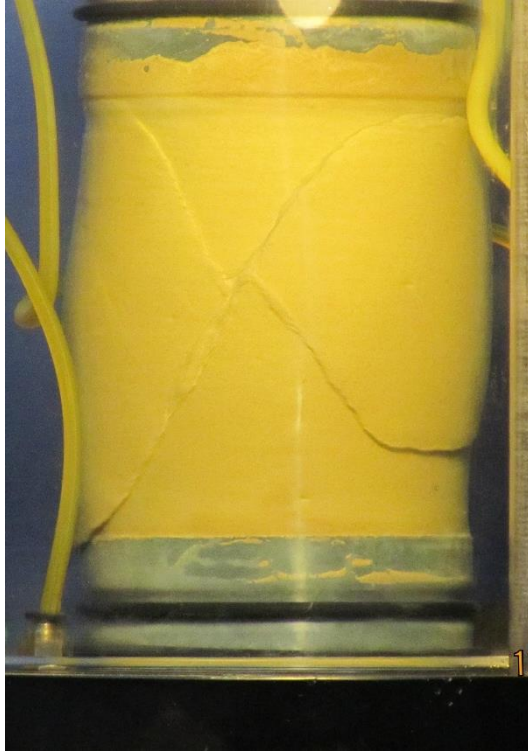$(\sigma_3 - u_a) = 100$ kPa
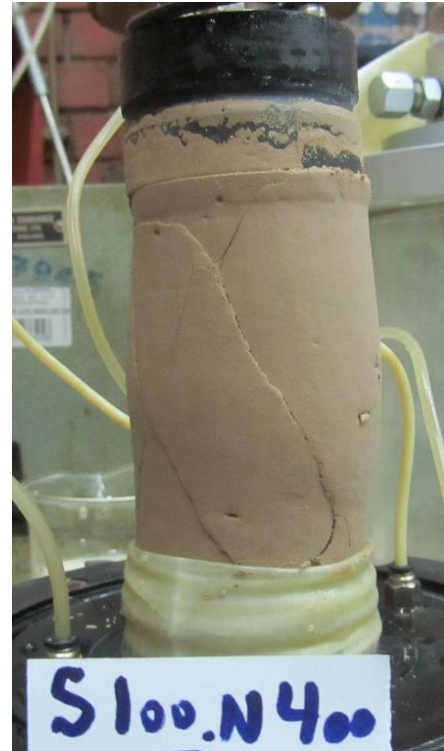
Figures C.23 Failure mode of IRS specimen at unsaturated condition s = 100 kPa, $(\sigma_3 - u_a) = 400$ kPa
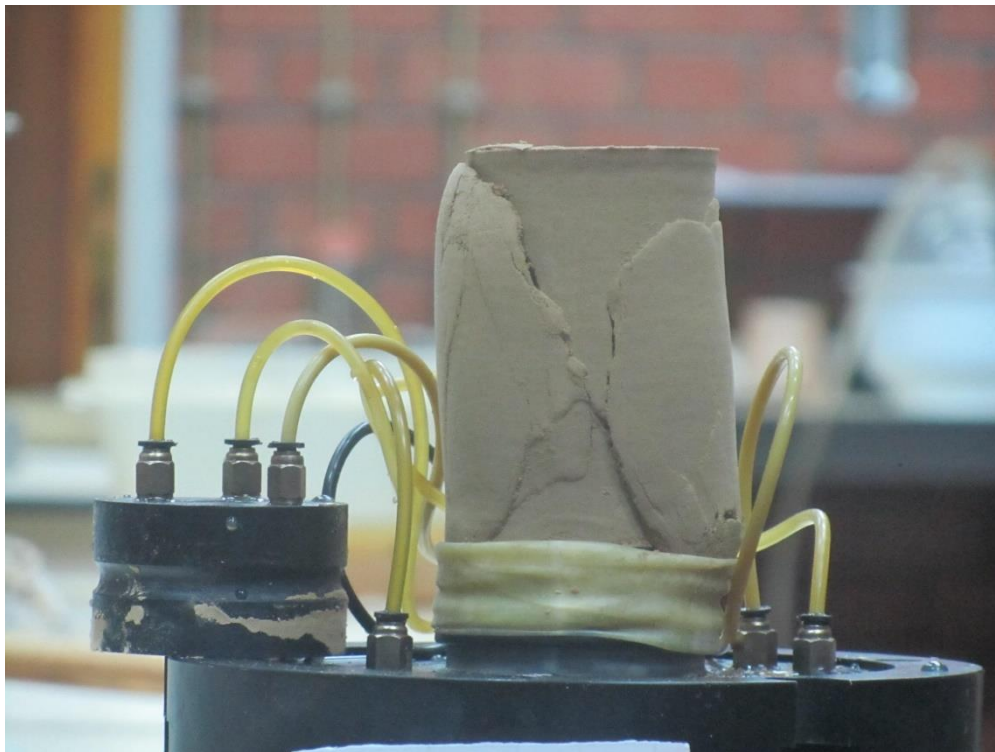
Figures C.24 Failure mode of IRS specimen at unsaturated condition s = 200 kPa, $(\sigma_3-u_a) = 25$ kPa

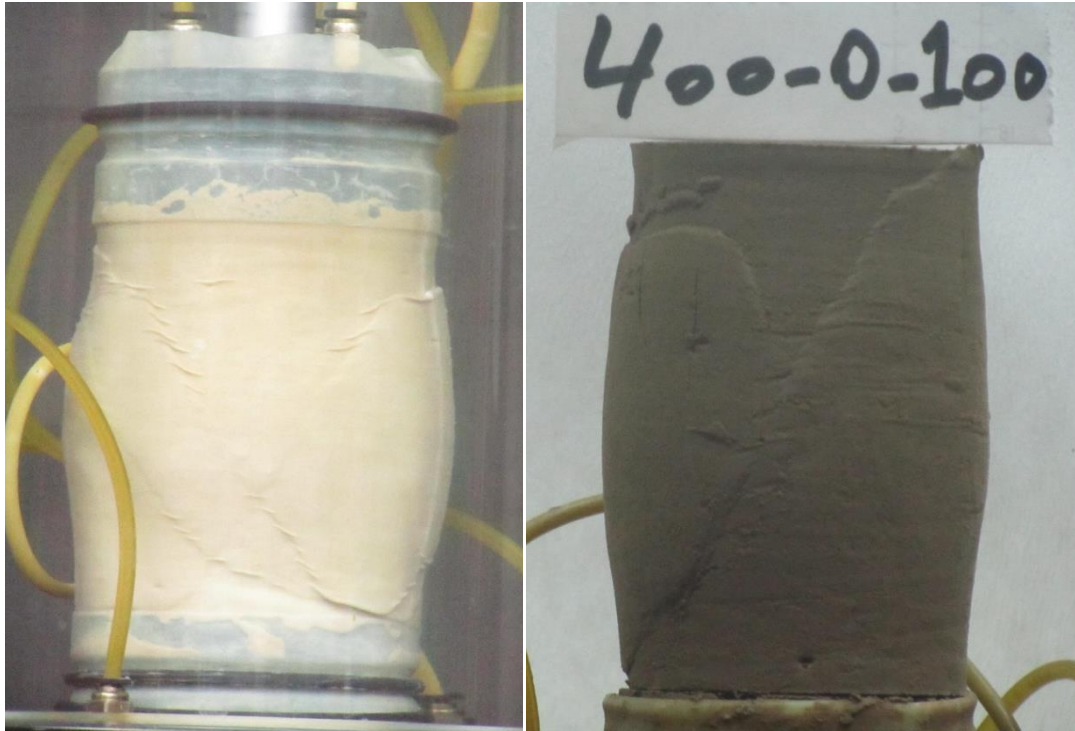Figures C.25 Failure mode of IRS specimen at unsaturated condition s = 200 kPa,
$(\sigma_3\text{-}u_a)$ = 100 kPa
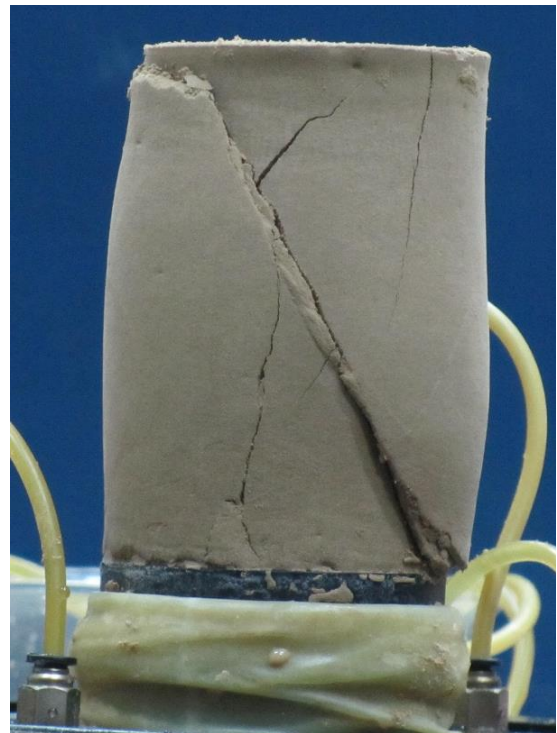
Figures C.26 Failure mode of IRS specimen at unsaturated condition s = 200 kPa,
$(\sigma_3\text{-}u_a)$ = 400 kPa
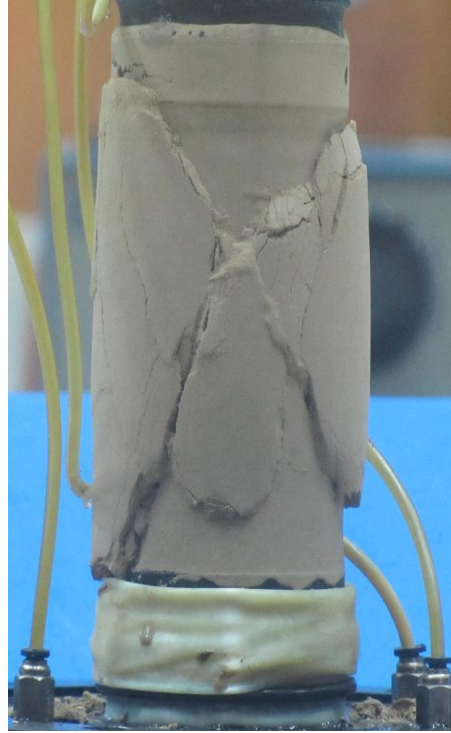
Figures C.27 Failure mode of IRS specimen at unsaturated condition s = 400 kPa,
$(\sigma_3-u_a) = 25$ kPa

Figures C.28 Failure mode of IRS specimen at unsaturated condition s = 400 kPa,
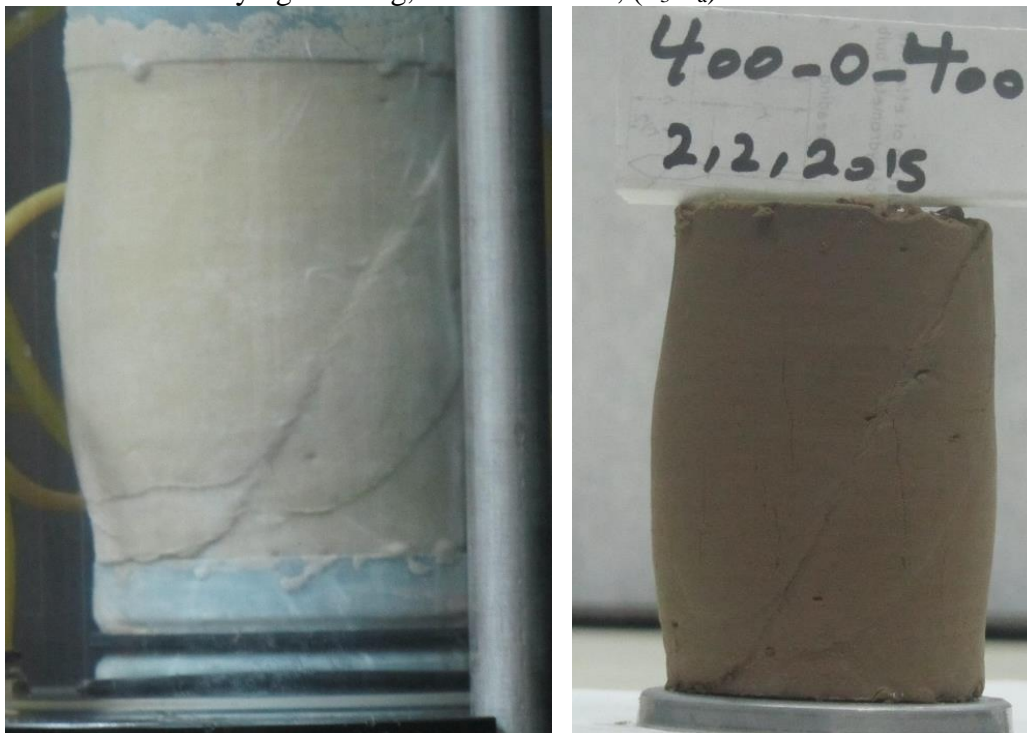$(\sigma_3-u_a) = 100$ kPa

Figures C.29 Failure mode of IRS specimen at unsaturated condition s = 400 kPa, $(\sigma_3 - u_a)$ = 400 kPa
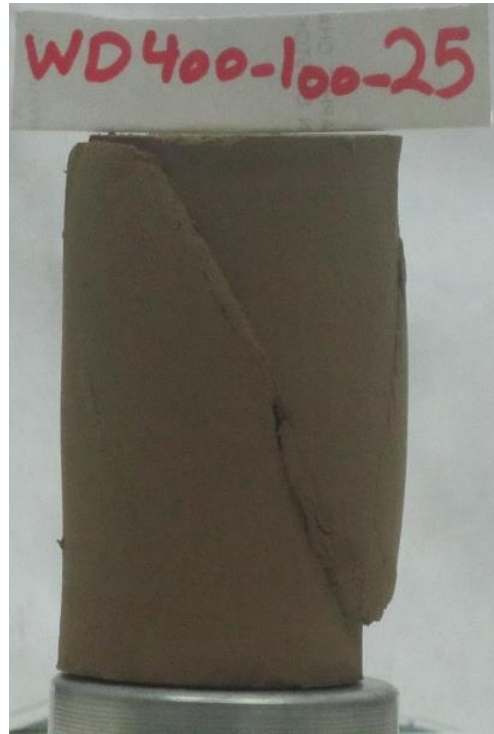
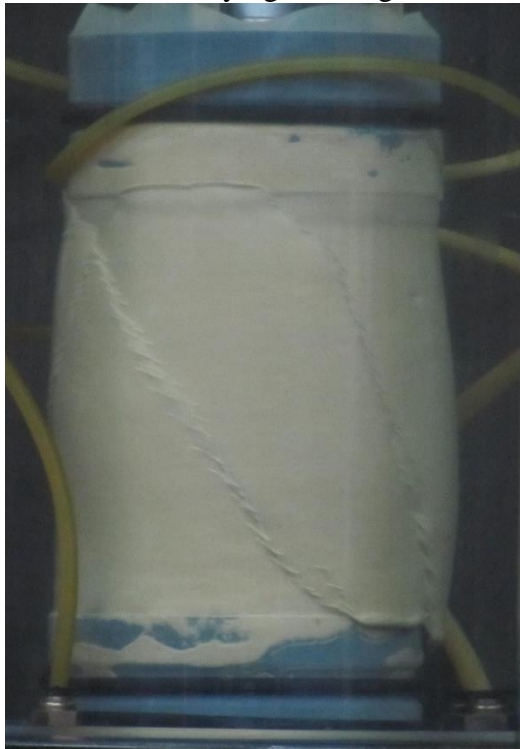**Unsaturated tests on IRS specimens with drying- wetting.**

Figures C.30 Failure mode of IRS specimen at unsaturated condition with drying- wetting, s = 400 - 0 kPa, $(\sigma_3 - u_a)$ = 100 kPa
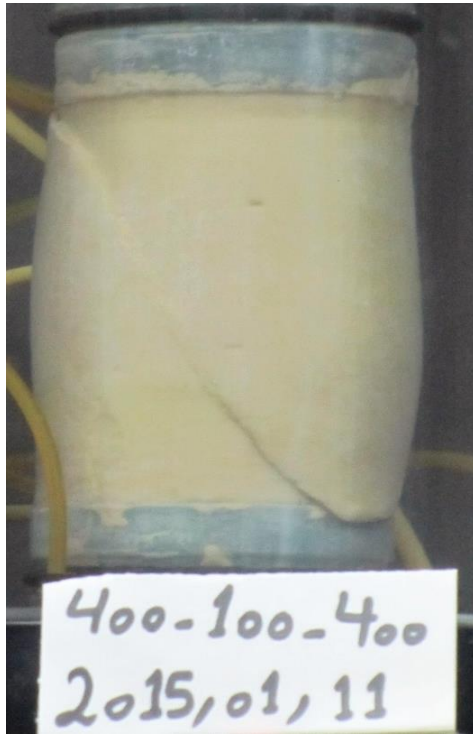

Figures C.31 Failure mode of IRS specimen at unsaturated condition with drying- wetting, s = 400 - 0 kPa, $(\sigma_3 - u_a)$ = 400 kPa

Figures C.32 Failure mode of IRS specimen at unsaturated condition with drying- wetting, s = 400 - 100 kPa, $(\sigma_3 - u_a)$ = 25 kPa

Figures C.33 Failure mode of IRS specimen at unsaturated condition with drying- wetting, s = 400 - 100 kPa, $(\sigma_3 - u_a)$ = 100 kPa

Figures C.34 Failure mode of IRS specimen at unsaturated condition with drying- wetting, s = 400 - 100 kPa, $(\sigma_3 - u_a)$ = 400 kPa
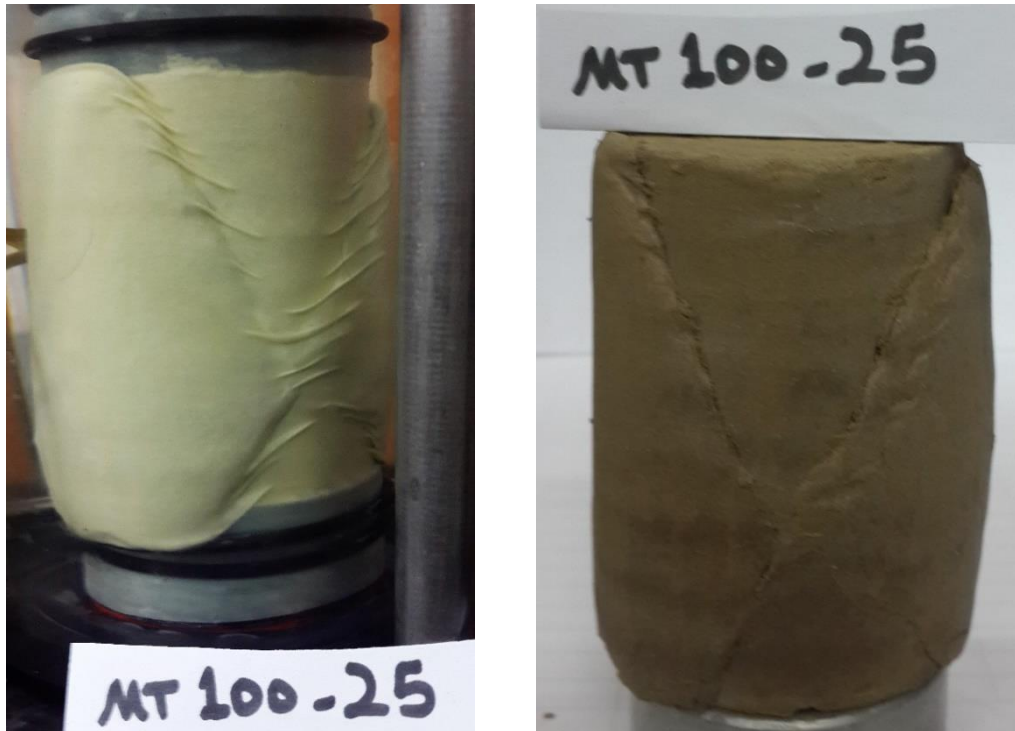

Figures C.35 Failure mode of IRS specimen at unsaturated condition with drying- wetting, s = 400 - 200 kPa, $(\sigma_3 - u_a)$ = 25 kPa
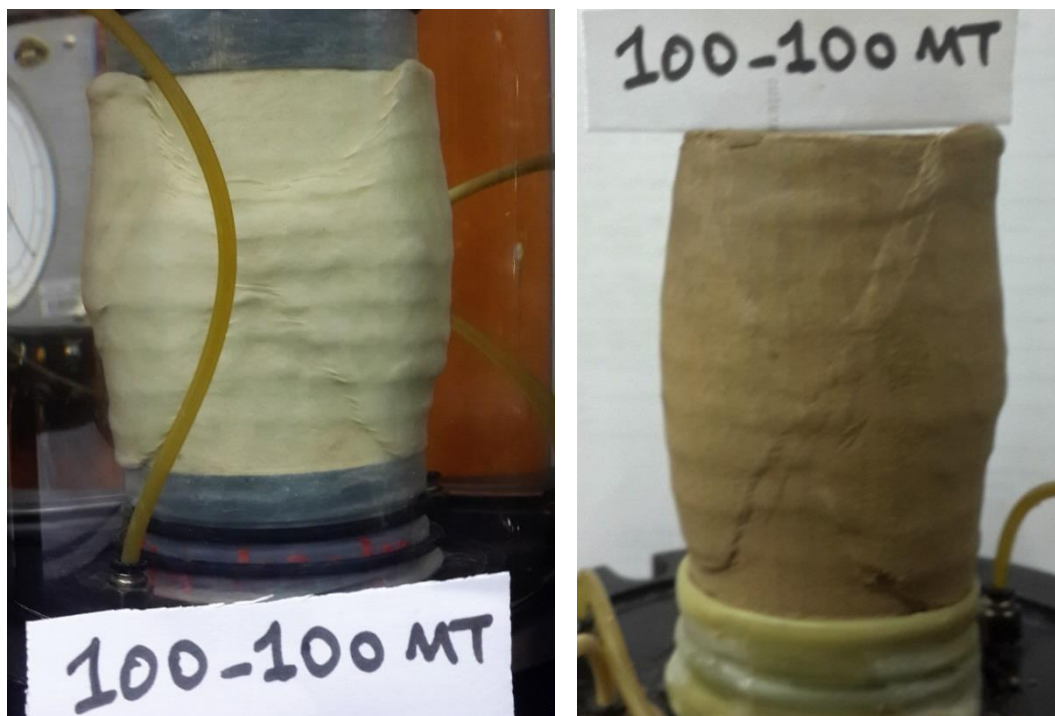
Figures C.36 Failure mode of IRS specimen at unsaturated condition with drying- wetting, s = 400 - 200 kPa, (σ_3-u_a) = 100 kPa

Figures C.37 Failure mode of MT specimen at unsaturated condition, s = 100 kPa, (σ_3-u_a) = 25 kPa

Figures C.38 Failure mode of MT specimen at unsaturated condition, s = 100 kPa, (σ_3-u_a) = 100 kPa

Figures C.39 Failure mode of MT specimen at unsaturated condition, s = 100 kPa, $(\sigma_3 - u_a)$ = 400 kPa

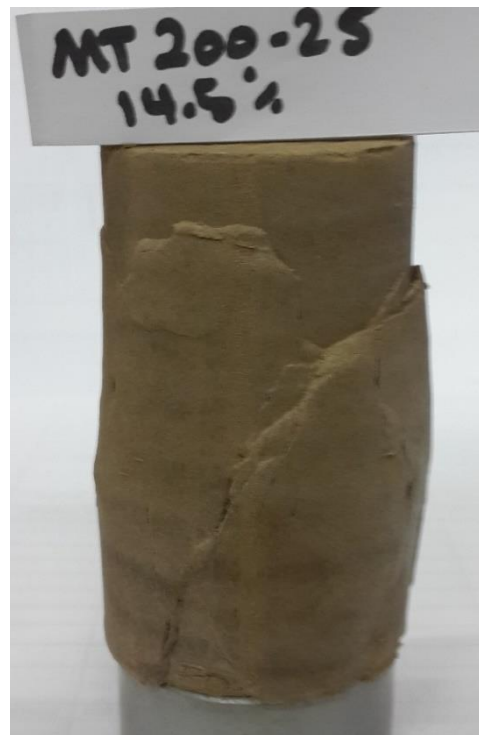
Figures C.40 Failure mode of MT specimen at unsaturated condition, s = 200 kPa, $(\sigma_3 - u_a)$ = 25 kPa

Figures C.41 Failure mode of MT specimen at unsaturated condition, s = 200 kPa, $(\sigma_3 - u_a)$ = 100 kPa

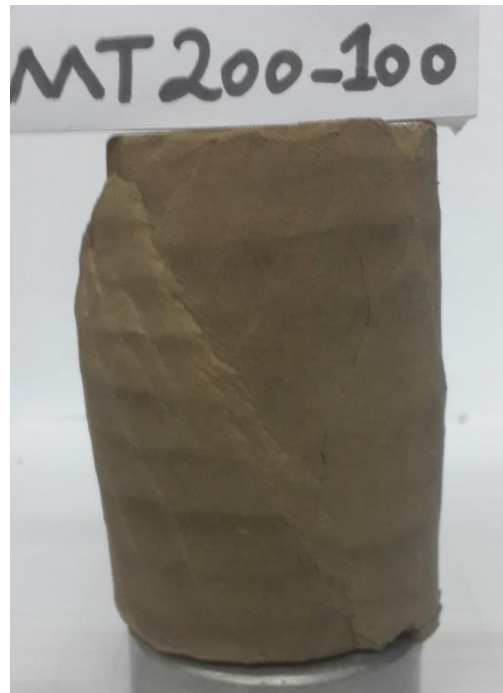
Figures C.42 Failure mode of MT specimen at unsaturated condition, s = 200 kPa, $(\sigma_3 - u_a)$ = 400 kPa

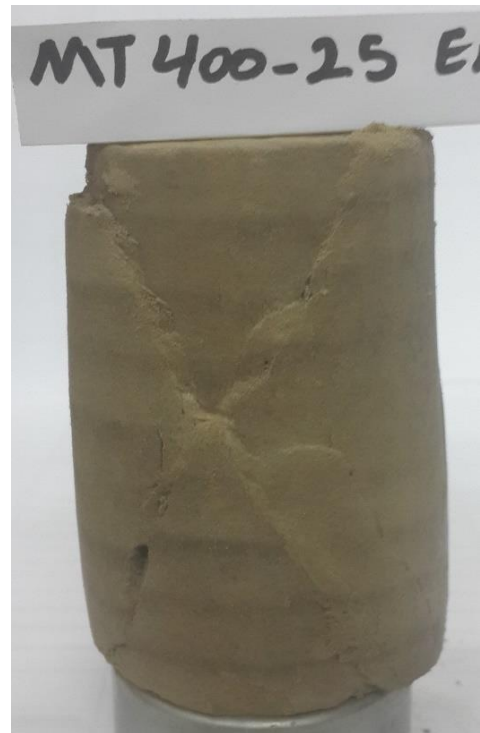Figures C.43 Failure mode of MT specimen at unsaturated condition, s = 400 kPa, (σ_3-u_a) = 25 kPa

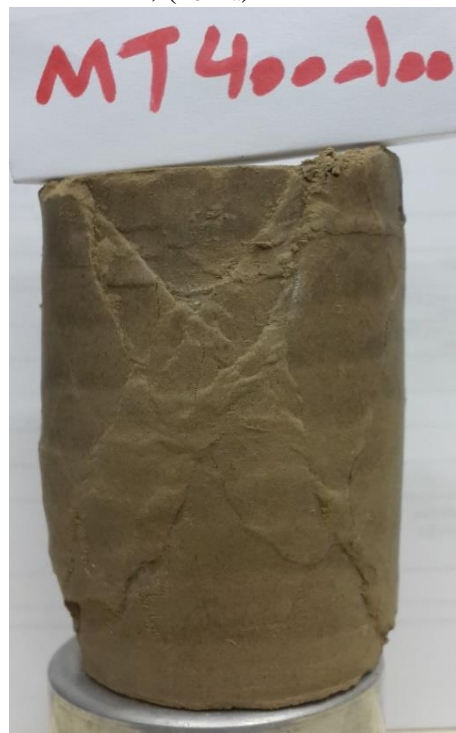

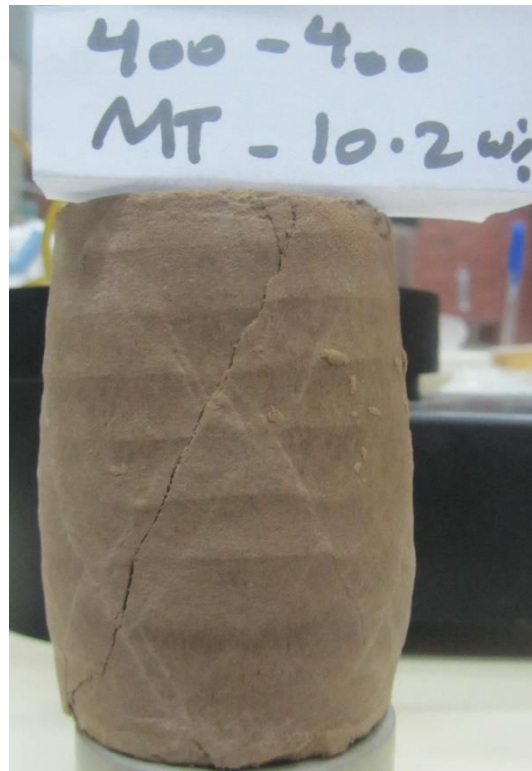Figures C.43 Failure mode of MT specimen at unsaturated condition, s = 400 kPa, (σ_3-u_a) = 25 kPa

Figures C.44 Failure mode of MT specimen at unsaturated condition, s = 400
kPa, (σ_3-u_a) = 400 kPa

PERSONAL INFORMATION

Surname, Name: Ahmadi Naghadeh, Reza

Nationality: Iranian

Date and Place of Birth: 2 May 1982, Naghadeh

Phone: +90 541 3769012

email: rnaghadeh@gmail.com

Education

- **Middle East Technical University**, Ankara, Turkey
    - Ph.D. in Geotechnical Engineering   Feb. 2010 - Jan. 2016

    - M.Sc. in Geotechnical Engineering   Sept. 2006 - Dec. 2008
    - B.S. in Civil Engineering   Sept. 2002 - Sept. 2006

Publications

Journal

- **Ahmadi-Naghadeh, R**., Toker, N. K., *Volume Change Measurement in Triaxial Tests by Monitoring Cell Fluid Volume Based on Viscoelastic Behavior of the Test Setup*, submitted to Geotechnical Testing Journal (Under review).
- **Ahmadi-Naghadeh, R**., Toker,N. K., *A new isotropic specimen preparation method from slurry for both saturated and unsaturated triaxial testing*, submitted to Geotechnical Testing Journal (Under review).

- **Ahmadi-Naghadeh, R**., Toker, N. K., *An exponential equation for predicting shear strength envelope of unsaturated soils* (ready for submission).

- **Ahmadi-Naghadeh, R**., Toker, N. K. Hydro-Mechanical Behavior of Unsaturated Specimens Isotropically Reconstituted from Slurry and Compacted Specimens (in preparation).

Conference Proceedings

- **Ahmadi-Naghadeh, R**. and Toker, N. K, *Volume change measurement in triaxial testing of unsaturated soils*. 3rd International Conference on New Developments in Soil Mechanics and Geotechnical Engineering, 2012, Cyprus.

- **Ahmadi-Naghadeh, R**., Toker, N. K. and Ahmadi-Adli, M., *Water content variability of unsaturated soil specimens in conventional strength tests*. 10th International Congress on Advances in Civil Engineering, 2012, Ankara, Turkey.

- Maghsoudloo, A., **Ahmadi-Naghadeh, R**., Toker, N.K., *Numerical comparison of retaining system behavior for a deep excavation case with and without ground improvement*, International Conference on Ground Improvement and Ground Control (ICGI 2012), 30 Oct.- 2 Nov. 2012, University of Wollongong, Wollongong , Australia.

- Toker, N.K, Ozlu, P., Maghsoudloo, A., **Ahmadi Naghadeh, R**., *Design of a deep excavation near metro tunnels in Ankara*, 6th Geotechnical Engineering symposium, November 2011, Ankara, Turkey.(in Turkish)

Honors and Awards

- Graduate fellowship, The Scientific and Technological Research Council of Turkey (Tübitak), 2010-2014.
- Full grant for summer school participation (Tübitak),
  - Unsaturated Soil Mechanics: From Fundamentals to Applications, Barcelona, Spain, 2015.
- Young Researchers and Elite Club, (2008-2010),
  - Three travel grant for attending national conferences.

Research Experience

Research Assistant (Ph.D. Research)

Projects

- Modifying the conventional triaxial setup to perform unsaturated soils tests (Matric suction control; volume changes measurement), 2013-2014, (BAP-07-02-2012-101-120).
- Coupled hydro-mechanical constitutive modeling of unsaturated soils prepared from slurry, 2014-2015, (BAP-07-02-2014-007-138).

Key Achievements:

- Developed a novel volume-change measurement technique in triaxial testing of unsaturated soil by monitoring cell fluid volume based on viscoelastic behavior of the test setup.
- Developed a novel procedure for preparation of specimens isotropically reconstituted from the slurry for use in both saturated and unsaturated soil testing.
- Performed a comprehensive laboratory-based study on both saturated and unsaturated specimens reconstituted from slurry and compacted specimens with drying-wetting cycles.
- Proposed an equation to predict shear strength of unsaturated soils.

Teaching Experience (Middle East Technical University)

- Teaching assistant of CE 7009 (Geotechnical laboratory techniques),
- Teaching assistant of laboratory session of CE363, CE364 (undergraduate soil mechanics).

Invited Talks

Laboratory Testing of Soils, CFU International Trade and Services LTD, Ankara, Turkey, January 2015.

Laboratory Experience

All commonly practiced soil testing methods, triaxial testing of saturated and unsaturated soil (along with axis translation and volume change measurement), high-capacity tensiometer, computer-automated data acquisition, equipment modification and design, measurement of soil moisture characteristic curves.

Computer Skills

- Engineering software:
    - PLAXIS 2D
    - Phase2
    - Autodesk AutoCAD
    - Slide (Rocscience)
    - GeoStudio

- Programming software:
    - MATLAB
    - Python (Elementary)